

https://dspace.org/

The effects of cement extenders and water to binder ratio on the heat evolution characteristics of concrete

Greensmith, Christopher Graeme

2006-10-31T08:51:29Z
http://hdl.handle.net/10539/1516

Downloaded from a DSpace repository. https://dspace.org/

THE EFFECTS OF CEMENT EXTENDERS AND WATER TO BINDER RATIO ON THE HEAT EVOLUTION CHARACTERISTICS OF CONCRETE

Christopher Graeme Greensmith

A research report submitted to the Faculty of Engineering and the Built Environment, University of the Witwatersrand, in fulfilment of the requirements for the degree of Master of Science in Engineering.

Johannesburg, 2005

Declaration

I declare that this research report is my own, unaided work. It is being submitted for the Degree of Master of Science in Engineering in the University of the Witwatersrand, Johannesburg. It has not been submitted before for any degree or examination in any other University.

_____

Christopher Graeme Greensmith

_____day of _____(year)_____

Abstract

The hydration of cement is an exothermic reaction, which begins almost immediately upon contact with water. This produces a large amount heat that subsequently raises the temperature of the concrete mixture, creating a temperature gradient across the member. The temperature rise associated with hydration induces thermo-mechanical stresses. These stresses can cause damage to the structure, affecting the durability and in extreme cases the functionality of the structure. If the maximum rate of heat evolution experienced can be minimised through the selection of the constituents of a concrete mixture, then the thermal stresses that develop in the concrete can be reduced. The main aim of this research is to develop a knowledge of how the heat evolution characteristics of concrete are affected by changing certain concrete mixture parameters and ingredients. The focus is on the addition of three different cement extenders and varying the water/cement ratio. This will be a step towards the development of a model for predicting the thermal properties of concrete. As a part of this investigation, a prediction model for the change in heat rate in concrete was developed. The model is intended to predict the contribution of the individual clinker crystallographic phases in cement and the heat liberated in concrete during hydration.

Acknowledgements

I would like to thank my supervisor, Professor Yunus Ballim, for his support, encouragement and expert guidance throughout this study. I would also like to thank Dr. Peter Graham and the materials laboratory staff at the School of Civil and Environmental Engineering at the University of the Witwatersrand for their help with the laboratory work done as a part of this investigation. Thanks to Holcim South Africa for providing the cement used in this research and the three different aggregate types tested. Thanks also goes to Mr. John Kellerman and the laboratory staff at the Holcim cement laboratory in Roodepoort for conducting the required XRF analyses for this study.

For my parents

Colin and Louise Greensmith

Table of Contents

Declaration....i

Abstract....ii

Acknowledgements....iii

Table of Contents....v

List of Figures....x

List of Tables....xiii

1. INTRODUCTION 1

1.1 Background....1

1.2 Scope of the Investigation....2

1.2.1 Statement of the Problem....2

1.2.2 Aims of the Research....5

1.3 Outline of the Investigation....6

1.4 Chapter References....7

2. LITERATURE REVIEW 9

2.1 Introduction....9

2.2 The Early History of Cement....10

2.3 The Chemistry and Hydration of Portland Cement....11

2.3.1 The Chemical Composition of Cement....11

2.3.2 The Hydration of Portland Cement....13

2.4 Thermal Cracking of Concrete....20

2.4.1 Background *20*

2.4.2 Thermal Stress and Strain *21*

2.4.3 Temperature Gradients and the Formation of Cracks *23*

2.4.4 Practical Measures to Avoid Thermal Cracking *25*

2.5 The Effect of Cement Extenders on the Hydration and Heat Evolution Characteristics of Concrete 26

2.5.1 Background *26*

2.5.2 Fly Ash *28*

2.5.3 Blastfurnace Slag *31*

2.5.4 Silica Fume *35*

2.6 Methods of Determining the Heat of Hydration 37

2.7 Summary and Conclusions 38

2.8 Chapter References 39

3. TEST METHODS AND MATERIALS **43**

3.1 Introduction 43

3.2 Sample Collection 44

3.3 Test Methods for Material Analysis 45

3.3.1 Chemical Analysis *45*

3.3.2 Clinker Morphology *47*

3.3.3 Sample Preparation for Microscopy Investigation *50*

3.3.4 Determination of Density and the Blaine Test *53*

3.4 Adiabatic Calorimeter 53

3.4.1 General Description *53*

3.4.2 Hardware *56*

3.4.3 Software *59*

3.4.4 Heat of Hydration Measurement *60*

3.5 Holcim Portland Cement and Clinker Characterisation 61

3.5.1 Holcim Portland Cement *61*

3.5.2 Dudflied Clinker *63*

3.5.3 Ulco Clinker *67*

3.6 Cement Extenders 72

3.7 Summary and Conclusions 73

3.8 Chapter References 74

4. ADIABATIC CALORIMETER RESULTS **76**

4.1 Introduction 76

4.2 Prediction of the Temperature Distribution in a Concrete Element 77

4.3 Concrete Maturity as Applied to Heat Evolution 78

4.3.1 Determining the Rate of Heat Evolution *79*

4.3.2 Maturity Functions *81*

4.4 Concrete Mixture Design 82

4.5 Adiabatic Calorimeter Test Results 84

4.5.1 Test Methodology *84*

4.5.2 Portland Cement Concretes *86*

4.5.3 Ground Granulated Blastfurnace Slag Concretes *89*

4.5.4 Fly Ash Concretes *92*

4.5.5 Condensed Silica Fume Concretes *94*

4.5.6 Effect of Aggregate Type on Heat Characteristics *97*

4.6 Comparing the Results of the Different Binders 99

4.6.1 Comparison between the GGBS Concretes and the PC Only Concretes *99*

4.6.2 Comparison between the FA Concretes and the PC Only Concretes *101*

4.6.3 Comparison between the CSF Concretes and the PC Only Concretes *104*

4.6.4 Comparison between the Different w/c Ratios *107*

4.7 Summary and Conclusions 114

4.8 Chapter References 116

5. MATURITY HEAT RATE MODEL **119**

5.1 Introduction 119

5.2 Multi-Component Heat of Hydration Model (Maekawa et al., 1999) 120

5.2.1 Basis of the Heat of Hydration Model 120

5.2.2 Reference Heat Generation Rates 123

5.2.3 Temperature Dependence of the Mineral Phases 125

5.2.4 Interdependence of Mineral Reactions 126

5.2.5 The Effect of Mineral Composition on the Rate of Heat Evolution 128

5.2.6 Structure of the Heat of Hydration Model 129

5.3 Modified Heat of Hydration Model 130

5.3.1 Maturity Heat Rate Model 130

5.3.2 Structure of the Maturity Heat Rate Model 131

5.3.3 Input Data 132

5.3.4 Free Water Calculations 132

5.3.5 Heat of Hydration Determination 134

5.4 Verification of the Maturity Heat Rate Model 140

5.4.1 Calibration of the Prediction Model 140

5.4.2 Verification of the Prediction Model 141

5.5 Summary and Conclusions 146

5.6 Chapter References 147

6. CONCLUSION **149**

6.1 Introduction 149

6.2 Adiabatic Calorimeter Results 149

6.3 Maturity Heat Rate Model 152

6.4 Possible Areas for Additional Research 152

6.5 Chapter References 153

APPENDIX A: VISUAL BASIC MACROS **154**

APPENDIX B: MATURITY HEAT RATE MODEL **166**

List of Figures

CHAPTER 2

Figure 2.1. A typical heat rate versus time curve for the hydration of cement.....15

Figure 2.2. Relationship between Stress, Strain and Temperature at an Internal Point in a Concrete Section (Bernander, 1998).....22

Figure 2.3. Superposition of the P- and S-Reactions in a PC/GGBS binder (De Schutter, 1998).....34

CHAPTER 3

Figure 3.1. Layout of the Adiabatic Calorimeters in the Laboratory 54

Figure 3.2. Schematic Diagram of the Adiabatic Calorimeter 55

Figure 3.3. Sketch of the Calorimeter Sample Chamber (not to scale) 58

Figure 3.4. Photograph of the Sample Chamber with a Temperature Probe in the sample jar alongside.....59

Figure 3.5. 400x Magnification of Dudfield clinker.....65

Figure 3.6. 100x Magnification of Dudfield clinker with belite nests.....66

Figure 3.7. 40x Magnification of Dudfield clinker - high concentration of belite. 66

Figure 3.9. 400x Magnification of Ulco clinker. 70

Figure 3.10. 200x Magnification of Ulco clinker - large amount of joined alite. 70

Figure 3.11. 100x Magnification of Ulco clinker - belite nest. 71

Figure 3.12. 200x Magnification of Ulco clinker - large belite nests. 71

CHAPTER 4

Figure 4.1. Total Heat – PC Only concretes.....87

Figure 4.2. Maturity Heat Rate – PC Only concretes 87

Figure 4.3. Total Heat – GGBS concretes 90
Figure 4.4. Maturity Heat Rate – GGBS concretes 90
Figure 4.5. Total Heat – FA concretes.....93
Figure 4.6. Maturity Heat Rate – FA concretes.....93
Figure 4.7. Total Heat – CSF concretes.....95
Figure 4.8. Maturity Heat Rate – CSF concretes.....95
Figure 4.9. Total Heat – Different Aggregate Types.....98
Figure 4.10. Maturity Heat Rate – Different Aggregate Types.....98
Figure 4.11. Total Heat and Maturity Heat Rate versus t_{20} Maturity – PC & GGBS comparison.....100
Figure 4.12. Total Heat and Maturity Heat Rate versus t_{20} Maturity – PC & FA comparison.....103
Figure 4.13. Total Heat and Maturity Heat Rate versus t_{20} Maturity – PC & CSF comparison.....106
Figure 4.14. Total Heat liberated at 400 t_{20} hours for different extenders.....108
Figure 4.15. Total Heat – Different Binders w/c = 0.4.....108
Figure 4.16. Total Heat – Different Binders w/c = 0.5.....109
Figure 4.17. Total Heat – Different Binders w/c = 0.6.....109
Figure 4.18. Maximum Maturity Heat Rate (peak 3) for different extenders 112
Figure 4.19. Maturity Heat Rate – Different Binders w/c = 0.4.....112
Figure 4.20. Maturity Heat Rate – Different Binders w/c = 0.5.....113
Figure 4.21. Maturity Heat Rate – Different Binders w/c = 0.6.....113

CHAPTER 5

Figure 5.1. Stages of PC Hydration (Maekawa et al., 1999).....123
Figure 5.2. Reference Heat Rates – Ettringite Formation (Maekawa et al., 1999)....124
Figure 5.3. Reference Heat Rates – Phase Hydration (Maekawa et al., 1999).....124
Figure 5.4. Thermal Activity – Hydration Components (Maekawa et al., 1999).....125
Figure 5.5. Multi-Component Heat of Hydration Model (Maekawa et al., 1999).....129

Figure 5.6. Outline of the Maturity Heat Rate Model 131
Figure 5.7. Steps of the Maturity Heat Rate Prediction Model 135
Figure 5.8. c_i values for w/c ratios – Hydration.....137
Figure 5.9. c_i values for w/c ratios – Ettringite & Monosulphate.....137
Figure 5.10. t_{0i} values for w/c ratios – Hydration.....138
Figure 5.11. Duration of Exothermic Peak 3.....139
Figure 5.12. Model & Laboratory Results – PC concrete w/c = 0.6 141
Figure 5.13. Model & Laboratory Results – PC concrete w/c = 0.5 142
Figure 5.14. Model & Laboratory Results – PC concrete w/c = 0.4 142
Figure 5.15. Model & Laboratory Results – Cement A1 to D2 (Graham, 2003).....143
Figure 5.16. Model & Laboratory Results – Cement E1 to H2 (Graham, 2003) 144
Figure 5.17. Model & Laboratory Results – Cement K1 to K2 (Graham, 2003).....145

APPENDIX B

Figure B.1. Progression of Maturity Heat Rate Model.....167

List of Tables

CHAPTER 2

Table 2.1. Major Oxides found in South African Clinkers (Addis, 2001) 12

Table 2.2. Chemical phases and compounds present in South African Portland cements (Addis, 2001).....12

Table 2.3. Chemical composition of South African Cement Extenders (Addis, 2001) 27

CHAPTER 3

Table 3.1. Chemical composition of Holcim Portland cement.....62

Table 3.2. Chemical composition of Dudfield clinker 63

Table 3.3. Chemical composition of Ulco clinker. 68

Table 3.4. Chemical composition of the cement extenders used.....72

CHAPTER 4

Table 4.1. Reference Concrete Mixture Design (Graham, 2003).....83

Table 4.2. Concrete Mixture Designs.....83

Chapter 1

INTRODUCTION

1.1 Background

A cement is an adhesive substance able to bind fragments or masses of solid matter into a compact whole (Blezard, 1998). Cements used in the construction industry however, are chemically similar and are made up of a mixture of materials containing calcium and silica. After this mixture is fired in a kiln, it is ground with gypsum to produce Portland cement.

The first known use of cementitious materials dates back to the ancient Greeks and Romans who used lime and natural pozzolans in the mortars for their construction. The technology of the Romans and Greeks was lost however, and it was not until Smeaton discovered the benefits of using a mixture of hydraulic lime and clay in 1756, that this was rediscovered. In 1824, Joseph Aspdin patented Portland Cement (PC) and this is widely considered to be the first cement of what is commonly known by the same name today. The cements used today however, are chemically very different from Aspdin's patent (Blezard, 1998).

Since Aspdin's publication, there has been a large volume of research conducted on cement and a large number of publications on the nature of cement and concrete. The research presented here however, is primarily concerned with the heat evolution characteristics of concrete and factors, which affect these characteristics.

1.2 Scope of the Investigation

1.2.1 Statement of the Problem

The mixing of cement and water leads to an exothermic reaction. This reaction begins almost immediately upon contact of the two materials, producing a large amount of heat. Hydration is the term used collectively for the reactions that take place between the crystallographic cement phases and water and the heat liberated is known as the heat of hydration. This heat subsequently raises the temperature of the concrete mixture constituents in contact with the water-cement paste. Consequently, a temperature gradient can be established across the concrete member in question, particularly in large sections. The heat liberated during hydration also creates a potential for cracking to occur due to thermally induced stresses in the concrete.

The temperature rise associated with hydration and the induced thermal-mechanical stresses can cause damage to the structure, affecting the durability and, in extreme cases, the functionality of the structure. This is a particularly serious problem in mass concrete sections such as dams and piers because of the large temperature difference experienced between the core and the surface of the section.

Hydration of Portland Cement

As mentioned, the mixing of water and cement causes in an exothermic reaction that begins almost instantaneously, and continues for an extended period thereafter. Hydration however, is a complex process because of the many different minerals found in cement. A series of individual reactions takes place between the water and the different components of the cement, both simultaneously and successively and can affect one another directly or indirectly. The combination of the various reactions results in chemical and physio-mechanical changes in the cement paste, particularly during hardening and setting of the paste or concrete (Odler, 1998).

There are four major minerals or crystallographic phases in PC that take part in hydration namely, tricalcium silicate or alite (C_3S), dicalcium silicate or belite (C_2S),

tricalcium alluminate (C_3A) and tetracalcium aluminoferrite or ferrite (C_4AF). Each of these minerals reacts differently with water, contributing to the heat of hydration at different times, in different amounts and at different rates. This implies that cements differ quite significantly in their heat evolution characteristics because of the varying amounts of the major phases present and different ways in which they affect the heat of hydration.

Copeland and Kanto (1972) note that the following assumptions are generally made with respect to the heat of hydration of the major phases of cement:

- The total heat of hydration is equal to the sum of the individual heats of hydration of the cement components.
- The C_2S present contributes the least to the heat of hydration and the C_3A contributes the most to the heat evolved, followed by the C_3S.

During the hydration of cement, there are at least two, and possibly up to four cycles of increasing and decreasing rates of reaction. Each of the major crystallographic phases contributes in different amounts and at different times to these stages and to the overall rate of heat evolution. This is discussed in detail in chapter 2.

Thermal Cracking of Concrete

Thermal cracking in concrete is caused by differential contraction due to temperature changes within a concrete member and can cause serious structural damage. When the strains caused by this contraction exceed the tensile capacity of the concrete, and any restraints in place that prevent this contraction from freely occurring, the member can crack (Harrison, 1981). One major source for possible temperature-induced cracking is in the setting of the concrete and the chemical reactions that take place during the hydration process.

Soon after the concrete has been poured and hydration has begun, some of the heat generated is retained inside the concrete member, causing a temperature rise in the material (Harrison, 1981). At this point, the rate of heat generation is greater than the rate of heat loss. Under unrestrained conditions, the concrete element would expand.

The fact that a section is always at least partially restrained and that heat can be dissipated from the surface of the concrete much quicker than from the interior implies that there is a non-uniform expansion of the section (Bernander, 1998). This resistance to thermally induced movement in the concrete causes stress in the section, which can result in cracks forming on the surface. These cracks however, are relatively shallow and usually not serious, and generally close up during the cooling phase of hydration when the member begins to contract (Bernander, 1998).

Once the concrete begins to cool down, contraction would occur freely under unrestrained conditions. This is prevented however, by the restraint the member is subjected to and by the stiffness developed in the concrete due to the onset of setting and hardening. The increased stiffness attracts more stress and, although the tensile capacity of the concrete is increasing, its relaxation capacity is decreasing (Ballim, 2001). This can cause serious internal cracks, known as through cracks, if the tension experienced exceeds the tensile capacity of the concrete (Bernander, 1998). These through cracks are relatively large and do not close.

Simultaneously, different points along the section at any one depth will be subjected to a different temperature at any particular time, as not all of the concrete can be poured at the same time (Ballim, 2001). The extent of hydration and the amount of heat produced therefore varies at each point across the structure, creating a further temperature gradient along the length of the section. This establishes another possible cause of the development of through cracks.

Designers and engineers therefore need to be aware of the development and evolution of heat in concrete sections and need to be able to predict the thermal behaviour of a mixture in order to control heat evolution and ultimately prevent early-age cracking. This topic is discussed in further detail in chapter 2.

1.2.2 Aims of the Research

Factors affecting the heat evolution of concrete

The main aim of this research is to develop a knowledge of how the heat evolution characteristics of concrete are affected by changing certain ingredients in the concrete mixture. This will be a step towards the development of a model for predicting the thermal properties of a concrete based on the concrete mixture design. This will hopefully aid engineers and concrete technologists in the prediction of the thermal cracking potential of a concrete based on the mixture constituents. Data produced in this research could be used to form part of a database for computer modelling of the hydration of concrete and the prediction of thermal stresses.

If the constituents of a concrete mixture can be chosen to minimise the maximum in the rate of heat evolution (see figure 2.1, chapter 2), then the thermal stresses that develop in the concrete can be reduced. This approach could also be used to ensure that the maximum tensile stress (see figure 2.2, chapter 2) occurs at a time when the concrete has developed sufficient strength to resist the induced tension without cracking. This could be achieved by delaying the occurrence of peak 3 in figure 2.1.

The focus of this investigation is on how the heat evolved from, and the rate of heat evolution of concrete is affected by various concrete mixture parameters and components during curing. Emphasis is on the following aspects affecting concrete mixture design, the results of which are presented in chapter 4:

- The effects of varying the water:cement or water:binder ratio (w/c). Note that water:binder ratio is represented by w/c throughout this investigation.
- The effects of different extenders used in place of a portion of the cement in the mixture.
- The effects of different aggregate types.

Development of a heat rate prediction model

If engineers are to design concrete structures with a minimum risk of thermally induced cracking, there is a need for a reliable prediction of the heat evolution

characteristics of the concrete used and the transfer of heat through the concrete element. Such tools would allow engineers to optimise the design of large concrete elements with respect to mixture constituents, element size, cooling systems, sequential pouring of concrete etc., without the need for costly and time-consuming laboratory tests.

In an attempt to develop such a tool, a heat rate prediction model was developed as a part of this investigation. The model is based on the work conducted by Maekawa et al. (1999) and Graham (2003). It predicts the contribution of the individual clinker phases in cement to the heat liberated in concrete during hydration. This is presented in chapter 5.

1.3 Outline of the Investigation

This investigation has been divided into the following four parts, which are discussed in depth in the chapters that follow:

1. A review of the literature concerning the heat of hydration of cement and thermal cracking of concrete.
    - The contributions of the different cement phases to the rate of heat evolution of cement are discussed in detail.
    - The mechanisms associated with thermal cracking in concrete.
    - The current knowledge regarding the effects of cement extenders on the heat evolution characteristics of concrete.
    - Current methods available for determining the heat of hydration of cement and concrete.
2. A discussion of the test methods and the materials used during this investigation.
3. The presentation and analysis of the adiabatic calorimeter results obtained for the purposes of this investigation. It is hoped that these results will add to what is known about the effects of varying the w/c ratio and the presence of

cement extenders on the progression of heat rate with respect to time in a concrete element.

4. The development of a maturity heat rate prediction model. It is hoped that this model will aid engineers to predict the type of results presented in chapter 4 more accurately and eliminate the need to costly, time-consuming laboratory tests.

1.4 Chapter References

Ballim, Y. (2001) Thermal properties of concrete and temperature development at early ages in large concrete elements. In: Addis, B. and Owens, G. (ed.), *Fulton's Concrete Technology, 8th Ed.*, Cement and Concrete Institute (CNCI), Midrand, South Africa, pp. 227-247.

Bernander, S. (1998) Practical measures to avoiding early age thermal cracking in concrete structures. In: Springedschmid, R. (ed.) *Prevention of thermal cracking in concrete at early ages*, RILEM Report 15, E&FN Spon, London, UK, pp. 255-314.

Blezard, R.G. (1998) The history of calcareous cements. In: Hewlett, P.C. (ed.), *Lea's chemistry of cement and concrete*, Arnold, London, UK, pp. 1-24.

Copeland, L.E. and Kanto, D.L. (1972) Chemistry of hydration of Portland cement at ordinary temperatures. In: Taylor, H.F.W. (ed.) *The chemistry of cements volume 1*, Academic Press, New York, USA, pp. 313-370.

Graham, P.C. (2003) *The heat evolution characteristics of South African cements and the implications for mass concrete structures*. Ph.D. Thesis, University of the Witwatersrand, Johannesburg, South Africa.

Harrison, T.A. (1981) *Early-age thermal crack control in concrete*, CIRIA Report 91, Construction Industry Research and Information Association (CIRIA), London, UK.

Maekawa, K., Chaube, R. and Kishi, T. (1999) Multicomponent model for the heat of hydration of Portland cement. *Modelling of Concrete Preformance: Hydration, microstructure formation and mass transport*, Routledge, New York, USA, pp. 178-248.

Odler, I. (1998) Hydration, setting and hardening of Portland cement. In: Hewlett, P.C. (ed.), *Lea's chemistry of cement and concrete*, Arnold, London, UK, pp. 241-297.

Chapter 2

LITERATURE REVIEW

2.1 Introduction

Cements are defined as adhesive substances that are able to bind fragments or masses of solid matter into a compact whole (Blezard, 1998). This definition however, encompasses a very wide range of different substances that are chemically and mechanically far removed from the Portland cement used in construction and civil engineering. Cements used in the construction industry generally bear a chemical resemblance to one another and constitute a mixture of compounds, with lime as the main ingredient.

Cement is a highly complex material and the topics that can be discussed are far reaching. For this reason, the literature review conducted was divided into the following five sections:

1. A brief history of cement and its early development and use.
2. The chemistry and hydration of Portland cement.
3. Thermal cracking of concrete.
4. The effects of cement extenders on concrete.
5. Methods of determining the heat of hydration.

2.2 The Early History of Cement

The Romans and Greeks were most likely the first to be aware of the use of lime and natural pozzolans in the mortars they used during construction. Some of the hydraulic properties associated with modern cement were achieved through the addition of tile fragments or pottery shards to the pozzolanic mixture. The properties of hydraulic lime however, were only recognised in 1756 when John Smeaton discovered the benefits of using limestone that contained a relatively large portion of clayey material. Joseph Aspdin's patent for Portland Cement in 1824 is often considered to be the first cement of what is known today by the same name. The cement of today however, is chemically different from Aspdin's material, which was essentially little more than a hydraulic lime. Cement manufacturing by Aspdin's method is however the forerunner to that of modern Portland cement. Since Aspdin patented Portland cement, there have been a large number of publications about the nature of cement and concrete. This chapter however, will only focus on aspects of cement and concrete that are pertinent to the heat evolution characteristics of these materials.

It has been well documented that early age temperature rises and temperature-induced stresses affect the functionality, durability and overall performance of a concrete structure and an ability to control these factors is vital (Branco et al., 1992 and van Breugel, 1998). Tetmeyer was one of the first researchers to recognise the importance of heat evolution in concrete when he began taking heat measurements of samples as early as 1883 (Springedschmid, 1998). Since then, particularly in the 1920's and 1930's, many authors have discussed the problem of temperature rises. The focus however, was mainly on methods of avoiding thermal cracking during the casting and construction phase of a concrete structure. In more recent times the focus has shifted towards the pre-construction phase, and is aimed at optimising the concrete mixture design and developing heat of hydration models for predictions of temperature in a concrete structure at the design stage.

2.3 The Chemistry and Hydration of Portland Cement

2.3.1 The Chemical Composition of Cement

Portland cement (PC) is classified as a hydraulic cement, which means that it hardens and gains strength after reacting with water to produce a water resistant product (Czernin, 1980). It is produced by grinding PC clinker with a small amount of calcium sulphate, usually in the form gypsum, to produce the fine grey powder recognisable as cement.

Clinkers are produced through the processing of predetermined amounts of suitable raw materials, which are burnt or clinkered at sufficiently high temperatures to form hard nodules. Two types of raw materials are generally used, one rich in calcium, such as limestone or chalk, and one rich in silica, such as clay or shale. These materials are used in order to obtain the calcium oxide, silica, alumina and iron oxide necessary for the formation of the major PC crystallographic phases. The clinker is then ground with between four and seven percent gypsum to produce Portland cement.

After investigations carried out by Bogue (1947) it was determined that five major components are present in PC, namely CaO, MgO, Al_2O_3, Fe_2O_3 and SiO_2. These components and their interactions are responsible for the formation of the four major crystallographic phases present in Portland cement (refer to table 2.1 and table 2.2). Under equilibrium conditions, the following reactions approximately represent the formation of the four major phases in cement (Bogue, 1947):

1. Fe_2O_3 reacts with Al_2O_3 and CaO to produce $4CaO.Al_2O_3.Fe_2O_3$ or C_4AF.
2. The remaining Al_2O_3 reacts with CaO to produce $3CaO.Al_2O_3$ or C_3A.
3. The remaining CaO reacts with SiO_2 to first form $2CaO.SiO_2$ (C_2S) and the calcium oxide left over reacts further with C_2S to produce $3CaO.SiO_2$ or C_3S. Any CaO that is still uncombined at this point remains as CaO in the cement.
4. The MgO present in cement remains virtually inert and uncombined.

It must be noted however, that it is highly unlikely that equilibrium conditions will be obtained during the production of Portland cement.

Oxide	Chemical Formula	Symbol	Average content by mass (%)
Calcium oxide	CaO	C	63 – 68
Silicon oxide (silica)	SiO_2	S	19 – 24
Aluminium oxide (alumina)	Al_2O_3	A	4 – 7
Iron oxide	Fe_2O_3	F	1 – 4
Magnesium oxide	MgO	M	0.5 – 3.5

Table 2.1. Major Oxides found in South African Clinkers (Addis, 2001)

Common Name	Pure Mineral Compound	Chemical formula	Symbol	Ave. content by mass (%)
Alite	Tricalcium Silicate	$3CaO.SiO_2$	C_3S	45 – 65
Belite	Dicalcium Silicate	$2CaO.SiO_2$	C_2S	10 – 35
Celite or Alluminate	Tricalcium Alluminate	$3CaO.Al_2O_3$	C_3A	4 – 10
Felite or Ferrite	Tetracalcium Aluminoferrite	$4CaO.Al_2O_3.Fe_2O_3$	C_4AF	5 – 10
Mangesia	Magnesium Oxide	MgO	M	0.3 – 4.0
Gypsum	Calcium Sulphate	$CaSO_4$	-	3.5 – 7.0
Free lime	Calcium oxide	CaO	C	0.3 – 2.5

Table 2.2. Chemical phases and compounds present in South African Portland cements (Addis, 2001)

Tables 2.1 and 2.2 show the major chemical compounds, crystallographic phases and other important compounds present in cement clinker and PC. These phases and compounds contribute to the unique characteristics of Portland cement, depending on the relative amounts present.

2.3.2 The Hydration of Portland Cement

When cement is mixed with water, an almost instantaneous exothermic reaction begins upon contact, producing a large amount of heat. Initially the mixture, or paste, is in a plastic state and over time it becomes rigid and sets/hardens. This setting is also associated with an increase in the strength of the paste. In general terms, hydration is the chemical combining of a compound with water, causing the water involved to be absorbed during the reaction (Bye, 1999). In cement chemistry terms, hydration is the term collectively used for the reactions that take place between the different cement phases present and water. The heat liberated during this process is known as the heat of hydration.

Hydration however, is a very complex process due to the heterogeneous nature of Portland cement. A series of individual reactions between the water present and the different components of the cement take place both simultaneously and successively and can affect one another directly or indirectly. Chemical and physio-mechanical changes occur in the cement paste due to the combination of the various reactions, particularly during hardening and setting of the paste or concrete (Massazza and Daimon, 1992).

The progress and kinetics of hydration of PC are influenced by a number of internal and external factors such as (Odler, 1998):

- The phase composition of the cement, not only in terms of the quantities of the four major crystallographic phases, but also with respect to the presence of foreign ions within the crystal lattice of the individual phases.
- The fineness of the cement – particle size distribution and specific surface area affect the rate of reaction.
- The water/cement or water/binder ratio, w/c.
- The temperature at which the sample is cured.
- The addition of any chemical admixtures that modify the rate of hydration and the physical properties of the cement paste, such as workability and flowability.

- The presence of any cement extenders such as fly ash, blastfurnace slag or silica fume.

Massazza and Daimon (1992) also noted how parameters such as non-evaporable water, chemical shrinkage and heat of hydration affect the degree of hydration.

The four major crystallographic compounds that participate in the hydration reactions are shown in Table 2.2. Each of these compounds reacts differently with water, contributing to the heat of hydration at different times, in different amounts and at different rates. Other participants in the hydration reaction include free CaO ions, alkali sulphates and gypsum (calcium sulphate) (Odler, 1998). Cements therefore differ quite significantly in their heat evolution characteristics because of the varying amounts of the major crystallographic phases present and different ways in which they affect the heat of hydration.

The assumption generally adopted however, is that the heat of hydration of cement is equal to the sum of the individual heats of hydration of the cement phases. The C_2S present contributes the least to the heat of hydration and the C_3A contributes the most to the heat evolved, followed by the C_3S (Copeland and Kanto, 1972). This supports the observation that cement with high C_3S and C_3A contents will have a large amount of heat evolved relative to cement with a large amount of C_2S. The alluminate and alite phases also hydrate far more rapidly than the other mineral components and this suggests that cements that hydrate quickly also produce a large amount of heat in the early stages of hydration.

The Mechanisms of Hydration

With the hydration of cement, there are at least two, and possibly up to four cycles of increasing and decreasing rates of reaction. Four distinct stages of hydration can be identified from the heat rate versus time curve shown in Figure 2.1. During the early stages, there are significant interactions between the main phases since most particles are smaller than 5 μm and there is a wide distribution of interstitial phases. During the later stages of hydration however, the phases can be considered to be hydrating

independently of one another because of the barriers created by the hydration products formed and the limited amount of free water available (Bye, 1999).

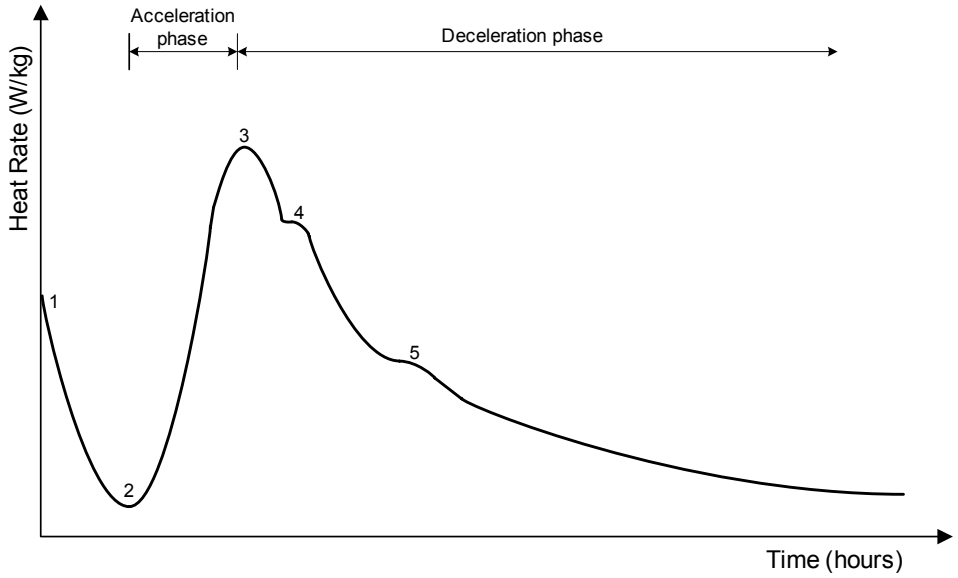

Figure 2.1. A typical heat rate versus time curve for the hydration of cement

Stage 1: Pre-induction Stage (peak 1). Almost immediately after the mixing of cement and water there is an initial maximum in the rate of heat evolution and a rapid dissolution of ions from the cement into a liquid phase occurs (Odler, 1998). This is due to the initial rapid hydration of C_3S and C_3A. If there is an inadequate amount of calcium sulphate present, there will be insufficient retardation of the reaction between the alluminate phase and water and flash set will occur (Copeland and Kanto, 1972).

A layer of calcium silicate hydrate (CSH) hydration product, or gel, begins to precipitate on the surface of the cement particles due to the C_3S hydration but the fraction of C_3S used up during this stage of the reaction is fairly low. C_3A dissolves rapidly and reacts with free calcium and sulphate ions in the liquid solution to form a type of calcium alluminate sulphate hydrate, known commonly as ettringite. The ettringite (AFt) crystals are deposited on the surface of the cement grains. C_4AF reacts in a similar way to C_3A, also yielding ettringite, but to a much smaller extent. Similarly, C_2S reacts in the same way as C_3S producing CSH gel (Odler, 1998).

Stage 2: Induction or Dormant Stage (trough 2). The early rate of hydration and heat evolution soon slows down quite rapidly as the layer of hydration products formed around the cement grains begins to act as a barrier between the cement particles and the water. The gypsum in the cement also begins to retard the hydration of C_3A in order to prevent false set from occurring. This dormant period occurs during the first few hours after mixing (Odler, 1998).

Stage 3: Acceleration Stage (peak 3). The end of the dormant period is signified by a sudden rapid increase in the rate of hydration and heat evolution of the paste roughly three to twelve hours after mixing. Initial set of the cement usually occurs on the lower side of trough 2, where the rate of heat evolution is still increasing. Final set generally occurs soon after the maximum exothermic peak is reached. (Copeland and Kanto, 1972).

Although all four of the major phases are involved in hydration during the acceleration stage, it is mainly the reaction of the alite, and to a lesser extent the alluminate phase, that results in peak 3 in figure 2.1. The reaction between C_3A and $CaSO_4$ produces ettringite. The increased rate of C_3S hydration leads to the formation of secondary CSH gel around the cement particles (Odler, 1998).

The hydration of alite governs the time and shape of peak 3 (Copeland and Kanto, 1972). At roughly the same time as initial set begins, the alite has hydrated sufficiently for CSH particles to start interlocking. This leads to final set of the cement and contributes to the strength development of the paste. The decrease in the rate of heat evolution after peak 3 is due to two main reasons; the surface area of unhydrated cement particles has decreased, and the layer of CSH gel coating the cement grains limits the ingress of water.

The rate of the C_3A reaction also increases as gypsum is consumed and more ettringite (AFt) crystals or rods are formed (Bye, 1999). The precipitation of a form of calcium hydroxide, known as Portlandite, from the liquid phase also plays a major role in the increased rate of heat evolution associated with peak 3. The hydration of

C_2S also increases, but at a much slower rate than that of the C_3S, and makes a greater contribution to the later stages of hydration.

Stage 4: Post-Acceleration Stage (peaks 4 and 5). The rate of hydration gradually slows down after the main peak in the rate of heat evolution, which, as mentioned, is due mainly to CSH and Portlandite formation. The progression of hydration is now largely controlled by the rate of diffusion of free ions in the liquid phase through the layer of hydration product surrounding each cement grain. CSH formation continues steadily and the contribution of C_2S to its production increases with time (Odler, 1998).

An additional peak or shoulder (peak 4) is often seen as the gypsum content is depleted and a short renewal of ettringite formation is seen coupled with the conversion of ettringite to monosulphate (AFm). The ettringite crystals usually stop forming about one day after initial mixing of the concrete. Occasionally a second shoulder (peak 5) occurs when C_3A reacts with some C_4AF causing some of the AFt crystals to be replaced by AFm plates, which are deposited on the surface of the cement grains (Bye, 1999).

The Kinetics of Hydration

The kinetics of cement hydration is affected by the relationship between the degree of hydration and the age of the paste, and any other factors that affect the two (Taylor, 1997). The kinetics also differs for the various constituent phases found in cement (Massazza and Daimon, 1992).

Hydration of Alite. The hydration of C_3S begins almost immediately when the cement and water come into contact. This initial reaction is rapid, but only lasts a few minutes before the dormant period begins. At this point, the reaction slows down quite dramatically, but does not cease. The reaction then speeds up again and continues to do so until a large portion of the available alite has been used up (Barret and Bertrandie, 1991). As the surface area or fineness of the alite crystals increases, so too does the rate of hydration of the alite. This leads to an increase in the amount

of heat evolved from the cement with respect to time and contributes to the size and shape of peak 3 in figure 2.1 (Bye, 1999). The rate of C_3S hydration also depends on its reactivity, which is governed to an extent by the following factors (Odler, 1998):

- The amount and quality of foreign ions present in the crystal lattice.
- Hydration of alite is accelerated in cements when greater amounts of SO_3 are present.
- Alite hydration decelerates with an increasing C_2S/C_3S ratio in the clinker.

According to Bye (1999), there are two distinct ways in which alite hydrates. The first is a through-solution mechanism where the rate of growth of CSH gel is dependent on the surface area of hydration product already formed. As hydration progresses, the CSH gel formed acts as a protective barrier around the cement grain, creating a situation where the rate of reaction is dependent on the rate of dissolution of water through this layer. For the second mechanism, alite hydration takes place at the surface of the CSH layer where ions are diffused from the cement particles into solution around the particles. The first mechanism is more dominant than the second mechanism during the early stages of hydration, and visa versa.

The formation of CH or portlandite, is also associated with the hydration of C_3S. Crystalline CH begins to form at the end of the dormant stage and the amount produced increases as alite hydration progresses (Odler, 1998).

Hydration of Belite. Belite exists in the form of four main polymorphs in cement, namely α-, α'-, β- and γC_2S. Although all four polymorphs are involved in the hydration of belite, only the β polymorph is of any real concern in the hydration of cement. βC_2S reacts in a very similar way to C_3S, producing similar hydration products (Bye, 1999). The difference between the alite and β-belite reactions is that the βC_2S reacts at a much slower rate and produces less CSH or CH hydration products than the C_3S. βC_2S also shows a period of secondary hydration, unlike alite. According to Bye (1999), this suggests that spalling of the layer of hydration product takes place at the surface of the unhydrated belite. C_2S therefore contributes very little to peak 3 in figure 2.1, but does increase concrete strength during the later stages if

hydration is allowed to continue. Since belite reacts very similarly to alite, the hydration products are the same, namely CSH gel and CH crystals.

Hydration of Tricalcium Alluminate. The C_3A in cement reacts extremely quickly when in contact with water, producing almost all the heat associated with peak 1 in figure 2.1. The gypsum present in cement however, acts as a retardant to the hydration of the alluminate phase. If gypsum were not present, the C_3A hydration would cause premature flash set of the concrete. Bye (1999) suggests that the retardation of C_3A in the presence of free calcium and sulphate ions in the aqueous phase is mostly due to the formation and deposition of ettringite crystals on the surface of the particles. Bye (1999) adds that retardation is further increased in the presence of calcium hydroxide, which causes the precipitation of a more compact layer of supersaturated crystals.

Between five and twenty five percent of the alluminate present reacts within the first five minutes of hydration according to Odler (1998). The reactivity depends on the quality and quantity of the alkalis present in the crystal lattice of the cement, and is increased in the presence of K^+ ions and decreased in the presence of Na^+ ions.

Hydration of Calcium Aluminoferrite. C_4AF hydration is similar to that of C_3A, only much slower and less volatile. The rate of hydration varies according to the A/F ratio in the cement (Odler, 1998).

Effect of w/c Ratio. The nature of the hydration reaction is unaffected by a change in the w/c ratio. The only observed variations are in the overall rate of hydration and the rate at which heat is evolved from the reactions (Copeland and Kanto, 1972). At a particular age, pastes with a higher w/c ratio will produce greater amounts of heat than pastes with a lower w/c, for a unit mass of cement. This is possibly due to a greater access to free water molecules and the greater availability of space for hydration products, in the higher w/c pastes. At later ages, the rate of heat evolution is greater in the pastes with the lower w/c ratios. This implies that by decreasing the w/c

ratio, the rate of hydration at intermediate ages can be decreased without limiting the overall extent to which hydration occurs.

Copeland and Kanto (1972) describes how the effect of the w/c ratio on hydration can be quantitatively explained in terms of the ratio of the volume of hydrated cement to the space available for the hydrated cement grains and the hydration products formed. This value is zero at the instant that the cement and water are mixed and the rate of hydration is therefore independent of w/c at this point. As the reactions progress, hydration products are deposited on the surfaces of the concrete mixture constituents. Eventually these products form a continuous layer around the mixture materials, which means that the reactants in the hydration process must diffuse through this coating in order for the reactions to continue. This slows down the rate of hydration as the space available for the hydration products is filled. The lower the w/c ratio of a paste, the more rapidly the rate of hydration decreases as there is less available water for the reactions to continue and therefore less space is freed up for hydration products to fill.

2.4 Thermal Cracking of Concrete

2.4.1 Background

In order to minimise the risk of thermal cracking, a thorough knowledge of the temperature profile of a concrete section during hydration is needed, in order to predict the thermal behaviour of the element. Factors that affect the rate of temperature rise, the maximum temperature experienced and the temperature distribution within a concrete section include (Morabito, 1998):

- The rate of heat evolution
- The total amount of heat evolved
- The cement composition and proportions of the phases present
- The dimensions of the concrete section under consideration
- The prevalent environmental conditions and the placing temperature

- The mixture proportions and the type of aggregate used.

The hydration of cement is an exothermic reaction and, consequently, a large amount of heat (of the order of 300-400 kJ/kg of cement) is generated during the process. This causes a temperature rise in the concrete section under consideration. This temperature rise would cause the specimen to expand equally and uninhibited in all directions in a controlled adiabatic environment where the concrete sample is free from all possible restraints. In practice however, conditions are far from this ideal, particularly in large concrete structures. This can create temperature differentials both within and across a concrete element.

2.4.2 Thermal Stress and Strain

There is no linear relationship between the thermal stresses present in a concrete element and the risk of cracking (Branco et al., 1992). Absolute temperatures and temperature differentials however, are important factors in the thermal analysis of concrete structures (van Breugel, 1998). Early-age thermal cracking in concrete is the result of differential expansion and contraction of the element due to temperature changes within the member. In other words, the strains caused by this expansion and/or contraction, exceed the tensile capacity of the concrete and any restraints in place that prevent this expansion/contraction from freely occurring cause the member to crack (Harrison, 1981). This can have serious consequences for a structure with respect to functionality, durability, appearance and more importantly structural integrity of the concrete.

The adequate development of the tensile strain capacity of the concrete however, is not the only factor to consider with respect to the development of thermally induced cracks. The increase in tensile strength with time suggests that the ability of the concrete to resist cracking is improved. However, as hydration progresses the elastic modulus of the concrete increases and the creep capacity decreases, leading to an increase in overall stiffness of the element. As thermally induced stresses and strains build up, the potential for cracking to occur becomes greater as the stiffness increases.

The tensile strength development therefore needs to take place at an adequate rate to counter the detrimental effects of the increasing stiffness. The development of thermal stress and strain within a concrete section is shown in figure 2.2.

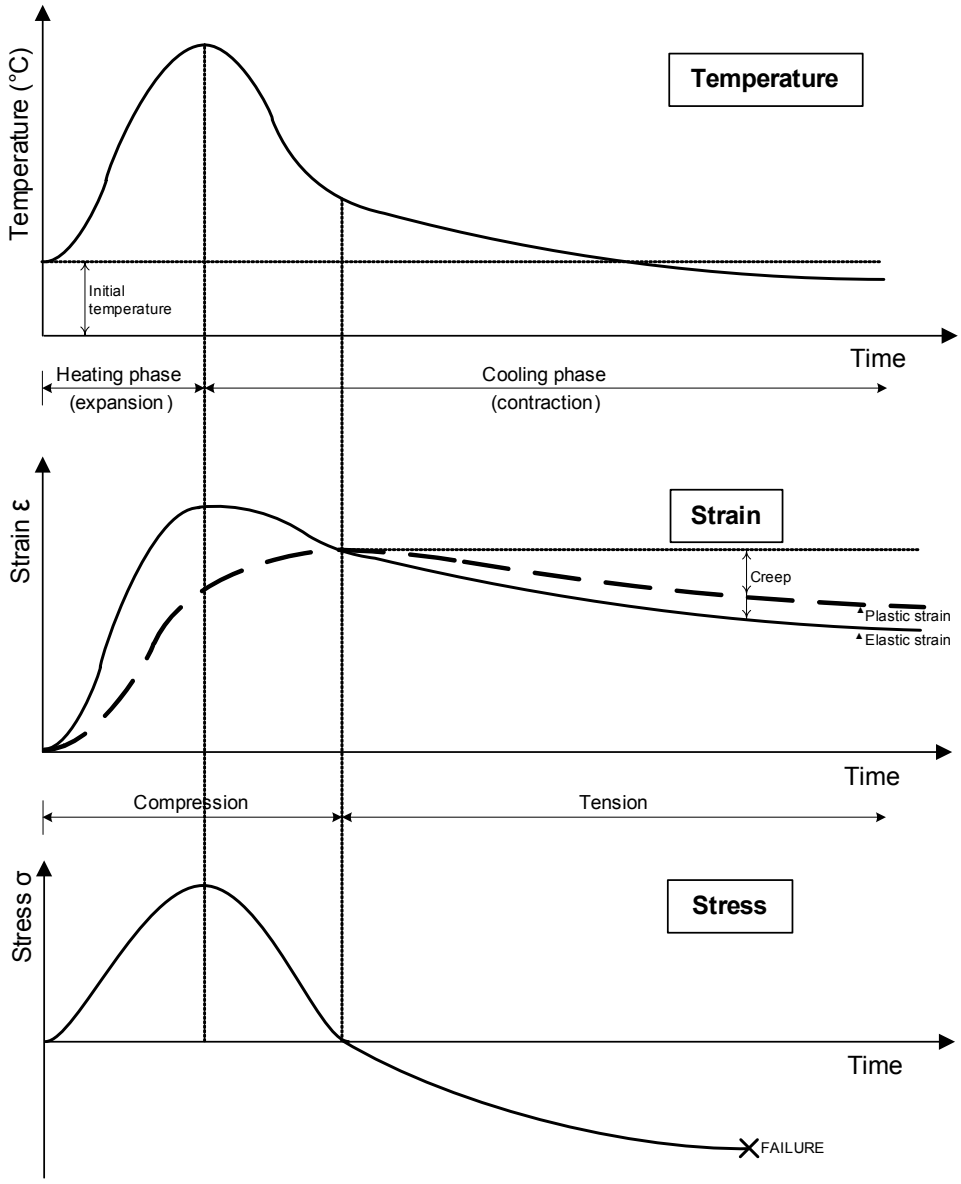

Figure 2.2. Relationship between Stress, Strain and Temperature at an Internal Point in a Concrete Section (Bernander, 1998)

2.4.3 Temperature Gradients and the Formation of Cracks

In the past, research in the area of crack control has been almost entirely focussed on temperature development, particularly the maximum temperature reached in a concrete mixture and the temperature differentials that exist within a section. According to Emborg and Bernander (1994) however, recent advances have shown that temperature is not the only important factor to consider. The degree of restraint to which the member is subjected and the transient mechanical properties of the hardening concrete, also need to be considered. This implies that the cracking sensitivity of a concrete element is a function of two parameters (Springenschmid and Breitenbücher, 1998), namely:

- Factors relating to the concrete mixture constituents such as the mixture composition, specific heat, temperature rise, the elastic modulus, and the coefficient of thermal expansion.
- Boundary conditions with respect to the dimensions of the element, degree of restraint, temperature of the surroundings and transfer of heat between the element and the environment.

In turn, temperature, restraint and the properties of fresh concrete are affected by factors such as the preconditions of both the concrete mixture materials and of the construction site, basic data concerning the concrete itself, the curing condition the concrete is subjected to and the environment in which the section is cast.

Cracks form during both the heating and cooling phases of the hydration process (see figure 2.2). During the heating phase, when the concrete has been poured and hydration has begun, some of the heat generated is retained inside the concrete member, causing a temperature rise in the material (Harrison, 1981). At this point, the rate of heat generation is greater than the rate of heat loss, and under ideal conditions in the absence of any restraint, the concrete would expand. The fact that a section is always at least partially restrained however, and that heat can be dissipated from the surface of the concrete at a much quicker rate than from the interior, implies that there is a non-uniform expansion of the section (Bernander, 1998).

Since the cooler outer areas of the element are not expanding at the same rate as the hotter inner sections, the expansion of the interior and the resistance to thermally induced movement can lead to a build up of tensile stress in the surface zone. This can eventually cause the formation of surface cracks on the concrete. As mentioned, this will only occur if the tensile stress on the surface exceeds the tensile capacity of the concrete at that point in time. Waller et al. (2003) however, note that the high creep capacity exhibited by concrete at early ages can help relieve the compressive stresses present in the centre of the element that induce the tensile stresses at the surface. Emborg and Bernander (1994) also note that the surface cracks are usually not serious and generally close up during the cooling phase of hydration when the member begins to contract. When coupled with the effects of an aggressive environment, ambient temperature variations and shrinkage however, surface cracks can have serious negative effects on the durability of a concrete structure and may even initiate through cracks (Bernander, 1998).

Once the concrete enters the cooling phase (figure 2.2), under ideal conditions where no restraint or temperature differentials exist, the concrete element would contract equally in all directions. However, the issues discussed earlier with regard to the expansion of the element during the heating phase, cause internal restraint and prevent this contraction from occurring freely. The higher rate of heat dissipation of the surface layers compared to the inner core of the concrete leads to the surface setting and hardening before the core has cooled down. The already stiff outer layers restrain the interior of the element as it begins to contract upon cooling. This induces a tensile stress within the material and once the tensile capacity of the concrete is exceeded, cracking can occur within the element. Emborg and Bernander (1994) refer to these internal cracks as *through cracks* and they can cause serious structural damage to a concrete element, as they do not close up.

Bernander (1998) however, notes that the effects of heat of hydration during the early stages are not always deleterious. Provided that cracking does not occur, the tensile stresses developed at the surface during the heating phase can be transformed into compressive stresses, contributing to a reduction in the overall amount of tension experienced in the section.

The progression of hydration with respect to time has a dual effect on the strength development and cracking potential of the concrete. As hydration proceeds, there is an increase in the stiffness and strength (both tensile and compressive) of the concrete. This increased stiffness however, attracts more stress and, although the tensile strength is increasing, the relaxation capacity of the element is decreasing (Ballim, 2001). This implies that, although the risk of cracking is reduced with the improved strength, the tendency for cracking increases since the corresponding increase in both stiffness and the modulus of elasticity reduces the creep capacity of the concrete (Waller et al., 2003).

The problem of a temperature gradient existing in the concrete is not only confined to the cross section of the element, but also along the length of the section. Different points along a section will be subjected to different time-temperature histories as all of the concrete cannot be poured at the same time. The rates of hydration and heat evolution are therefore different along the element at any particular depth (Ballim, 2001). This additional temperature gradient establishes another possible cause for the development of through cracks but is usually not as serious as the temperature differentials created through the cross section.

2.4.4 Practical Measures to Avoid Thermal Cracking

In general, the specifications that are put forward by engineers in an effort to control thermal cracking are largely inadequate because the focus is on reducing the maximum allowable temperature in an element rather than accounting for the cracking potential. According to Emborg and Bernander (1994), the potential for cracking in a section is a function of time and the degree of hydration, and a temperature difference is required to induce cracks rather than an excessively high maximum temperature. The focus therefore needs to be on issues such as reducing the temperature differentials experienced across and within a structure, minimising the degree of restraint that causes the build up of stresses in the concrete, and the use of concrete with mechanical properties that maximise the resistance to cracking.

Regarding concrete mixture design (a factor that is relevant to this research), Ballim (2001) suggests some practical measures that can be considered in an attempt to avoid thermally induced cracking of a concrete section. These include:

- Maximising the proportions of cement replacement materials such as fly ash and blastfurnace slag, which reduce the maximum heat rate experienced and cause it to occur at a later age compare to a plain cement concrete.
- Using materials that reduce the required water content, which in turn reduces the required binder amount needed for a given w/c ratio.
- Designing a concrete mixture with a low early strength development.

2.5 The Effect of Cement Extenders on the Hydration and Heat Evolution Characteristics of Concrete

2.5.1 Background

Often materials such as fly ash, blastfurnace slag or silica fume are added to a concrete mixture as a replacement material for a portion of the cement present. Such replacement materials are commonly referred to as cement extenders. Most of these additional materials react with some of the components of the cement paste yielding desirable characteristics such as improved strength, workability and better durability. This section discusses the effects ground granulated blastfurnace slag (GGBS) and two pozzolanic materials, fly ash (FA) and condensed silica fume (CSF), have on the properties of a concrete mixture. These three extenders have been considered as cement replacement materials in this investigation with respect to their effects on the heat evolution characteristics on concrete. Table 2.3 shows the common oxides found in three cement extenders commercially available in South Africa.

Many of the materials used as cement extenders are pozzolans. A pozzolan is a material which, when combined with free lime in the presence of water, reacts forming cementitious compounds (Addis, 1986). The basis for the use of pozzolans as cement replacement materials is the ability of the alkaline media produced during

hydration to break down the silica or alumina-silica networks that exist in the extender particles and produce CSH gel (Bye, 1999). For this to occur however, the reaction between a pozzolan and water must take place in the presence of an adequate amount of alkaline material. This material is a product of the water-cement reactions, and is needed to break down the silica or alumina-silica networks. As mentioned, two pozzolans were used in this investigation, namely FA and CSF.

GGBS		FA		CSF	
Oxide	**Average content by mass (%)**	**Oxide**	**Average content by mass (%)**	**Oxide**	**Average content by mass (%)**
SiO_2	34 – 40	SiO_2	45 – 50	SiO_2	92
CaO	32 – 37	CaO	4 – 8	CaO	0.6
Al_2O_3	11 – 16	Al_2O_3	25 – 30	Al_2O_3	1.5
MgO	10 – 13	MgO	2 – 4	MgO	0.6
Fe_2O_3	0.3 – 0.6	Fe_2O_3	9 – 11	Fe_2O_3	1.2
MnO	0.7 – 1.2	Na_2O + 0.658 K_2O	1 – 3	K_2O	0.6
K_2O	0.8 – 1.3			H_2O	0.8
S	1.0 – 1.7				
TiO_2	0.7 – 1.4				

Table 2.3. Chemical composition of South African Cement Extenders (Addis, 2001)

Some important points to note regarding the hydration of concrete binders containing pozzolanic materials include (Bye, 1999):

- The reactivity of a pozzolan is highly dependent on the surface area of the material and the proportion and reactivity of the glass content present.
- The large surface area of pozzolans promotes the formation of non-swelling CSH gel, which is precipitated in the presence of free calcium ions when portlandite produced from the PC hydration is consumed by the particular pozzolan present.

2.5.2 Fly Ash

Fly ash (FA) is obtained from the ash produced from coal-burning power stations removed by electrostatic precipitators (Addis, 1986). A major part of the dust carried out from the burning of the coal contains a glassy material that is derived from the clay present in the pulverised coal (Bye, 1999). FA is a fine powder consisting of round, hollow spherical particles that constitute mainly glass and quartz, mullite and calcium oxide. The fineness of the FA plays an important role with respect to the reactivity of the material and the workability of the concrete in which it is used. As a general rule, the finer the fly ash, the greater the pozzolanic activity and the better the workability of the concrete mixture. If however, too fine a FA is used in a concrete mixture that already contains a significant proportion of fines, the concrete could lose workability and become sticky.

Advantages and disadvantages of using FA

Addis (1986) and Langan et al. (2002) note some of the advantages and disadvantages of using FA as a replacement material in the binder:

- A reduction in the cost of materials and a saving on energy, as less cement is used resulting in a reduction in CO_2 emissions
- Better workability and concrete cohesiveness
- A reduction in construction costs as workability is improved
- Reduced water penetration
- Reduced shrinkage
- Reduced heat of hydration
- Reduced cracking tendency
- Slower strength development due to the accompanying pozzolanic activity.

The Influence of FA on Concrete Properties

The most notable effect of adding FA to a concrete mixture is the reduced water demand and great improvement in workability and flow. This is often the main reason for adding FA to a concrete mixture. According to Bye (1999), this is the result of the

absorption of negatively charged particles of silica-alumina glass on the cement grain surfaces. Flow and workability are improved by the mutual repulsion of these negative charges in the paste. The extent of this improvement depends on the fineness and carbon content of the FA and, as mentioned, the finer the material, the greater the effect (Addis, 1986). The carbon content however, has the reverse effect and the more carbon present the more detrimental the effect on the workability of the concrete.

The hydration of FA cements differs from that of Portland cement with respect to the rate of hydration of the different cement phases, the amount of portlandite formed, the composition of the hydration products and the additional compounds formed as a result of the reactions involving the fly ash itself (Ramachandran et al., 2003). Lower amounts of portlandite are formed in the presence of FA because of the pozzolanic nature of FA and the reaction that occurs between the FA present in the binder and the lime produced during the PC hydration reactions (Lilkov et al., 1997). Many FA materials however, are unsuitable for use in concrete because of their low pozzolanic activity (Ramachandran et al., 2003).

According to Lilkov et al. (1997), FA has the effect of generally retarding the early stages of hydration and then accelerating the hydration process during the middle and later stages, particularly the hydration of alite present (Langan et al., 2002). This early retardation is because of the slowing of the calcium hydroxide saturation rate in the liquid phase due to the presence of FA. C_3A and C_4AF also experience the same trend of decelerated hydration in the early stages and accelerated reactions towards the later stages. This has the overall effect of reducing the rate and amount of heat evolved in the concrete during hardening in the presence of FA. According to Addis (1986), the percentage of heat reduction in fly ash cement at twenty-eight days is approximately equal to percentage of FA replacement of PC with respect to the total mass of the binder material.

The composition of the alite and belite hydrates in the paste of a three-day-old FA/PC concrete is very similar to that of a plain PC concrete. The main difference is that the proportions of the hydration products differ (Ramachandran et al., 2003). During the later stages of hydration, the FA reduces the C/S ratio in the CSH gel produced and

increases the A/C ratio. The greater the FA content, the greater these effects become. The condensation of silicate anions with respect to the C_3S present is also more rapid when FA is introduced into the concrete mixture.

The presence of FA reduces the amount of CH in the hydration product because of the dilution effect it has during the consumption of calcium hydroxide in the pozzolanic reactions. Initially however, the formation of solid calcium hydroxide from the hydration of C_3S is greater than the consumption of CH in the pozzolanic reaction, but eventually the amount of CH present in the hardening paste peaks and then begins to decline (Bye, 1999). The replacement of solid CH with CSH gel in the hardened paste also creates the potential to reduce the permeability of the concrete by modifying the distribution of pore sizes. This can have positive effects on the durability of the concrete since the possible ingress of deleterious foreign materials is reduced due to a reduction in permeability.

The presence of fly ash consequently reduces the magnitude of the main exothermic heat rate peak (peak 3, in figure 2.1) and delays the time at which it occurs (Langan et al., 2002). This delay is greater in the presence of FA with a greater calcium content. Bye (1999) states that with a thirty percent cement replacement with fly ash, the principle peak in heat rate is delayed between three and four hours and the presence of FA depresses the maximum value. The rate of hydration however, is also dependent on the fineness of the FA used and generally, as particle size is decreased the exothermic heat rate peaks as seen in figure 2.1 become sharper and occur sooner in the hydration process (Ramachandran et al., 2003).

If FA is to be used with a view to reducing the heat of hydration, Ramachandran et al. (2003) recommend that a high volume (greater than fifty percent binder content) FA cement be used with a low calcium FA because low calcium FA has shown to have the following benefits:

- Low temperature rise
- Adequate early age strength (depending on the w/c ratio)
- Higher later age strengths.

Results from testing have suggested that high volume, low calcium FA cements result in a more homogeneous hydration product with a low $Ca(OH)_2$ content, a lower C/S ratio and a CSH gel that exhibits a stronger structure.

2.5.3 Blastfurnace Slag

Blastfurnace slag is a non-metallic molten by-product formed during of the smelting of iron ore. This liquid generally contains siliceous and alluminosilicate impurities from the iron ore and coke involved. The principle oxides found in slag include lime, silica and alumina and hence it is made up of similar chemical compounds to those found in Portland cement, but in different proportions (Bye, 1999). If cooled slowly, slag crystallises and the material possesses little or no cementing properties. If however, it is cooled rapidly to below 800°C the slag forms a granular, glassy material with the hydraulic properties of a cementitious material. This is the type of slag used as a cement replacement material in concrete. The slag is usually ground down into a fine powder, hence the common industry name ground granulated blastfurnace slag (GGBS).

The Influence of GGBS on Concrete Properties

The addition of GGBS to a concrete mixture can influence certain properties of the concrete such as compressive strength development, heat of hydration characteristics, flexural strength and construction cost. According to Addis (1986), some of the effects of using GGBS as a cement replacement material in a mixture include:

- Lower cost of binder material.
- When comparing concretes with equivalent mixture parameters and w/c ratio, the compressive strength of slag cement is generally lower than that of PC before 28 days. The long-term strength development is also slower. The difference in strength however, tends to disappear by about 90 days of curing.
- GGBS concretes exhibit lower heats of hydration than plain PC concretes. It is for this reason that many mass concrete elements have slag in the cement binder in order to reduce the potential for thermal cracking. The extent to which slag reduces the heat evolved is difficult to predict because the effect of

the slag varies depending on the composition of the GGBS and the ratio of PC to GGBS in the binder. The reduction in heat rate in the GGBS/PC cements is also more pronounced during the first three days of curing than over the first seven days.

- Early flexural strength of GGBS concretes is generally lower than that of equivalent PC concretes during the first three days. The opposite is true however, at seven and twenty eight days of curing. This observation indicates a slower, yet improved flexural strength development in concretes containing GGBS.

Strength development and heat of hydration effects of blastfurnace slag on the properties of concrete depend on the ability of the slag to react in the cement paste system (Coole, 1988). The reactivity of GGBS depends on a number of factors such as the glass content, the bulk composition and the fineness of the powder (Ramachandran et al., 2003). These factors are all affected by the rate of cooling to below 800°C. It must be noted however, that a slag is only noticeably reactive in a concrete mixture if it has been activated. This is usually achieved if and when GGBS is in the presence of calcium sulphate (gypsum) or substances such as NaOH, $Ca(OH)_2$ or water glass. Portland cement itself acts as an effective GGBS activator (Bye, 1999), but this is only once an adequate amount of alkalis and portlandite has been produced from the cement hydration reactions (De Schutter, 1998)

The microstructure and principle hydration products of a slag cement paste are essentially the same as those of a plain cement paste. The major difference lies in the fact that the CaO/SiO_2 ratio in the CSH hydrate of slag cement is somewhat lower. The glass content of GGBS also has a major effect on the strength development of the concrete (Ramachandran et al., 2003) as it influences the reactivity.

The presence of GGBS retards the hydration reactions of the major cement phases during the stages 1 and 2 of the hydration process, except for the reaction between C_3A, $CaSO_4$ and $Ca(OH)_2$. During stage 3, approaching the main exothermic heat rate peak (peak 3, figure 2.1), all of the phases undergo an accelerated hydration. If the surface area of the slag is large enough however, it may result in the accelerated

hydration of alite during the first two stages of hydration (Ramachandran et al., 2003). In addition, the finer the slag the more intense the peaks in the heat rate versus time curve tend to be and the earlier the peaks occur. The rate of GGBS hydration is also dependent on the efficiency of its dispersion in the concrete mixture and generally the reaction rate decreases as slag content increases and the w/c ratio decreases (Bye, 1999).

Coole (1988) showed that in concrete mixtures where the slag replacement level is less than sixty percent, only blastfurnace slag with a low glass content are effective in lowering the maximum temperature reached in the concrete. Coole (1988) also showed that, in general, the addition of blastfurnace slag is an effective means of reducing the rate of heat evolution, even if the maximum temperature is not reduced. This fact may help reduce the tensile stresses and strains experienced in a structure and lessen the potential for cracking.

According to Ramachandran et al. (2003), the heat rate peaks in figure 2.1 are generally more symmetrical in plain PC concretes than in those containing GGBS. Peak 3, which is mainly associated with the hydration of alite, tends to appear at a later age in slag cements. This indicates that the presence of GGBS retards the hydration of the major cement phases. It must be remembered that the total heat liberated and the corresponding heat rate of a slag cement depends on the quality and amount of blastfurnace slag used.

De Schutter (1998) showed that the hydration of a cement binder containing blastfurnace slag could be split up into two different reactions, the P- and S-reactions. The principle of superposition can be applied to find the overall heat rate from the contributions of the two separate reactions. This concept is shown in figure 2.3.

Essentially, the P-reaction is the contribution of the Portland cement present to the heat of hydration and similarly the S-reaction is the contribution of the slag. The rate of heat of hydration is therefore equal to the sum of the contributions from the P- and S-reactions. From figure 2.3, it can be seen that the S-reaction does not begin

immediately once water is added to the concrete mixture. This is because the hydration of blastfurnace slag only begins once the material has been activated, as discussed earlier.

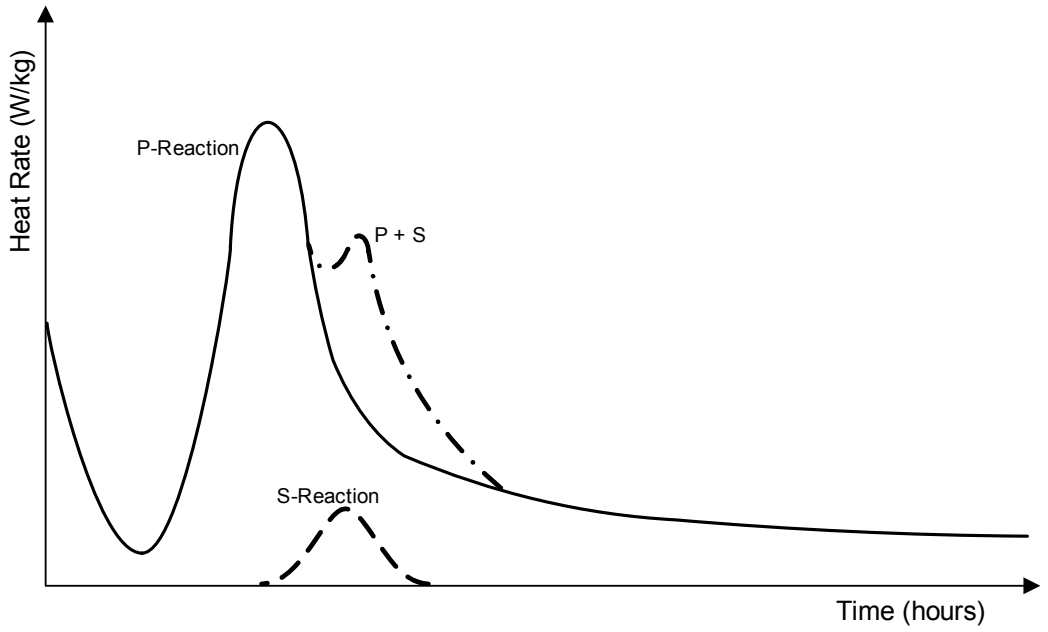

Figure 2.3. Superposition of the P- and S-Reactions in a PC/GGBS binder (De Schutter, 1998)

De Schutter (1998) was able to standardise curves for both the P- and S-reactions and develop a hydration model for concrete made with a blastfurnace slag binder. The P-reaction curves are typical of those seen for Portland cement binders. The S-reaction curves are more symmetrical and indicate that the S-reaction ends more rapidly than the P-reaction. This can be seen in figure 2.3.

Ramachandran et al., (2003) and Bye (1999) also noted some other important points regarding the effect of slag on cement hydration:

- The presence of GGBS leads to a decrease in the portlandite content of the paste. This is because of the dilution effect due to the consumption of lime by the slag during hydration.

- GGBS concretes tend to produce significantly greater amounts of ettringite than PC only concretes.
- The hydration products of the GGBS and PC present form separately at the respective grain surfaces and extend inwards with time.
- GGBS does not react with or absorb water rapidly, which can have a positive effect on the workability of a concrete mixture. The slower early reaction rate of the slag causes a slower decline in the loss of slump/workability and a slower heat build up compared to an equivalent plain PC concrete. The hydration of slag can be accelerated however if curing temperatures exceed approximately 40°C. Such temperatures are likely to occur in mass concrete elements.

2.5.4 Silica Fume

Silica Fume is a by-product from the manufacture of silicon or ferrosilicon alloys by the reduction of silica with carbon in an electric furnace. The gases produced are condensed into an extremely fine powder with a high silica content, hence the term condensed silica fume or CSF. It is a highly active pozzolan and this high reactivity is due to the fineness, high silica content and amorphous nature of the silica (Addis, 1986). Coatings of carbon on the surface of the silica particles however, can greatly reduce the pozzolanic activity of silica fume.

The Influence of CSF on Concrete Properties

When w/c ratio and binder content are kept constant, the most notable effect of CSF on concrete is the dramatic increase in compressive strength over the first 28 days of curing (Lagan et al., 2002). This of course depends on the amount and nature of silica fume present. The increase in strength is also accompanied by a decrease in the permeability of the concrete, aiding in improving the durability characteristics (Addis, 1986).

Silica fume has significant effects on the rate of hydration of concrete. Many investigators however, have reported that the hydration rates in silica fume cements are highly variable because many CSF powders differ in their physical and chemical nature (Ramachandran et al., 2003). Almost all of the stages of hydration, with respect to the hydration of pure cement phases, are accelerated by the addition of silica fume. Bye (1999) has reported that, although the early rate of heat liberation is increased in a CSF concrete mixture because of the high reactivity of silica, the replacement of a portion of PC with CSF progressively reduces the total heat generated.

A small amount of CSF speeds up the hydration of alite and causes the maximum exothermic peak (peak 3, figure 2.1) to occur earlier and as the amount of SiO_2 present in the CSF increases, the peak occurs at an earlier age (Langan et al., 2002). This effect can be attributed to the fineness of the CSF being so much greater than that of the PC in the binder as the increased surface area provides sites for preferential nucleation of hydration products (Ramachandran et al., 2003). The pozzolanic silica particles also offer a surface at which the CSH hydration product can be precipitated. This allows for the removal of free calcium and silicate ions, resulting in a thinner layer of CSH gel (Langan et al., 2002), reducing the impermeability of this layer and allowing the hydration process to be accelerated. The maximum heat rate experienced also increases as the fineness of the CSF increases but conversely it decreases as the specific area of the SiO_2 increases.

Other important points to note regarding the effect of CSF on concrete include (Ramachandran et al., 2003):

- The total heat of reaction per unit mass of binder is greater in concretes containing silica fume.
- At all stages during hydration, the $Ca(OH)_2$ content of the concrete is lower in the CSF concretes compared to PC only concretes. This is due to the pozzolanic nature of silica fume.
- In the presence of CSF, the heat rate curves indicate that there is no secondary ettringite or monosulphate produced during hydration.

2.6 Methods of Determining the Heat of Hydration

A number of different test methods have been developed for measuring temperature rise in concrete. The ideal test however, should be capable of predicting an accurate time-temperature profile of the concrete during casting. Morabito (1998) divides the test methods into three broad categories:

1. Isothermal methods, which are usually applied to pure cement pastes.
2. Adiabatic methods, which make use of a calorimeter.
3. Semi-adiabatic methods, where there is a limited heat exchange between the sample and environment.

As mentioned, isothermal methods are used with pure cement pastes. The tests measure the amount of heat generated by the hydrating paste, which is maintained at a constant temperature. These methods do not account for the change in cement reactivity that occurs during hydration with an ever-changing temperature. Coupled with the fact that the test is conducted using a paste only and not concrete, this makes it difficult to predict the temperature profile that an actual structure will experience.

Adiabatic calorimetry allows for the temperature rise in a concrete sample to be recorded with no exchange of heat between the sample and its environment (Morabito, 1998). This is usually achieved by controlling the outside temperature relative to the sample. Measuring temperature in this way allows for the determination of the amount of heat produced due to hydration and the rate of heat evolution, without any external interference (Gibbon, 1995). Although true adiabatic conditions are very difficult to achieve, the results obtained from an adiabatic calorimeter are the most accurate for predicting the temperature distribution in an actual concrete structure (Graham, 2003). This is particularly true in mass concrete sections where the material at the centre of the element experiences near adiabatic conditions due to the inability of the core of the element to dissipate heat. Semi-adiabatic tests also produce reliable results with the difference being that heat exchange with the surroundings is limited rather than prevented.

Another test method is that of conduction calorimetry where the heat-flow of a hydrating cement paste is determined. The data recorded can be used to calculate the rate of heat evolution at various stages during the hydration process (Gibbon et al., 1997). Unfortunately, samples tested by this method are never able to attain the same temperatures experienced in an actual concrete structure (Graham, 2003).

From the above discussion, it is evident that adiabatic calorimetry is the most appropriate test method for the laboratory work conducted for this research. The School of Civil and Environmental Engineering at the University of the Witwatersrand has two such calorimeters, both of which were used to test the various concrete samples discussed in Chapter 4. A detailed description of the adiabatic calorimeters used can be found in Chapter 3.

2.7 Summary and Conclusions

Portland cement is a highly complex material made up of an array of compounds that are generally all involved in cementing reactions to some degree. The range of reactions that take place between water and the cement phases cannot be predicted exactly with respect to the products formed, the time over which the reactions occur, and the heat that is liberated during hydration. The mechanisms of hydration and the heat produced as a consequence of the process, are greatly affected by the chemical properties and composition of the binder material used in the concrete. Factors such as particle fineness, w/c ratio and the quantity and type of cement extender present all affect the amount of heat evolved. All of this in turn affects the ability of a concrete element to resist thermally induced stresses and strains due to excess rises in temperature and the presence of temperature gradients within and across a section. This can either help prevent or exacerbate the problem of thermal cracking. Adiabatic calorimetry provides the most accurate, realistic and effective way of determining the temperature profile of a mass concrete element.

2.8 Chapter References

Addis, B. (2001) Cementitious Materials. In: Addis, B. and Owens, G. (ed.), *Fulton's Concrete Technology, 8th Ed.*, Cement and Concrete Institute (CNCI), Midrand, South Africa, pp. 1-15.

Addis, B.J. (ed) (1986) Temperature effects and thermal properties of concrete. In: *Fulton's concrete technology 6th Ed.*, Portland Cement Institute, Midrand, South Africa, pp. 515-575.

Ballim, Y. (2001) Thermal properties of concrete and temperature development at early ages in large concrete elements. In: Addis, B. and Owens, G. (ed.), *Fulton's Concrete Technology, 8th Ed.*, Cement and Concrete Institute (CNCI), Midrand, South Africa, pp. 227-247.

Barret, P. and Bertrandie, D. (1986) Fundamental hydration kinetic features of major cement constituents: Tricalcium silicate (Ca_3SiO_5) and β-dicalcium silicate (β-Ca_2SiO_4), *J. Chim. Phys. Phys.-Chim.Biol*, vol. 83, no. 11-12, pp. 765-775.

Bernander, S. (1998) Practical measures to avoiding early age thermal cracking in concrete structures. In: Springedschmid, R. (ed.) *Prevention of thermal cracking in concrete at early ages*, RILEM Report 15, E&FN Spon, London, UK, pp. 255-314.

Blezard, R.G. (1998) The history of calcareous cements. In: Hewlett, P.C. (ed.), *Lea's chemistry of cement and concrete*, Arnold, London, UK, pp. 1-24.

Bogue, R.H. (1947) *The chemistry of Portland cement*, Reinhold Publishing, New York, USA.

Branco, F.A., Mendes, P.A. and Mirambell, E. (1992) Heat of hydration effects in concrete structures, *ACI Materials Journal*, vol. 89, no. 2, American Concrete Institute (ACI), Detroit, USA, pp. 139-145.

Bye, G.C. (1999) *Portland cement: Composition, production and properties*, 2nd ed. Thomas Telford, London, UK.

Coole, M.J. (1988) Heat release characteristics of concrete containing ground granulated blast furnace slag in simulated large pours, *Magazine of Concrete Research*, vol. 40, no. 144, Thomas Telford, London, UK, pp. 152-158.

Copeland, L.E. and Kanto, D.L. (1972) Chemistry of hydration of Portland cement at ordinary temperatures. In: Taylor, H.F.W. (ed.) *The chemistry of cements volume 1*, Academic Press, New York, USA, pp. 313-370.

Czernin, W. (1980) *Cement chemistry for civil engineers, 2nd English Ed.*, George Godwin Ltd., London, UK.

De Schutter, G. (1998) Hydration and temperature development of concrete made with blast-furnace slag cement, *Cement and Concrete Research*, vol. 29 (1999), Pergamon Publishing, pp. 143-149. Retrieved April 2004, from http://www.sciencedirect.com.

Emborg, M. and Bernander, S. (1994) Assessment of risk of thermal cracking in hardening concrete, *Journal of Structural Engineering,* vol. 120, no. 10, American Society of Civil Engineering (ASCE), New York, USA, pp. 2893-2912.

Gibbon, G.J. (1995) *Laboratory test procedures to predict the thermal behaviour of concrete*, PhD Thesis, University of the Witwatersrand, Johannesburg, South Africa.

Gibbon, G.J., Ballim, Y. and Grieve, G.R.H. (1997) A low-cost computer-controlled adiabatic calorimeter for determining the heat of hydration of concrete, *Journal of Testing and Evaluation (JTEVA),* vol. 25, no. 2, American Society for Testing Materials (ASTM), West Conshohocken, USA, pp. 261-266.

Graham, P.C. (2003) *The heat evolution characteristics of South African cements and the implications for mass concrete structures*. Ph.D. Thesis, University of the Witwatersrand, Johannesburg, South Africa.

Harrison, T.A. (1981) *Early-age thermal crack control in concrete*, CIRIA Report 91, Construction Industry Research and Information Association (CIRIA), London, UK.

Langan, B.W., Weng, K. and Ward, M.A. (2002) Effect of silica fume and fly ash on heat of hydration of Portland cement, *Cement and Concrete Research*, vol. 32, Elsevier Science Ltd., pp. 1045-1051. Retrieved March 2004, from http://www.sciencedirect.com.

Lilkov, V., Dimitrova, E. and Petrovo, E. (1997) Hydration process of cement containing fly ash and silica fume: the first 24 hours, *Cement and Concrete Research*, vol. 27, no. 4, Elsevier Science Ltd., pp. 577-588. Retrieved March 2004, from http://www.sciencedirect.com.

Massazza, F. and Daimon, M. (1992) Chemistry of hydration of cements and cementitious materials. In: *Proceedings of the 9th International Congress on the Chemistry of Cement (ICCC)*, New Delhi, India, pp. 383-429.

Morabito, P. (1998) Methods to determine the heat of hydration of concrete. In: Springedschmid, R. (ed.) *Prevention of thermal cracking in concrete at early ages*, RILEM Report 15, E&FN Spon, London, UK, pp. 1-25.

Odler, I. (1998) Hydration, setting and hardening of Portland cement. In: Hewlett, P.C. (ed.), *Lea's chemistry of cement and concrete*, Arnold, London, UK, pp. 241-297.

Ramachandran, V.S., Paroli, R.M., Beaudoin, J.J. and Delgado, A.H. (2003) Supplementary cementing materials and other additions. In: *Handbook of thermal analysis of construction materials*, Noyes Publications/William Andrew Publishing, Norwich, USA, pp. 293-319.

Springedschmid, R. (ed.) (1998) *Prevention of thermal cracking in concrete at early ages*, RILEM Report 15, E&FN Spon, London, UK.

Springenschmid, R. and Breitenbücher, R. (1998) Influence of constituents, mixture proportions and temperature on cracking sensitivity of concrete. In: Springedschmid, R. (ed.) *Prevention of thermal cracking in concrete at early ages*, RILEM Report 15, E&FN Spon, London, UK, pp. 40-50.

van Breugel, K. (1998) Prediction of temperature development in hardening concrete. In: Springedschmid, R. (ed.) *Prevention of thermal cracking in concrete at early ages*, RILEM Report 15, E&FN Spon, London, UK, pp. 51-75.

Waller, V., d'Aloïa, L. Cussigh, F. and Lecrux, S. (2004) Using the maturity method in concrete crack control at early ages, *Cement and Concrete Composites*, vol. 26, issue 5, Elsevier Science Ltd., 9pp. 589-599. Article still in press at the time of retrieval. Retrieved November 2003, from http://www.sciencedirect.com.

Chapter 3

TEST METHODS AND MATERIALS

3.1 Introduction

With any set of laboratory tests conducted using a particular material, the results obtained will show a general trend of what is occurring during testing. Where the aim is to assess the effects of the characteristics of that material on the results however, the actual figures produced are specific to that particular material and its chemical, physical and mechanical properties. If the same experiments are carried out with an almost identical material, there is likely to be a difference between the two sets of results obtained. By the same token, it is also important that a standard set of tests is used and tests and their methodology are reproducible if the test results are to have any accuracy and validity.

Graham (2003) showed that the chemical composition of cement affects the heat evolution characteristics of the concrete, with all other ingredients in the concrete mixture remaining constant. It is therefore vital that the cement used for a batch of tests (particular where heat evolution of concrete is concerned) is characterised to allow for the possibility that differences between similar tests can be attributed to the characteristics of the cement used. This is of course provided that an established trend exists between the test results and all other variables in the concrete mixture are relatively constant. Similarly, there is a need to characterise any other materials that might be present in the concrete mixture.

This chapter covers the following two sections. Firstly, a description of the various tests used in characterising the concrete materials and a detailed description of the adiabatic calorimeter used for testing the concrete samples. Secondly, the chemical composition and properties of the various materials used in the test concretes as well as the physical characteristics and attributes of the clinker crystal phases are discussed.

3.2 Sample Collection

The cement used in this research, and the clinkers from which it was produced were obtained from the Roodepoort mill of Holcim South Africa, west of Johannesburg. The Holcim cement was produced from clinkers obtained at two different sources: one sourced at Ulco and the other sourced at Dudfield. For consistency of the characterisation, it was necessary to ensure that the cement and clinkers collected were from the same production batch. This was accomplished by removing a sample of clinker from the production line before it entered the mill for grinding and then extracting a sample of cement from the mill, approximately ten minutes later, after grinding and blending of the two different clinkers with gypsum, had been completed.

Approximately 25 kg of each of the Ulco and Dudfield clinkers was extracted from the mill and of this amount, about 500 g from each batch was set aside for the preparation of specimens for the microscopy investigation. A pocket of cement (approximately 50 kg) was drawn from the plant for testing purposes in the adiabatic calorimeter. Approximately 300 g to 500 g of the cement and clinkers were sent for XRF analysis and the rest of the cement was kept for sample testing in the adiabatic calorimeter. The clinkers and XRF analysis samples were sealed in durable plastic bags and the cement was doubled sealed in two plastic bags and placed in an airtight bin in order to minimise the possibility of exposure to moisture.

The extenders used (fly ash, blastfurnace slag and silica fume) were available in the concrete materials laboratory at the School of Civil and Environmental Engineering at the University. Samples of these were also sent for XRF analysis at Holcim

laboratory in Roodepoort. Three different 13.2 mm coarse aggregates, granite, dolomite and andesite, and corresponding sands were used for investigating the effects of aggregate type on the heat evolution characteristics of concrete. These aggregates were again supplied by Holcim.

3.3 Test Methods for Material Analysis

3.3.1 Chemical Analysis

XRF Analysis

The Holcim cement laboratory in Roodepoort conducted X-ray fluorescence spectroscopy (XRF) in order to determine the contents of the chemical elements in each of the Dudfield and Ulco clinkers, the cement and the three extenders used in this investigation.

XRF is a method of determining the chemical elements found in a material, both qualitatively and quantitatively, by exposing the material to X-rays (Lawrence, 1998). The primary beam from the X-ray tube irradiates the sample, exciting each of the chemical elements present. Each element then in turn emits a secondary spectral line, with a wavelength characteristic of that particular element, with an intensity related to the concentration of the element in the clinker. Potential negative effects associated with particle size and mineralogy of the clinker are prevented by mixing the sample with lithium tetraborate and lanthanum oxide before exposure to the X-rays. Intensities of each wavelength of secondary spectral lines are measured and the chemical composition is then determined using previously established calibrations.

Bogue Calculation

The elements found in the clinker and the cement samples from the XRF analysis can be used to estimate the proportions of the four major crystallographic phases (C_3S, C_2S, C_3A and C_4AF) found in cement. Other minor components generally only make up less than two percent of the cement and it is therefore reasonable to neglect them

in the calculations (Lawrence, 1998). The theoretical phase content is found using equations based on the chemical phase diagrams for the C-S-A-F system found in clinker and the American Standard ASTM C150 is the general standard adopted worldwide for this purpose. These equations are based on the Bogue calculation (Bogue, 1947) and the formulae are as follows (Lawrence, 1998):

1. $\%C_4AF = 3.043(\%Fe_2O_3)$ (3.1)
2. $\%C_3A = 2.650(\%Al_2O_3) - 1.692(\%Fe_2O_3)$ (3.2)
3. $\%\beta C_2S = 2.867(\%SiO_2) - 0.7544(\%C_3S)$ (3.3)
4. $\%C_3S = 4.071(\%CaO) - 7.600(\%SiO_2) - 6.718(\%Al_2O_3) - 1.430(\%Fe_2O_3) - 2.852(\%SO_3)$ (3.4)

The main assumption made with the Bogue calculation is that chemical equilibrium is established at the clinkering temperature and is maintained throughout the critical phase of the cooling period (Lawrence, 1998). This introduces errors in the results obtained from equations 3.1 to 3.4. These discrepancies are further exaggerated by the formation of minor compounds that are produced during clinkering but are ignored in the analysis because of their small quantities. The formation of solid solutions with both minor and major elements in the clinker also adds to the error in the estimated phase components.

It is therefore generally accepted that the Bogue calculation provides somewhat inaccurate estimates of the major PC phases, especially with respect to the C_3S and C_3A amounts. This is because chemical equilibrium cannot be maintained during cooling. According to Lawrence (1998), when comparing the calculated Bogue values to those obtained using an X-ray analysis, it can be seen that the Bogue calculation underestimates the alite content and overestimates the alluminate content. This might prove to be a serious problem where accuracy is important. For the purposes of this investigation however, where the main concern is the characterisation of the materials used, equations 3.1 to 3.4 are considered to be sufficient.

If more accurate quantitative values are required, there are a variety of modifications to the Bogue calculation available. The most widely accepted of these modifications

is that proposed by Taylor (1997). Taylor uses more realistic phase compositions derived from micro analytical data that give more representative results of the major phases (Lawrence, 1998 and Taylor, 1997).

Lime Saturation Factor

The lime saturation factor (LSF) is a measure of the amount of calcium oxide available in the clinker or cement for the formation of C_3S. It is calculated using the following equation:

$$LSF = \frac{\%CaO}{2.8(\%SiO_2) + 1.1(\%Al_2O_3) + 0.7(\%Fe_2O_3)} \tag{3.5}$$

A LSF of 100 would indicate that the clinker contains only C_3S and a solid solution or matrix of C_4AF, i.e. the belite and alluminate phases will not be present. According to the PCA (1994) the LSF should lie somewhere between 88 and 94 for reasonable burnability of the clinker in the kiln. A low LSF would suggest a low alite content, which will negatively affect early age strength development in concrete. A higher LSF will make clinkering of the cement raw materials very difficult.

3.3.2 Clinker Morphology

Examination of the Clinkers

Clinker morphology was examined with the aid of an optical microscope in the materials laboratory at the School of Civil and Environmental Engineering at the University of the Witwatersrand. Clinker samples were mounted on an epoxy resin to be viewed under the reflected light of the microscope. For this purpose, a universal polarising microscope, capable of reflecting and transmitting light, was used.

The microscope used is trinocular, allowing for binocular viewing and a monocular tube that allows for the attachment of a camera or projector. The eyepiece has a magnification of 10X and is connected to a rotating nosepiece with four objective lenses, namely 4X, 10X, 20X and 40X. This in turn allows the magnification of the

images to 40X, 100X, 200X and 400X with the combinations allowed for by the different lenses.

A Polaroid digital camera is mounted to the monocular tube in order to photograph the images viewed through the microscope. The camera has a variety of resolution options with a maximum capability of 1600x1200 pixels. The software provided with the camera (Micrografx 6.0©) makes it possible to view and enhance each image and to set a scale to each photograph taken.

A freeware image analysis programme, *ImageJ*, was used to conduct a limited analysis of the photographs taken of the clinker specimens. The programme allowed for alite and belite crystal sizes to be estimated and for an approximation of the matrix area around the alite and belite crystals to be obtained. ImageJ can be downloaded at the following internet address: http://rsb.info.nih.gov//nih-image/. The applications available on this programme are rather limited however.

Microscopic Characteristics of the Clinker Phases

When viewing crushed clinker under a microscope it must be remembered that an attempt is being made to analyse the three-dimensional skeletal structure of the crystals by examining a two-dimensional image of a section through the clinker. According to Campbell (1999), the interference of colours under a microscope depends mainly on the natural colour of the phase, the thickness of the phase, the crystallographic orientation of the crystal with respect to the light from the microscope, and the difference between the indices of refraction of the different light rays.

In general, a cross section through a typical clinker will have the following characteristics (Campbell, 1999):

- A loosely bound network of C_3S crystals
- Single C_2S crystals between the C_3S framework with some clusters or nests

- A matrix of C_3A and C_4AF formed in the liquid phase, surrounding the alite and belite crystals.

Alite (C_3S). Alite is the most abundant of the phases found in clinker and forms a discontinuous three-dimensional loose framework of linked crystals stacked on top of one another. The other phases are present in the voids contained within this structure (Campbell, 1999). The crystals are usually six-sided in cross-section and are typically formed as a combination of two rhombohedra or pyramids along one face. The crystal surfaces are generally free of any striations etc. apart from noticeable cracks and planes. Average crystal sizes range from 25 μm to 65 μm. The crystals may sometimes contain inclusions of rounded belite particles and matrix material formed during early cooling, and may have a belite coating. It is also common for alite crystals to cluster together into large areas or zones. This is known as crystal zonation.

According to Campbell (1999), there are two modes of C_3S growth, stable and unstable. Stable growth exhibits very few inclusions of foreign materials in the alite crystals and a general trend towards crystal faceting during formation. Unstable growth is evident if there are large amounts of entrapped material in the alite, such as belite and free lime, and by irregular crystal shapes. Campbell (1999) suggests that the presence of secondary belite and its growth from the alite into the surrounding matrix is indicative of the formation of an impenetrable barrier formed during early crystallisation of C_4AF.

Belite (C_2S). Belite crystals are generally well rounded with many markings/scratches branching out in all directions. This is known as a laminar structure. There are three varieties of belite found in clinker, αC_2S, βC_2S and γC_2S, all of which form at progressively lower temperatures during the cooling phase of the clinker. The most abundant of the three types is the βC_2S and usually has a yellow, spotted surface with no striations.

Tricalcium Alluminate (C_3A). Also sometimes referred to as celite, tricalcium alluminate usually appears as small, uniform crystals in the matrix surrounding the C_3S and C_2S. The crystals generally show no outward form, or at most a slight rectangular shape. The finer the C_3A matrix, the more rapidly the clinker has been cooled and generally, cements made from rapidly cooled clinkers tended to have better compressive strengths and slower setting time than those allowed to cool gradually (Campbell, 1999).

Ferrite (C_4AF). Ferrite crystals in the matrix tend to form part of an orthorhombic solid solution. They can be dendritic, prismatic or fibrous/blade-like, depending on the rate of cooling of the clinker. Slowly cooled crystals have a blade-like form, moderately cooled crystals tend to be more prismatic, whilst rapidly cooled crystals are usually dendritic (Campbell, 1999).

3.3.3 Sample Preparation for Microscopy Investigation

Approximately 300 g of each of the Dudfield and Ulco clinkers were crushed using a steel pestle in order to prepare samples for microscopy. The crushed material was then sieved and the clinker passing the 2.36 mm sieve and retained on the 1.18 mm sieve was kept for encapsulating and mounting the samples.

Encapsulation and mounting

Two 30 mm diameter moulds were prepared for each of the clinkers, giving a total of four specimens. The following methodology was used for casting samples into the detachable plastic moulds:

- The inside of each mould was smeared with petroleum jelly (Vaseline) to allow the easy removal of each specimen after setting.
- A depth of about 5 mm of clinker was placed into each mould.
- The rest of the mould was filled with a low viscous epoxy resin mixture. The clinker and the resin were mixed to ensure proper coating of the clinker grains and to remove as many voids as possible.

- The samples were then placed in a desicator (vacuum chamber) and the vacuum pressure was set to 75 kPa. This was done to remove any additional trapped air voids in the moulds.
- The specimens were placed overnight in an oven and the temperature was set at 50°C to allow the resin-clinker mixture to set and harden.

Note: the aim of the process is to try to ensure that the epoxy resin completely coats the clinker and fills up any voids between clinker grains. This procedure however, is not always successful and it is sometimes necessary to discard samples.

Grinding and Polishing

Grinding and polishing of the clinker specimens was done once the samples were removed from the oven and the moulds were taken off. The following procedure was adopted:

- Initially the samples were ground against a rotating disc sander with a paper grade of 600. This was to establish a visibly flat surface and to remove all pits from the clinker surface.
- The specimens were then placed on a flat glass surface and sanded by hand with grade 600 sandpaper. The flatness of the sample surfaces was periodically checked by eye using a steel straight edge.
- The samples were cleaned using isopropyl alcohol in an ultrasonic bath before being checked under a binocular microscope for surface scratches. If any scratches were found, the specimens were sanded again with the grade 600 paper on the glass surface.
- The four samples were simultaneously polished using a Struer's Rotopol 31 Lapping Machine with a Struer's Rotoforce 4 mounting arm. The samples were polished with three different grades (6.0 μm, 3.0 μm and 0.25 μm) of diamond particle (DP) suspensions and a corresponding DP pan cloth discs. The following method was applied for each of the three grades of DP:
    - The disc was cleaned with alcohol to remove any impurities that might scratch the samples and interfere with polishing.
    - The DP pan cloth disc was placed in the lapping machine.

- The DP suspension was sprayed over the pan cloth and smeared over the cloth with the face of the specimens to be polished.
- The samples were mounted in the arm and a downward force and time were set for polishing. For the 6 μm DP suspension and cloth, a force of 15 N was applied for ten minutes; for the 3 μm DP suspension and cloth a force of 10 N was applied for ten minutes; and for the 0.25 μm DP suspension and cloth a force of 5 N was applied for five minutes.
- After each set of polishing, the specimens were removed from the arm and washed in isopropyl alcohol in the ultrasonic bath. The polished surfaces were then viewed under the microscope for any scratches and the polishing was repeated if any were found.

Etching

Etching was done to samples in order to distinguish between the different crystallographic phases found in the clinker. The etching process adopted was based on the work done by Graham (2003). A nitol etch was superimposed over a potassium hydroxide (KOH) etch which allows for all four of the major clinker phases (C_3S, C_2S, C_3A and C_4AF) to be recognised under a microscope. This combination of etching gives C_3S a green to blue colour, C_2S a brown to blue colour, C_3A a light brown colour in the matrix, and C_4AF a white colour, also in the matrix.

The following methodology was adopted:

- Four petrie dishes were set out for the four different solutions to be used.
  - One dish with a 10% solution of KOH and ethyl alcohol.
  - A second dish with ethyl alcohol only.
  - A third dish with 1.5 ml HNO_3 and 100 ml isopropyl alcohol. This solution constitutes nitol.
  - A fourth dish with isopropyl alcohol only.
- The polished face of the specimen was dipped in the KOH solution for a period of twenty seconds.

- The sample was then rinsed in the ethyl alcohol and patted dry with paper towels to stop the reaction between the clinker specimen and the KOH from continuing.
- The specimen was dipped in the nitol solution for a period of twelve seconds.
- It was then rinsed in the isopropyl alcohol and dried off.

This process produced results that were adequate for viewing the clinker specimens and identifying the different phases under a microscope.

3.3.4 Determination of Density and the Blaine Test

The Blaine test conducted on the Holcim cement was done according to SABS Method 748 in order to determine the fineness of the cement. This gives an indication of the reactivity of the material. SABS Method 747 was used to determine the density of the cement used in this investigation. Both of these test methods have since been replaced by SANS 50192-6, but the principles remain the same. The tests were conducted in the materials laboratory at the School of Civil and Environmental Engineering and the University of the Witwatersrand.

3.4 Adiabatic Calorimeter

3.4.1 General Description

Gibbon (1995) originally developed the adiabatic calorimeter used to conduct the laboratory tests included in this investigation. It consists of the following basic items, which can be seen in figures 3.1 and 3.2:

- A chamber in which the concrete sample is placed and surrounded by a pocket of air.
- A 120 *l* water tank in which the sample chamber is placed.
- Temperature probes for measuring the temperatures in the concrete sample and the water tank.
- A heating element in the tank, used to maintain adiabatic conditions.

- A personal computer with an analogue to digital (A/D) converter for interpreting the temperature measurements sent from the probes via a signal-conditioning unit.
- A set of interface circuits and relays that allow the personal computer to switch the heating element in the tank on and off while maintaining the adiabatic environment.
- An uninterrupted power supply (UPS) in order to allow testing to continue for a limited period of time in the event of an unexpected power failure.

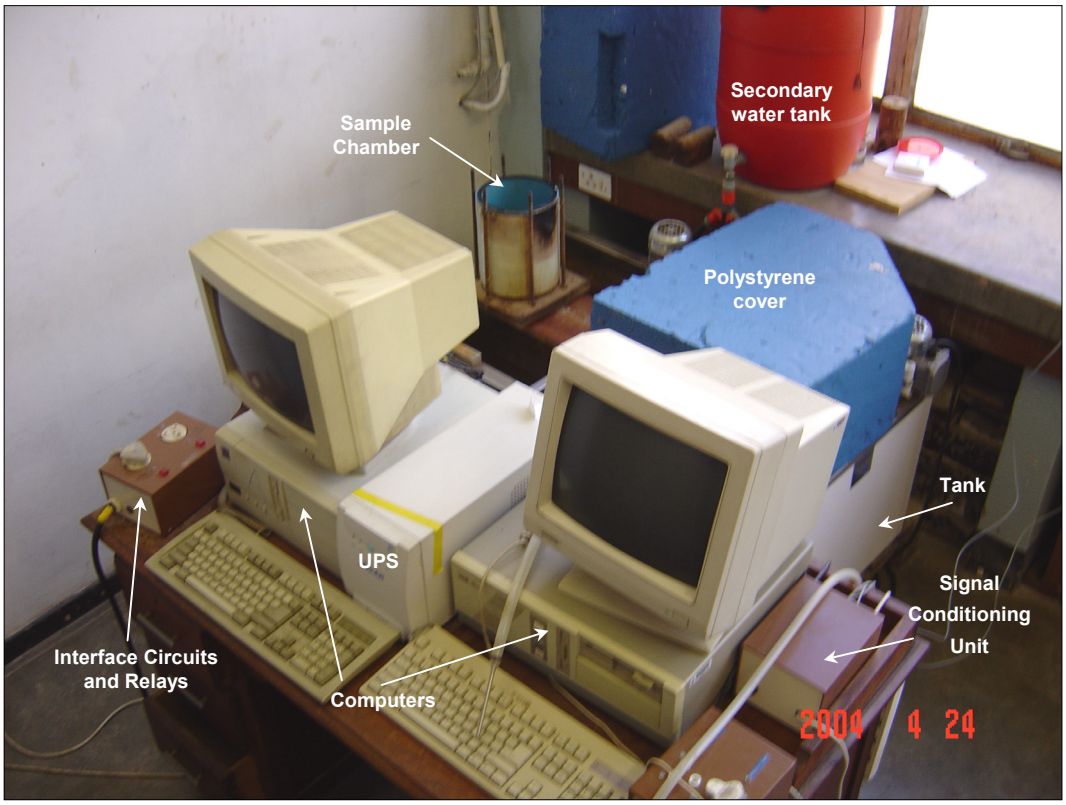

Figure 3.1. Layout of the Adiabatic Calorimeters in the Laboratory

The concrete sample under consideration is cast in a 1 *l* plastic jar with a thermal probe embedded roughly in the centre of the sample in order to take temperature measurements. The sample is placed inside a sealed chamber wherein it is surrounded by a pocket of air and is insulated from the outside environment. This chamber is then placed in the water tank, with the water level set at roughly forty to fifty millimetres

above the top surface of the chamber. A second probe in the tank monitors the water temperature.

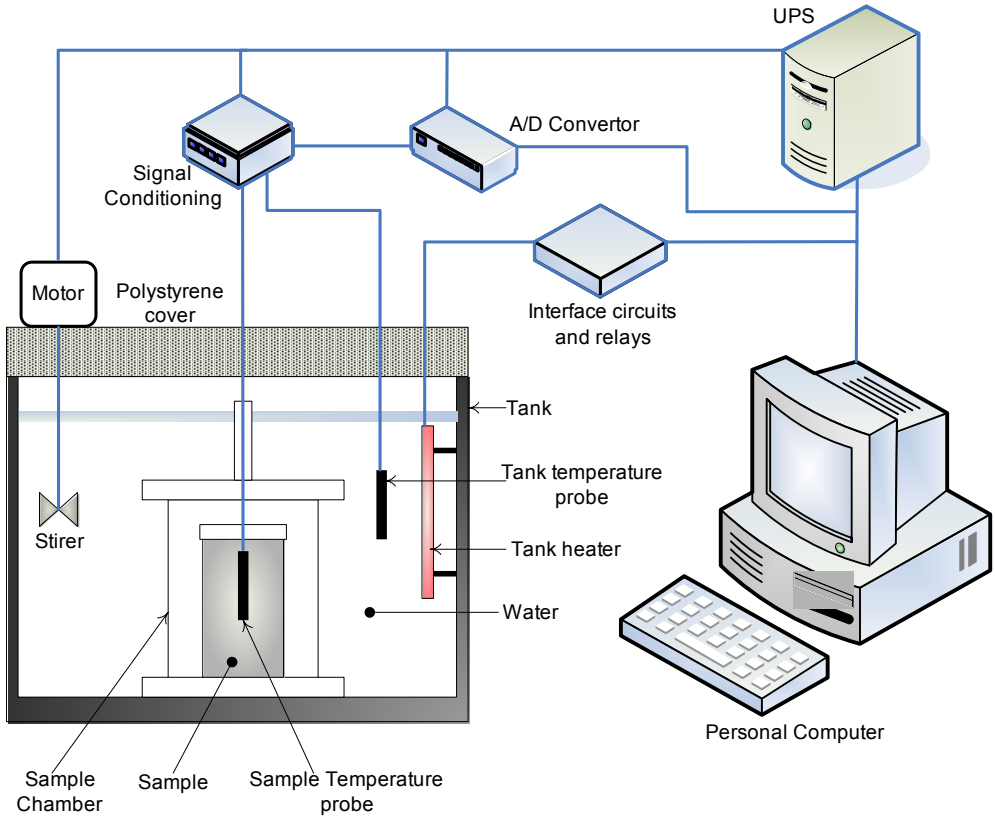

Figure 3.2. Schematic Diagram of the Adiabatic Calorimeter

Both temperature probes are connected to a signal-conditioning unit and an A/D converter, which relay the temperature measurements to the computer. The computer then switches the heating element in the tank on or off according to the reading from the sample probe, in order to maintain adiabatic conditions between the sample and the water in the tank. This ensures that no heat is transferred between the concrete in the chamber and the water surrounding it in the tank.

The tank is raised off the ground by a wooden platform and the room in which the adiabatic calorimeter is housed is kept a constant ambient temperature of 20°C ± 2°C

at all times. This achieved with an air-conditioning unit. A more detailed description of the calorimeter and its components follows.

3.4.2 Hardware

The calorimeter used is based on the design of Gibbon (1995). An IBM compatible personal computer with a 486 processor, 640 kB of RAM, a 1.44 MB 3.5" floppy disk drive and a 609 MB hard disk drive was used. A 12-bit PC-26 A/D converter card was connected to the computer as well as a 24-line PC-36 digital interface (I/O) card. The calorimeter system is fitted with a 200 W UPS connected to the computer and signal conditioning unit. The UPS allows for a power failure of up to forty-five minutes and during such time, the software used on the computer allows a test to be restarted or continued if the power failure has been longer than fifteen minutes. During long power interruptions however, the water in the tank can drop to a temperature that is low enough for adiabatic conditions to be lost. In this case the test should be discarded.

Signal Conditioning Unit

The signal-conditioning unit converts the temperature readings from the probes in the sample and the tank into a voltage that can be interpreted by the computer through the A/D converter. It converts temperatures from 0°C to 100°C to voltages from 0 to 10 V. Commercially available signal converters with the following specifications were used:

- Model: 1100L
- Supply: 200 V 50 Hz
- Input: PT100: 0 to 100°C, three wire
- Output: 0 to 10 volts

A/D Converter Card

The output voltages from the signal-conditioning unit are transferred to the computer via an analogue to digital converter card for interpretation by the software. The A/D card used in the computer has the following specifications:

- Type: PC-26
- A/D resolution: 12 bit
- A/D input ranges: 0 – 10 V, -5 – 5 V, -10 – 10 V
- A/D throughput rate: 25kHz
- The A/D card gives a resolution of 0.024°C

Interface Circuits and Relays

The computer controls the heating element in the tank through a PC-36 digital I/O board. The circuitry includes an interface design by Gibbon (1995) that provides a buffer between the relays controlling the power supply of the heater and the I/O board.

120 *l* Water Tank

A 120 *l* double walled, insulated, stainless steel water tank is used in maintaining the adiabatic environment around the sample chamber. The tank has a 2 kW heater that can raise the water temperature by 12°C per hour and an electric stirrer, which keeps the water in constant motion in order to maintain an even temperature distribution throughout the tank. A float valve connected to a secondary water tank is used to account for water lost by evaporation and heat and vapour loss is minimised with a thick polystyrene covering over the tank during testing.

Sample Chamber

The sample chamber is shown in figures 3.3 and 3.4. It consists of a plastic tube into which the concrete specimen is placed, with two Perspex plates at its ends. The plates are fastened against the tube with six threaded rods and wing nuts, giving an airtight seal. Before placing the chamber in the tank, the concrete sample is cast in a 1 *l* plastic jar and placed on a polystyrene layer inside the chamber. A temperature probe is inserted into the concrete and run through a plastic sheath in the top Perspex cover. This sheath is then plugged with cotton wool, providing thermal insulation. The air pocket in the chamber surrounding the sample helps to damp the harmonic response

between the sample and the water in the tank due to over and under runs created when switching the heaters on and off or due to intrinsic errors in the probes (Graham, 2003).

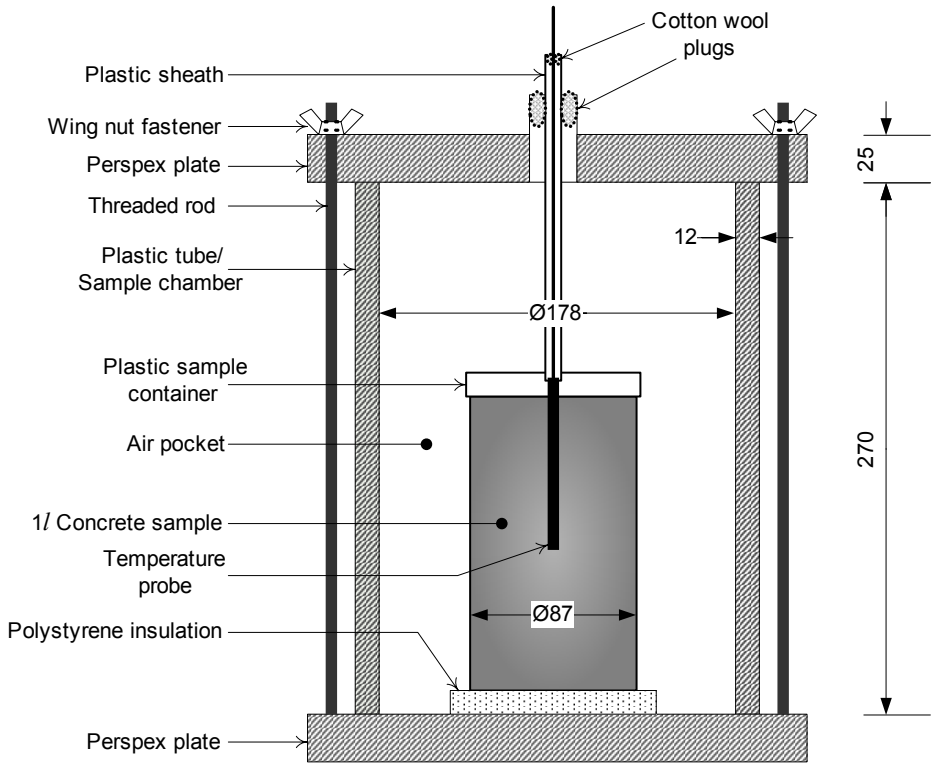

Figure 3.3. Sketch of the Calorimeter Sample Chamber (not to scale)

Temperature Probes

Temperature sensors sealed in 60 mm long stainless steel tubing with a 6 mm diameter are used to measure the temperatures experienced in the concrete sample and the water tank. They are guaranteed to have an accuracy of 0.5°C and are connected to the signal-conditioning unit in order to transmit the readings to the personal computer. No calibration factors are included in the hardware with respect the temperature measurements, but this is accounted for in the software.

3.4.3 Software

Gibbon (1995) originally developed the software used for recording the temperature of the sample during the course of testing, in conjunction with the School of Electrical Engineering at the University of the Witwatersrand. The programme allows the user to enter sample information, change test parameters, plot previously measured data and calibrate the calorimeter. The test parameters can also be modified while an experiment is in progress. An "ON-OFF" control algorithm is used to control the heating element in the water tanks during testing. The programme simply switches the heater on or off depending on the sample temperature, in order to maintain adiabatic conditions.



Figure 3.4. Photograph of the Sample Chamber with a Temperature Probe in the sample jar alongside

3.4.4 Heat of Hydration Measurement

Temperature readings taken from the adiabatic calorimeter can be used to determine the amount of heat produced due to the hydration of the cement present at any point in time. This is done using equation 3.6 below:

$$Q_i = C_p m \Delta T \tag{3.6}$$

Where:

Q_i = heat produced from hydration during the time interval $\Delta t = (t_i - t_{i-1})$

m = sample mass

ΔT = $T_i - T_{i-1}$ = temperature change/rise over time Δt

C_p = specific heat capacity of the concrete sample.

The total heat gain is simply the summation of the Q_i values over i time periods:

$$Q_t = \sum_{i=1}^{i=n} C_p m\left(T_i - T_{i-1}\right) \tag{3.7}$$

The specific heat capacity of concrete is usually calculated as the weighted sum of the individual components in the concrete mixture. Although Gibbon (1995) recognises that the C_p value of the cement paste changes throughout the hydration process, he shows that this method is sufficiently accurate for the results obtained from the calorimeter. Thus:

$$C_p = \left(\sum_{i=1}^{i=n} C_i m_i\right) \Big/ m_c \tag{3.8}$$

Where:

C_p = specific heat capacity of the concrete sample

C_i = specific heat capacity of the ith component in the concrete mixture

m_c = mass of the concrete sample

m_i = mass of the ith component in the concrete mixture.

The heat generated per unit mass of cement or binder can then be calculated from equation 3.9:

$$q_t = Q_t / m_c \tag{3.9}$$

The rate of heat evolution of the concrete sample can then be determined from equation 3.10:

$$q'_t = \frac{dq_t}{dt} \tag{3.10}$$

Results obtained with equation 3.10 are only comparable if tests are conducted with the same initial temperature. Ballim and Graham (2003) developed a mathematical approach in terms of concrete maturity in order to allow for test results to be independent of starting temperature. This is discussed in detail in chapter 4.

3.5 Holcim Portland Cement and Clinker Characterisation

As mentioned, the cement used in this research was supplied by Holcim South Africa in Roodepoort. Holcim manufactures its cement using two clinkers, one from sourced Dudfield and one sourced from Ulco, that are ground together with between four and five percent gypsum. The cement consists of an overall clinker content of 25% Dudfield clinker and 75% Ulco clinker. The chemical XRF analyses for the results that follow were conducted by the Holcim laboratory in Roodepoort.

3.5.1 Holcim Portland Cement

This section provides details of the Holcim PC used. The mass percentages of the oxides found in the cement powder can be seen in table 3.1.

When comparing the values shown in table 3.1 to those presented by Addis (2001) in tables 2.1 and 2.2 in chapter 2, it can be seen that the major oxides present in the Holcim cement fall within the average ranges for South African cements. This is true for all of the oxides except for the alumina present, which is slightly short of the

minimum value suggested. The silica and magnesium oxide amounts however, lie towards the upper end of the ranges suggested by Addis (2001).

Chemical Composition of Holcim PC by XRF Analysis	
Chemical Determinant	Percentage in Cement (%)
CaO	65.9
SiO_2	22.6
Al_2O_3	3.6
Fe_2O_3	2.4
MgO	3.1
LOI	1.8
SO_3	2.6
TiO_2	0.3
Mn_2O_3	0.9
P_2O_5	0.1
Phase Composition by Bogue Calculation	
Crystalline Phase	Percentage in Clinker (%)
C_3S	61.5
C_2S	18.4
C_3A	7.3
C_4AF	5.5
Other Properties	
Lime Saturation Factor	95.6
Density (kg/m^3)	3230
Blaine (cm^2/g)	4275

Table 3.1. Chemical composition of Holcim Portland cement

The major crystallographic phase amounts all fall quite comfortably within the average ranges for South African cements. This indicates that the cement used for this investigation is a typical PC used in the construction industry in South Africa. The LSF of the Holcim cement is above 94, which suggests that a fair amount of alite is present. This is confirmed by the fact the C_3S content is near the upper end of the range presented in table 2.2. The density and Blaine values obtained, are also

somewhat high for cement. This suggests that the reactivity of the material will be higher that most other cements.

3.5.2 Dudfield Clinker

This section provides details of the Dudfield clinker used by Holcim Cement in the production of its PC. The Dudfield clinker constitutes 25% of the clinker used in the manufacturing of the PC used in this research.

Chemical Properties

Chemical Composition of Dudfield Clinker by XRF Analysis	
Chemical Determinant	Percentage in Clinker (%)
CaO	67.3
SiO_2	22.7
Al_2O_3	4.2
Fe_2O_3	2.7
MgO	1.6
LOI	0.4
SO_3	0.4
TiO_2	0.3
Mn_2O_3	0.2
P_2O_5	0.1
Phase Composition by Bogue Calculation	
Crystalline Phase	Percentage in Clinker (%)
C_3S	72.1
C_2S	14.3
C_3A	6.6
C_4AF	8.2
Lime Saturation Factor	96.0

Table 3.2. Chemical composition of Dudfield clinker

Table 3.2 shows the chemical analysis of the Dudfield clinker. When the composition of the Dudfield clinker is compared to the average values presented by Addis (2001)

in Table 2.1, chapter 2, it can be seen that the major oxides of CaO, SiO_2, Al_2O_3, and Fe_2O_3 all fall with the specified range. The high LSF of 96 supports the high Bogue calculation estimates of C_3S and C_4AF in the clinker. This is further supported on examination of the clinker under the microscope seen in the photographs in figures 3.5 to 3.8.

Microscopy Investigation

A number of photographs were taken for the microscopy investigation of the Dudfield clinker. Those pertinent to this discussion are shown in figures 3.5 to 3.8 that follow. The photographs taken during the microscopy examination show that the surface of the Dudfield clinker samples is relatively free from scratches and markings. This indicates that it is a fairly hard material, especially when compared to the Ulco clinker.

The crystal phases are well formed and can be clearly distinguished from one another. In the matrix in particular, the difference between the alluminate phase (darker areas) and the ferrite phase (lighter, more white areas) is quite distinct, which is not very often the case. The area of the matrix around the clinker crystals is about 7.6% of the total clinker area, which gives an indication of the fact that there is very little matrix material present.

When viewed under the microscope, the alite present in the Dudfield clinker has a green to yellow colouring. The C_3S crystals show a fair amount of impurities and inclusions (figures 3.5 and 3.8). However, a very small amount of the included material seems to be belite. The crystals generally show a well defined hexagonal shape with sharp angular edges. In contrast to the Ulco clinker, not many of the alite crystals are joined together, with only two or three being combined at most.

Figures 3.6 to 3.8 indicate that the C_3S forms a loosely tied framework with very few areas with a high concentration of joined alite crystals. There is some evidence of belite coatings around a few alite crystals, but this is fairly minimal. The individual

alite crystals vary in size from approximately 12 μm to 79 μm with an average crystal size of about 44 μm.

The C_2S crystals exhibit a variety of colours under the microscope from a reddish brown/black colour to a bright pink-purple in some areas. This variation is most likely due to the crystals reacting differently to the etching process. Some of the purple crystals also have what look like green inclusions, similar to the colour exhibited by the alite phase. This could possibly be due the formation of secondary C_2S from C_3S. The sizes of the belite crystals range from about 9 μm to 70 μm with a mean crystal size of roughly 32 μm. There is a substantial number of belite nests or clusters of crystals throughout the clinker samples (figures 3.6 and 3.7) and these nests tend be rather large. The crystals have the typically rounded, oval shape with rough, needle-like edges. They also exhibit a lamellar structure, with many surface striations in all directions. The C_2S crystals are small in comparison to the C_3S crystals, but there are a number of large crystals present in the clinker and some evidence of crystal joining, which is not very common in belite (Campbell, 1999).

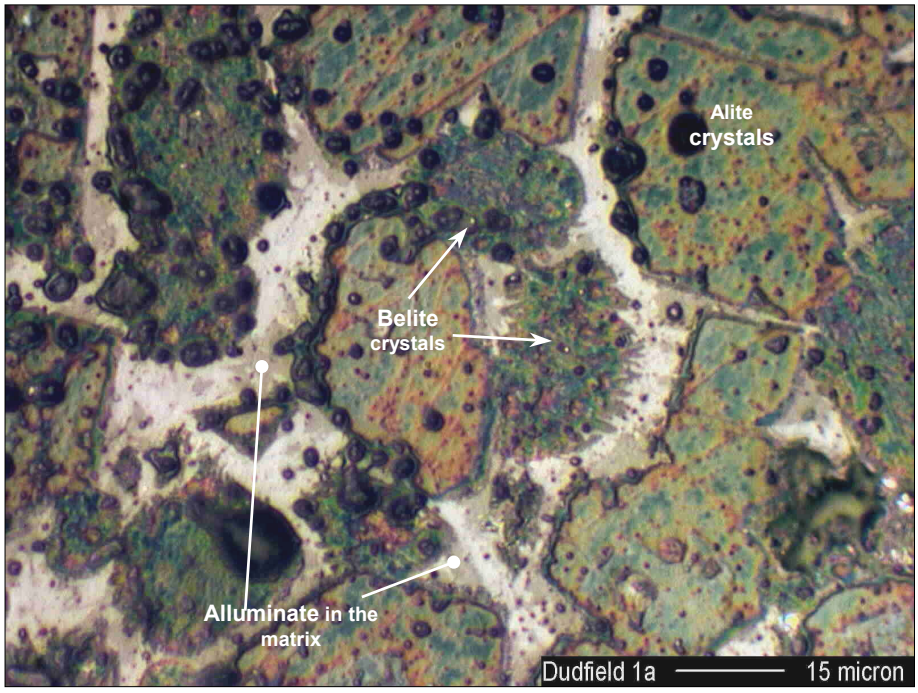

Figure 3.5. 400x Magnification of Dudfield clinker.

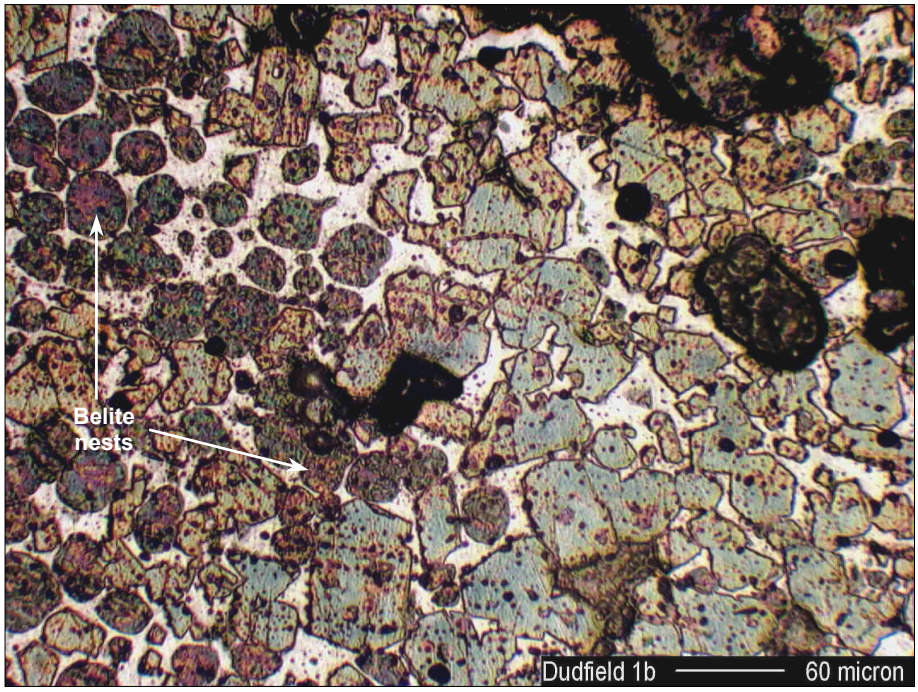

Figure 3.6. 100x Magnification of Dudfield clinker with belite nests

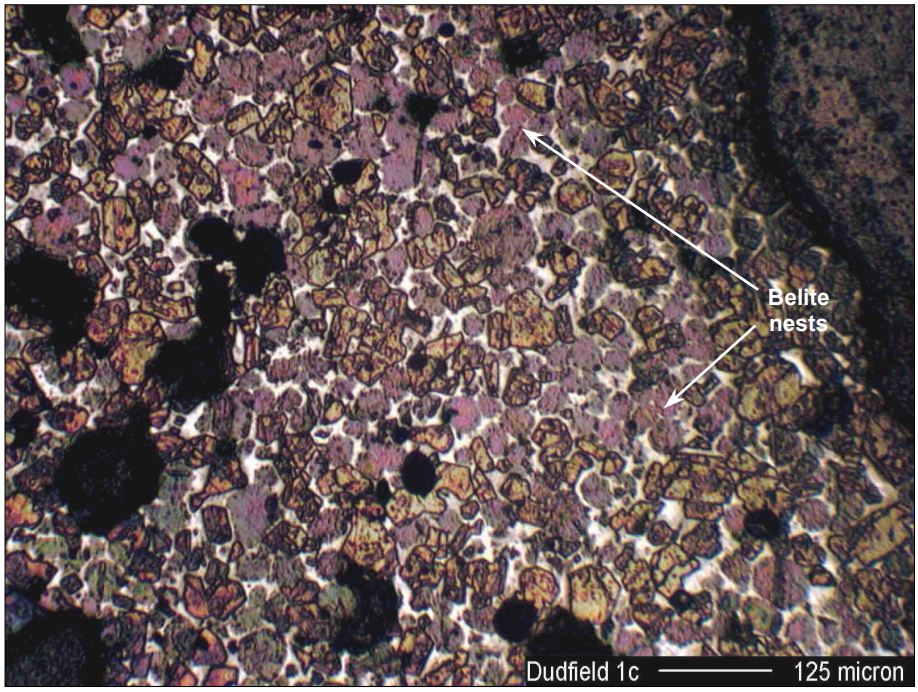

Figure 3.7. 40x Magnification of Dudfield clinker - high concentration of belite.

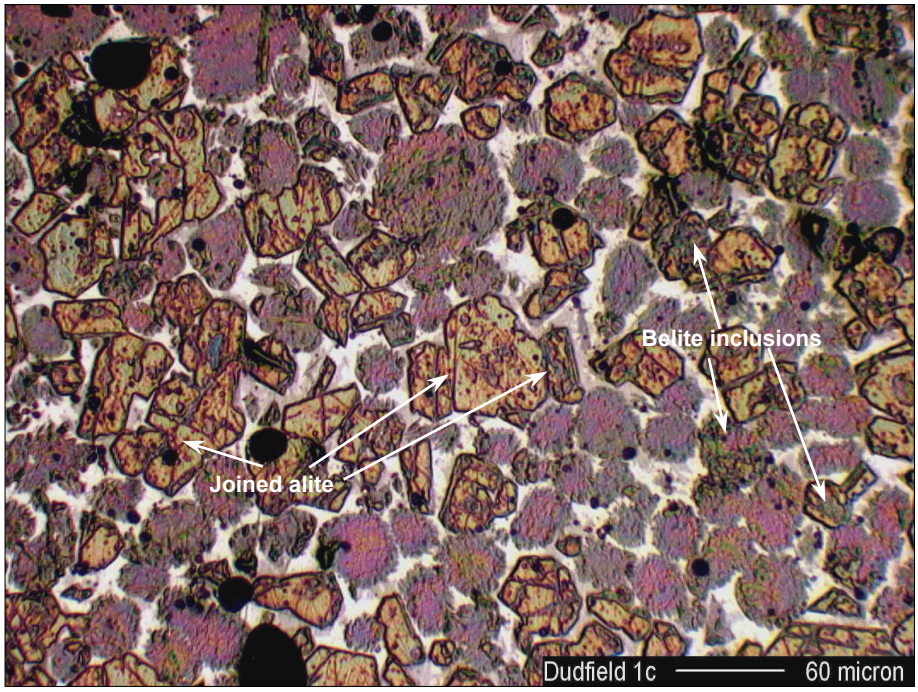

Figure 3.8. 100x Magnification of Dudfield clinker - high concentration of belite nests with joined alite crystals and C_2S inclusions.

3.5.3 Ulco Clinker

This section provides details of the Ulco clinker used by Holcim Cement in the production of its PC. The Ulco clinker constitutes 75% of the clinker used in the manufacturing of the PC used in this research.

Chemical Properties

Table 3.3 shows the chemical analysis of the Ulco clinker. Comparing the composition of the Ulco clinker to average values put forward by Addis (2001) in Table 2.1, it can be seen that the major oxides of CaO, SiO_2, Al_2O_3, and Fe_2O_3 all fall within the given ranges, with the exception of the Al_2O_3 content being slightly less than the norm. The Ulco composition is also very similar to that of the Dudfield clinker, shown in table 3.2.

As with the Dudfield clinker, the high LSF of 98.8 supports the high Bogue calculation estimates of the alite and ferrite present. This is further supported by the microscopy investigation discussed in this chapter and seen in the photographs in figures 3.9 to 3.12.

Chemical Composition of Ulco Clinker by XRF Analysis	
Chemical Determinant	Percentage in Clinker (%)
CaO	66.6
SiO_2	22.0
Al_2O_3	3.6
Fe_2O_3	2.6
MgO	2.6
LOI	1.5
TiO_2	0.7
Mn_2O_3	0.7
SO_3	0.3
P_2O_5	0.1
Phase Composition by Bogue Calculation	
Crystalline Phase	Percentage in Clinker (%)
C_3S	75.2
C_2S	6.4
C_3A	5.1
C_4AF	7.9
Lime Saturation Factor	98.8

Table 3.3. Chemical composition of Ulco clinker.

Microscopy Investigation

A number of photographs were also taken for the microscopy investigation of the Ulco clinker. Those relevant to this discussion are shown in figures 3.9 to 3.12 that follow. From the images captured using the microscope and digital camera it can be seen that the Ulco clinker samples are fairly scratched, especially when compared to the Dudfield samples. This suggests that the Ulco clinker is softer than the Dudfield material, since all samples were subjected to the same grinding and polishing process.

Under the microscope the C_3S present in the Ulco clinker generally has a green to yellow colour (figures 3.9 and 3.10), with a pink-red-purple colouring in some areas. This could be due to the etching and the variations could be because of the softness of the clinker or the formation of secondary C_2S. When examining the alite, figure 3.10 indicates many joined crystals, forming long chains.

In contrast to the Dudfield clinker, the C_3S makes up a tight framework in some areas with very little C_3A and C_4AF matrix surrounding the alite (figures 3.10 to 3.12). Most of the crystals are typically angular and show a definite hexagonal shape, which is very common for alite crystals (Campbell, 1999). Some of the crystals show a somewhat rounded shape, particularly near the edges of the faces. There are also very few visible fracture planes and a small number of inclusions, especially compared to the Dudfield clinker. The alite crystals have an average size of 38 μm, with sizes ranging from 15 μm to 75 μm. The belite crystals range from about 9 μm to 62 μm with an average size of 29 μm. Comparing these values to those of the Dudfield clinker, it can be seen that there is a fair amount of uniformity of the crystal size gradings of the two clinkers. This suggests that there will be very little difference between these values and those of the cement made from the combination of the Dudfield and Ulco clinkers. The average area of the matrix material of the Ulco clinker is approximately 5.92% of the total area of the clinker samples. This is significantly less than that of the Dudfield clinker, but this smaller amount of matrix material is supported by the lower amounts of C_3A and C_4AF found in the Ulco clinker, as determined from the chemical analysis.

Only very small traces of belite can be seen in some areas of the samples and there are some C_2S inclusions in the alite crystals. The belite tends to show up with a brownish-black colouring under the microscope, making it difficult at times to distinguish it from other impurities in the clinker. There is not a great deal of space available to be filled with matrix material because of the close spacing and joining of the alite crystals. The matrix appears to have more lighter areas than dark patches, which suggests more C_4AF than C_3A and this observation is confirmed by the results of the Bogue calculation in table 3.3.

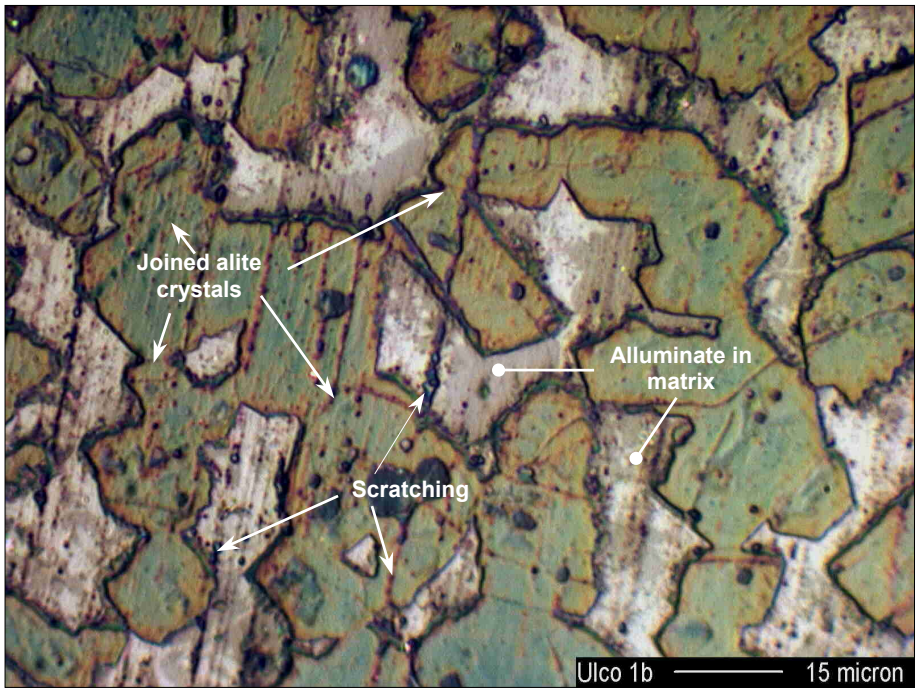

Figure 3.9. 400x Magnification of Ulco clinker.

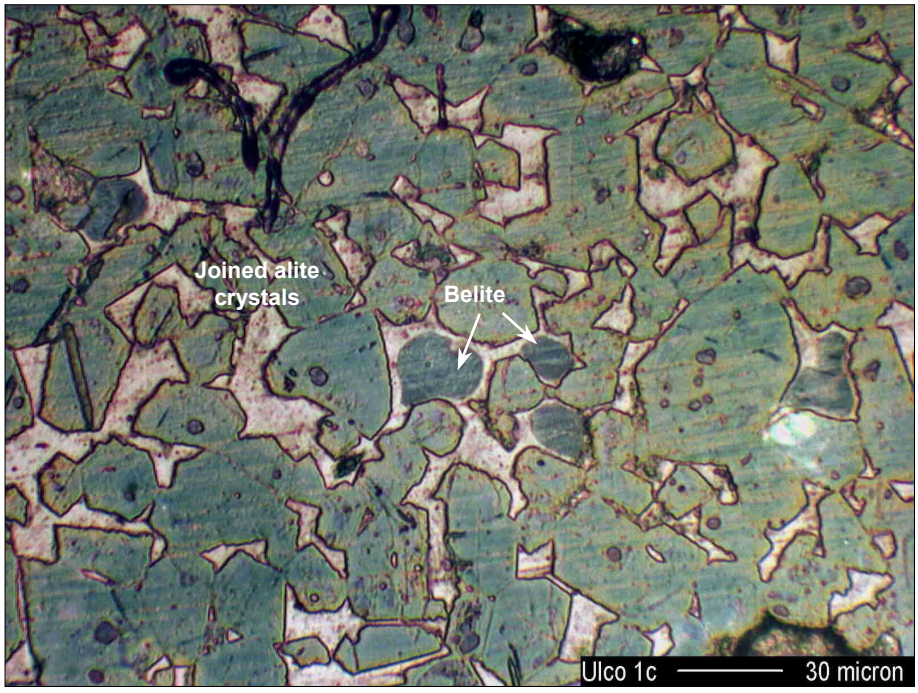

Figure 3.10. 200x Magnification of Ulco clinker - large amount of joined alite.

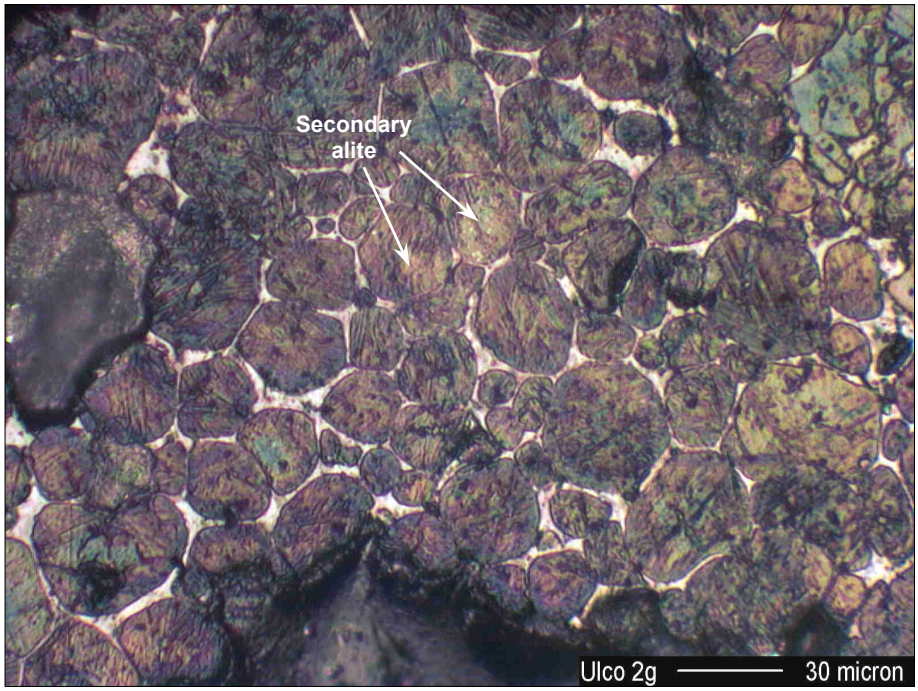

Figure 3.11. 100x Magnification of Ulco clinker - belite nest.

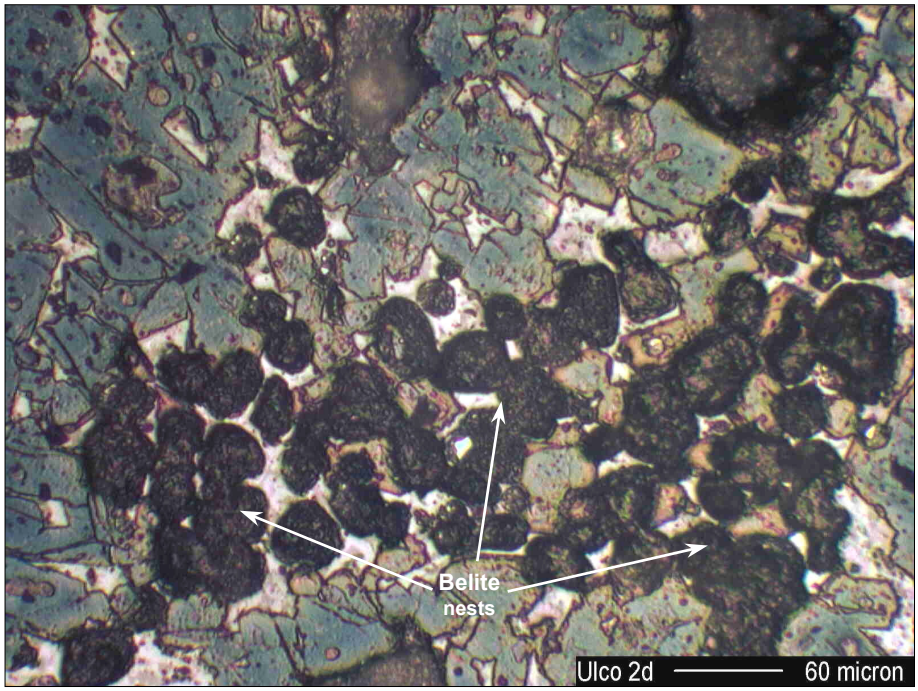

Figure 3.12. 200x Magnification of Ulco clinker - large belite nests.

3.6 Cement Extenders

Table 3.4 shows the mass percentages found in the three cement extenders used in this research. These values can be compared against the average values suggested by Addis (2001) in table 2.3 in chapter for common South African extenders.

Oxide	Average content by mass for the Cement Extenders used (%)		
	FA	GGBS	CSF
SiO_2	55.1	37.8	93.6
Al_2O_3	29.7	15.6	0.5
Fe_2O_3	5.7	1.2	4.0
CaO	7.5	39.4	3.6
MgO	1.1	11.0	0.4
K_2O	0.8	0.9	1.2
TiO_2	1.8	0.6	0.2
Mn_2O_3	0.1	1.2	0.3
P_2O_5	0.4	<0.1	0.1
LOI	0.7	0.7	3.8

Table 3.4. Chemical composition of the cement extenders used

Comparing the actual values in table 3.4 to those presented by Addis (2001) in table 2.3, the following points can be noted:

- The amount of SiO_2 present in the FA is rather high at more that 5% above the suggested average value. Although the amount Al_2O_3 falls within the suggested range, it is at the upper end at the range at just under 30%. The magnesium and iron oxides amounts are both well below the minimum amounts subscribed by Addis (2001).
- In general, the oxides present in the GGBS fall within the average ranges in table 2.3, with the exceptions of CaO and Fe_2O_3. These values are both slightly above the maximum values put forward by Addis (2001).
- The CSF values are approximately of the same order as those in table 2.3 except for the CaO amount, which is approximately six times greater than that suggested by Addis (2001).

3.7 Summary and Conclusions

This chapter has described the test methods used for determining the heat of hydration of the concrete materials under investigation in this research. The characterisation of these materials and the methods used for this purpose, are also discussed.

The Holcim Portland cement used shows similar characteristics to most commercially available cements in South Africa. The Blaine value however, is rather high, which indicates that the cement reactions with water will be fast acting during the hydration process. This would suggest that steep, rapidly approached peaks at peak 1 and 3 in figure 2.1 and a fairly short dormant period (see chapter 2) could be expected from the calorimeter results.

Under the microscope, the Dudfield clinker (which makes up 25% of the clinker material used in the Holcim PC) has well defined phases, with very little matrix material between the alite and belite crystals. The material also appears to be reasonably hard, with almost no evidence of scratching. There are a fair amount of inclusions in the C_3S crystals and very little joining of the alite as well as some secondary belite formed from the alite, especially when compared to the Ulco clinker. There are a large number of extensive C_2S nests and there is even evidence of joining of belite crystals, which is very uncommon in clinkers.

When examining the Ulco clinker (which makes up 75% of the clinker material used) under the microscope, the surface of the material appears to be very scratched. This indicates that the material is rather soft, particularly when compared to the Dudfield clinker. There is some evidence of secondary C_2S in the C_3S but as mentioned, it is very little compared to that of the Dudfield material. A large proportion of the alite crystals are joined to one another forming long chains in a tight framework of C_3S. This leaves very little space for matrix material between crystals. There is also very little evidence of belite in the Ulco clinker, with a few crystals and nests scattered throughout the samples.

3.8 Chapter References

Addis, B. (2001) Cementitious Materials. In: Addis, B. and Owens, G. (ed.), *Fulton's Concrete Technology, 8th Ed.*, Cement and Concrete Institute (CNCI), Midrand, South Africa, pp. 1-15.

American Standard ASTM C150-04**,** *Standard Specification for Portland Cement,* ASTM International, West Conshohocken, PA, USA.

Ballim, Y. and Graham, P.C. (2003) *A maturity approach to the rate of heat evolution in concrete*, Magazine of concrete research, vol. 55 no. 3, Thomas Telford, London, UK, pp. 249-256.

Bogue, R.H. (1947) Calculation of Phase Composition. In: *The chemistry of Portland cement*, Reinhold Publishing, New York, USA, pp 184-203.

Campbell, D.H. (1999) Microscopic characteristics of clinker phases. In: *Microscopical examination and interpretation of Portland cement and clinker, 2nd Ed.*, Portland Cement Association (PCA), Skokie, USA, pp. 29-42.

Gibbon, G.J. (1995) *Laboratory test procedures to predict the thermal behaviour of concrete*, PhD Thesis, University of the Witwatersrand, Johannesburg, South Africa.

Graham, P.C. (2003) *The heat evolution characteristics of South African cements and the implications for mass concrete structures*. Ph.D. Thesis, University of the Witwatersrand, Johannesburg, South Africa.

Lawrence, C.D. (1998) The constitution and specification of Portland cement. In: Hewlett, P.C. (ed.), *Lea's chemistry of cement and concrete, 4th Ed.*, Arnold Publishing, London, UK, pp. 131-191.

Portland Cement Association (PCA). (1994) *Research and development information: Cement*, PCA, Skokie, USA.

South African Bureau of Standards (SABS). (1971) *SABS Method 747: Density of cement*, SABS, South Africa, pp. 1-3.

South African Bureau of Standards (SABS). (1971) *SABS Method 748: Specific surface of cement*, SABS, South Africa, pp. 1-6.

Taylor, H.F.W (1997) *Cement chemistry, 2nd Ed.*, Telford, London, UK.

Chapter 4

ADIABATIC CALORIMETER RESULTS

4.1 Introduction

The temperature of a concrete sample recorded over time during an adiabatic test can be manipulated in order to find the total heat generated and the rate at which heat is evolved. In turn, the thermal responses of different concretes can be assessed and compared. This information could also be used as input to mathematical models for the prediction of the hydration process of cement and the heat transfer within large concrete elements, such as a dam wall.

In order to produce accurate predictions of the temperature distribution or progress of hydration in concrete, there is a need for an accurate determination of the rate of heat evolution from the concrete due to the hydration of the cement present. This is not an easy task since the heat rate is not only dependent on time, temperature and the rate of hydration but also on the boundary conditions of the element. The issue is further complicated by the unique time-temperature profile that exists for each point in the element. This implies that each point in a concrete structure will be subjected to a different heat rate at a particular point in time, as discussed in section 2.2. In order to predict a generalised heat rate for the entire structure, the heat rate curves for each point in the element under consideration need to be normalised. This will allow the results to be expressed in terms of the advance of hydration rather than time, thus making the results independent of the individual time-temperature histories.

This chapter discusses the adiabatic calorimeter tests conducted for this investigation that could be used for prediction and modelling purposes. A description of the method developed by Ballim and Graham (2003) for normalising the heat rate curves produced from adiabatic calorimeter test results is also included. This method allows the various results to be independent of the starting temperature of the concrete sample.

The following topics and test results are discussed in this chapter:

- The concept of concrete maturity as applied to heat evolution, including a discussion on two different maturity functions available for this purpose.
- The concrete mixture design approach applied to the samples tested.
- The adiabatic calorimeter test results for the different w/c ratios (0.4, 0.5 and 0.6), the different cement extenders (GGBS, FA and CSF) and three different aggregate types (granite, dolomite and andesite). Discussions of and comparisons between the different results are also included.

With regard to a hydration model, work done by Kishi et al. (1993) and Maekawa et al. (1999) has shown reasonable accuracy in predicting the rate of heat evolution of concrete with respect to time. Graham (2003) was able to apply this work to his research with reasonable success. This is discussed in more detail in Chapter 5.

4.2 Prediction of the Temperature Distribution in a Concrete Element

The Fourier equation (shown in equation 4.1) is used to predict the distribution of temperature within a concrete element, allowing for transient conditions within three dimensions, as is experienced on site. The solution of this equation is beyond the scope of this investigation however, but information regarding its use and application can be found in the text by Holman (1990), work done by Ballim and Graham (2003) and by Graham (2003).

In its application to concrete, the Fourier equation is as follows:

$$\rho \cdot C_p \cdot \frac{\partial T}{\partial t} = k\left(\frac{\partial^2 T}{\partial x^2} + \frac{\partial^2 T}{\partial y^2} + \frac{\partial^2 T}{\partial z^2}\right) + q_t' \tag{4.1}$$

Where:

ρ = concrete density

C_p = the specific heat capacity of the concrete

T = the concrete temperature

x, y, z = coordinates of point in question

q_t = the total heat generated per unit mass of binder as a function time t

4.3 Concrete Maturity as Applied to Heat Evolution

Ballim and Graham (2003) describe a mathematical approach for expressing the amount of heat developed and the rate of heat evolution in terms of an equivalent maturity rather than an actual clock time. This approach helps normalise the heat rate curves produced from adiabatic calorimeter test results in order to make the results independent of the starting temperature of the concrete. This concept will be discussed below and was applied to the test results obtained for this research.

Maturity is a concept generally used to correlate the engineering properties of concrete, such as strength, to the degree of hydration of the cement. As a concept, maturity is intended to describe the extent of hydration of concrete, and is a function of the temperature history of the element. It is usually expressed as a time-temperature function or an equivalent maturity age. In mathematical terms, maturity is defined as:

$$M = \int_0^t f(t)dt \tag{4.2}$$

4.3.1 Determining the Rate of Heat Evolution

The rate of heat evolution from a concrete sample is easily determined from adiabatic test results obtained for that concrete. First, the amount of heat produced by a specimen at a given point in time must be calculated. This is done using the following equation:

$$q_t = C_p \cdot (T_t - T_0) \cdot \frac{m_s}{m_c} \tag{4.3}$$

Where:

q_t = the total heat generated per unit mass of binder at time t

C_p = the specific heat capacity of the concrete

T_t = the sample temperature at time t

T_0 = the sample temperature at the start of the test

m_s = the mass of the sample

m_c = the mass of the cement/binder present in the concrete mixture.

The rate of heat evolution, q'_t, can be found by differentiating equation 4.3 with respect to time:

$$q'_t = \frac{dq_t}{dt} \tag{4.4}$$

A major problem with determining the temperature distribution and rate of heat evolution in a concrete element in this fashion is that the results obtained from adiabatic testing in a laboratory will be very different to the actual temperature distribution in a concrete structure. This is because:

- Every point within the structure will have been subjected to a different time-temperature distribution. No unique time based function can therefore completely describe the heat evolution of the entire concrete element.
- The rate of heat evolution is dependent on the range of temperatures that the concrete has already been exposed to, and adiabatic testing cannot account for the effect of the environmental conditions on the temperature distribution within the concrete and amount of heat liberated.

In order to overcome the problem associated with different time-temperature profiles and varying degrees of hydration within a structure, the time component can be expressed in terms of concrete maturity. Wang and Dilger (1994) proposed the following formulae as a means of calculating the rate of heat evolution from a sample with respect to maturity:

$$\begin{aligned} q_t' &= 0.5 + 0.54M^{1/2} \quad \text{for } M \le 10hrs \\ q_t' &= 2.2\exp\left[-0.0286(M-10)\right] \quad \text{for } M \ge 10hrs \end{aligned} \tag{4.5}$$

Where M is the maturity of the concrete relative to that of a sample cured at a constant 20°C.

Ballim and Graham (2003) however, note that the approach of Wang and Dilger (1994) has two serious flaws, namely:

- The approach ignores the initial temperature at which the adiabatic test was conducted. This will influence the rate of hydration and heat liberation.
- The approach ignores the fact that if the concrete temperature were to be reduced to -10°C (when hydration is considered to have ceased) the rate of heat evolution should be reduced to zero. If equation 4.5 were to be applied this would not be the case, since the formulae are dependent on cumulative maturity, which remains constant regardless of the concrete temperature.

Ballim and Graham (2003) addressed these issues by expressing the heat liberated in terms of a *maturity heat rate*. This is a function of cumulative maturity as opposed to actual clock time. The maturity heat rate is therefore expressed as:

$$q_M' = \frac{dq_t}{dM} \tag{4.6}$$

A time-based rate of heat evolution, as required to solve the Fourier equation (4.1), can then be determined from equation 4.4 and 4.6, with respect to the maturity heat rate:

$$q_t' = q_M' \cdot \frac{dM}{dt} \tag{4.7}$$

4.3.2 Maturity Functions

There are two generally accepted equations used to describe concrete maturity. One is the Nurse-Saul equation, which expresses maturity as a time-temperature factor and the other is the Arrhenius equation, which expresses maturity as an equivalent age, usually in hours. Through a series of adiabatic calorimeter tests where the starting temperature of each concrete sample was varied, Ballim and Graham (2003) showed that the Arrhenius maturity function is more suitable than the Nurse-Saul equation for expressing heat evolution characteristics in terms of maturity when trying to normalise the heat rate curves. Waller et al. (2003) also agree that the Arrhenius equation is the more appropriate of the two to use for this purpose.

The Arrhenius Equation

The Arrhenius function is a temperature-rate equation that is based on the kinetics of the hydration reactions. In the form of equation 4.2, the Arrhenius function can be written as:

$$M = k\int_0^t \exp\left(-\frac{E}{RT_k}\right)dt \tag{4.10}$$

Where:

k = Proportionality constant

T_k = temperature (K)

E= Activation Energy for concrete = 33.5 kJ/mole (Bamford and Tipper, 1969)

R= universal gas constant = 8.314 J/mol°C

t = time

Ballim and Graham (2003) refined equation 4.10 in order to develop an equation for expressing maturity in terms of an equivalent age in a way that is suitable for analysing the results obtained from the adiabatic calorimeter tests. The equation is as follows:

$$t_{20} = \sum_{i=1}^{i=n} \exp\left[\frac{E}{R}\left(\frac{1}{293} - \frac{1}{273 + 0.5(T_i + T_{i-1})}\right)\right] \cdot (t_i - t_{i-1}) \tag{4.11}$$

Where:

t_{20} = the equivalent maturity time as discussed earlier (hours)

T_i = temperature at the end of the ith interval (°C)

t_i = time at the end of the ith interval

Equation 4.11 was used for analysing the results obtained from the adiabatic calorimeter for this research based on the work done by Ballim and Graham (2003).

4.4 Concrete Mixture Design

Different concrete samples were tested in the adiabatic calorimeters at the School of Civil and Environmental Engineering at the University of the Witwatersrand. As discussed, the aim of the tests was to determine the practical implications for heat evolution and thermal cracking prevention of different aspects of a concrete mixture and mixture design. The following factors were considered:

1. The effect of varying the w/c ratio
2. The effect of different cement extenders in the binder material
3. The effect of different aggregate types.

A standard concrete mixture was developed with a w/c ratio of 0.6, 9 mm silica aggregate and graded silica sand. This concrete mixture was based on the work done by Graham (2003) shown in table 4.1. The concrete mixture was modified accordingly when considering the different factors above. In all cases, only the sand and binder contents were adjusted according to the changing w/c ratio and the water and stone amounts were kept constant. This was done in order to maintain a similar fines content and mixture consistency across the various samples that were tested. These concrete mixture designs are shown in table 4.2.

Concrete Mixture Component	Mass per cubic metre of concrete (kg/m^3)
Portland cement (CEM I)	350
9.5 mm Silica stone	850
Graded silica sand	885
Water	233
w/c ratio	0.67

Table 4.1. Reference Concrete Mixture Design (Graham, 2003)

Concrete Mixtures	w/c Ratio	Mixture Parameter Content (kg/m^3)				
		PC (CEM I)	Extender	Stone	Sand	Water
PC only Concretes	**0.4**	631	-	1034	907	253
	0.5	505	-	1034	1012	253
	0.6	421	-	1034	1081	253
GGBS Concretes	**0.4**	379	253	1034	890	253
	0.5	303	202	1034	998	253
	0.6	253	168	1034	1069	253
FA Concretes	**0.4**	442	189	1034	850	253
	0.5	354	151	1034	996	253
	0.6	295	126	1034	1043	253
CSF Concretes	**0.4**	568	63	1034	881	253
	0.5	454	50	1034	991	253
	0.6	379	42	1034	1040	253
Concrete Mixtures	**Aggregate**	**PC (CEM I)**	**Extender**	**Stone**	**Sand**	**Water**
Different Aggregate Concretes	**Dolomite**	421	-	1122	1173	253
	Andesite	421	-	1142	1193	253
	Granite	421	-	1070	1119	253

Table 4.2. Concrete Mixture Designs

In an attempt to make the results as practically representative as possible, commercially available Portland cement was obtained from Holcim South Africa for

testing purposes. Common industry practices were also adopted with respect to w/c ratios used, amounts of extenders present in binders and commercially available aggregates. These include:

- w/c ratios of 0.4, 0.5 and 0.6 were used.
- The following binders were used in conjunction with the three w/c ratios:
  - CEM I PC only (referred to as the PC only concretes),
  - 70% PC and 30% FA (the FA concretes),
  - 60% PC and 40% GGBS (the GGBS concretes),
  - 90% PC and 10% CSF (the CSF concretes).
- Three different commercial 13.2 mm aggregates and crusher sands, namely granite, andesite and dolomite.

4.5 Adiabatic Calorimeter Test Results

4.5.1 Test Methodology

Fifteen different concrete mixtures, described in table 4.2, were tested as a part of this investigation. Twelve concretes were used for investigating the effects of binder type and w/c ratio were and three concretes were tested for investigating the effects of aggregate type. The testing was conducted according to the following methodology:

1. Testing concrete samples for effects of different binder types and w/c ratios with standard silica aggregates:
   a. Testing 0.4, 0.5 and 0.6 w/c ratios with 100% PC binder content.
   b. Testing 0.4, 0.5 and 0.6 w/c ratios with 60/40 PC/GGBS binder content.
   c. Testing 0.4, 0.5 and 0.6 w/c ratios with 70/30 PC/FA binder content.
   d. Testing 0.4, 0.5 and 0.6 w/c ratios with 90/10 PC/CSF binder content.
2. Testing concrete samples for different aggregate types with 13.2 mm stone and a w/c ratio of 0.6.
   a. Test concrete with granite sand and stone aggregates.
   b. Test concrete with dolomite sand and stone aggregates.
   c. Test concrete with andesite sand and stone aggregates.

In order to check the reproducibility of the calorimeter tests, a number of test samples were randomly selected for repeat testing in the laboratory. In almost all cases, the differences between the original and repeat tests were negligible. However, when a discrepancy was evident between two tests, the sample was retested until a set of almost identical results were obtained for a particular concrete sample. In this way, the reproducibility and credibility of the results presented in this investigation has been maintained.

The total amount of heat produced and the maturity heat rate could be calculated and plotted against cumulative maturity or equivalent age, t_{20}, using the temperature measurements made over the duration of each test. These results are shown in figures 4.1 to 4.21 that follow. The results obtained using the different extenders for the three different w/c ratios are compared individually to the corresponding PC only concretes.

In order to analyse the temperature readings obtained from the calorimeter, a set of spreadsheet macros were developed using Microsoft Visual Basic 6.3. The macros first convert the time readings into hours and then filter the results in order to smooth the curves to be plotted. The filter is designed to eliminate the oscillatory effect that the changing water temperature has on the readings recorded by the personal computer connected to the calorimeter (refer to chapter 3). The rises and falls in temperature are very small and are caused by the switching on/off of the calorimeter tank heater while maintaining adiabatic conditions. For the first twelve hours, the macro filters out time readings less than fifteen minutes apart. Thereafter, time readings less than one hour apart are ignored. This filtering process was adequate enough to allow the results to be plotted along a smooth curve. Thereafter the macros calculate equivalent maturity, total heat liberated and the maturity heat rate and plot graphs of total heat and maturity heat rate versus t_{20} maturity. These macros can be found in Appendix A. For comparative purposes, the macros developed were adapted for the analysis of two, three and four different sets of calorimeter results respectively at a time.

4.5.2 Portland Cement Concretes

Figures 4.1 and 4.2 show the total heat (q_t) and maturity heat rate (q'_M) versus the Arrhenius maturity (t_{20}). The curves in figure 4.1 show the effects of varying the w/c ratio on the total heat liberated from the concrete during hydration. Figure 4.2 illustrates the effect of the w/c ratio on the maturity heat rate with respect to cumulative maturity.

Figure 4.2 can be compared to the general curve for heat rate versus time shown in figure 2.1 in chapter 2. Although figure 4.2 is in terms of maturity as opposed to actual clock time as in figure 2.1, the curves are comparable with respect to the stages of hydration, as discussed in chapter 2. The pre-induction phase and peak 1 in figure 2.1 however, are ignored in the discussions that follow for all of the various concrete mixtures. This is due to the difficulty associated with recording the heat liberated from a sample from outset of hydration. Since hydration begins almost immediately upon mixing of the cement and water, the initial heat produced cannot be recorded accurately, if at all, since the sample cannot be placed in the calorimeter immediately.

Figure 4.1 indicates that as the w/c ratio decreases, the total heat liberated per unit mass of binder decreases. During approximately the first 65 t_{20} hours of hydration the total heat produced is roughly independent of the w/c ratio, but as time progresses the total heat graphs begin to diverge. Although the 0.5 and 0.6 w/c tests do not reach final maxima in figure 4.1, it is apparent that the higher the w/c ratio the greater the amount of total heat produced per kilogram of binder. The maximum amount of heat occurs at a later maturity and at a slower rate in the higher w/c concretes.

The difference in the maximum total heat value and the maturity at which it occurs between the different w/c ratios is less significant as the w/c ratio increases. This can be attributed to the greater possibility of contact between the water and cement particles in the higher w/c pastes, where more water is available in the later stages of hydration to continue the reactions. This results in a larger portion of the binder being hydrated in the higher w/c concretes, and thus more heat is produced.

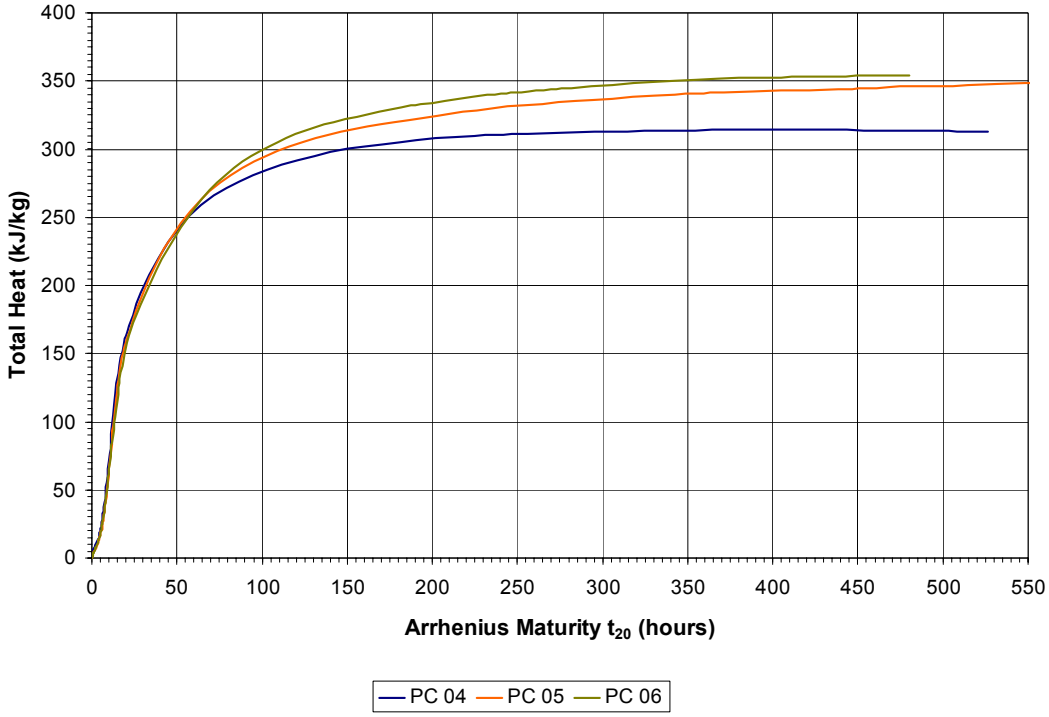

Figure 4.1. Total Heat – PC Only concretes

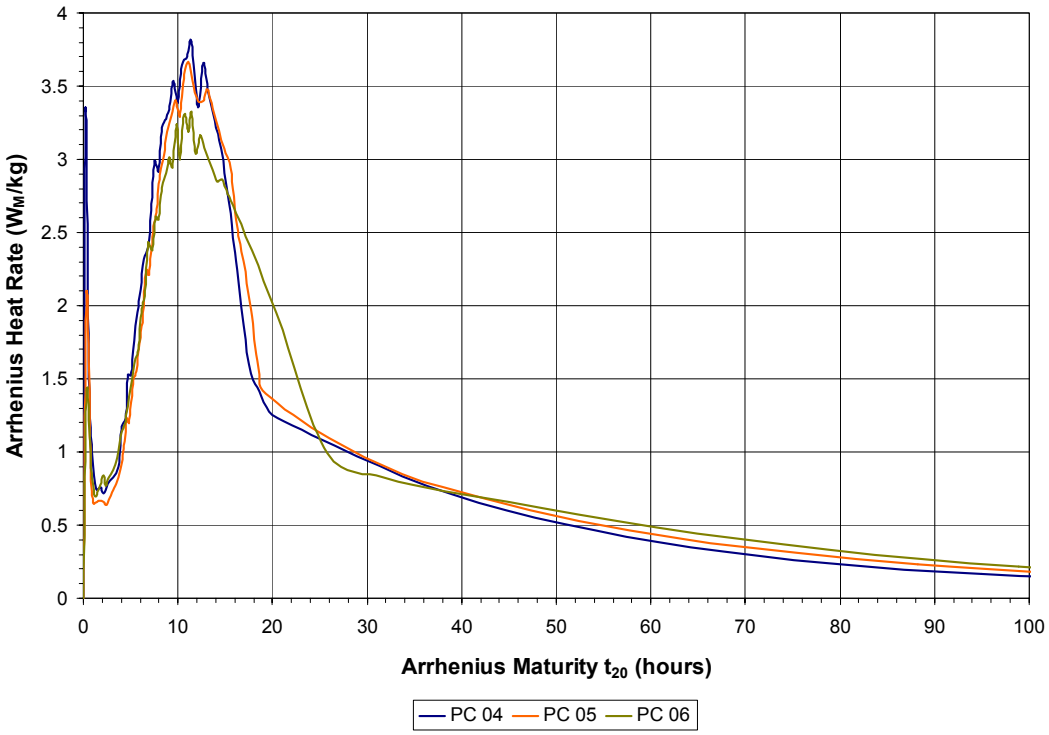

Figure 4.2. Maturity Heat Rate – PC Only concretes

Self-dessication can also explain the decrease in the maximum total heat with a lower w/c ratio. In cases such as the calorimeter tests of this investigation, where the concrete is sealed after mixing, hydration can be halted if the w/c ratio is below a critical value. This value is generally accepted to be around 0.25. At the critical w/c ratio, there may be sufficient water to react with the cement particles and fill the gel pores, but the capillary pores will not contain any water. If the w/c ratio is below this value, the concrete mixture will have insufficient water to hydrate the cement completely (Addis, 2001).

Above the critical w/c ratio, the capillary pores will be partially filled and hydration will continue. This implies that concretes with a higher w/c ratio will produce more hydration products at later ages and that these products will be of a better quality since hydration will have continued for longer. At the micro-level however, the process of hydration can seal off access to unhydrated cement grains, which in turn can halt the reactions, even though the w/c ratio may be above the theoretical lower limit for true self-dessication. In practice, the critical w/c ratio is therefore larger than the theoretical lower limit.

In figure 4.2, there is an indication that the greater the w/c ratio the lower the maximum value of the exothermic peaks and troughs as shown in figure 2.1 in chapter 2. The peaks occur at approximately the same maturity, which suggests that a change in the w/c of a concrete mixture will not cause any significant delays in the progress of hydration. The dormant period also lasts for approximately the same period of time across the three test results.

During the first five t_{20} hours, the minimum maturity heat rate of trough 2 is lower in the higher w/c pastes. This could be the result of a larger initial availability of cement particles for hydration and ettringite formation in the lower w/c concretes.

From approximately five to thirty t_{20} hours, the rate of change in the maturity heat rate is approximately the same for all three concretes approaching peak 3. Peak 3 also occurs at roughly the same maturity in all three concretes. This suggests that the w/c

ratio does not significantly affect the rate of reaction during the acceleration stage. The peak 3 maxima are greater in the lower w/c pastes. However, the difference between maxima decreases as the w/c ratio increases. Graham and Ballim (2003) noted that the significance of these differences is likely to be dependant on the binder content of the concrete and the size of the concrete member in question.

The rate of hydration during the later stages is greater in the concrete mixtures with the larger w/c ratios. This is evident by the greater amounts of heat produced (figure 4.1) and the slower rate at which the heat rate approaches zero (figure 4.2). The greater the w/c ratio the more noteworthy peak 4 is during the post acceleration stage, suggesting greater delayed ettringite production from the hydration of the alluminate phase. As with the total amount of heat produced, this can be attributed to the greater availability of free water in the higher w/c concretes during the later stages of hydration.

From the points above, it can be deduced that the w/c ratio only plays a significant role in changing the heat evolution characteristics of concrete during the intermediate and later stages of hydration. This is evident when considering the points in time where the curves begin to separate from one another in figures 4.1 and 4.2. These observations are in agreement with Copeland and Kanto (1972), as discussed in chapter 2.

4.5.3 Ground Granulated Blastfurnace Slag Concretes

As mentioned, three 60/40 PC/GGBS concretes mixtures were tested in an adiabatic calorimeter with w/c ratios of 0.4, 0.5 and 0.6. The results of these tests are found in figures 4.3 and 4.4, showing total heat per unit mass of binder and maturity heat rate against t_{20} maturity hours. The effects of varying the w/c ratio and of the addition of GGBS on the heat evolution characteristics of the concrete with respect to cumulative maturity can be noted from figures 4.3 and 4.4.

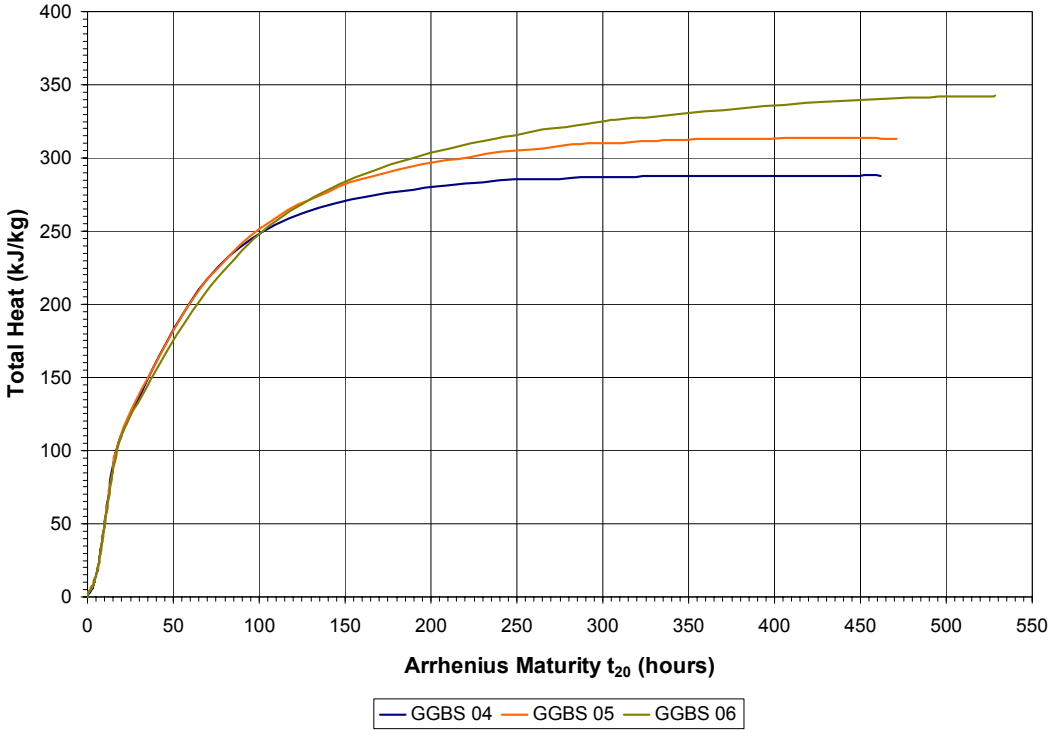

Figure 4.3. Total Heat – GGBS concretes

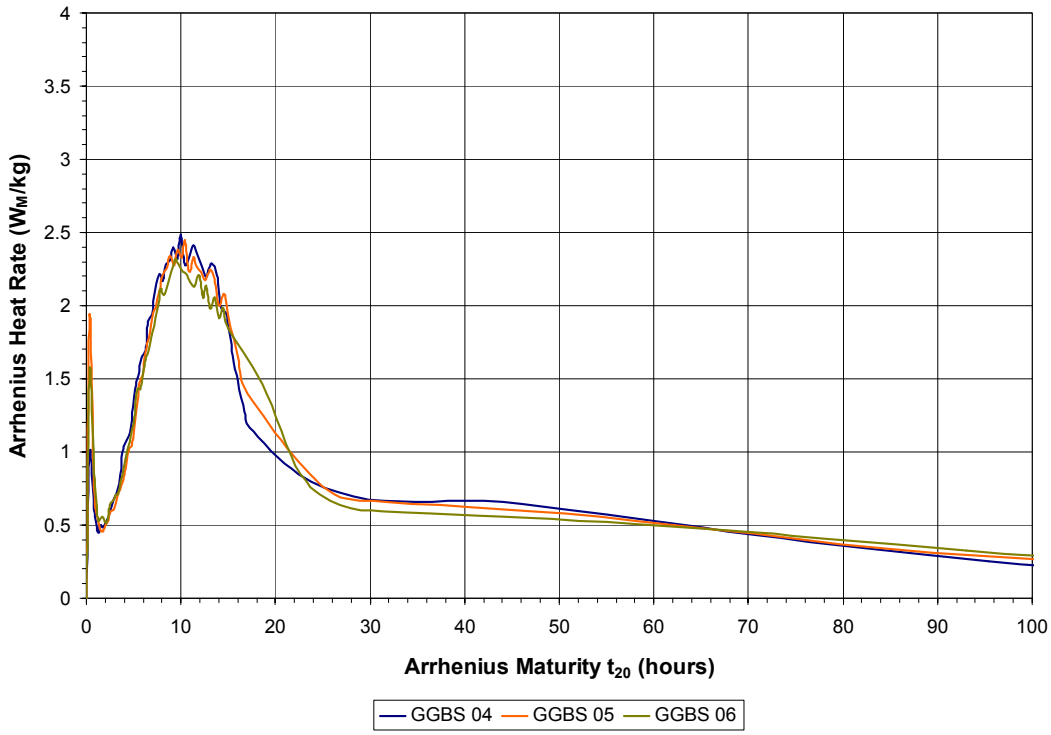

Figure 4.4. Maturity Heat Rate – GGBS concretes

Although the w/c 0.6 GGBS concrete does not reach a final maximum total heat in figure 4.3, it is also evident that the lower the w/c ratio, the lower the maximum total heat reached. As the w/c ratio increases, the difference in total heat liberated per unit mass of binder decreases slightly, as shown in figure 4.3. This is similar to the trend seen in the PC only concretes, except that the difference in total heat liberated is greater in the GGBS samples. This could be attributed to the late contribution of the S-reaction discussed in chapter 2, and the increased availability of free water in the higher w/c concretes during the later stages of hydration.

The graphs in figures 4.4 suggest that the greater the w/c ratio, the greater the value of trough 2, although the difference is only marginal between the 0.4 and 0.5 w/c ratios. The dormant period appears to last for roughly the same length of t_{20} hours across all three samples. This also indicates that the w/c ratio has almost no effect on the hydration process during this stage. Similarly, the w/c has a negligible effect on the acceleration stage of hydration since the progress of hydration appears to proceed at the same rate in all three GGBS mixtures from approximately 5 to 15 t_{20} hours in figure 4.4.

Changing the w/c ratio only has a small effect on the maximum heat rate in the GGBS concretes. From figure 4.4, it is evident that the maximum maturity heat rate (peak 3) only decreases slightly with a higher w/c ratio. The difference between the heat rate peaks however, is more evident as the w/c ratio increases. The maximum also occurs at the same maturity in all three samples. This suggests that the use of GGBS helps to reduce the negative effects associated with a lower w/c ratio paste increasing the maximum heat rate because the cement content of the concrete is higher. It is possible that this is due to the late contribution of the S- reaction to the heat liberation of the concrete, as discussed. This could be useful in designing a concrete mixture that has reduced chances of thermal cracking.

The effects of the S-reaction (De Schutter, 1998) discussed in chapter 2 are evident in the post acceleration stage in figure 4.4. The curves in figure 4.4 support the theory of a P- and an S-reaction developed by De Schutter (1998) and the contribution of the hydration of GGBS to peak 4 is visible in figure 4.4 between 40 and 50 t_{20} hours.

There is no definite trend with respect to the contribution of the GGBS present to peak 4, although from figure 4.4 it may be reasonable to assume that, as the w/c decreases, the contribution of GGBS to the value of peak for will increase. This could be because of the greater amount of GGBS present per kilogram of binder as the w/c ratio decreases, for a constant PC/GGBS ratio.

The greater rate of reaction seen in the higher w/c concretes during the later stages of hydration (figure 4.4) could also be attributed to the fact that, there is more space available to be filled by hydration product because there is less binder material and a greater amount of available water. This increases the chance for cement grains to come into contact with free water in the later stages of hydration. A similar effect can be noted with the PC only concretes as shown in figure 4.2, but it is more pronounced in the GGBS concretes. It also suggests that the hydration of GGBS only significantly contributes to the heat liberated during the later stages.

4.5.4 Fly Ash Concretes

Three concretes containing 30% FA and 70% PC binder content were tested in the adiabatic calorimeter for the three different w/c ratios as discussed earlier. The results of these tests are shown in figures 4.5 and 4.6, which respectively show total heat and maturity heat rate versus t_{20} maturity. The effects varying the w/c ratio and of the addition of FA to the binder can be noted from figures 4.5 and 4.6.

From figure 4.5, it is evident that there is no significant difference between the three different FA concretes for approximately the first 50 t_{20} hours. Thereafter, the three graphs begin to diverge from one another, although the difference in the rate of change in heat liberated is not substantial. The FA concrete samples with the higher w/c ratios reach a greater maximum total heat amount compared with the lower w/c samples and the maximum heat liberated tends towards that of the high w/c concrete. i.e. as the w/c ratio increases, the difference in total heat liberated per unit mass of binder between two samples, is less. This trend appears to become less significant as the w/c ratio increases.

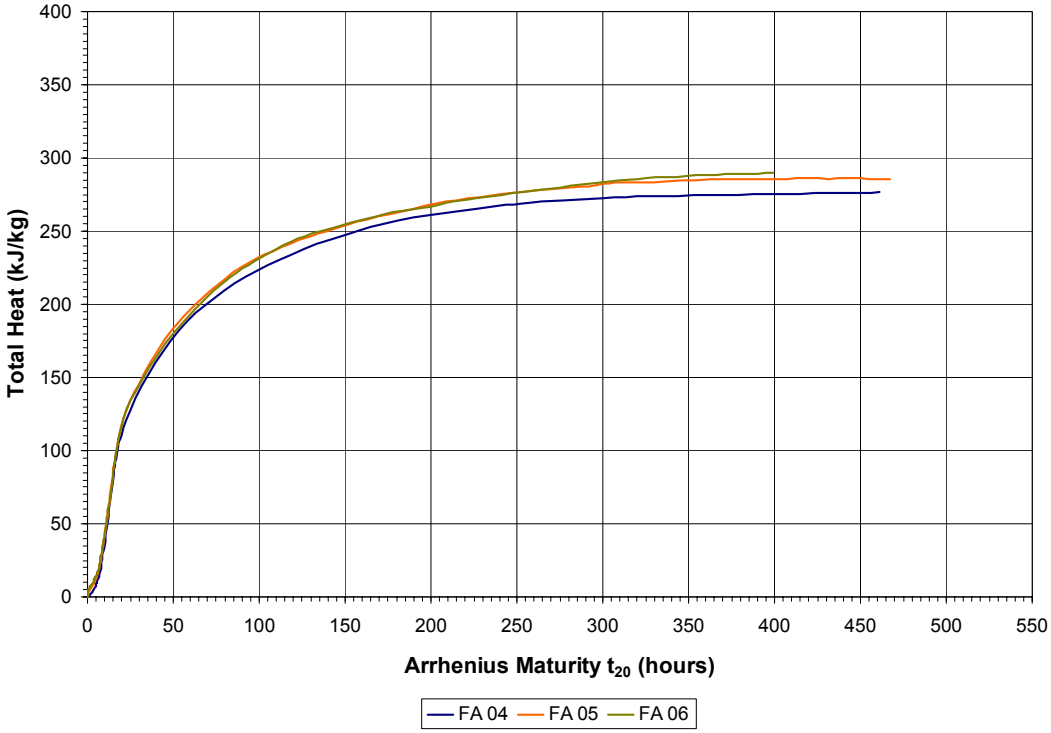

Figure 4.5. Total Heat – FA concretes

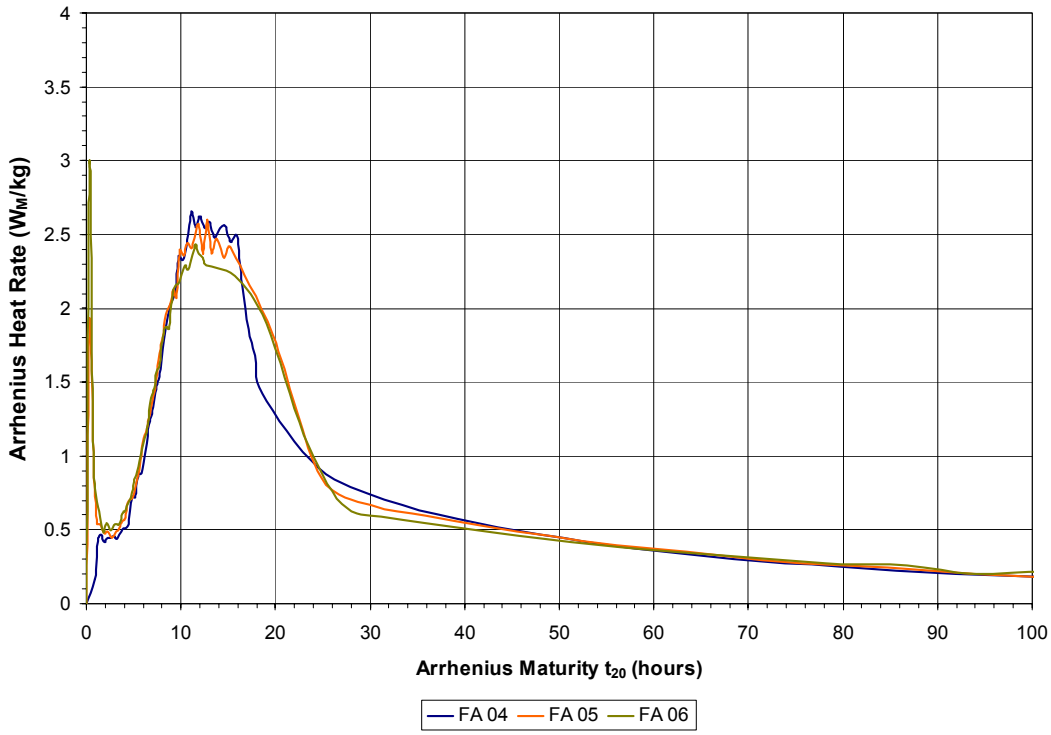

Figure 4.6. Maturity Heat Rate – FA concretes

Figure 4.6 shows the maturity heat rates versus t_{20} hours for the three different FA concrete mixtures. In all three sets of results, the dormant period during hydration lasts for approximately the same length of t_{20} hours. The minimum q'_M value at trough 2 is also approximately the same for all three FA concrete mixtures and occurs at the same maturity for the three concretes. After trough 2, the change in maturity heat rate approaching peak 3 is constant across the three tests.

The main effect of FA and different w/c ratios can be seen at peak 3 in figure 4.6. Figure 4.6 indicates that the lower the w/c ratio of a concrete containing FA, the higher the maximum maturity heat rate will be. This trend becomes less significant however as the w/c ratio increases and peak 3 tends towards the maximum value of the highest w/c. Peak 3 also occurs at the same maturity for all three concretes.

The decrease in maturity heat rate during the deceleration phase is more rapid in the lower w/c concretes, although this difference tends to become negligible as the w/c increases. This could again be attributed to the greater availability of free water in the higher w/c concretes.

Peak 4 in the hydration process is almost non-existent in the FA concretes, particularly in the higher w/c ratio concrete mixtures (i.e. as the w/c ratio increases the contribution of peak 4 to the maturity heat rate decreases). After peak 4 at between 40 and 50 t_{20} hours, the rate of decrease in the maturity heat rate is approximately the same for all three concretes. This is also evident when considering the change in heat liberated after 50 t_{20} hours in figure 4.5.

4.5.5 Condensed Silica Fume Concretes

Three samples with different w/c ratios, containing 10% CSF and 90% PC binder content were tested in the adiabatic calorimeter as discussed earlier. Figure 4.7 and figure 4.8 illustrate the results of these tests, which respectively show total heat liberated and maturity heat rate per kilogram versus t_{20} maturity. The effects of the addition of CSF to concrete and of varying the w/c are discussed below.

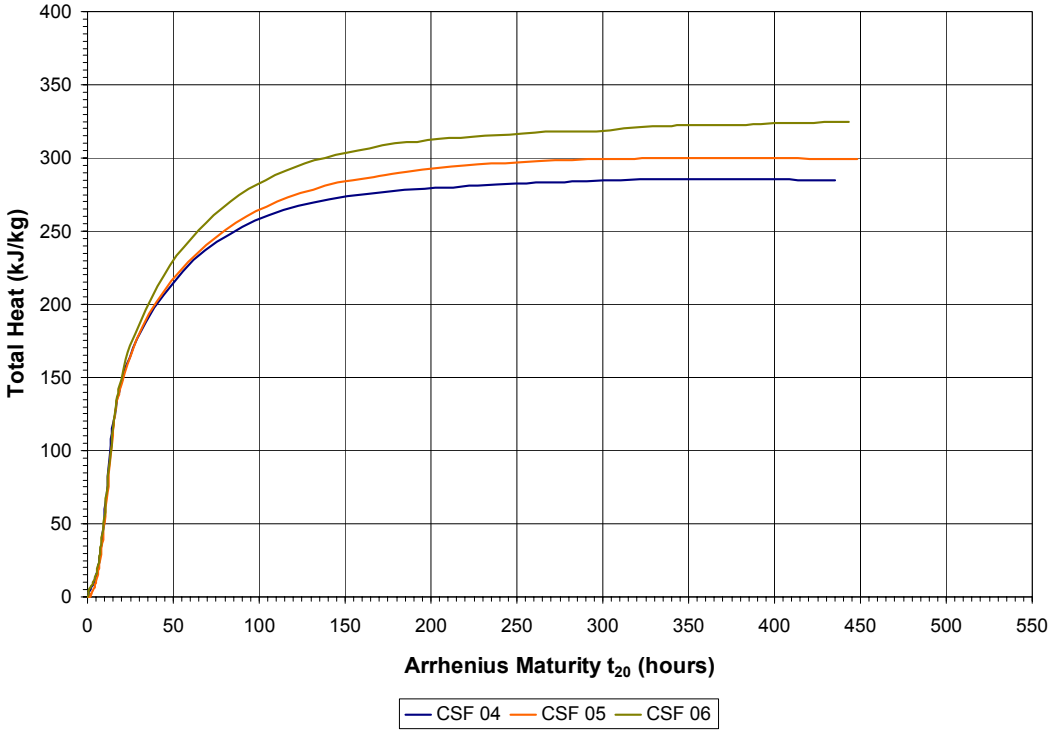

Figure 4.7. Total Heat – CSF concretes

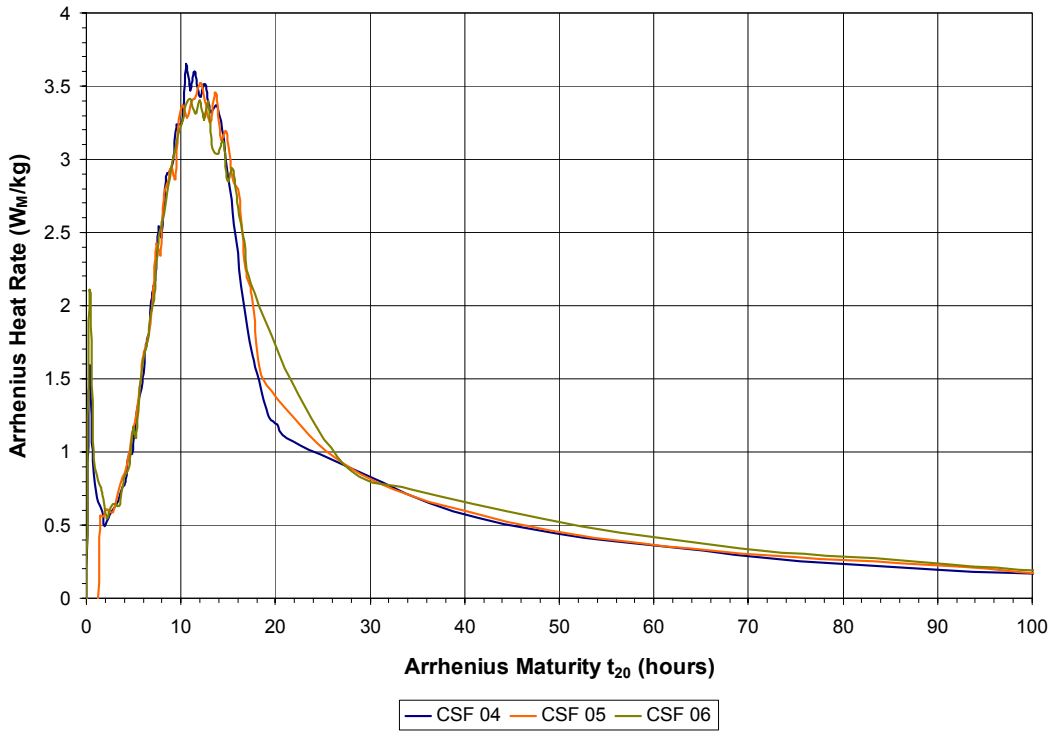

Figure 4.8. Maturity Heat Rate – CSF concretes

Figure 4.7 indicates that there is no significant difference between the three CSF concretes with different w/c ratios during the first 25 t_{20} hours, with respect to total heat liberated per kg. After roughly 25 t_{20} hours however, the three curves begin to diverge and the higher w/c CSF concretes produce a greater amount of total heat. When comparing the different w/c concretes, the difference in total heat liberated increases with a greater w/c ratio, i.e. $q_{0.6} - q_{0.5} > q_{0.5} - q_{0.4}$.

Figure 4.8 shows the maturity heat rate versus cumulative maturity for the three CSF concretes. In all three CSF test samples, trough 2 occurs at approximately the same t_{20} maturity. The dormant period associated with trough 2 also lasts for approximately the same t_{20} duration in each of the different CSF concretes. This suggests that the w/c ratio has a minimal effect on the heat evolution characteristics of a concrete containing CSF during the early stages of hydration.

The main exothermic peak, peak 3, occurs at approximately the same maturity in all three of the CSF concretes. Figure 4.8 indicates that a CSF concrete with a lower w/c ratio, produces a greater maximum exothermic heat rate peak, although the difference in this maximum between the CSF concretes, is very small. Peak 3 also decreases at a roughly uniform rate with an increasing w/c ratio, as shown in figure 4.18. This can be attributed to the fact that less binder is available to react with the water in the concrete mixture at the greater w/c ratios and can consequently contribute less to the heat evolution of the concrete.

The decrease in maturity heat rate during the post acceleration phase of hydration after peak 3 is more rapid in the CSF concretes with a lower w/c ratio. At approximately 50 t_{20} hours, the curves approach a minimum value at the same rate. There is almost no evidence of an additional exothermic peak due to the conversion of ettringite to monosulphate (peak 4 in figure 2.1.) and this is more apparent in the lower w/c CSF concretes.

4.5.6 Effect of Aggregate Type on Heat Characteristics

As mentioned, the effect of using three different commercially available 13.2 mm aggregates and corresponding crusher sands, namely granite, andesite and dolomite was also considered for this investigation. A w/c ratio of 0.6 was used for each of the mixtures and the results from the calorimeter tests are presented in figures 4.9 and 4.10.

It is evident from figures 4.9 and 4.10 that there is no noticeable effect on the total heat produced per kg of binder by concrete or the rate of heat evolution with respect to maturity for the similar concretes with different aggregate materials only. However, when figures 4.2 and 4.10 are compared, the maximum maturity heat rate for the w/c = 0.6 PC only concrete in figure 4.2 is less that of the different aggregate concretes shown figure 4.10.

The differences between figures 4.2 and 4.10 could be attributed to aggregate size, since 13.2 mm coarse aggregates were used here compared to the 9 mm aggregates used for the different binder type concretes. More heat energy is required to heat the larger aggregate particles since they occupy a larger volume. Consequently, the rate at which heat is liberated increases as more energy is used per unit mass. This is evident when comparing figures 4.2 and 4.10 where peak 3 for the concrete with the larger coarse aggregates produces a greater maximum heat rate. This however, is beyond the scope of this investigation, but is another possible research topic for the future.

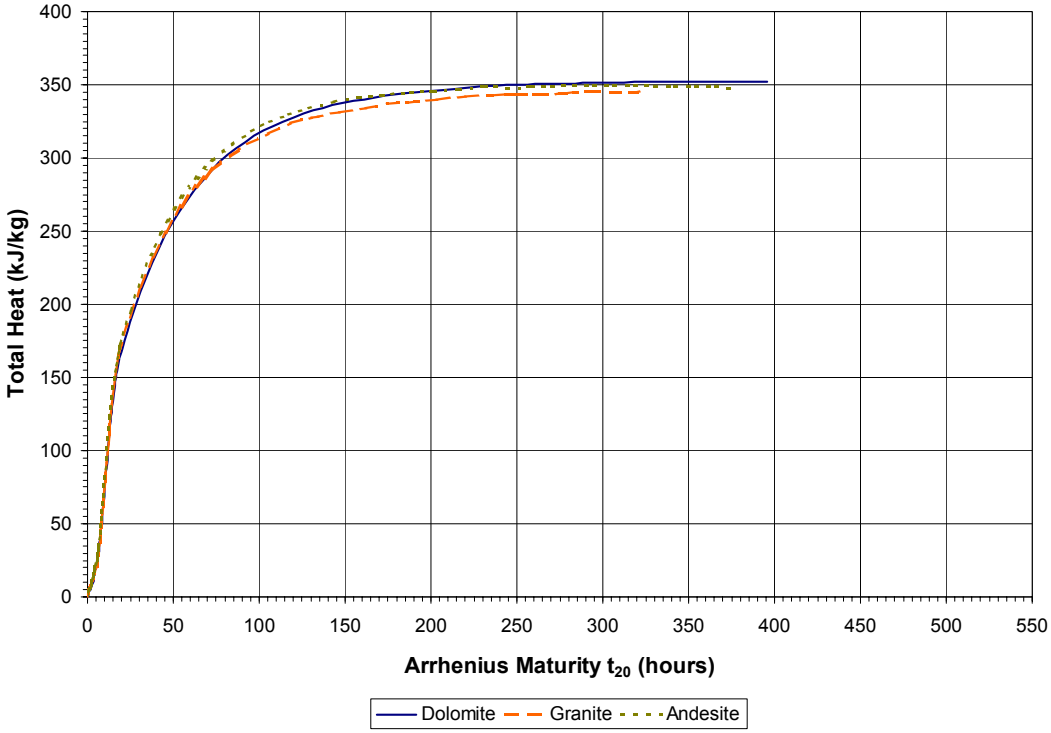

Figure 4.9. Total Heat – Different Aggregate Types

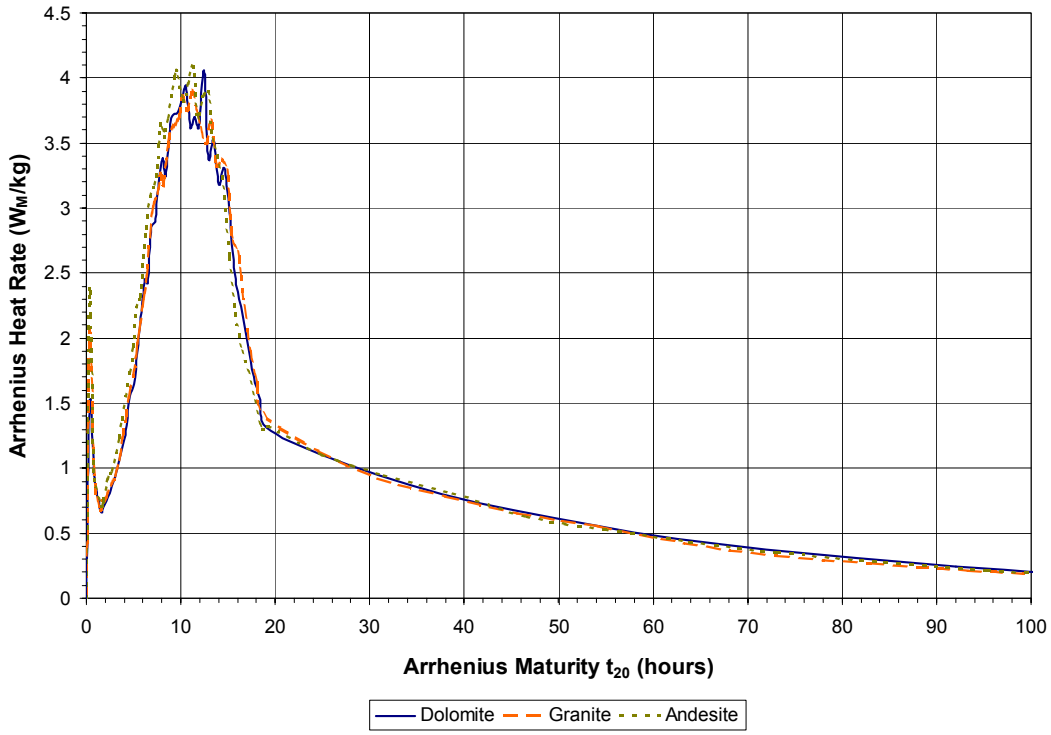

Figure 4.10. Maturity Heat Rate – Different Aggregate Types

4.6 Comparing the Results of Different Binders

4.6.1 Comparison between the GGBS Concretes and the PC Only Concretes

The calorimeter results for the GGBS concrete mixtures in figures 4.3 and 4.4 can be compared to figures 4.1 and 4.2 respectively for the PC only concrete mixtures. Figures 4.14 and 4.18 show the difference between maximum values of heat liberated and maturity heat rate for the different binder types. Additional graphs comparing the GGBS concretes to the PC only concretes for the different w/c ratios are shown in figure 4.11.

The following points can be noted with respect to total heat liberated versus maturity in figures 4.1, 4.3, 4.11 and 4.14:

- Initially the total heat versus maturity curves for the GGBS concretes have the same rate of change in total heat per unit mass as the PC only concretes for the corresponding w/c ratios. This trend is more significant in the concretes with a higher w/c ratio, i.e. the total heat curves begin to diverge at an earlier age for a higher w/c ratio.
- The GGBS concretes reach a maximum amount of heat liberated at a roughly the same t_{20} maturity as the PC only concretes. The GGBS concretes however, produce less heat per unit mass of binder during the later stages of hydration. This could be attributed to the smaller amount of cement in the binder material of the GGBS concretes and also possibly to the S-reaction contributing to the total heat liberated at a later stage.

The differences between the GGBS and PC only test results with regards to the maturity heat rate versus cumulative maturity in figures 4.2, 4.4, 4.11 and 4.18. The differences are discussed in terms of the major peaks and troughs that occur in the general heat rate curve for concrete as described in chapter 2 and shown in figure 2.1. The following observations are noted.

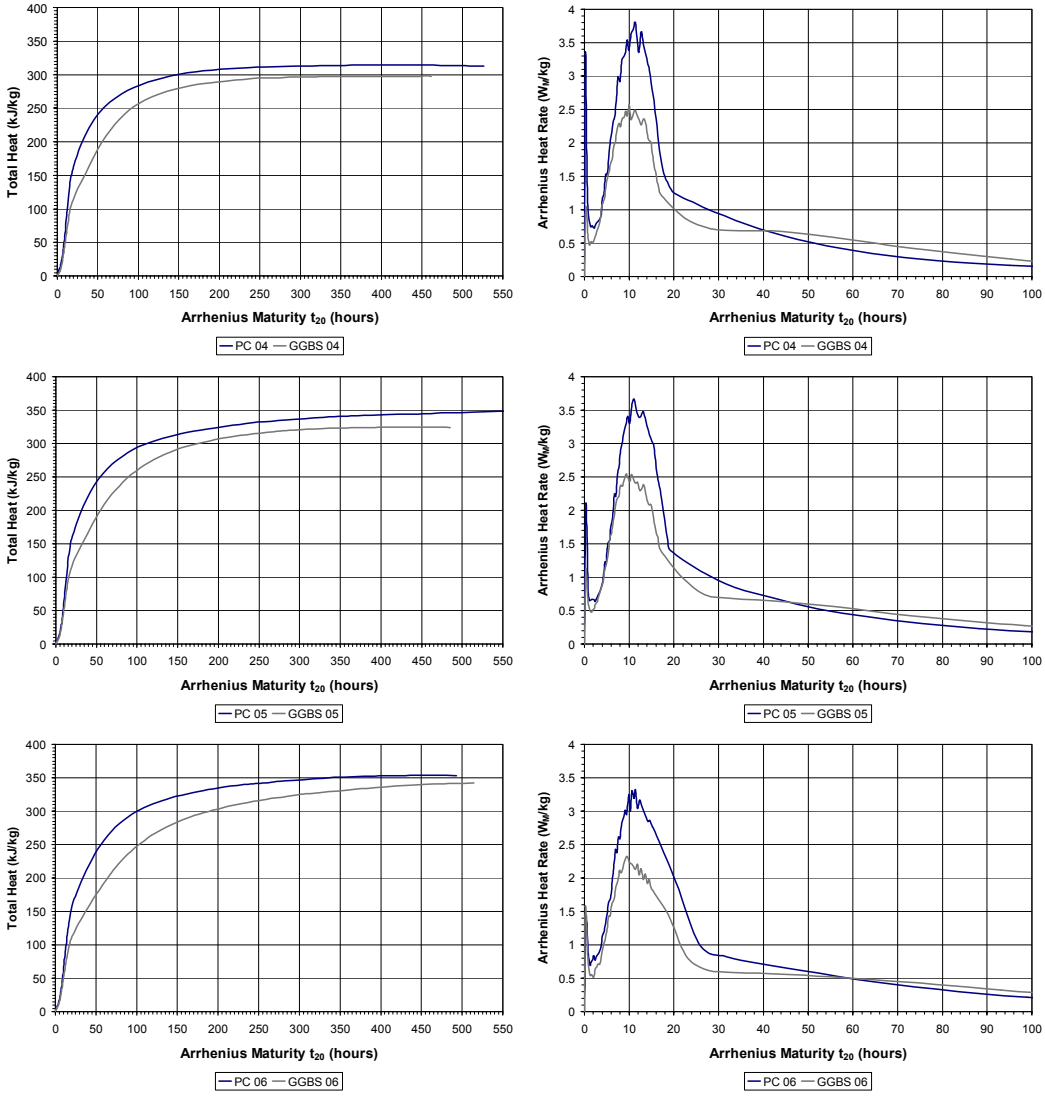

Figure 4.11. Total Heat and Maturity Heat Rate versus t_{20} Maturity – PC & GGBS comparison

Dormant Period and Trough 2. The minimum value of trough 2 is lowered by the presence of GGBS in the concrete mixture in comparison to the maturity heat rate values of trough 2 in the PC only concretes. This difference however is not very appreciable. The addition of GGBS appears to shorten the length of t_{20} hours over which the dormant period lasts, particularly in the concretes with a lower w/c ratio. The rate of increase in maturity heat rate after trough 2 is more gradual in the GGBS concretes than in the PC only concretes. This could be due to the lower amounts of cement present in the GGBS concretes. This trend is only significant in the lower w/c

concretes, which could be attributed to the decreased free water availability in the lower w/c concretes.

Peak 3. In general, the value of maximum exothermic peak in the maturity heat rate curves is much greater in the PC only concretes than in the GGBS concretes. As the w/c ratio increases, the peak heat rates of the GGBS and PC concretes tend towards the same value. This suggests that the effects of GGBS become less appreciable as the w/c ratio increases. Peak 3 also occurs at a slightly earlier t_{20} maturity in the GGBS samples compared to the PC only samples, and this difference in maturity is roughly the same for all w/c ratios. The PC only concretes experience a more rapid decrease in maturity heat rate than the GGBS concretes during the post acceleration stage of hydration before peak 4 is reached. This underlines the late hydration of the GGBS and the contribution of the S-reaction to the heat liberated.

Post-acceleration Stage and Peak 4. There is greater evidence of Peak 4 in the GGBS concretes than in the PC only concretes. This could be due to the effects of the S-reaction described by De Schutter (1998), as discussed earlier. The maximum value of peak 4 occurs at a later maturity in the GGBS concrete mixtures and it lasts for a longer time. The PC only concretes approach a minimum maturity heat rate more rapidly than the GGBS concretes and consequently reach a minimum value at an earlier t_{20} maturity. The differences between the GGBS and PC only concretes during the post acceleration stage of hydration become less significant as the w/c ratio increases.

4.6.2 Comparison between the FA Concretes and the PC Only Concretes

The calorimeter results for the FA concrete mixtures in figures 4.5 and 4.6 can be compared to those of the PC only concrete mixtures in figures 4.1 and 4.2 respectively. This illustrated in figure 4.12. Figures 4.14 and 4.18 also show the difference between maximum values of heat liberated and maturity heat rate for the different binder types.

The following can be noted with respect to total heat liberated from the curves shown in figures 4.1, 4.5 4.12:

- During approximately the first ten t_{20} hours, there is no appreciable difference in the change in total heat with respect to maturity between the FA concretes and the PC only concretes. Thereafter, the curves begin to diverge from one another rapidly with an increase in maturity.
- The samples containing FA approach the maximum amount of total heat liberated more gradually than the PC only samples. The maximum heat produced by the FA concretes is also substantially lower than that of the PC only concretes, and this trend increases as the w/c ratio increases.

With regard to the maturity heat rate curves in figures 4.2 and 4.6, the differences between the two sets of results are discussed in terms of the major peaks and troughs that occur in the general heat rate curve for concrete. This is discussed in detail in chapter 2 and shown in figure 2.1. By comparing figures 4.2, 4.6 and 4.12, the following can be noted.

Dormant Period and Trough 2. In general, trough 2 in the FA concretes has a lower minimum value than that of the corresponding PC only concretes and occurs at a later t_{20} maturity. This difference in trough 2 maturity heat rates appears to remain constant when comparing the FA and PC only concretes at corresponding w/c ratios. The dormant period also lasts for a longer time in the FA concretes compared to the PC only concretes. This suggests that the presence of FA extends the retardation of the alluminate phase slightly since trough 2 ends at a later age in the FA concrete mixtures. It also indicates that the presence of FA possibly delays the hydration of alite since the dormant period lasts for a greater t_{20} maturity in the FA concretes. The magnitude of the effect of FA on trough 2 however, is not significantly affected by the w/c ratio of the concrete in question.

Peak 3. Figures 4.2 and 4.6 show that the maximum maturity heat rate in the FA concretes is considerably lower than the maximum values seen in the PC only concretes. Peak 3 in the FA results also occurs at a later maturity than that of the

corresponding PC only concrete, which implies that the presence of FA reduces the rate of the hydration reactions. This delay in the occurrence of peak 3 is roughly constant for all w/c ratios. The presence of FA in the binder therefore reduces the maximum exothermic heat rate value quite markedly, and causes the main exothermic peak to occur at a later age. This could be useful in cases where there is a need to reduce the maximum heat rate experienced in a large concrete element and a need for this maximum to occur at an age where the concrete has developed enough tensile strain capacity to resist the possibility of through cracking. The magnitude of this difference in heat rate in the FA concretes increases with an increasing w/c ratio.

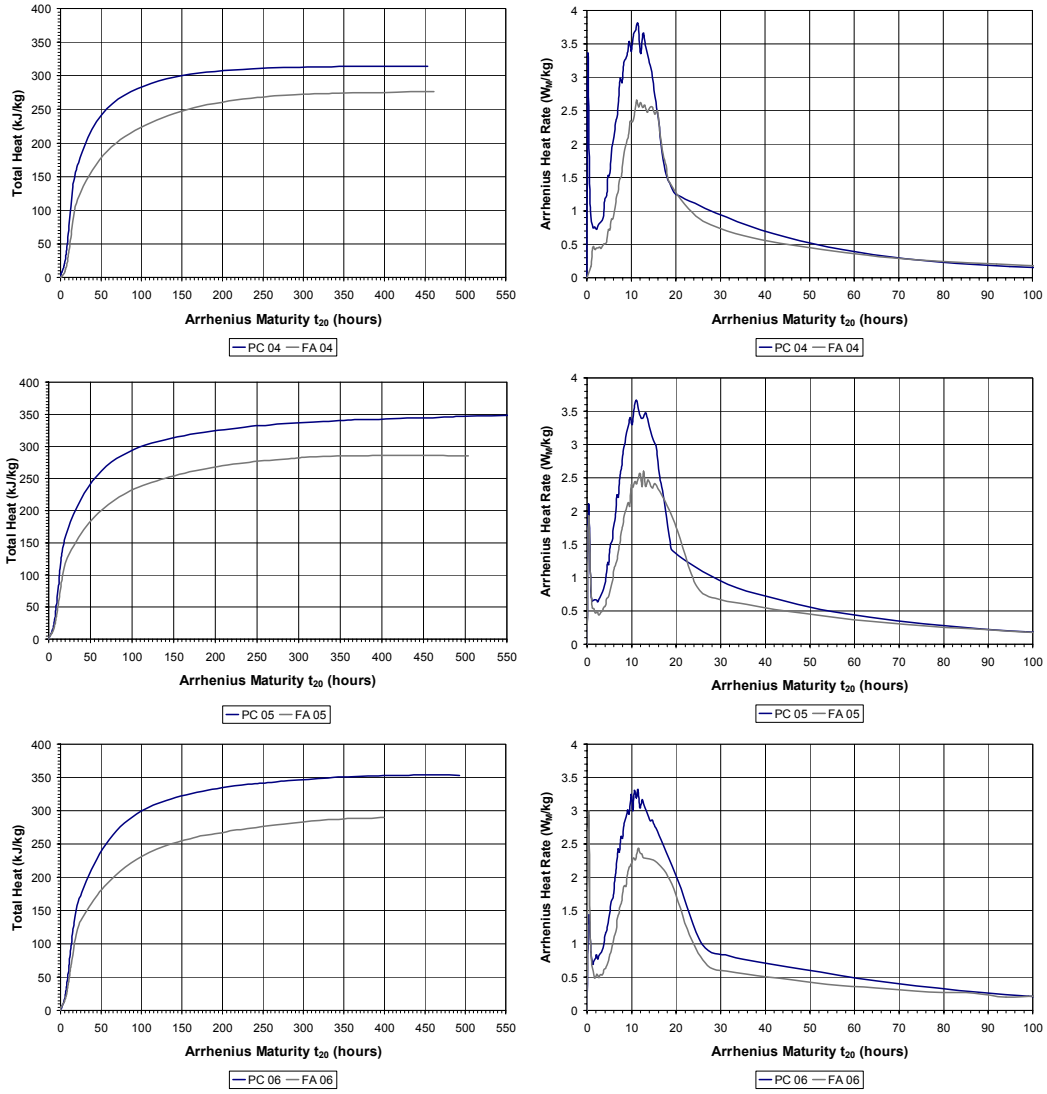

Figure 4.12. Total Heat and Maturity Heat Rate versus t_{20} Maturity – PC & FA comparison

Post-acceleration Stage and Peak 4. The presence of peak 4 is more significant in the PC only concretes compared to those containing FA in the binder, particularly at the higher w/c ratios. This suggests that the presence of FA reduces the secondary production of ettringite and the conversion to monosulphate usually associated with peak 4. This in turn could be due to the fact that FA consumes some of the Portlandite produced during cement hydration by the ferrite and alluminate phases. Peak 4 also occurs at a later t_{20} maturity in the FA concretes compared to the PC only concretes. Thereafter however, the decrease in maturity heat rate of both the FA and PC concretes is roughly the same. The point at which the decrease in heat rate becomes the same in the respective PC and FA concretes occurs later in the higher w/c concretes.

4.6.3 Comparison between the CSF Concretes and the PC Only Concretes

The adiabatic calorimeter results for the PC only concrete mixtures in figures 4.1 and 4.2 can be compared to those of the CSF concrete mixtures in figures 4.7 and 4.8 respectively. A set of graphs individually comparing the CSF concretes to the PC only concretes for the different w/c ratios can be found in figure 4.13. The difference between maximum values of heat liberated and maturity heat rate for the different binder types are shown in figures 4.14 and 4.18.

When figures 4.1, 4.7 and 4.13 are examined and the results of CSF concretes are compared to the results of the PC only concretes with respect to total heat liberated, the following points can be noted:

- The rate of change of total heat with respect to maturity is initially the same for both the PC only and CSF concretes during approximately the first 30 t_{20} hours. The curves start to diverge from one another during the acceleration phase of hydration. The concrete mixtures with the lower w/c ratios begin to diverge at an earlier maturity than those with a higher w/c ratio.
- After the curves for the PC only and CSF concretes have begun to diverge, the rate of increase of total heat liberated is, in general, more gradual in the PC only samples than in the CSF samples. The overall total heat produced per

kg of binder, is also less in the CSF concretes and it is reached at an earlier t_{20} maturity. However, there is no specific trend for the difference in maximum total heat at the corresponding maturity between the PC only and CSF concretes with respect to different w/c ratios.

The differences between the curves of maturity heat rate versus t_{20} maturity in figures 4.2, 4.6 and 4.13 are discussed in terms of the major peaks and troughs that occur in the general heat rate curve for concrete. As mentioned, this is discussed in detail in chapter 2 and shown in figure 2.1. The following points can be noted.

Dormant Period and Trough 2. In general, the minimum maturity heat rate at trough 2 is lower in the CSF concretes than in the PC only concretes. This difference is approximately the same (0.1 W_M/kg) when comparing the results of the CSF samples and the PC only samples with corresponding w/c ratios. The minimum of trough 2 also occurs roughly one t_{20} hour later in the CSF concretes compared to the PC only concretes. The dormant period however, lasts for approximately the same length of t_{20} hours in the CSF and PC only concretes. This suggests that although the presence of CSF delays the onset of the dormant period, it does not affect its duration and therefore does not extend the retardation of the hydration reactions any further.

Peak 3. The rate of increase of maturity heat rate approaching peak 3 is roughly the same in the corresponding CSF samples and PC only samples despite the acceleration phase beginning slightly later in the CSF concretes. Peak 3 therefore occurs at a later maturity in the CSF concretes than in the corresponding PC only concretes. In the w/c = 0.4 results, peak 3 is greater in the PC concrete than in the CSF concrete. The same is true for the w/c = 0.5 tests, although the difference in peak 3 maxima is less compared to that for the w/c = 0.4 concretes. In the w/c = 0.6 concretes however, peak 3 is greater in the CSF concrete than in the PC only concrete. Desiccation of the CSF in the lower w/c pastes could account for this discrepancy. The higher w/c CSF concretes have a greater access to water for the continued hydration of both CSF and PC.

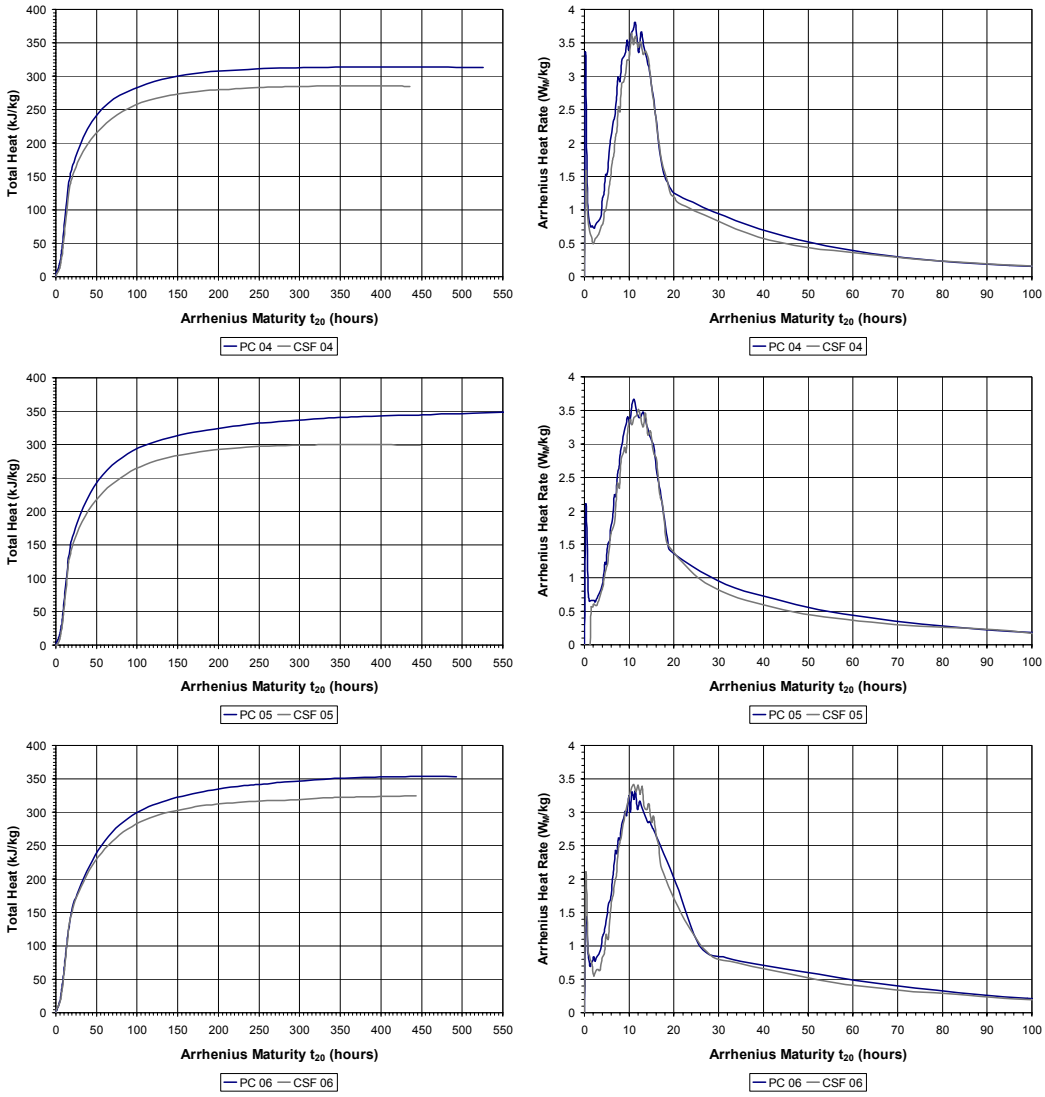

Figure 4.13. Total Heat and Maturity Heat Rate versus t_{20} Maturity – PC & CSF comparison

Post-acceleration Stage and Peak 4. The CSF concretes show no signs of the presence of a fourth exothermic peak in the maturity heat rate compared to the PC only concretes. This suggests that the presence of CSF significantly retards the production of secondary ettringite and its conversion to monosulphate during the post-acceleration stage. This could be due to the fact that CSF consumes some of the Portlandite produced during cement hydration. This trend is equally noticeable in all three w/c ratios. Once peak 4 has passed, the PC only and CSF curves converge again and decrease towards a minimum maturity heat rate together.

4.6.4 Comparison between the Different w/c Ratios for Different Binders

This section discusses the effects that the three extenders, namely GGBS, FA and CSF, have on the concrete samples tested with different w/c ratios. The results can be seen figures 4.14 to 4.21. These figures show total heat and maturity heat rate versus t_{20} maturity.

Figures 4.14 and 4.21 show the maximum heat liberated at 400 t_{20} hours and the maximum maturity heat rate for the different w/c ratios tested. A linear regression line was fitted to each set of results and from this, the coefficient of determination (R^2) was calculated. The R^2 value is an indication of the degree to which the fitted regression line is in agreement with the actual results obtained, i.e. it is the proportion of variability of the results. R^2 always lies between zero and one. The closer the value is to one, the more accurately the fitted line represents the results (Montgomery et al, 2004). Both the change in maximum total heat (at 400 t_{20} hours) and maximum maturity heat rate (peak 3) vary approximately linearly with respect to the w/c ratio, since the R^2 values of the fitted linear regressions are all greater than 0.9. Such a trend could be used in the prediction of the heat evolution characteristics of a binder with respect to the w/c ratio.

The Effects on Total Heat Liberated

The results of total heat versus t_{20} maturity of the three different w/c ratios for the different binder types, can be seen in figures 4.14 to 4.17. From these graphs, the following points can be noted.

Initially during approximately the first 20 t_{20} hours the total heat versus maturity curves follow one another closely. This suggests that the binder type and w/c ratio have a negligible effect on the total heat liberated during the early stages of hydration.

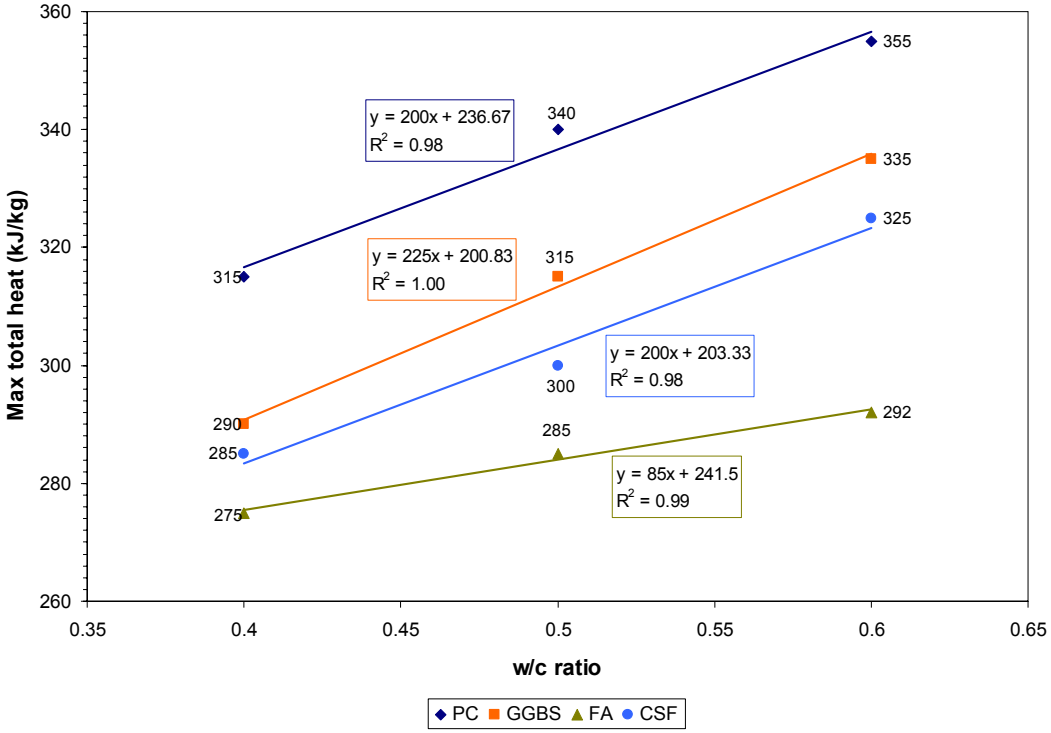

Figure 4.14. Total Heat liberated at 400 t_{20} hours for different extenders

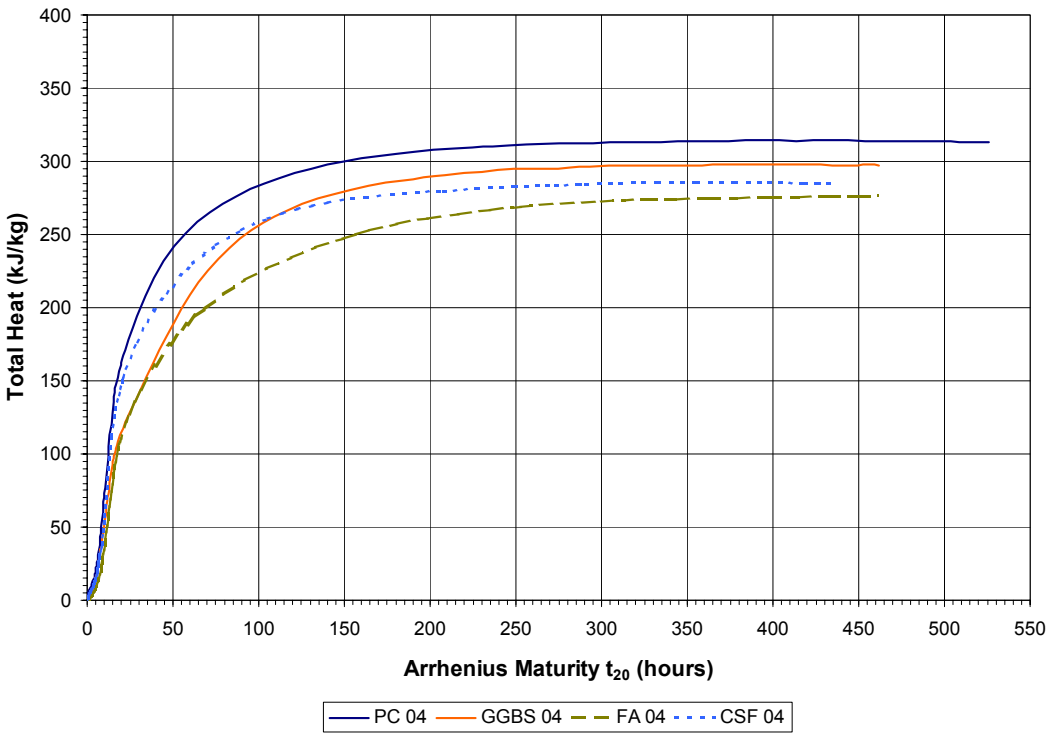

Figure 4.15. Total Heat – Different Binders w/c = 0.4

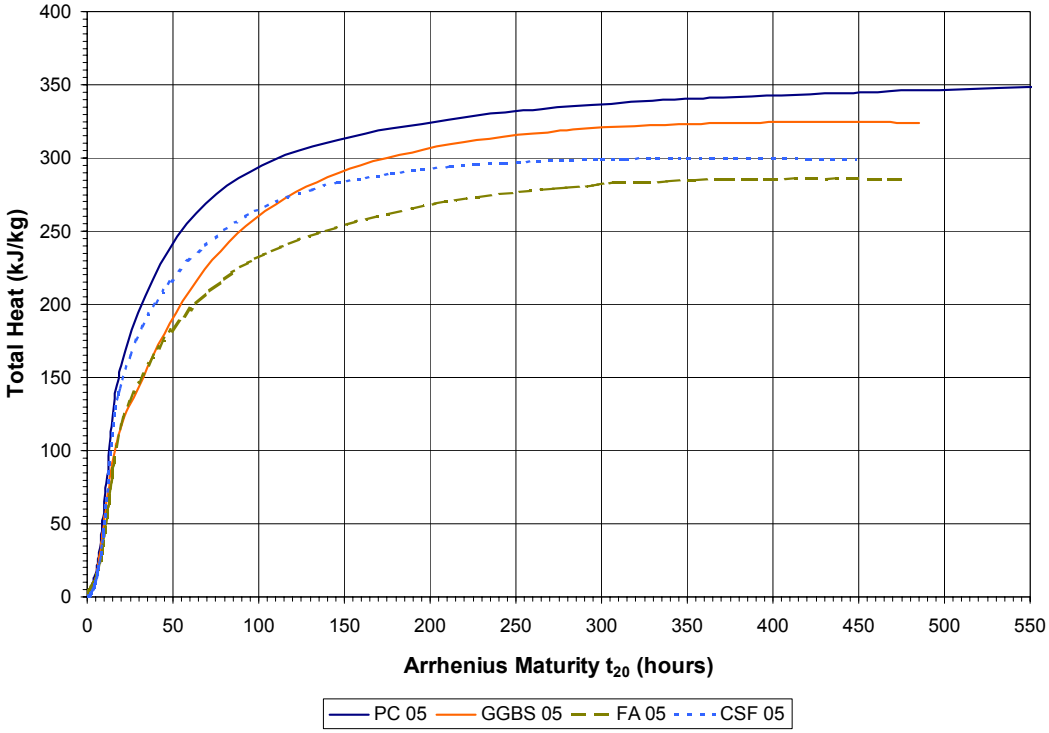

Figure 4.16. Total Heat – Different Binders w/c = 0.5

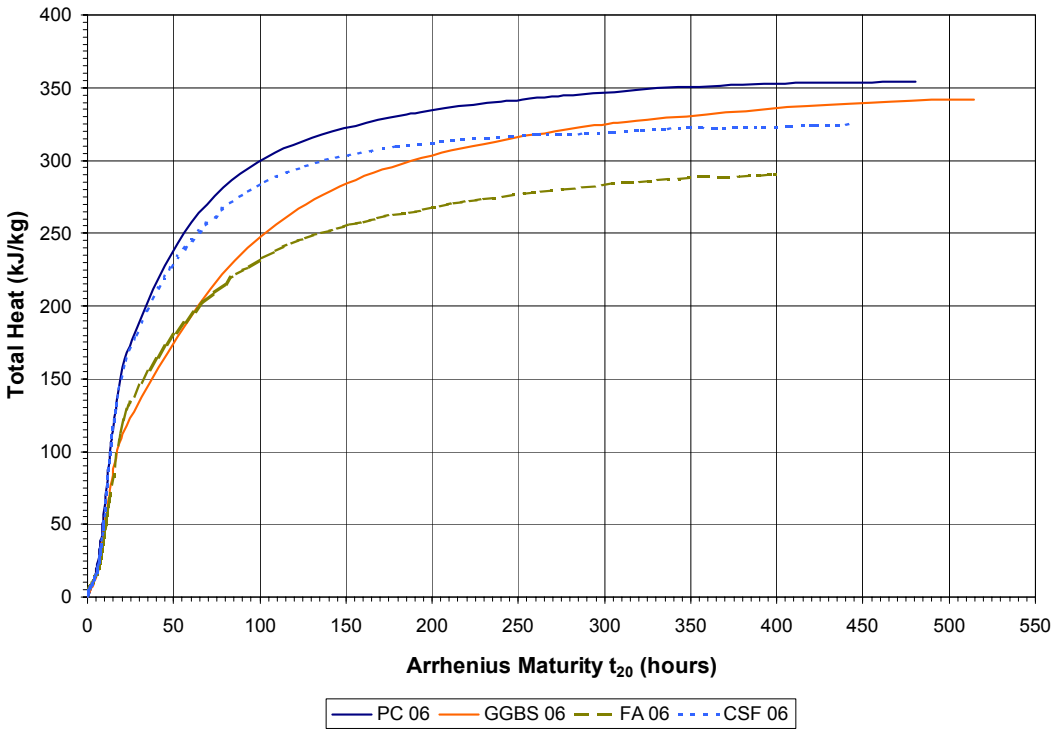

Figure 4.17. Total Heat – Different Binders w/c = 0.6

At 400 t_{20} hours, it is evident that $q_{FA} < q_{CSF} < q_{GGBS} < q_{PC}$. It can be expected that the FA concretes liberate less heat per unit mass of binder than the CSF concretes, which in turn produces less heat than the PC only concretes, since there is a greater amount of cement per kilogram in the CSF and PC only binders. Applying this idea, it would then be expected that the GGBS concretes would produce the least amount of heat, since they contain the smallest percentage of cement in the binder material. Figures 4.15 to 4.17 illustrate that this is not the case. This could be attributed to the delayed nature of the GGBS hydration and the contribution of S-reaction during the later stages of hydration.

The FA concretes tend to produce the least amount of total heat and generally have the slowest rate of increase in total heat with respect to maturity as the curves approach the maximum values. As the w/c ratio increases, this trend becomes more pronounced.

The FA and GGBS curves follow one another very closely until approximately 40 t_{20} hours. Thereafter the curves diverge and the GGBS concretes produce more heat that the corresponding FA concretes. This is roughly the point where the S-reaction begins to contribute to the heat liberated by the GGBS concretes, increasing the total heat produced.

The curves for the CSF concretes follow those of the PC only concretes more closely than any of the other results. The CSF concrete samples however, produce less heat since CSF uses up a portion of the portlandite hydration product. This consequently reduces the amount of secondary ettringite and monosulphate produced. The point where the CSF and PC only curves begin to diverge corresponds approximately to the time in the deceleration phase where secondary ettringite and monosulphate are usually produced.

From the slopes of the regression lines in figure 4.14, the following points are evident:

- The presence of CSF does not affect the sensitivity of the amount of heat liberated per unit mass of binder, with respect to a change in the w/c ratio, i.e., the slope of the CSF regression line is the same as that of the PC only line.
- The GGBS concretes are the most sensitive with respect to total heat produced for different w/c ratios.
- The FA concretes are the least sensitive to changes in the w/c ratio.

The above implies that, adherence to the concrete mixture design parameters pertinent to the w/c ratio, is important when GGBS is used as a binder replacement material, and heat of hydration effects are critical with regards to thermally-induced cracking. Conversely, the use of FA reduces the sensitivity of the concrete mixture to variation in the w/c ratio. This could be important when quality control is difficult to maintain on a construction site.

The Effects on the Maturity Heat Rate

The results of maturity heat rate versus t_{20} maturity are displayed in figures 4.18 to 4.21. The effects of the presence of the extenders at different w/c ratios on the maturity heat rate can be noted from these figures. These results are compared in terms of the stages of hydration discussed in detail in chapter 2 and shown in figure 2.1. Peak 1 is ignored in the discussion, as explained earlier.

Dormant Period and Trough 2. The minima of trough 2 occur at the earliest maturity in the PC only and GGBS concretes and are seen progressively later in the CSF and FA concretes respectively. The FA concretes also have the lowest minimum value at trough 2, followed by the GGBS, CSF and PC concretes respectively. This indicates that the dormant period and the retardation of the alluminate hydration is greater in the FA and CSF concretes than in the GGBS and PC only concretes. The rate of increase in maturity heat rate approaching peak 3 is greatest in the PC and CSF concretes and slowest in the GGBS and FA concretes respectively. This suggests that the presence of the extenders slows the rate of the hydration reactions before the acceleration stage begins.

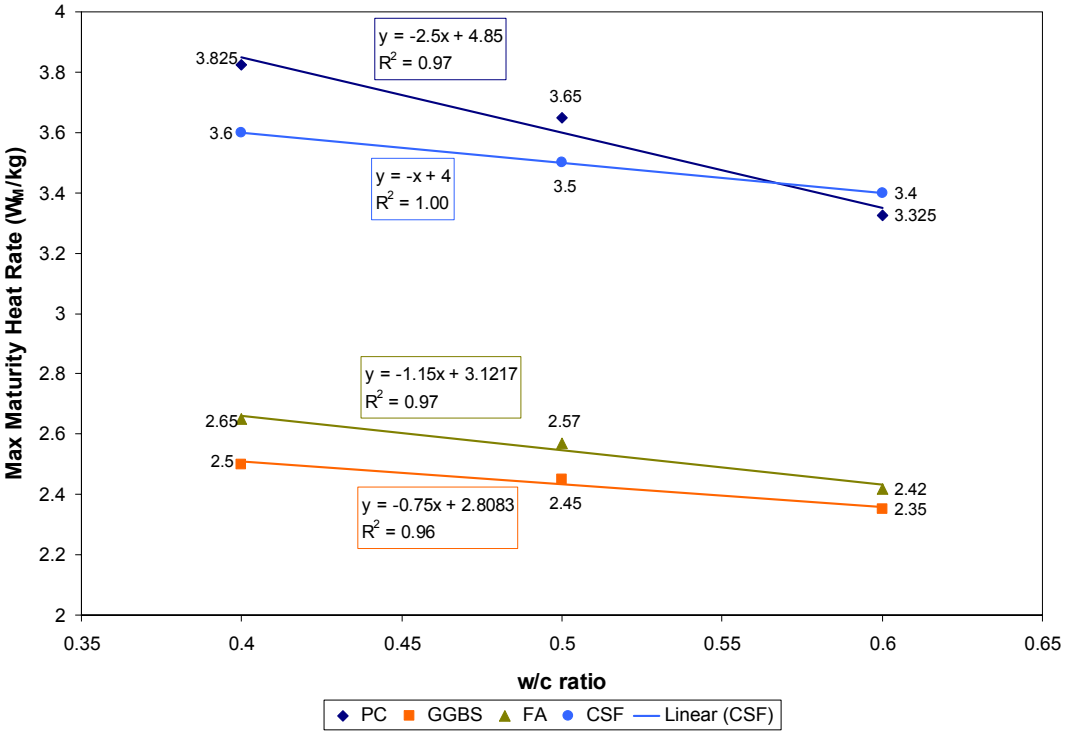

Figure 4.18. Maximum Maturity Heat Rate (peak 3) for different extenders

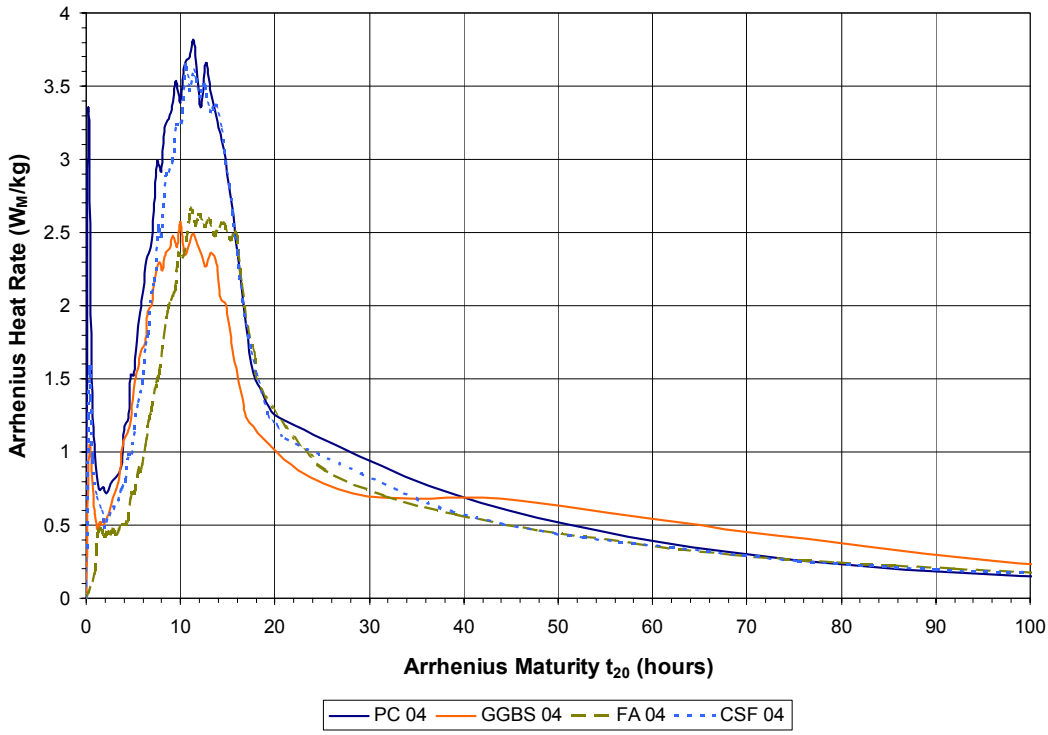

Figure 4.19. Maturity Heat Rate – Different Binders w/c = 0.4

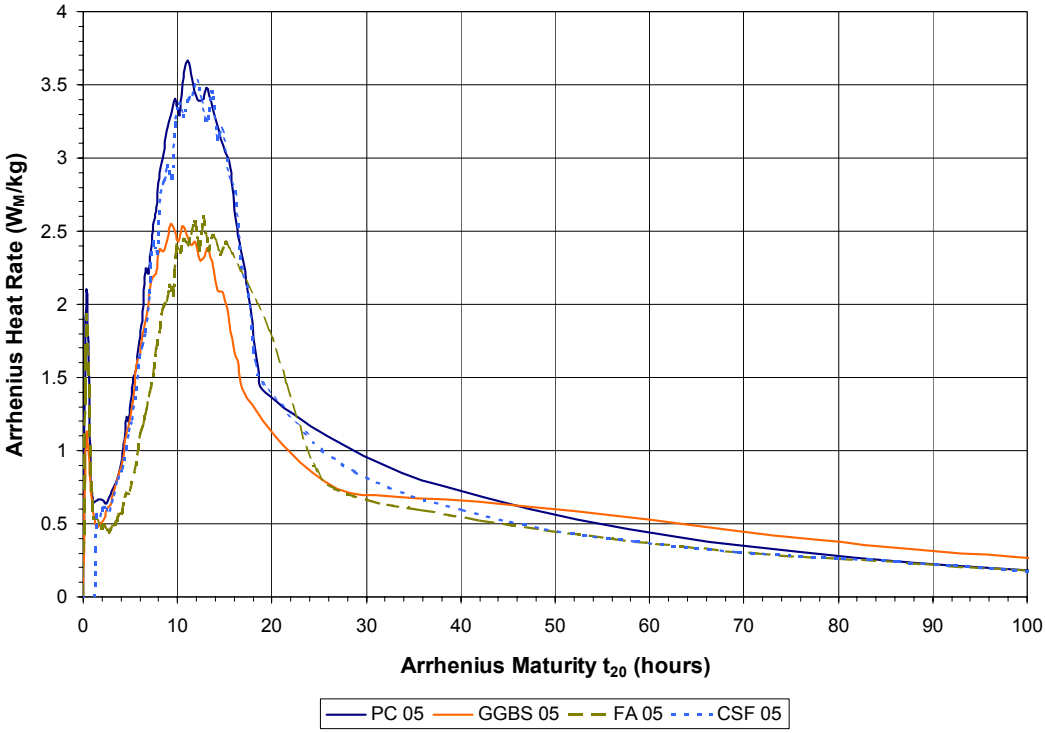

Figure 4.20. Maturity Heat Rate – Different Binders w/c = 0.5

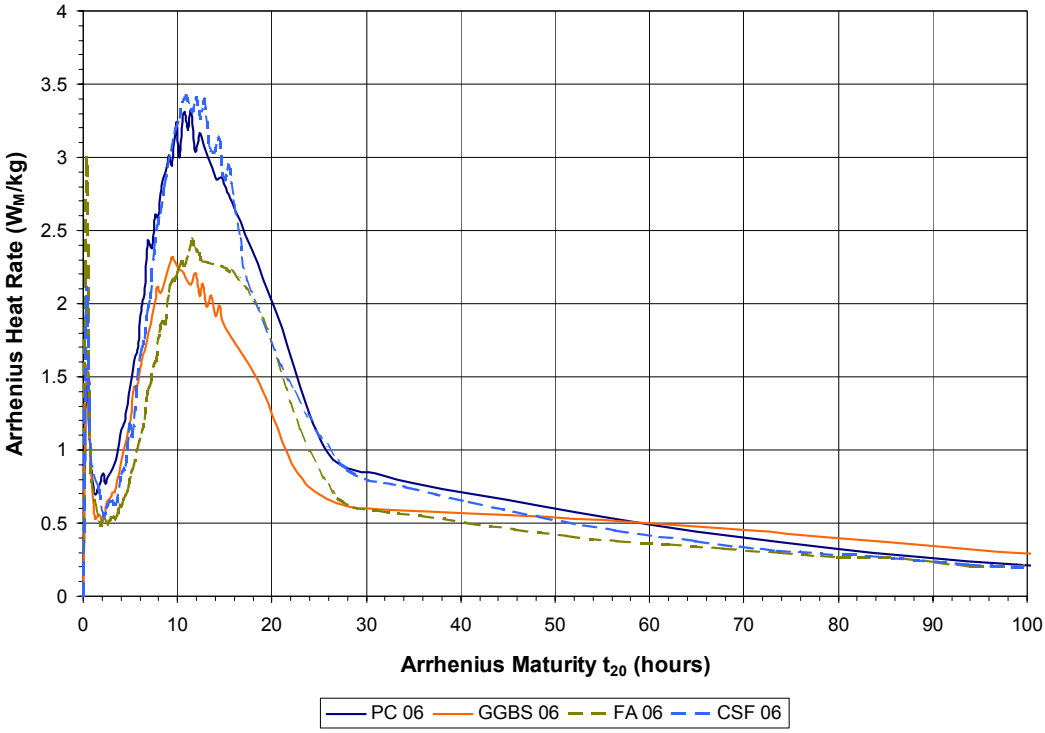

Figure 4.21. Maturity Heat Rate – Different Binders w/c = 0.6

Peak 3. The only extenders that significantly affect the maximum exothermic peak are FA and GGBS. The difference between PC only and CSF concretes with respect to peak 3 is negligible, both in terms of magnitude, and in terms of the t_{20} maturity at which peak 3 occurs. The GGBS and FA concretes produce significantly lower maturity heat rate peaks in the end of the acceleration stage, and the peaks of the FA concretes occur at a later maturity than the other samples.

Post-acceleration Stage and Peak 4. Peak 4 is the most pronounced in the GGBS concretes due to the effects of the S-reaction discussed in chapter 2. In all of the CSF concretes, there is almost no evidence of peak 4 occurring. In all cases, peak 4 occurs at the earliest maturity in the PC only concretes followed by the FA and GGBS concretes respectively. These trends are less significant as the w/c ratio increases.

With all of the different binder types, as the w/c ratio increases, the rate of increase and decrease of the maturity heat rate with t_{20} maturity becomes more similar across the four different sets of results. This suggests that as the w/c ratio is increased, the effects of cement extenders on the heat evolution characteristics of a concrete is less significant. From figure 4.18, it can also be noted that the presence of any of the cement extenders in the binder material reduces the sensitivity of the maximum maturity heat rate with changes in the w/c ratio. GGBS and FA appear to be the least sensitive in this regard.

4.7 Summary and Conclusions

Ballim and Graham (2003) showed how the heat rate curve for a concrete mixture could be normalised so that the results obtained can be described independently of initial casting temperature. This is achieved by expressing the clock time in terms of an equivalent age or maturity and the rate of heat evolution as a maturity heat rate. They further showed that the Arrhenius equation is the most suitable function for this purpose.

In general, the following points regarding the calorimeter test results obtained can be noted:

- The higher the w/c ratio, the greater the amount of heat liberated per unit mass of binder.
- The higher the w/c ratio the lower value of the main exothermic heat rate peak.
- The w/c ratio has a negligible effect on the maturity at which the exothermic heat rate peaks and troughs occur.
- The change in the maxima of total heat and maturity heat rate vary approximately linearly with respect to a changing w/c ratio.
- Aggregate type has no significant effect on the heat evolution characteristic of concrete. The size of coarse aggregate used however, could potentially affect the rate of heat evolution and the amount of heat liberated.

From the PC only concretes it was shown that, a decrease in the w/c ratio results in a lower maximum in the total heat liberated per kilogram of binder. There is also an increase in the main exothermic heat rate peak and a quicker rate at which both maximum values are approached in the lower w/c ratios. The same trends were noticeable in the CSF concrete test results. The PC only concretes with a greater w/c showed increased signs of monosulphate conversion from ettringite in the later stages of hydration. This could be attributed to a greater availability of free water in the higher w/c concretes during the later stages of hydration.

The results from the GGBS concretes suggested that the greater the w/c ratio the greater the maximum total heat produced, as was the case with the PC only concretes. The difference in total heat produced between the different w/c ratio concretes is greater in the GGBS results compared to the PC only results. This suggests that the presence of GGBS makes the concrete more sensitive to changes in the w/c ratio with respect to the heat evolution characteristics. The presence of GGBS seemed to normalise the maturity heat rate to an extent, causing there to be no significant differences between the maximum heat rates of different GGBS concretes. The main exothermic peak occurs at a later maturity in the GGBS concretes compared to the PC only concretes. The presence of GGBS also causes a substantial increase in peak 4 in

the hydration process. This is due to the effects of the S-reaction described by De Schutter (1998). This effect was greater as the w/c decreased.

The FA concretes indicate that as the w/c ratio decreases, both the total heat produced and the maximum maturity heat rate observed decrease. This trend however, is not as significant in the FA concretes as it is in the other test results, suggesting that the presence of FA tends towards normalising the heat evolution characteristics of a concrete. There are also no measurable signs of ettringite conversion to monosulphate in the presence of FA.

The use of GGBS or FA would be preferable to PC only or CSF when considering the heat evolution characteristics of a concrete. GGBS and FA reduce the maximum heat rate achieved and show a more gradual changes in the rate of heat evolution compared to the PC only and CSF concretes. This could aid designers in choosing a concrete mixture with a reduced temperature gradient across and through the section. This in turn will reduce the tendency towards thermally induced cracking. FA has the added benefit of delaying the occurrence of the main exothermic heat rate peak. The FA concretes also appear to be less sensitive to changes in the w/c ratio than the GGBS concretes. By delaying this occurrence of peak 3, the concrete tensile resistance has more time to develop and thus the possibility of thermally induced cracking is possibly reduced.

4.8 Chapter References

Ballim, Y. and Graham, P.C. (2003) A Maturity Approach to the Rate of Heat Evolution in Concrete. *Magazine of Concrete Research*, vol. 55, no. 3, Thomas Telford, London, UK, pp. 249-256.

Bamford, C.H. and Tipper, C.F.N. (1969) The Practice of Kinetics. In: *Comprehensive Chemical Kinetics*, vol. 1, Elsevier Publishing, New York, USA, pp. 404.

Copeland, L.E. and Kanto, D.L. (1972) Chemistry of hydration of Portland cement at ordinary temperatures. In: Taylor, H.F.W. (ed.) *The chemistry of cements volume 1*, Academic Press, New York, USA, pp. 313-370.

De Schutter, G. (1998) Hydration and temperature development of concrete made with blast-furnace slag cement, *Cement and Concrete Research* 29 (1999), Pergamon Publishing, pp. 143-149. Retrieved April 2004, from http://www.sciencedirect.com.

Graham, P.C. (2003) *The heat evolution characteristics of South African cements and the implications for mass concrete structures*. Ph.D. Thesis, University of the Witwatersrand, Johannesburg, South Africa.

Graham, P.C. and Ballim, Y. (2003) *Early-age heat evolution characteristics of South African cements in relation to clinker chemistry and crystallography*. Proceedings of the 11th International Congress on the Chemistry of Cement (ICCC). Grieve, G and Owens, G (ed). Durban, South Africa.

Holman, J.P. (1997) *Heat Transfer 8th Edition*, McGraw-Hill, New York, USA, pp. 1-6.

Kishi, T., Shimomura, T. and Maekawa, K. (1993) Thermal crack control design of high performance concrete, in the *Proceedings of Concrete 2000*, Dundee, Scotland, E&FN Spon, London, UK, pp. 447-456.

Maekawa, K., Chaube, R. and Kishi, T. (1999) Multicomponent model for the heat of hydration of Portland cement. *Modelling of Concrete Preformance: Hydration, microstructure formation and mass transport*, Routledge, New York, USA, pp. 178-248.

Montgomery, D.C., Runger, G.C. and Hubele, N.F. (2004) *Engineering Statistics 3rd Edition*, John Wiley & Sons, Inc., New York, USA, pp. 261-315.

Ramachandran, V.S., Paroli, R.M., Beaudoin, J.J. and Delgado, A.H. (2003) Supplementary cementing materials and other additions. In: *Handbook of thermal analysis of construction materials*, Noyes Publications/William Andrew Publishing, Norwich, USA, pp. 293-319.

Waller, V., d'Aloïa, L. Cussigh, F. and Lecrux, S. (2004) Using the maturity method in concrete crack control at early ages, *Cement and Concrete Composites*, vol. 26, issue 5, Elsevier Science Ltd., pp. 589-599. Article still in press at the time of retrieval. Retrieved November 2003, from http://www.sciencedirect.com

Wang, C.H. and Dilger, W.T.T (1995) Prediction of Temperature Distribution in Hardening Concrete. In: Springenschmid, R. (ed.) *Thermal Cracking in Concrete at Early Ages: Proceedings from RILEM Symposium 25, Munich 1994*, E & FN Spon, London, UK, pp. 21-28.

Chapter 5

MATURITY HEAT RATE MODEL

5.1 Introduction

In order for engineers to design concrete structures with a minimum risk of thermally induced cracking, there is a need for a reliable prediction of the heat evolution characteristics of the concrete used and the transfer of heat through the concrete element under consideration. With such tools, engineers and designers could optimise the design of large concrete elements with respect to concrete mixture constituents, element size, cooling systems, sequential placing of concrete etc., without the need for costly and time-consuming laboratory tests.

This chapter focuses on the development of a maturity heat rate model that can be used to predict results similar to those obtained for this investigation in chapter 4. The model is based on the heat of hydration produced by the individual crystalline phases present in cement, and attempts are made to account for variations in the relative phase amounts and the effects of different w/c ratios. Work done by Kishi et al. (1993) and Maekawa et al. (1999) has shown reasonable accuracy in predicting the rate of heat evolution of concrete with respect to time. Graham (2003) was able to apply this work to his research with reasonable success. The model developed as a part of this study is based on the work of Maekawa et al. (1999) and attempts to build on the modifications proposed by Graham (2003).

The work covered in this chapter is divided into three parts:

1. A description of the heat of hydration model developed by Maekawa et al. (1999) and a discussion of the aspects of the model relevant to this research.
2. The development and calibration of a maturity heat rate model based on the results of laboratory tests conducted on concrete samples in an adiabatic calorimeter.
3. Verification of the results produced by the maturity heat rate model.

5.2 Multi-Component Heat of Hydration Model (Maekawa et al., 1999)

5.2.1 Basis of the Heat of Hydration Model

The heat of hydration model developed by Maekawa et al. (1999) was based on the work originally done by Suzuki et al. (1990). The model attempts to describe the heat liberated during cement hydration in terms of the individual reactions of the major crystalline phases. The rate of heat evolution of each of the pure clinker components is combined depending on the percentage of the phase present in the cement and the amount of free water available for hydration. These individual heat rates are described using two material functions developed by Maekawa et al. (1999). The first function is a reference heat generation rate at a specified constant temperature and the second function is referred to by the authors as the *thermal activity* of the cement phase in question. The thermal activity helps describe the temperature-dependent nature of the individual reactions of each crystallographic phase.

The Maekawa et al. (1999) model considers the heat produced due to the following reactions of the individual mineral phases and binder components with water:

- The formation of ettringite from C_3A and C_4AF during the early stages of hydration.
- The hydration of the four main phases, namely C_3S, C_2S, C_3A and C_4AF, after the dormant period.

- The conversion of ettringite (AFt) to monosulphate (AFm) during the post acceleration stage of hydration.
- The effects of GGBS, FA and superplasticisers in the heat of hydration of cement.

Using the same notation as used by Maekawa et al. (1999), the total heat liberated during hydration is expressed as the sum of the heat liberated from each of the individual components taking part in the process:

$$H_c = \sum p_i H_i \tag{5.1}$$

Where:

H_c = the rate of heat evolution of the entire cement/binder

p_i = the mass ratio of the ith component present in the binder, determined using the Bogue Calculations (see equations 3.1 to 3.4, chapter 3)

H_i = rate of heat evolution of the ith component

The rate of heat evolution of each of the individual components involved in the hydration reactions is calculated using equation 5.2:

$$H_i = \gamma \beta_i \lambda \mu s_i H_{i,T_0}(Q_i) \cdot \exp\left[-\frac{E_i}{R}\left(\frac{1}{T} - \frac{1}{T_0}\right)\right] \tag{5.2}$$

Where:

γ = a coefficient allowing for the delaying effects of FA and superplasticisers

β_i = a coefficient allowing for the reduction of the heat rate due to the decrease in the amount of available water for reaction and available space for hydration products to fill

λ = A coefficient accounting for the change in heat rate due to a reduction of CH in concrete with either GGBS or FA present

μ = a coefficient accounting for the changes in heat rate due to different mineral compositions of the phases

s_i = a coefficient accounting for variations in cement fineness

$H_{i,T0}(Q_i)$ = the reference heat rate of the ith component at a constant temperature T_0

E_i = the activation energy of the ith component

R = the universal gas constant = 8.314 J/mol°C

T = the concrete sample absolute temperature at the time in question

Q_i is the accumulated heat of the ith component over time and is related to H_i in the following equation:

$$Q_i = \int H_i dt \quad \text{Or} \quad H_i = q_i = \frac{dQ_i}{dt} \tag{5.3}$$

Maekawa et al. (1999) define $-E_i/R$ as the thermal activity of the ith crystallographic phase and the reference temperature T_0 as 293 K (= 20°C).

For the purposes of this investigation however, an attempt was only made to develop a model for predicting the rate of heat evolution of a concrete sample without any extenders or superplasticisers present. An attempt is made to develop a general model that is applicable to cements with different w/c ratios. Equation 5.2 can therefore be simplified as follows:

$$H_i = \beta_i \mu s_i H_{i,T_0}(Q_i) \cdot \exp\left[-\frac{E_i}{R}\left(\frac{1}{T} - \frac{1}{T_0}\right)\right] \tag{5.4}$$

The process of hydration is divided into three distinct stages shown in figure 5.1, which are similar to those discussed in chapter 2. It is assumed that ettringite is formed from the alluminate and ferrite phases from the outset and ends once the dormant period has passed. The hydration of the four major phases then takes place, dominated by the reactions involving the alite present. Once the main exothermic peak has passed, the conversion of ettringite to monosulphate begins. The conversion ends roughly at the transition between stages 2 and 3 below. From Stage 3 onwards the hydration process becomes diffusion controlled.

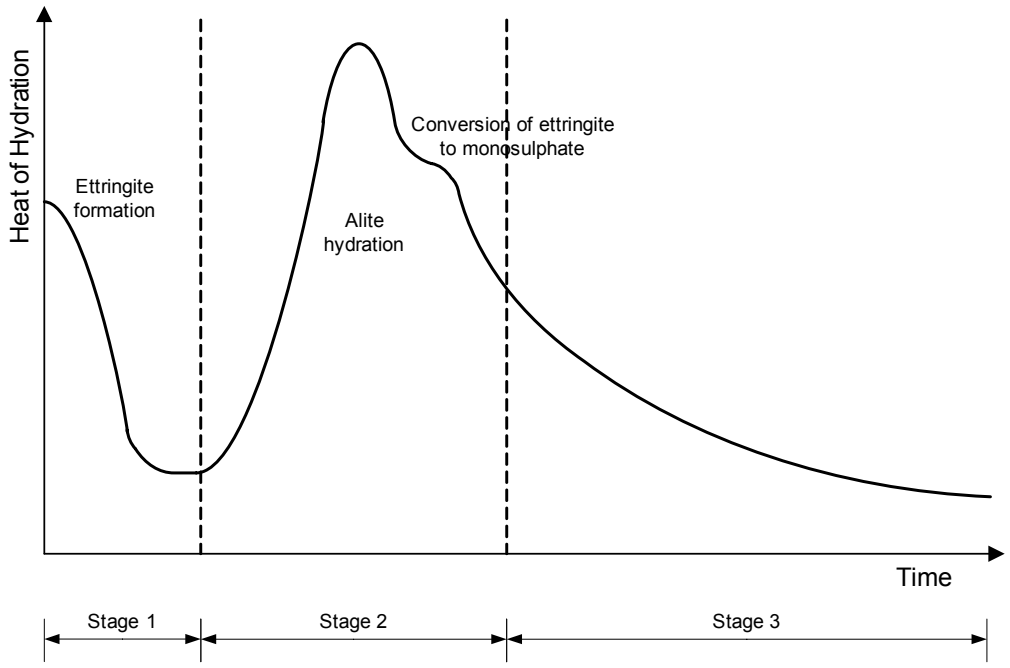

Figure 5.1. Stages of PC Hydration (Maekawa et al., 1999)

5.2.2 Reference Heat Generation Rates

Maekawa et al. (1999) developed a set of reference heat generation rates, $H_{i,T0}$, for each of the binder components involved in the hydration reactions. These are general reference values for the mineral composition of PC at a constant temperature of 20°C and are shown in figures 5.2 and 5.3. The $H_{i,T0}$ (or q_i) function in equation 5.4 can be obtained from these graphs at various time intervals for each of the hydration reactions considered. The reference heat rates shown in figures 5.2 and 5.3 however, are for a cement with a specific fineness. Since material fineness affects the rate of reactions, there is a need to account for variations in fineness if a general heat rate model is to be developed. This is achieved using the s_i coefficient is equation 5.4, which can be determined from the following relationship:

$$s_i = S_i / S_{i0} \tag{5.5}$$

Where S_i is the Blaine value (cm^2/g) of the ith component and S_{i0} is the reference Blaine value used by Maekawa et al. (1999). The reference values given by Maekawa et al. (1999) are 3380, 4330 and 3280 cm^2/g for PC, GGBS and FA respectively.

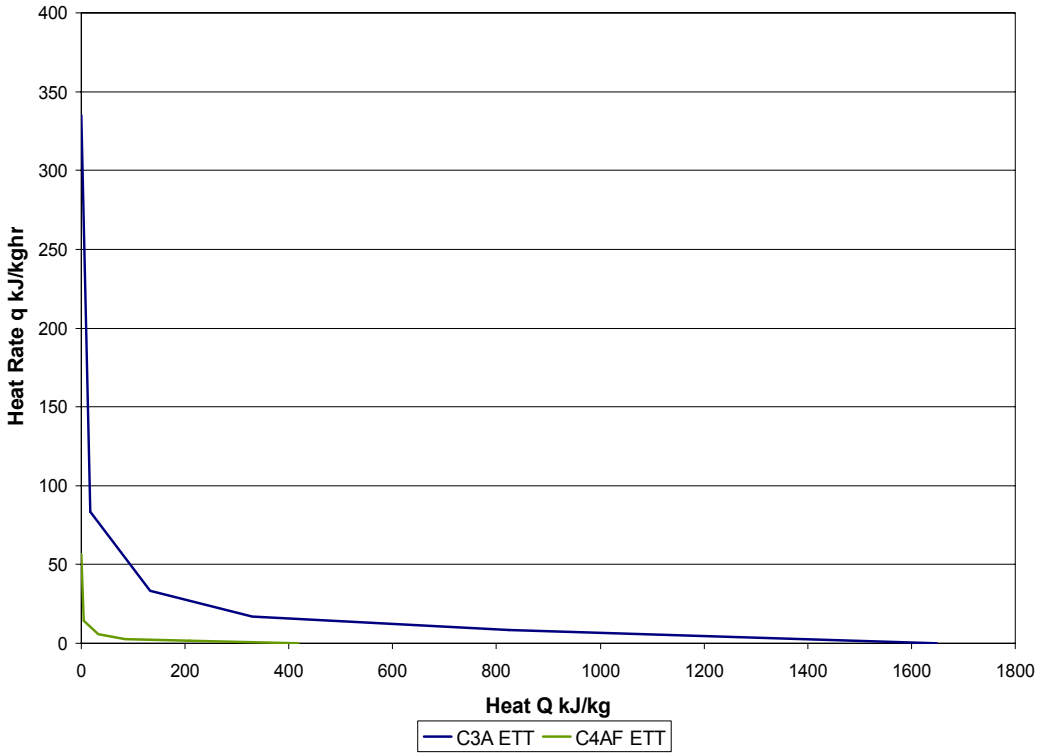

Figure 5.2. Reference Heat Rates – Ettringite Formation (Maekawa et al., 1999)

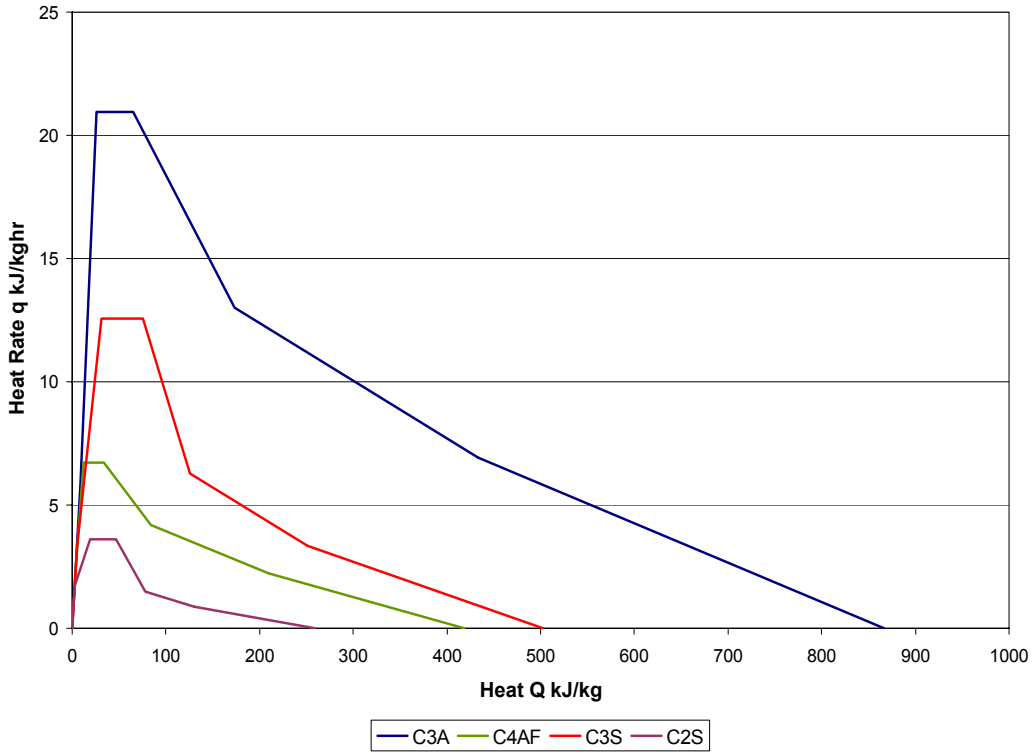

Figure 5.3. Reference Heat Rates – Phase Hydration (Maekawa et al., 1999)

5.2.3 Temperature Dependence of the Mineral Phases

The temperature dependence of each reaction in the hydration process is different for each mineral during every stage of hydration. The most highly reactive minerals dominate hydration during the early stages and, as time passes, the less reactive components begin to take over. If the temperature dependence is different for each crystallographic phase, it can be expected that the thermal activity, $-E_i/R$, will change as the accumulated heat produced increases.

Maekawa et al. (1999) modelled the temperature dependence in terms of the thermal activity of each component, shown in figure 5.4. From these graphs, the following order to the degree of reactivity can be assumed: $C_3A > C_3S > C_4AF > C_2S$. The thermal activities for each mineral phase are also assumed to remain constant during hydration.

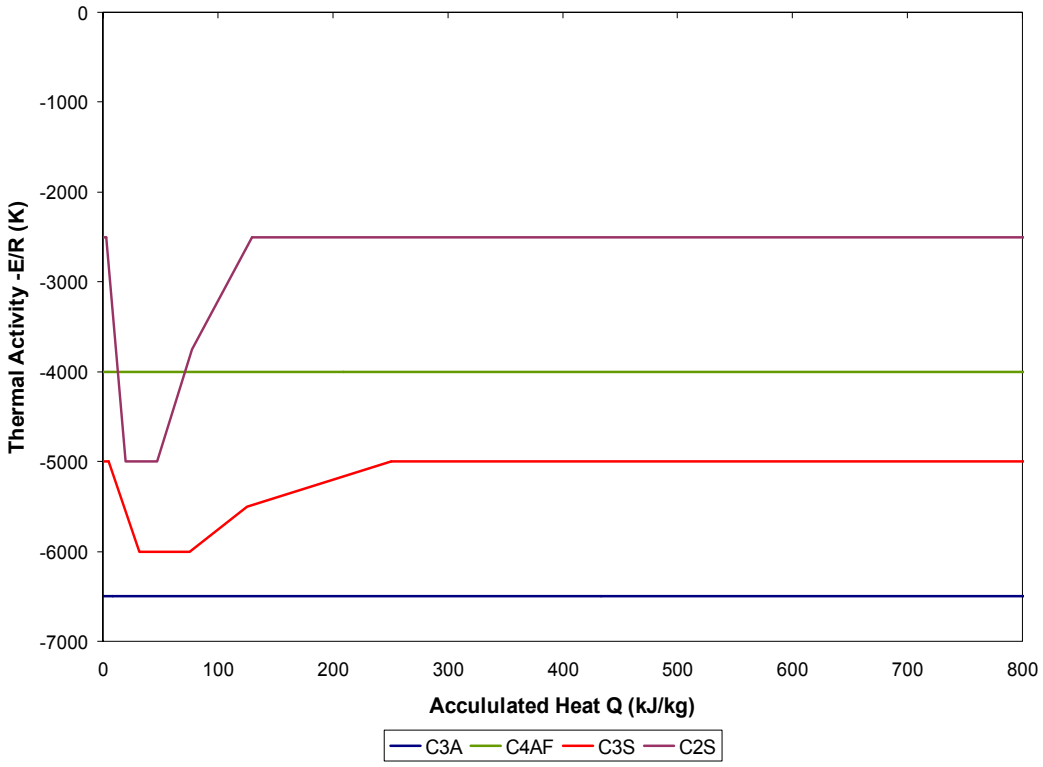

Figure 5.4. Thermal Activity – Hydration Components (Maekawa et al., 1999)

5.2.4 Interdependence of Mineral Reactions

In order to make the model proposed by Maekawa et al., (1999) representative of cement hydration as a whole, the authors needed to account for the interdependence of the individual mineral reactions. One factor that can be considered as possibly influencing mineral interdependence is the amount of free water that the phases share when reacting in the presence of one another. The amount of water consumed by each of the reactions can be determined from the chemical equations that follow in equations 5.6 to 5.13.

For ettringite formation (stage 1, figure 5.1):

$$C_3A + 3C\overline{S}H_2 + 26H \longrightarrow C_3A \cdot 3C\overline{S} \cdot H_{32} \quad (5.6)$$

$$C_4AF + 3C\overline{S}H_2 + 27H \longrightarrow C_3(AF) \cdot 3C\overline{S} \cdot H_{32} + CH \quad (5.7)$$

For the conversion of ettringite to monosulphate (end of stage 2, figure 5.1):

$$2C_3A + C_3A \cdot 3C\overline{S} \cdot H_{32} + 4H \longrightarrow 3\left[C_3A \cdot C\overline{S} \cdot H_{12}\right] \quad (5.8)$$

$$2C_4AF + C_3(AF) \cdot 3C\overline{S} \cdot H_{32} + 6H \longrightarrow 3\left[C_3(AF) \cdot C\overline{S} \cdot H_{12}\right] + 2CH \quad (5.9)$$

For the hydration of the mineral phases (stages 2 and 3, figure 5.1):

$$C_3A + 6H \longrightarrow C_3AH_6 \quad (5.10)$$

$$C_4AF + 2CH + 10H \longrightarrow C_3AH_6 + C_3FH_6 \quad (5.11)$$

$$2C_3S + 6H \longrightarrow C_3S_2H_3 + 3CH \quad (5.12)$$

$$2C_2S + 4H \longrightarrow C_3S_2H_3 + CH \quad (5.13)$$

Where:

$$C \equiv CaO,\ A \equiv Al_2O_3,\ F \equiv Fe_2O_3,\ \overline{S} \equiv SO_3, S \equiv SiO_2,\ CH \equiv Ca(OH)_2,\ H \equiv H_2O$$

The amount of water consumed per mole of mineral reacting (or the bound water ratio) can be obtained from equations 5.6 to 5.13 for each of the reactions. For example, in equation 5.6, one mole of alluminate reacts with twenty-six moles of water giving a bound water ratio of 26. The actual amount of bound water can then be determined by multiplying the bound water ratio by the degree of hydration of each mineral at a particular time and by the mass percentage of the phase in the cement.

The degree of hydration, which is based on the amount of heat liberated at a particular time, is defined in equation 5.14.

$$\text{Degree of Hydration} = \frac{Q_i}{Q_{i,\infty}} \tag{5.14}$$

Where $Q_{i,\infty}$ is the maximum accumulated heat for the ith component and can be obtained from figures 5.2 and 5.3 for each mineral.

It must be noted however, that the bound water ratio is only concerned with the water that is chemically bound and has been consumed in the above reactions. Some of the water in the concrete mixture is also physically trapped and unable to participate in the hydration process. According to van Bruegel (1992), this is generally about fifteen percent of the mass of the cement or binder present in the concrete mixture.

Maekawa et al. (1999) assume that the decline experienced in the heat rate is the result of a shortage of available water for reactions. This in turn is due to a reduction in the probability of contact between the reacting mineral surfaces and the available free water. The degree to which the heat rate declines due to a lack of free water is determined using equation 5.15.

$$\beta_i = 1 - \exp\left\{-5\left[\left(\frac{\omega_{free}}{100\eta_i}\right)\sqrt{s_i}\right]^{2.4}\right\} \tag{5.15}$$

Where:

ω_{free} = the free water ratio at a particular point in time during hydration

η_i = the thickness of the internal hydration product layer of the ith component at the same point in time

$$\omega_{free} = \frac{W_{total} - \sum W_i}{C} \tag{5.16}$$

$$\eta_i = 1 - \left(1 - \frac{Q_i}{Q_{i,\infty}}\right)^{1/3} \tag{5.17}$$

Where:

W_{total} = the total amount of water in the concrete mixture in kg

W_i = the physically bound water plus the water consumed by the reactions involving the ith component at a time t and is fixed by the reaction constituents in equations 5.6 to 5.13.

C = the total amount of cement in the concrete mixture in kg.

W_{total} includes both the chemically and physically bound water. W_i is equal to the amount of chemically bound water, determined from equations 5.6 to 5.13, plus an additional fifteen percent of the cement mass weighted according to the mineral composition of the cement. In other words, W_i is the amount of water consumed by the reaction of the ith component plus an additional 15% of the cement mass not consumed in this reaction at time t.

5.2.5 The Effect of Mineral Composition on the Rate of Heat Evolution

The rate of heat evolution of each of the mineral phases in cement is dependent on the individual proportions of each phase present. The heat evolution characteristics of concrete are therefore dependent on the cement composition and the proportioning of the major clinker phases in the cement. The model developed by Maekawa et al. (1999) considers the effect of mineral composition on heat rate by using the ratio of alite to belite, as shown in Equation 5.18. The approach yields the coefficient μ in equation 5.4, which is only applied to the hydration of C_3S and C_2S during stage 3 of the hydration process (figure 5.1). In all other cases, the effects of mineral composition are ignored, i.e. $\mu = 1$.

$$\mu = 1.4\left\{1 - \exp\left[-0.48\left(\frac{p_{C_3S}}{p_{C_2S}}\right)^{1.4}\right]\right\} + 0.1 \qquad (5.18)$$

5.2.6 Structure of the Heat of Hydration Model

Figure 5.5 shows the structure of the multi-component heat of hydration model developed by Maekawa et al. (1999), combining all the model elements that have been discussed thus far.

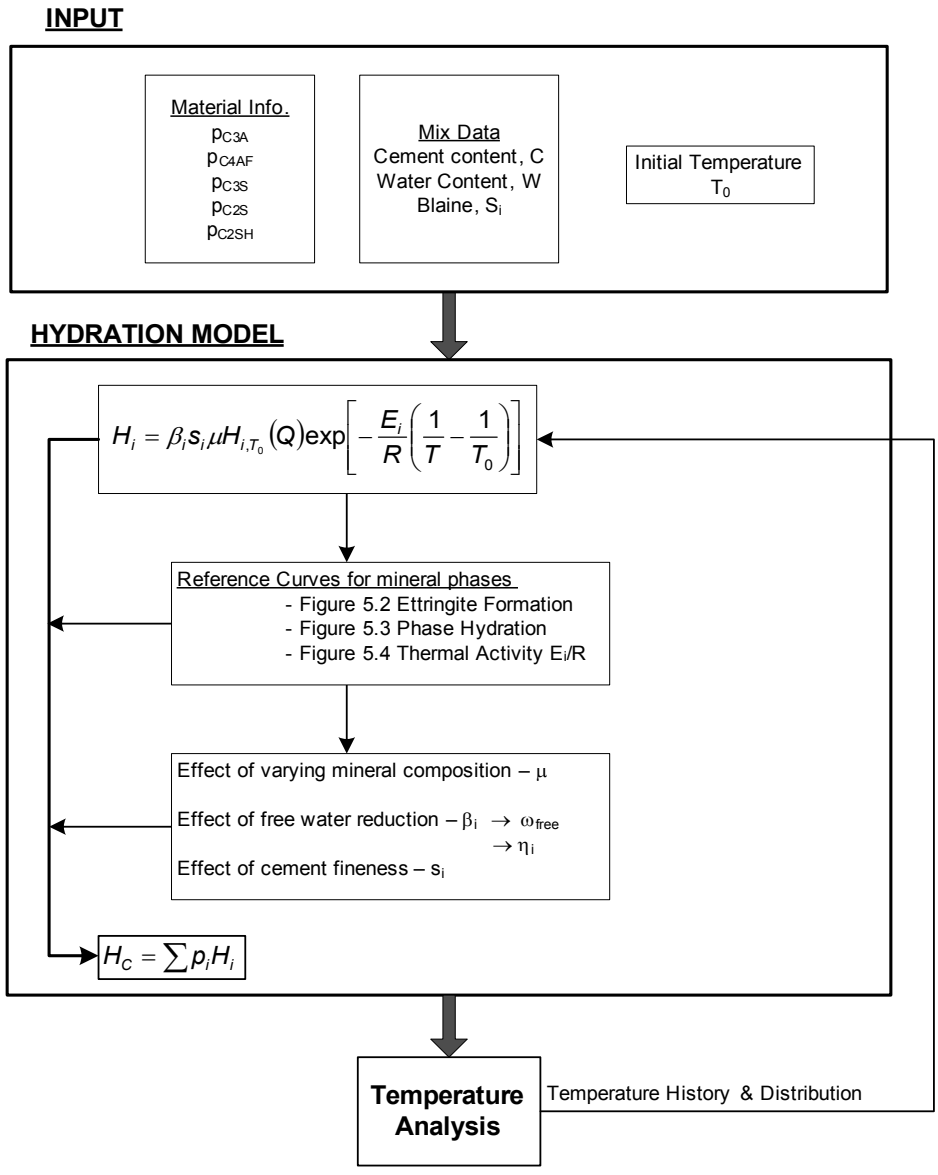

Figure 5.5. Multi-Component Heat of Hydration Model (Maekawa et al., 1999)

5.3 Modified Heat of Hydration Model

5.3.1 Maturity Heat Rate Model

A computer-based model was developed in a spreadsheet environment based on the work of Maekawa et al. (1999). A breakdown of the model can be found in Appendix B. The new model is a maturity heat rate model that determines the maturity heat rate and corresponding equivalent age (or maturity) for concrete, as discussed in chapter 4. It uses the same basic principles as the Maekawa et al. (1999) multi-component heat of hydration model, namely:

- The heat of hydration is determined for each of the major reactions in equations 5.6 to 5.13 in a stepwise fashion and summed over time.
- The heat produced by the crystallographic phases and their reactions with water is dependent on the amount of free water available for each reaction and on the amount of each phase present in the cement.

The model proposed by Maekawa et al. (1999) however, was unsuitable for different w/c ratios. In order to account for the effects of different w/c ratios, a modified version of the Maekawa et al. (1999) model is proposed. This is part of an attempt to develop a prediction model that is generally applicable to any concrete, regardless of the w/c ratio. The calibrations required for this purpose were developed using the results of three PC only concretes with different w/c ratios (discussed in chapter 4). A comparison is made between the results produced by the model and the laboratory test results obtained in this project as well as those obtained by Graham (2003). This was done in order to check the accuracy and general suitability of the prediction model. The new model was also adjusted to account for the different contributions made to the overall heat rate by the various cement phases at different times during the hydration process, as suggested in figure 5.1. This was achieved by varying the starting time of each of the reactions in equations 5.6 to 5.13.

5.3.2 Structure of the Maturity Heat Rate Model

Figure 5.6 shows the outline of the maturity heat rate prediction model developed as a part of this investigation. The model consists of four main parts as shown in figure 5.6, and discussed in this chapter. Appendix B contains screen shots of the model and the progression of the model in the spreadsheet environment is summarised in figure B.1.

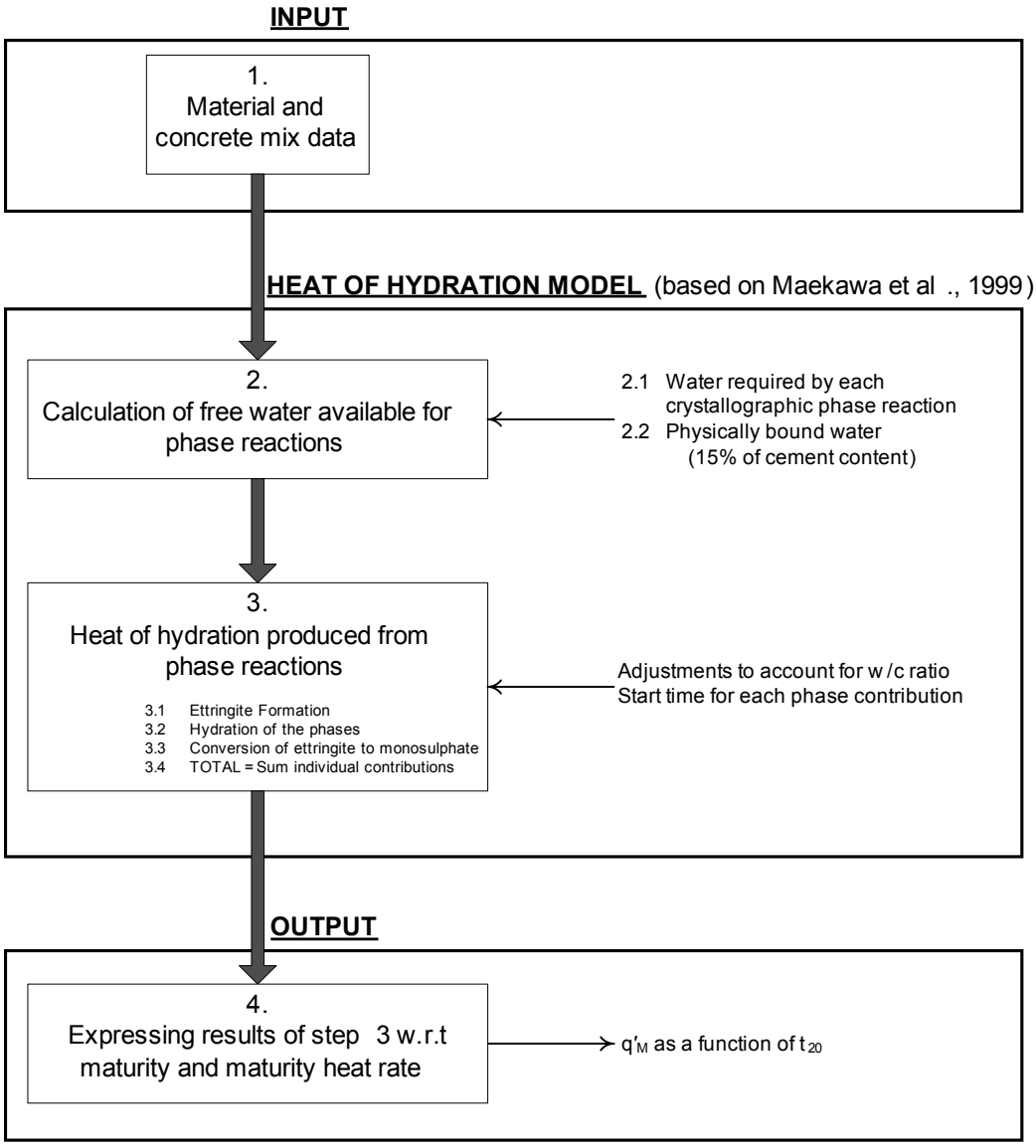

Figure 5.6. Outline of the Maturity Heat Rate Model

5.3.3 Input Data

In the model, the user is required to enter data pertaining to composition of the cement and concrete mixture. The input stage can be summarised as follows:

- The amounts of CaO, SiO_2, Al_2O_3, Fe_2O_3 and SO_3 in the cement are entered into the model, from which the Bogue Calculations (equations 3.1 to 3.4 in chapter 3) are used to compute the percentages of the crystalline phases present.
- The initial temperature of the sample is entered. This is generally been taken to be 20°C.
- The concrete mixture details are entered. These consist of the amount of cement, sand, stone and water in the concrete mixture (in kg/m^3). The user is also required to enter the individual specific heat capacity (C_p) of the concrete mixture constituents. From these values, the w/c ratio and the concrete C_p are calculated.
- The Blaine value, S_i, is entered and used in equation 5.5 to calculate s_i.

5.3.4 Free Water Calculations

The first stage of the heat of hydration model calculates the free water available in the concrete mixture for the reactions that take place between the cement mineral phases and the water present. It also determines the amount of water used in the hydration reactions at each stage in the process. The amount of water required for each of the reactions involving of the crystallographic phases (equations 5.6 to 5.13) can be found using the following relationship:

$$(RW)_i = M_H \times BWR \tag{5.19}$$

Where:

$(RW)_i$ = the reaction water required for the complete hydration of the ith cement phase, according to equations 5.6 to 5.13

M_H = the molar mass of water

BWR = the bound water ratio, determined from equations 5.6 to 5.13 as discussed earlier.

The amount of water required for complete hydration of the phases present in the cement can then be determined using the relationship:

$$(RQW)_i = p_i \times (RW)_i \tag{5.20}$$

Where:

$(RQW)_i$ = water required for complete hydration of the ith cement phase

p_i = the mass ratio of the ith component present in the cement.

The amount of physically bound water, which is assumed to remain uninvolved in the hydration reactions, is taken as fifteen percent of the mass of the cement present, as already mentioned. This was applied to each of the cement phases in the following fashion:

$$(PBW)_i = 0.15 p_i C \tag{5.21}$$

Where:

$(PBW)_i$ = the amount of physically bound water with respect to the ith component present in the cement.

It must be noted that as the hydration reactions progress, and cement and water are consumed in the process, the amounts of $(RW)_i$ and $(PBW)_i$ change, i.e. $(RW)_i$ and $(PBW)_i$ increase as the amounts of available cement and water decrease with time.

The values obtained from equations 5.19 and 5.21 represent the total amount of water consumed by each cement phase at the end of the hydration process. In order to predict the rate of heat evolution, the amount of water consumed needs to be known at each time interval considered in the model. This means that W_i in equation 5.16 needs to be calculated at each time t. For this purpose, it was assumed that the amount of water consumed by a particular phase was directly proportional to the degree of hydration of that phase at time t, i.e.:

$$W_i = [(RQW)_i + (PBW)_i] \times \frac{Q_i}{Q_{i,\infty}} \tag{5.22}$$

Where Q_i and $Q_{i,\infty}$ are obtained from the reference graphs in figures 5.2 and 5.3.

From equations 5.19 to 5.22, the free water ratio, ω_{free}, can be calculated for each time step using equation 5.16.

5.3.5 Heat of Hydration Determination

Once the amount of water available for reacting with the different phases is known for each time step, the heat produced from the reactions in equations 5.6 to 5.13 can be determined using equation 5.4. In the modified prediction model however, the β_i term in equation 5.4 is modified in order to account for concretes with different w/c ratios. The different reactions are also assumed to occur at different times during the hydration process. The heat of hydration model essentially consists of four parts:

1. The heat produced due to the formation of ettringite in stage 1 of the hydration process.
2. The heat produced from the hydration of the four main crystallographic phases during stages 2 and 3 of the hydration process.
3. The conversion of ettringite to monosulphate during stages 2 and 3 of the hydration process.
4. The combination of the above three steps in order to obtain the total amount of heat produced during hydration.

The same methodology is applied to the different stages of the model in parts 1 to 3 above. This is summarised in figure 5.7.

Time Step Determination

The time steps of the heat of hydration prediction are based on the reference curves produced by Maekawa et al. (1999), shown in figures 5.2 and 5.3. The graphs were interpolated to find Q_i and H_i values, and the corresponding time was determined using the relationship $H = dQ/dt$ or $\Delta t \approx \Delta Q/H$.

Free Water Calculation and Adjustment

The amount of free water available for the reactions involving the cement phases can be determined as discussed in section 5.3.3. Once ω_{free} and η_i have been found for

each time interval, the degree to which the heat rate declines due to a lack of free water, β_i, can be determined from equation 5.15.

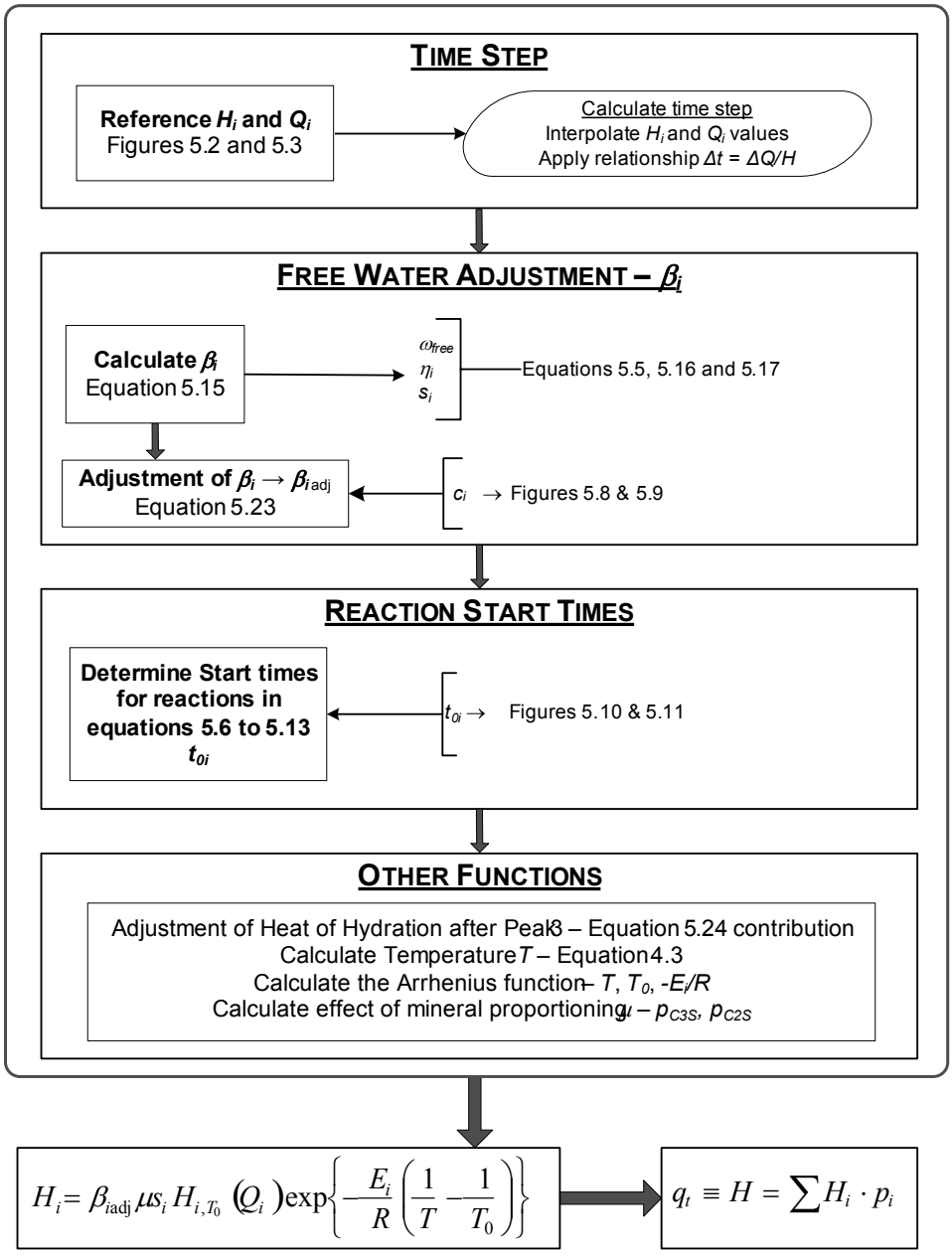

Figure 5.7. Steps of the Maturity Heat Rate Prediction Model

In order to account for the effects of different w/c ratios and cement phase compositions on the degree to which the heat rate declines due to a lack of free water,

β_i had to be adjusted. For this purpose, the following empirical equation was developed based on the results of the three PC only concretes in chapter 4.

$$\beta_{i\text{adj}} = \beta_i \left(\frac{0.6}{w/c} \right)^{c_i} \tag{5.23}$$

Where:

$\beta_{i\text{adj}}$ = the adjusted β_i value to account for the effects of w/c ratio

c_i = an experimental coefficient to account for different w/c ratios. This can be determined from the curves in figures 5.8 and 5.9 for the different cement phases.

The c_i coefficient was developed empirically for each major cement phase using the three PC only concretes described in chapter 4. Initially the original β_i values, as determined by equation 5.15, were used in the prediction of the heat rate curves for the three PC only concretes. These predicted curves were compared to the original curves shown in figure 4.2. Values for c_i were then empirically chosen such that, when the β_i values were replaced with $\beta_{i\text{adj}}$ in equation 5.23, the predicted results matched the actual maturity heat rate curves as closely as possible. The different empirical c_i values for the three PC only concretes were plotted against the respective w/c ratios. A trend line was fitted to the data, in order to obtain the curves shown in figures 5.8 and 5.9. The values of c_i where adjusted such that each fitted curve has an R^2 value of greater than 0.9. The equations for the original curves fitted for figures 5.8 and 5.9 can be found in Appendix B in the model screenshots 7 and 8 in section B.3.3.

The adjustment to β_i is only applied to stages 1 and 2 of the hydration process, as shown in figure 5.1. This is because it is assumed that the effects of a different w/c ratio are no longer significant during stage 3 because the reactions become diffusion controlled (as discussed in chapter 2) rather than being dependent on the amount of available reaction water.

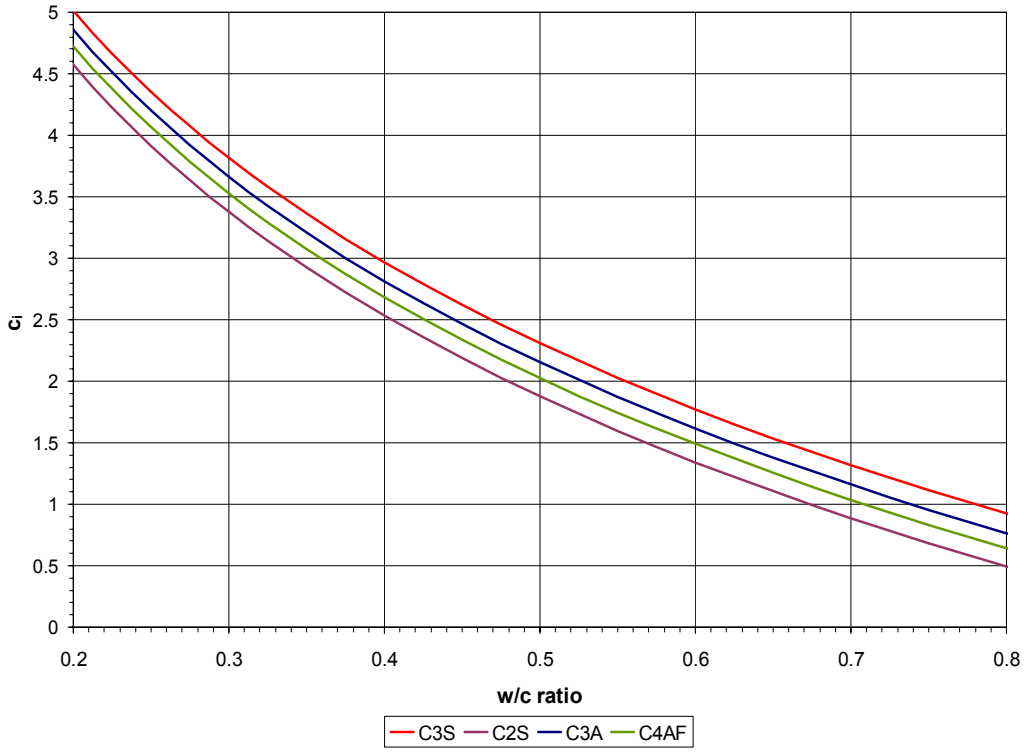

Figure 5.8. c_i values for w/c ratios – Hydration

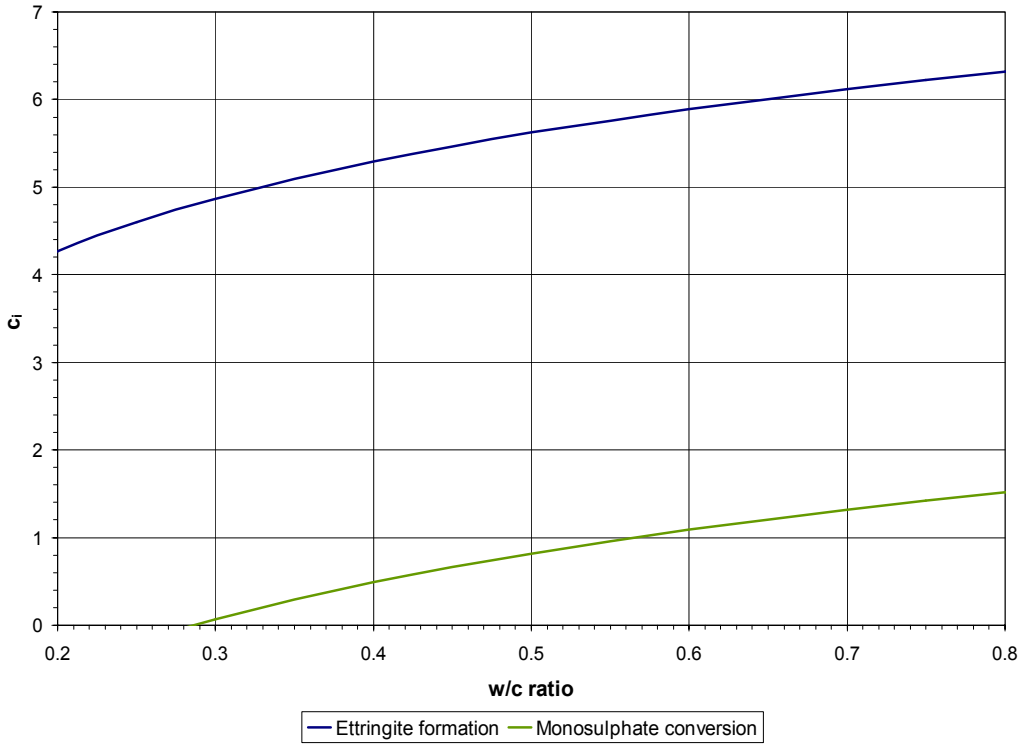

Figure 5.9. c_i values for w/c ratios – Ettringite & Monosulphate

Determination of the Reaction Start Times

For the heat produced by the various cement phase reactions to contribute to the overall heat of hydration curve at the correct stage of hydration, the start time for each reaction is varied. Reaction start times can be determined from the curves in figure 5.10 where t_{0i} is the start time for the reaction of the ith component in order to account for the effects of different w/c ratios. The reaction start times and the curves shown in figures 5.10 and 5.11 were empirically developed using the three PC only concretes in chapter 4. This was done in the same manner as the c_i values and curves were produced for the β_i adjustment. The length of time over which the main exothermic peak (peak 3) lasts is also adjusted, and can be determined from figure 5.11. This is seen as the flat portion over peak 3 in figures 5.12 to 5.17. The equations for the original curves fitted for figures 5.10 and 5.11 can be found in Appendix B in the model screenshots 7 and 8 in section B.3.3.

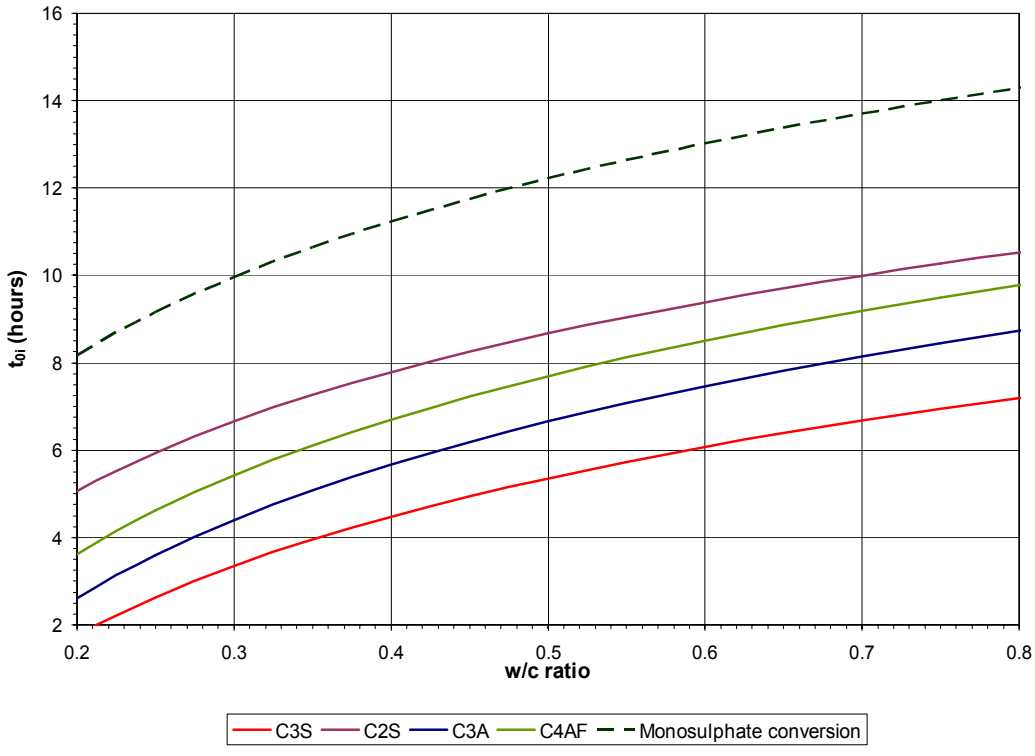

Figure 5.10. t_{0i} values for w/c ratios – Hydration

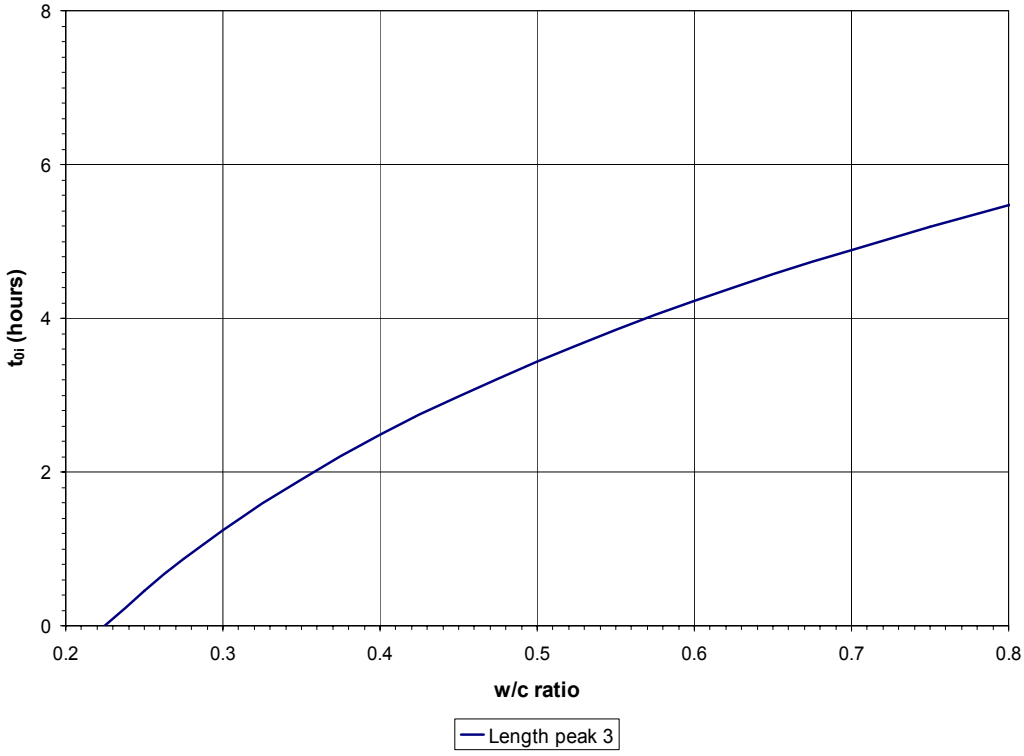

Figure 5.11 Duration of Exothermic Peak 3

Adjustment of Heat of Hydration after the Peak Heat Rate

After the maximum exothermic heat rate is reached, the Maekawa et al. (1999) model underestimates the rate of heat liberation quite considerably. This is due to the application of β_i in equation 5.4, which decreases sharply from approximately stage 3 of the hydration process onwards. In an attempt to predict the rate of heat evolution in the later stages of hydration more accurately, Graham (2003) proposed that the declining portion of the heat rate curve be represented by equation 5.24.

$$H_C = H_{C\max} \cdot \exp\left(-0.04\left(t_{20i} - t_{20H_{\max}}\right)\right) \tag{5.24}$$

Where:

H_C = the sum of the heat rate of the cement phases

$H_{C\max}$ = the maximum total heat rate achieved

t_{20i} = the concrete maturity at the ith interval in t_{20} hours

$t_{20H\max}$ = the concrete maturity when the maximum total heat rate is achieved.

The intention is for equation 5.24 to replace equation 5.1 after the maximum exothermic heat rate peak has passed. For the lower w/c concretes however, equation 5.24 overestimates the rate of heat evolution. It was therefore decided that once the maximum heat rate peak has passed, the heat rate would consist of a sixty percent contribution from equation 5.24 and a forty percent contribution from equation 5.1 for all w/c ratios.

Other Functions

The other functions required for solving Equation 5.4 are calculated in the same manner as in the model developed by Maekawa et al. (1999). The thermal activities for the Arrhenius function in equation 5.4 are taken from figure 5.3 for each of the mineral phases, as discussed earlier. The temperature of the sample is calculated using equation 4.3 in chapter 4. This approach is considered suitable because the aim of the model is to predict the maturity heat rate curve for a concrete under adiabatic conditions. This allows for the results obtained from the model to be comparable to those obtained in a laboratory in an adiabatic calorimeter.

As described in figure 5.7, the values obtained for the functions discussed in this section are used as input into equation 5.4 for each of the cement crystalline phases. This in turn is used in equation 5.1 to find the total heat of hydration of the cement at each time interval. The heat of hydration determined from the model, and the corresponding time are then converted into maturity functions using equations 4.6 and 4.11, as discussed in chapter 4.

5.4 Verification of the Maturity Heat Rate Model

5.4.1 Calibration of the Prediction Model

The maturity heat rate model discussed in this chapter was empirically calibrated using the three PC only adiabatic calorimeter test results obtained for this research.

The accuracy of the model was checked using laboratory results obtained by Graham (2003) by comparing these results to those produced by the prediction model.

5.4.2 Verification of the Prediction Model

The results obtained from the desktop computer model and the output curves produced were compared to the actual laboratory results. Figures 5.12 to 5.17 show the results of all the concrete mixtures entered into the model. The three PC only concretes used in this investigation and the concrete mixtures investigated by Graham (2003) are included.

Figures 5.12 to 5.17 show a graphical comparison between the model prediction and the experimental results for the particular cement or concrete under consideration. From the figures, the following observations regarding the accuracy of the maturity heat rate model can be noted.

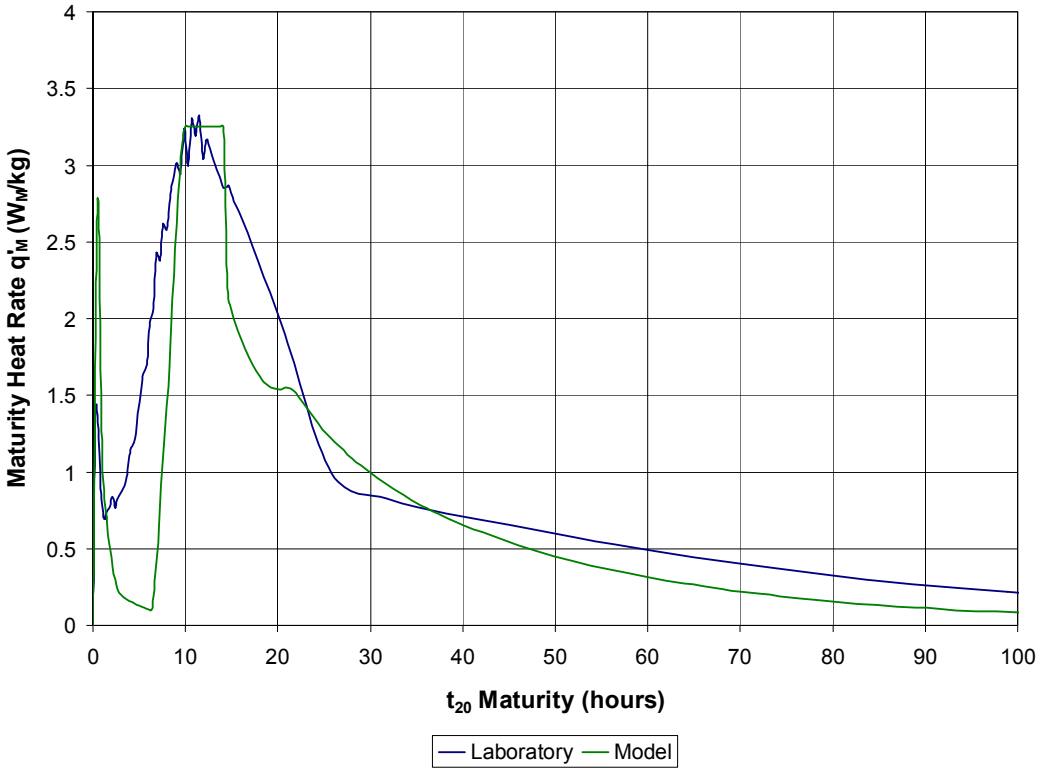

Figure 5.12. Model & Laboratory Results – PC concrete w/c = 0.6

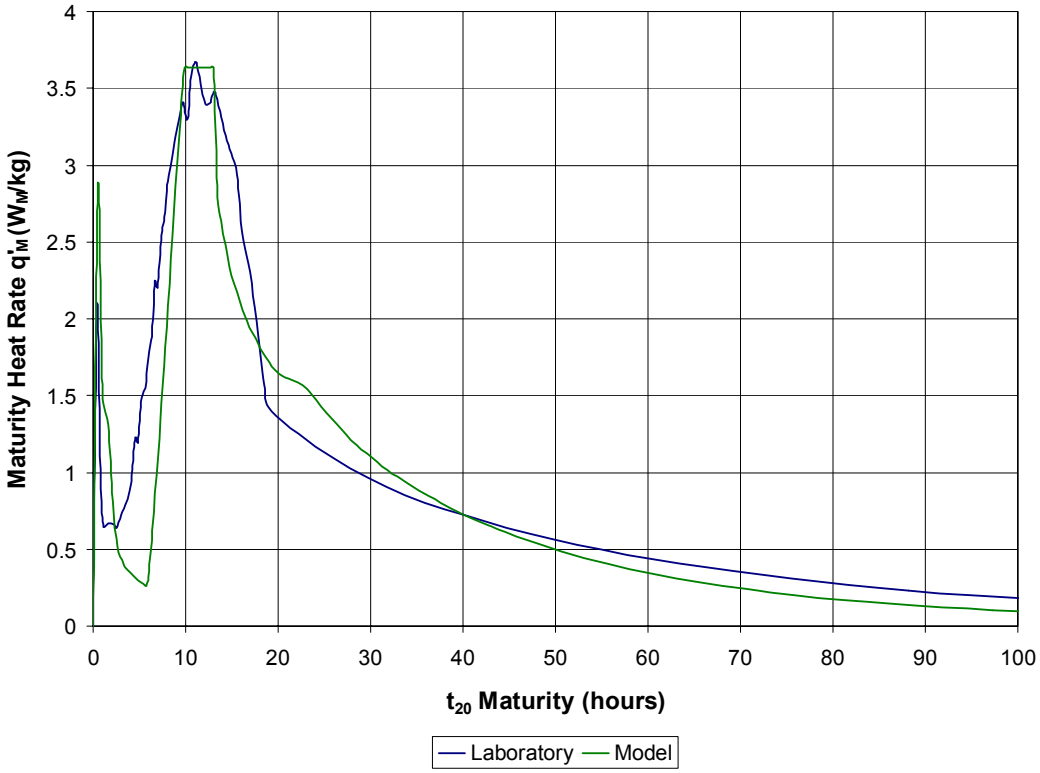

Figure 5.13. Model & Laboratory Results – PC concrete w/c = 0.5

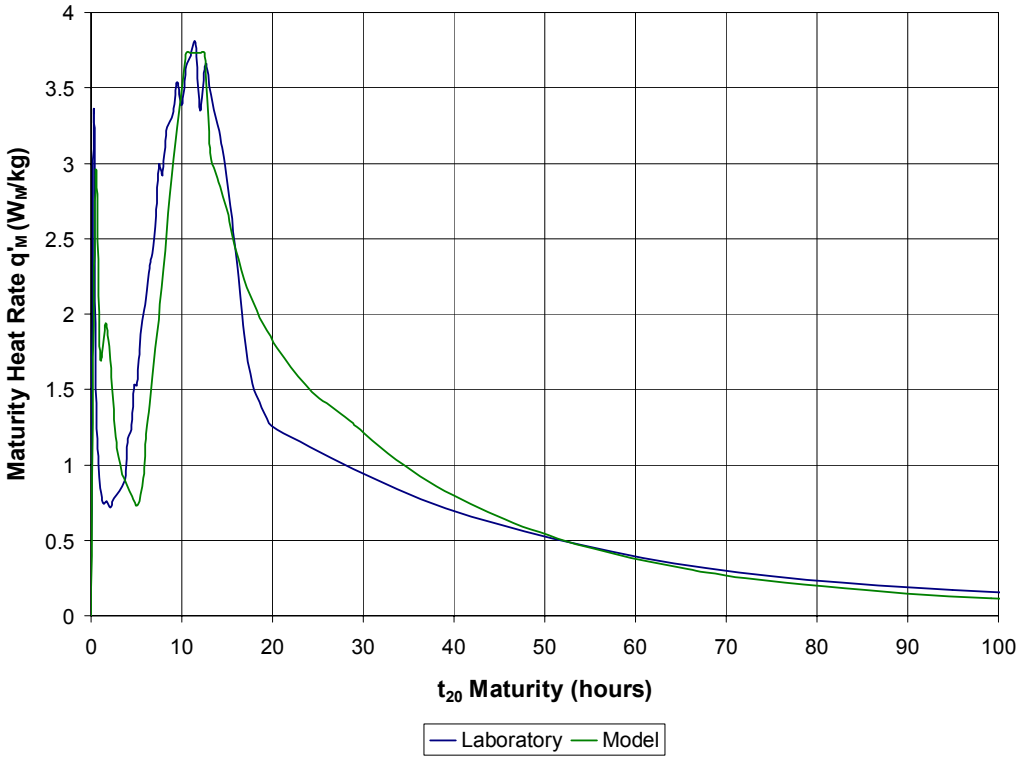

Figure 5.14. Model & Laboratory Results – PC concrete w/c = 0.4

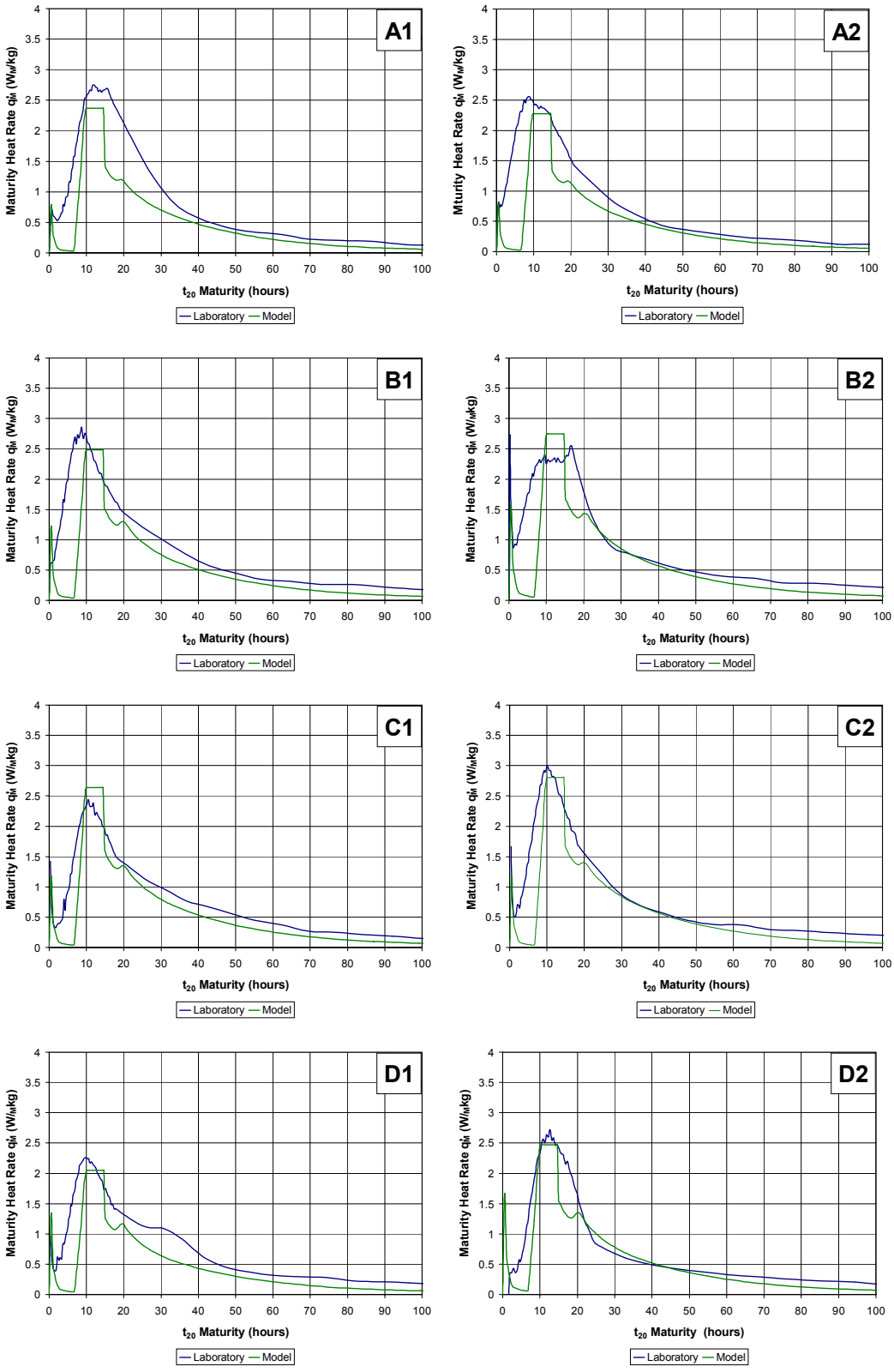

Figure 5.15. Model & Laboratory Results – Cement A1 to D2 (Graham, 2003)

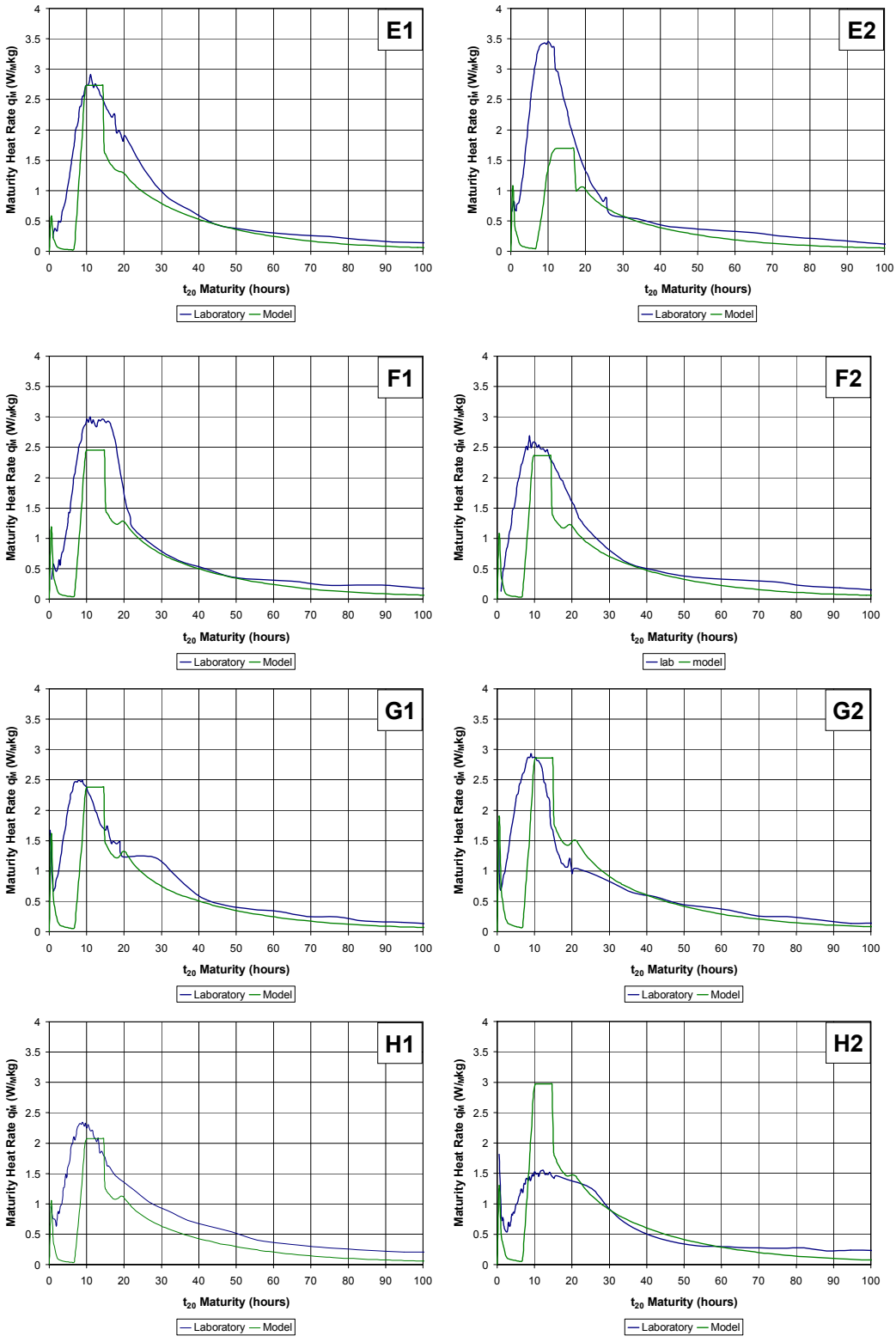

Figure 5.16. Model & Laboratory Results – Cement E1 to H2 (Graham, 2003)

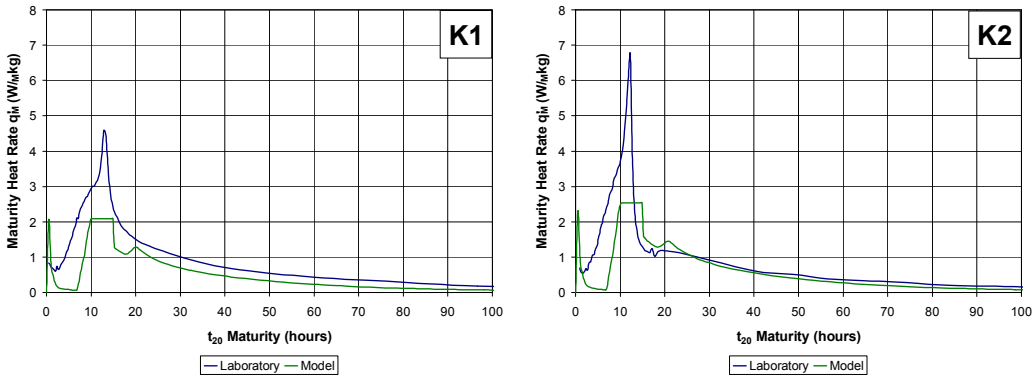

Figure 5.17. Model & Laboratory Results – Cement K1 to K2 (Graham, 2003)

The model provides a reasonably good prediction for the main exothermic heat rate peak (peak 3 in figure 2.1 in chapter 2), both with respect to the maximum maturity heat rate reached and the occurrence of the maximum. With some of the results however, the maximum predicted maturity heat rate occurs at a later equivalent t_{20} age than that of the experimental results (Cements A2, B1, C2, D1, F2, G2 and H1 (Graham, 2003)).

There is also an indication that the model occasionally over- or underestimates the maximum maturity heat rate. This could be a result of the filtering process applied to the laboratory test results and/or the magnitude of the time steps used in the prediction model. The intrinsic error in the temperature measurement of the adiabatic calorimeter may also limit the detection of small temperature variations, creating a small inaccuracy in the results produced. The inaccuracy of the Bogue calculation (discussed in Chapter 3) may also add to this discrepancy, since the model is dependent on the cement phase composition as determined using Bogue's method.

The model produces an inaccurate prediction of peak 1 and trough 2 (see figure 2.1, chapter 2). In most cases, the predicted maturity heat rate at trough 2 is substantially lower than the experimental value. The period of time for which the dormant period lasts is also much longer in the model compared to the laboratory results. These trends seem amplified as the w/c ratio increases. Trough 2 in the results obtained from the model tends to occur between two and five t_{20} hours later than it does in the

laboratory results. This is consistent throughout the results and implies that the model will predict a more rapid increase towards the maximum maturity heat rate than will be experienced in an actual concrete sample. These inaccuracies could be attributed to the highly unpredictable nature of the reactions involving gypsum in the production of ettringite and the effects of gypsum on the retardation of the hydration reactions during the early stages.

The model shows a general tendency to underestimate the maturity heat rate during the deceleration phase of the hydration process (figure 2.1, chapter 2). This is particularly true from about the time that the conversion of ettringite to monosulphate should have finished. The predicted maturity heat rate curves approach a zero heat rate more rapidly than the laboratory results do. This may be a function of the adiabatic calorimeter used in the tests. The inherent error of temperature measurement limits the ability of the system to detect small temperature increases and this is recorded as a zero heat rate.

5.5 Summary and Conclusions

The maturity heat rate model presented in this chapter was developed in a spreadsheet environment as an instrument for predicting the rate of heat evolution in concrete. Such a model would be an invaluable tool to engineers in the design of large concrete structures where thermally induced cracking is a potential problem. At this stage, the model is limited to cements with different phase compositions and concretes with different w/c ratios because of the complex nature of the heat of hydration produced by cement.

The heat rate model developed by Maekawa et al (1999) was adjusted using empirical factors in order to account for the effects w/c ratio on the heat evolution characteristics of a cement. The aim of these adjustments is to refine the model presented by Maekawa et al. (1999) in order to deal with the prediction errors noted by Graham (2003), and to extend the applicability of the model to include the effects of changing the w/c ratio. When compared to results not used for the purposes of

calibrating the adjustment factors, the model showed reasonably good accuracy, particularly with respect to the main exothermic peak in the heat rate curve.

The model can be improved and extended further to include more factors that might influence the heat of hydration of a concrete element. Such factors include:

- A more accurate prediction of the heat of hydration during the early and later stages of the hydration process. This might require a more in-depth study into the contributions of the reactions producing ettringite and later monosulphate, and the retarding effect of gypsum.
- The presence of cement extenders, particularly FA and GGBS, which are often used in concretes where high temperatures and heat evolution are potential problems, as discussed in chapter 2.
- The presence of additional materials such water-reducing agents and superplasticisers.
- The effects of variations in aggregate sizes and types on the heat evolution characteristics of concrete (a topic that has not been considered in this investigation).
- Defining functions based on a wider range of experimental results in order to make the empirically derived adjustment factors more accurate.

5.6 Chapter References

Graham, P.C. (2003) *The heat evolution characteristics of South African cements and the implications for mass concrete structures*. Ph.D. Thesis, University of the Witwatersrand , Johannesburg, South Africa.

Kishi, T., Shimomura, T. and Maekawa, K. (1993) Thermal crack control design of high performance concrete, in the *Proceedings of Concrete 2000*, Dundee, Scotland, E&FN Spon, London, UK, pp. 447-456.

Maekawa, K., Chaube, R. and Kishi, T. (1999) Multicomponent model for the heat of hydration of Portland cement. *Modelling of Concrete Preformance: Hydration, microstructure formation and mass transport*, Routledge, New York, USA, pp. 178-248.

Suzuki, Y., Tsuji, Y., Maekawa, K. and Okamura, H. (1990) Quantification of hydration-heat generation process of cement in concrete, *Concrete Library of JSCE*, no.19, pp 111-124.

van Breugel, K. (1992) Numerical simulation of hydration and microstructural development in hardening cement-based materials, *Heron*, vol. 37, no. 2, Delft University of Technology, Delft, Netherlands.

Chapter 6

CONCLUSION

6.1 Introduction

It has been shown that Portland cement is a highly complex material. It consists of a wide range of compounds, which, in general, are all involved in the hydration process. It is not possible to describe the range of reactions that take place between water and cement with complete accuracy. This makes predicting the hydration process difficult with respect to the products formed, the time over which the reactions occur, and the heat that is liberated during hydration.

The literature review in chapter 2 indicates that the chemical properties and composition of the binder material greatly affect the mechanisms of hydration and the amount of heat liberated. Other factors such as particle fineness, w/c ratio and the quantity and type of cement extender present in the binder also affect the heat evolved during hydration. All of this in turn affects ability of concrete to resist thermally induced stresses and strains due to excess rises in temperature and the presence of temperature gradients within and across a section. This can either help prevent or exacerbate the problem of thermal cracking.

6.2 Adiabatic Calorimeter Results

The main purpose of this study was to develop a knowledge of how the heat evolution characteristics of concrete (caused by the hydration of Portland cement) are affected

by changing the concrete mixture design. In particular, the focus was placed on the effects of varying the w/c ratio and the presence of different commonly used cement extenders on the heat of hydration. This was investigated in a series of adiabatic calorimeter tests conducted at the School of the Civil and Environmental Engineering, at the University of the Witwatersrand.

In order for the different adiabatic calorimeter test results to be comparable with one another, the heat rate curves obtained from the time-temperature histories of the samples had to be normalised. This allows the results obtained to be described independently of initial casting temperature. Maturity heat rate functions developed by Ballim and Graham (2003) were used for this purpose. Using the Arrhenius function, the actual clock time is expressed with respect to equivalent age or maturity and the rate of heat evolution is expressed as a maturity heat rate. This allows for a comparison of results in terms of the heat liberated from a concrete sample independently of the initial temperature or heat present in the system.

The following points regarding the calorimeter test results obtained can be noted from Chapter 4:

- For the PC only concretes, the higher the w/c ratio, the greater the amount of heat liberated per unit mass of binder and the lower the value of the main exothermic heat rate peak. The w/c ratio has no significant effect on the maturity at which the exothermic heat rate peaks and troughs occur. The change in the maxima of total heat and maturity heat rate also vary approximately linearly with respect to the w/c ratio. The same trends were also noticeable in the CSF concretes.
- The results from the GGBS concretes suggested that the greater the w/c ratio the greater the maximum total heat liberated. Compared to the PC only concretes, the presence of GGBS tends to normalise the maturity heat rate to an extent, causing there to be no significant differences between the maximum heat rates of different GGBS concretes. The main exothermic peak occurs at a later maturity in the GGBS concretes compared to the PC only concretes. The presence of GGBS causes substantial increase in peak 4 in the hydration

process due to the late contribution of the GGBS S-reaction described in Chapter 2.

- The FA concretes indicate that as the w/c ratio decreases, both the total heat produced and the maximum maturity heat rate observed decrease. The presence of FA also tends to normalise the heat evolution characteristics of concrete, making the effects of varying the w/c ratio less significant compared to the PC only concretes.
- Aggregate type has no significant effect on the heat evolution characteristic of concrete. The size of coarse aggregate used however, could potentially affect the rate of heat evolution and the amount of heat liberated.

From the calorimeter test results in chapter 4, the following trend is evident: $q_{FA} < q_{CSF} < q_{GGBS} < q_{PC}$. The fact that the GGBS concretes have a greater maturity heat rate than the PC only concretes during the later stages, underlines the late contribution of the S-reaction to the heat of hydration. The only cement extenders that significantly affect the maximum exothermic heat rate peak are FA and GGBS. The difference between PC only and CSF concretes with respect to peak 3 is negligible, both in terms of magnitude of the peak and the t_{20} maturity at which it occurs. The GGBS and FA concretes produce significantly lower peaks in the maturity heat rate at the end of the acceleration stage of hydration, and the peaks of the FA concretes occur at a later maturity than the other samples.

The following conclusions can be drawn from this investigation if the aim of designing a concrete mixture is to reduce maximum in the rate of heat evolution and ensure that the maximum tensile stress occurs at a time when the concrete has developed sufficient strength:

1. Use a concrete with the greatest possible w/c ratio.
2. Use of GGBS or FA rather than PC only or CSF in the binder material.

It must be remembered however, that the concrete will still have to meet the strength and durability requirements and structural specifications of the intended structure.

6.3 Maturity Heat Rate Model

The second area of investigation in this study was the development of a maturity heat rate model. A reliable prediction of the rate of heat evolution of concrete would aid engineers in optimising the design of large concrete elements with respect to concrete mixture constituents, element size, cooling systems, sequential pouring of concrete etc., without the need for costly and time-consuming laboratory tests. This would be a valuable tool in the design concrete structures with a minimum risk of thermally induced cracking.

The model developed in this study predicts the contribution of the individual clinker phases in cement to the heat liberated in concrete during hydration. It was developed in a spreadsheet environment based on the work conducted by Maekawa et al. (1999) and Graham (2003). Empirical calibrations were applied in an attempt to improve the accuracy and general suitability of the prediction. The model is limited however, to cements with different phase compositions and concretes with different w/c ratios. When the laboratory and predicted results were compared, the model showed reasonably good accuracy, particularly with respect to the main exothermic peak in the heat rate curve. It does however, require improvements in the following areas:

- A more accurate prediction of the heat of hydration during the early and later stages of the hydration process. This might require a more in-depth study into the contributions of the reactions producing ettringite and later monosulphate.
- Defining functions that are based on a wider range of experimental results in order to make the empirically derived adjustment factors more accurate.
- The inclusion of cement extenders.

6.4 Possible Areas for Additional Research

As mentioned, cement is a complex material and the hydration of the material in the presence of water is just as multifaceted. This makes predicting the progress of the hydration reactions and the associated heat evolution difficult. This study has only

focused on a few areas pertinent the to heat evolution characteristics of concrete and if a complete knowledge of these characteristics is to be acquired, further investigation is needed. Other possible areas of investigation include:

1. With respect to concrete mixture design parameters:
    i. The effects of superplasticisers and other admixtures commonly used in the construction industry on the heat evolution characteristics of concrete.
    ii. The effects of different aggregate sizes on the heat of hydration.
2. With respect to the development of a heat rate prediction model:
    i. Including the effects of the presence of cement extenders in the binder material. Particular consideration should be paid to including FA and GGBS, which have shown to have positive effects on the heat evolution characteristics of concrete.
    ii. Including the effects of admixtures and aggregate size on the heat evolution of concrete, as discussed in the previous point.

6.5 Chapter References

Ballim, Y. and Graham, P.C. (2003) A Maturity Approach to the Rate of Heat Evolution in Concrete. *Magazine of Concrete Research*, vol. 55, no. 3, Thomas Telford, London, UK, pp. 249-256.

Graham, P.C. (2003) *The heat evolution characteristics of South African cements and the implications for mass concrete structures*. Ph.D. Thesis, University of the Witwatersrand, Johannesburg, South Africa.

Maekawa, K., Chaube, R. and Kishi, T. (1999) Multicomponent model for the heat of hydration of Portland cement. *Modelling of Concrete Preformance: Hydration, microstructure formation and mass transport*, Routledge, New York, USA, pp. 178-248.

Appendix A

VISUAL BASIC MACROS

A.1 About the VB Macros

Visual Basic macros were written for use in a spreadsheet environment to analyse the temperature readings taken from an adiabatic calorimeter test. This appendix shows the two basic macros used; one for converting the clock time into hours and for filtering the data for plotting purposes, and one for calculating the parameters necessary for plotting the graphs shown in chapter 4. These basic macros were extended to enable an analysis of, and a comparison between two, three and four different test results at a time.

A.2 Time and Filter VB Macro

The macro that follows converts the time readings obtained from the calorimeter from days, hours and minutes to hours only. The macro then filters the results. This is done to smooth the oscillatory effects caused by the rising and falling of the temperature during testing. The rises and falls in temperature are very small and are caused by the switching on/off of the calorimeter tank heater while maintaining adiabatic conditions. For the first twelve hours, the macro filters out time readings less than fifteen minutes apart. Thereafter, time readings less than one hour apart are ignored. This filtering process was adequate enough to allow the results to be plotted along a smooth curve.

```
Sub Time_Filter()

Application.ScreenUpdating = False

' Time to hours Macro
' Macro recorded 1/22/2004 by CG Greensmith
' Converting time recorded to hours
Range("I20").Select
ActiveCell.FormulaR1C1 = "=RC[-8]*24+RC[-7]+RC[-6]/60"
ActiveCell.Range("A1").Select
Range(Selection, Selection.End(xlDown)).Select
Selection.FillDown
Range(Selection, Selection.End(xlDown)).Select
Selection.NumberFormat = "0.000"

' Filter for Adiabatic Calorimeter Results Macro
' Macro recorded 7/31/2002 by Y Ballim
' Modified 21/01/2004 by CG Greensmith
Range("I21").Select
CheckAge:
    If ActiveCell < 12 Then
    GoTo CheckLow
    Else
    GoTo CheckHigh
    End If
CheckLow:
    If ActiveCell = 0 Then
    End
    Else
    GoTo AssessLow
    End If
AssessLow:
    If ActiveCell - ActiveCell.Offset(-1, 0) < 0.25 Then
    GoTo DeleteRow
    Else
    ActiveCell.Offset(1, 0).Select
    GoTo CheckAge
```

```
    End If
CheckHigh:
    If ActiveCell = 0 Then
    End
    Else
    GoTo AssessHigh
    End If
AssessHigh:
    If ActiveCell - ActiveCell.Offset(-1, 0) < 2 Then
    GoTo DeleteRow
    Else
    ActiveCell.Offset(1, 0).Select
    GoTo CheckAge
    End If
DeleteRow:
    ActiveCell.Range("A1").Select
    Range(Selection, Selection.Offset(0, -8)).Select
    Selection.Delete
    ActiveCell.Range("I1").Select
     If ActiveCell.Offset(2, 0) <> 0 Then
     GoTo CheckAge
     Else: End
     End If

Application.ScreenUpdating = True

End Sub
```

A.3 Calculations and Graph-plotting Macro

The macro shown below uses the temperature readings taken from a sample during testing in the calorimeter and calculates total heat, heat rate, maturity and maturity heat rate using the theory discussed in chapter 4. The macro then plots graphs of total heat and maturity heat rate, both versus t_{20} maturity respectively.

```
Sub Calcs_Graphs()

Application.ScreenUpdating = False

' Calculations for Analysis of Adiabatic Calorimeter Results and  graph
plotting Macro
' Macro recorded 1/22/2004 by CG Greensmith
'
' Calcuating total heat
   Range("J20").Select
   ActiveCell.FormulaR1C1 = "=R13C[-4]*(RC[-4]-R20C[-4])*R15C[-
 7]/(1000*(R8C[-7]+R9C[-7]))"
     ActiveCell.Range("A1").Select
     Range(Selection, Selection.End(xlDown)).Select
     Selection.FillDown
     Range(Selection, Selection.End(xlDown)).Select
     Selection.NumberFormat = "0.000"

' Calculating Heat Rate
    Range("K20").Select
     ActiveCell.FormulaR1C1 = "=0"
     Range("K21").Select
     ActiveCell.FormulaR1C1 = "=(RC[-1]-R[-1]C[-1])/(3.6*(RC[-2]-   R[-
1]C[-2]))"
     ActiveCell.Range("A1").Select
     Range(Selection, Selection.End(xlDown)).Select
     Selection.FillDown
     Range(Selection, Selection.End(xlDown)).Select
     Selection.NumberFormat = "0.000"

' Calculating Arrhenius Maturity Function t20
    Range("L20").Select
    ActiveCell.FormulaR1C1 = "=0"
    Range("L21").Select
    ActiveCell.FormulaR1C1 = _
        "=R[-1]C+(EXP(R9C[-2]*(1/293-(1/(273+0.5*(RC[-6]+R[-1]C[-
 6])))))*(RC[-3]-R[-1]C[-3]))"
```

```
    ActiveCell.Range("A1").Select
    Range(Selection, Selection.End(xlDown)).Select
    Selection.FillDown
    Range(Selection, Selection.End(xlDown)).Select
    Selection.NumberFormat = "0.000"

' Calculating Arrhenius Maturity Heat Rate
    Range("M20").Select
    ActiveCell.FormulaR1C1 = "=0"
    Range("M21").Select
    ActiveCell.FormulaR1C1 = "=(RC[-3]-R[-1]C[-3])/(3.6*(RC[-1]-   R[-
1]C[-1]))"
    ActiveCell.Range("A1").Select
    Range(Selection, Selection.End(xlDown)).Select
    Selection.FillDown
    Range(Selection, Selection.End(xlDown)).Select
    Selection.NumberFormat = "0.000"


' Total_heat_graph Macro
' Macro recorded 1/22/2004 by CG Greensmith
'
    Dim intRow As Integer
    Dim CountA As Double
    Range("L20").Select
    CountA = Range(Selection, Selection.End(xlDown)).Count
    intRow = 20
    intRowA = intRow + CountA - 1

    Charts.Add
    ActiveChart.ChartType = xlXYScatterSmoothNoMarkers
    ActiveChart.SetSourceData
    Source:=Sheets("Sheet1").Range("O28")
    ActiveChart.SeriesCollection.NewSeries
    ActiveChart.SeriesCollection(1).XValues =
    Worksheets("Sheet1").Range("L20:L" & intRowA)
    ActiveChart.SeriesCollection(1).Values =
```

```
   Worksheets("Sheet1").Range("J20:J" & intRowA)
   ActiveChart.Location Where:=xlLocationAsNewSheet, Name:="Total
Heat"
   With ActiveChart
        .HasTitle = True
        .ChartTitle.Characters.Text = "Total Heat"
        .Axes(xlCategory, xlPrimary).HasTitle = True
        .Axes(xlCategory, xlPrimary).AxisTitle.Characters.Text = _
        "Arrhenius Maturity t20 (hrs)"
        .Axes(xlValue, xlPrimary).HasTitle = True
        .Axes(xlValue, xlPrimary).AxisTitle.Characters.Text =
"Total Heat (kJ/kg)"
   End With
   With ActiveChart.Axes(xlCategory)
        .HasMajorGridlines = True
        .HasMinorGridlines = False
   End With
   With ActiveChart.Axes(xlValue)
        .HasMajorGridlines = True
        .HasMinorGridlines = False
   End With
   ActiveChart.HasLegEnd = False

   ActiveChart.PlotArea.Select
   With Selection.Border
        .ColorIndex = 57
        .Weight = xlThin
        .LineStyle = xlContinuous
   End With
   Selection.Interior.ColorIndex = xlNone
   ActiveChart.Axes(xlValue).Select
   With Selection.Border
        .Weight = xlHairline
        .LineStyle = xlAutomatic
   End With
   With Selection
        .MajorTickMark = xlOutside
```

```
    .MinorTickMark = xlOutside
    .TickLabelPosition = xlNextToAxis
End With
With ActiveChart.Axes(xlValue)
    .MinimumScaleIsAuto = True
    .MaximumScaleIsAuto = True
    .MinorUnit = 5
    .MajorUnitIsAuto = True
    .Crosses = xlAutomatic
    .ReversePlotOrder = False
    .ScaleType = xlLinear
    .DisplayUnit = xlNone
End With
Selection.TickLabels.NumberFormat = "General"
ActiveChart.Axes(xlCategory).Select
With Selection.Border
    .Weight = xlHairline
    .LineStyle = xlAutomatic
End With
With Selection
    .MajorTickMark = xlOutside
    .MinorTickMark = xlOutside
    .TickLabelPosition = xlNextToAxis
End With
With ActiveChart.Axes(xlCategory)
    .MinimumScaleIsAuto = True
    .MaximumScaleIsAuto = True
    .MinorUnit = 1
    .MajorUnitIsAuto = True
    .Crosses = xlAutomatic
    .ReversePlotOrder = False
    .ScaleType = xlLinear
    .DisplayUnit = xlNone
End With
ActiveChart.ChartTitle.Select
Selection.AutoScaleFont = True
With Selection.Font
```

```
        .Name = "Arial"
        .FontStyle = "Bold"
        .Size = 14
        .Strikethrough = False
        .Superscript = False
        .Subscript = False
        .OutlineFont = False
        .Shadow = False
        .Underline = xlUnderlineStyleNone
        .ColorIndex = xlAutomatic
        .Background = xlAutomatic
    End With
    ActiveChart.Axes(xlCategory).AxisTitle.Select
    Selection.Characters.Text = "Arrhenius Maturity t20 (hrs)"
    Selection.AutoScaleFont = False
    With Selection.Characters(Start:=1, Length:=20).Font
        .Name = "Arial"
        .FontStyle = "Bold"
        .Size = 10
        .Strikethrough = False
        .Superscript = False
        .Subscript = False
        .OutlineFont = False
        .Shadow = False
        .Underline = xlUnderlineStyleNone
        .ColorIndex = xlAutomatic
    End With
    Selection.AutoScaleFont = False
    With Selection.Characters(Start:=21, Length:=2).Font
        .Name = "Arial"
        .FontStyle = "Bold"
        .Size = 10
        .Strikethrough = False
        .Superscript = False
        .Subscript = True
        .OutlineFont = False
        .Shadow = False
```

```
        .Underline = xlUnderlineStyleNone
        .ColorIndex = xlAutomatic
    End With
    ActiveChart.ChartArea.Select
    ActiveChart.HasLegEnd = True
    ActiveChart.LegEnd.Select
    Selection.Position = xlBottom
    ActiveChart.SeriesCollection(1).Name =
Worksheets("Sheet1").Range("C1")

' Heat_rate_graph Macro
' Macro recorded 1/22/2004 by Civil Engineering
'
    Charts.Add
    ActiveChart.ChartType = xlXYScatterSmoothNoMarkers
    ActiveChart.SetSourceData
    Source:=Sheets("Sheet1").Range("O28")
    ActiveChart.SeriesCollection.NewSeries
    ActiveChart.SeriesCollection(1).XValues =
    Worksheets("Sheet1").Range("L20:L" & intRowA)
    ActiveChart.SeriesCollection(1).Values =
    Worksheets("Sheet1").Range("M20:M" & intRowA)
    ActiveChart.Location Where:=xlLocationAsNewSheet, Name:="Heat
 Rate"
    With ActiveChart
        .HasTitle = True
        .ChartTitle.Characters.Text = "Heat Rate"
        .Axes(xlCategory, xlPrimary).HasTitle = True
        .Axes(xlCategory, xlPrimary).AxisTitle.Characters.Text = _
        "Arrhenius Maturity t20 (hrs)"
        .Axes(xlValue, xlPrimary).HasTitle = True
        .Axes(xlValue, xlPrimary).AxisTitle.Characters.Text = "Arrhenius
Heat Rate (W/kg)"
    End With
    With ActiveChart.Axes(xlCategory)
        .HasMajorGridlines = True
        .HasMinorGridlines = False
```

```
End With
With ActiveChart.Axes(xlValue)
    .HasMajorGridlines = True
    .HasMinorGridlines = False
End With
ActiveChart.HasLegEnd = False

ActiveChart.PlotArea.Select
With Selection.Border
    .ColorIndex = 57
    .Weight = xlThin
    .LineStyle = xlContinuous
End With
Selection.Interior.ColorIndex = xlNone
ActiveChart.Axes(xlValue).Select
With Selection.Border
    .Weight = xlHairline
    .LineStyle = xlAutomatic
End With
With Selection
    .MajorTickMark = xlOutside
    .MinorTickMark = xlOutside
    .TickLabelPosition = xlNextToAxis
End With
ActiveChart.ChartTitle.Select
Selection.AutoScaleFont = True
With Selection.Font
    .Name = "Arial"
    .FontStyle = "Bold"
    .Size = 14
    .Strikethrough = False
    .Superscript = False
    .Subscript = False
    .OutlineFont = False
    .Shadow = False
    .Underline = xlUnderlineStyleNone
    .ColorIndex = xlAutomatic
```

```
    .Background = xlAutomatic
End With
ActiveChart.Axes(xlCategory).Select
With Selection.Border
    .Weight = xlHairline
    .LineStyle = xlAutomatic
End With
With Selection
    .MajorTickMark = xlOutside
    .MinorTickMark = xlOutside
    .TickLabelPosition = xlLow
End With
With ActiveChart.Axes(xlCategory)
    .MinimumScale = 0
    .MaximumScaleIsAuto = True
    .MinorUnit = 0.5
    .MajorUnitIsAuto = True
    .Crosses = xlAutomatic
    .ReversePlotOrder = False
    .ScaleType = xlLinear
    .DisplayUnit = xlNone
End With
With ActiveChart.Axes(xlValue)
    .MinimumScale = 0
    .MaximumScaleIsAuto = True
    .MinorUnitIsAuto = True
    .MajorUnitIsAuto = True
    .Crosses = xlAutomatic
    .ReversePlotOrder = False
    .ScaleType = xlLinear
    .DisplayUnit = xlNone
End With
ActiveChart.Axes(xlCategory).AxisTitle.Select
Selection.Characters.Text = "Arrhenius Maturity t20 (hrs)"
Selection.AutoScaleFont = False
With Selection.Characters(Start:=1, Length:=20).Font
    .Name = "Arial"
```

```
            .FontStyle = "Bold"
            .Size = 10
            .Strikethrough = False
            .Superscript = False
            .Subscript = False
            .OutlineFont = False
            .Shadow = False
            .Underline = xlUnderlineStyleNone
            .ColorIndex = xlAutomatic
        End With
        Selection.AutoScaleFont = False
        With Selection.Characters(Start:=21, Length:=2).Font
            .Name = "Arial"
            .FontStyle = "Bold"
            .Size = 10
            .Strikethrough = False
            .Superscript = False
            .Subscript = True
            .OutlineFont = False
            .Shadow = False
            .Underline = xlUnderlineStyleNone
            .ColorIndex = xlAutomatic
        End With
        ActiveChart.ChartArea.Select
        ActiveChart.HasLegEnd = True
        ActiveChart.LegEnd.Select
        Selection.Position = xlBottom
        ActiveChart.SeriesCollection(1).Name =
        Worksheets("Sheet1").Range("C1")

    Application.ScreenUpdating = True
    End Sub
```

Appendix B

MATURITY HEAT RATE MODEL

B.1 Introduction

This appendix contains screen shots of the spreadsheet-based maturity heat rate prediction are also presented here for the purposes of completeness of chapter 5. These illustrate the stepwise process adopted for the prediction model as summarised in figures 5.6 and 5.7 in chapter 5.

B.2 Screenshots of the Prediction Model

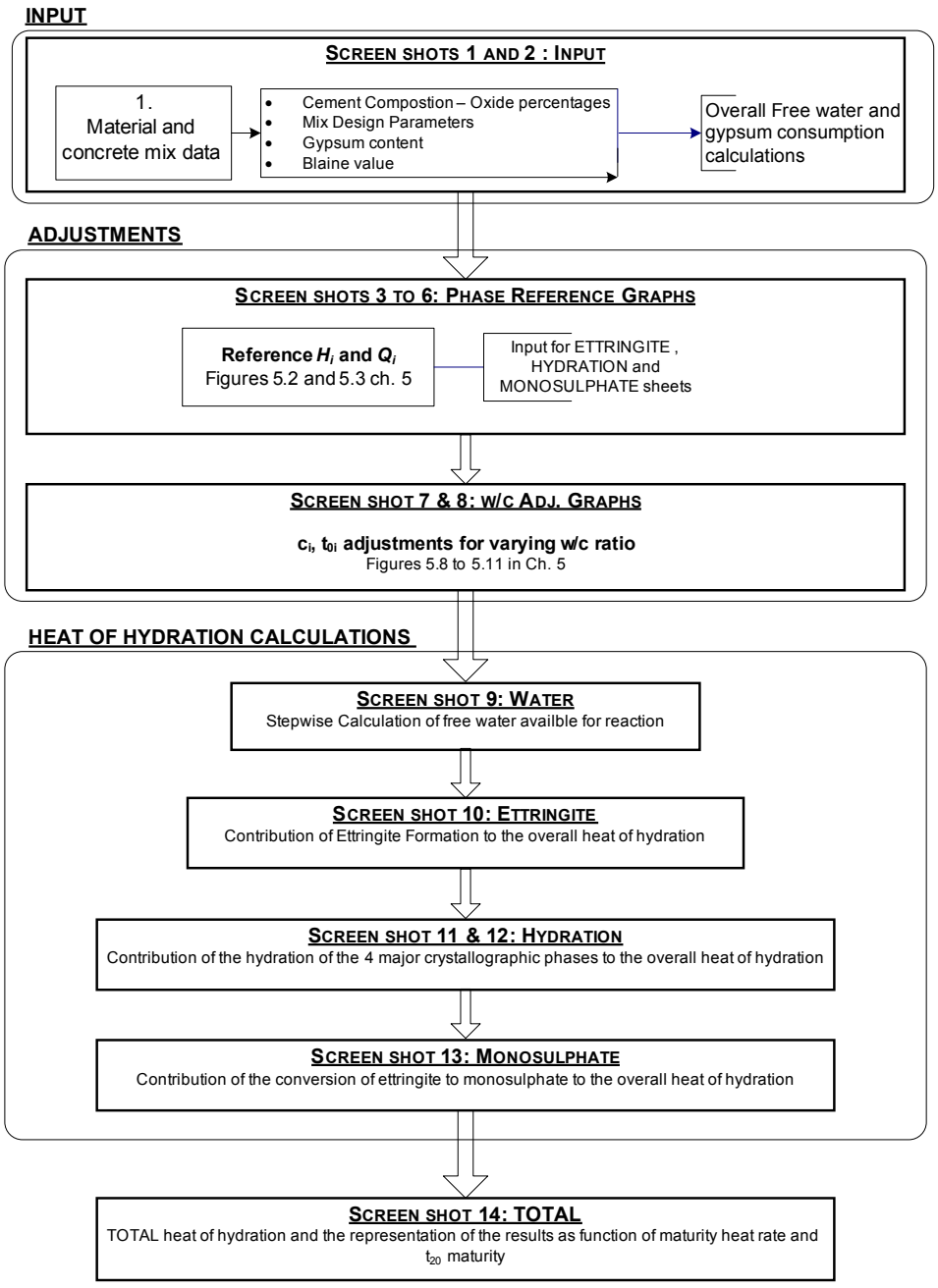

Figure B.1. Progression of Maturity Heat Rate Model

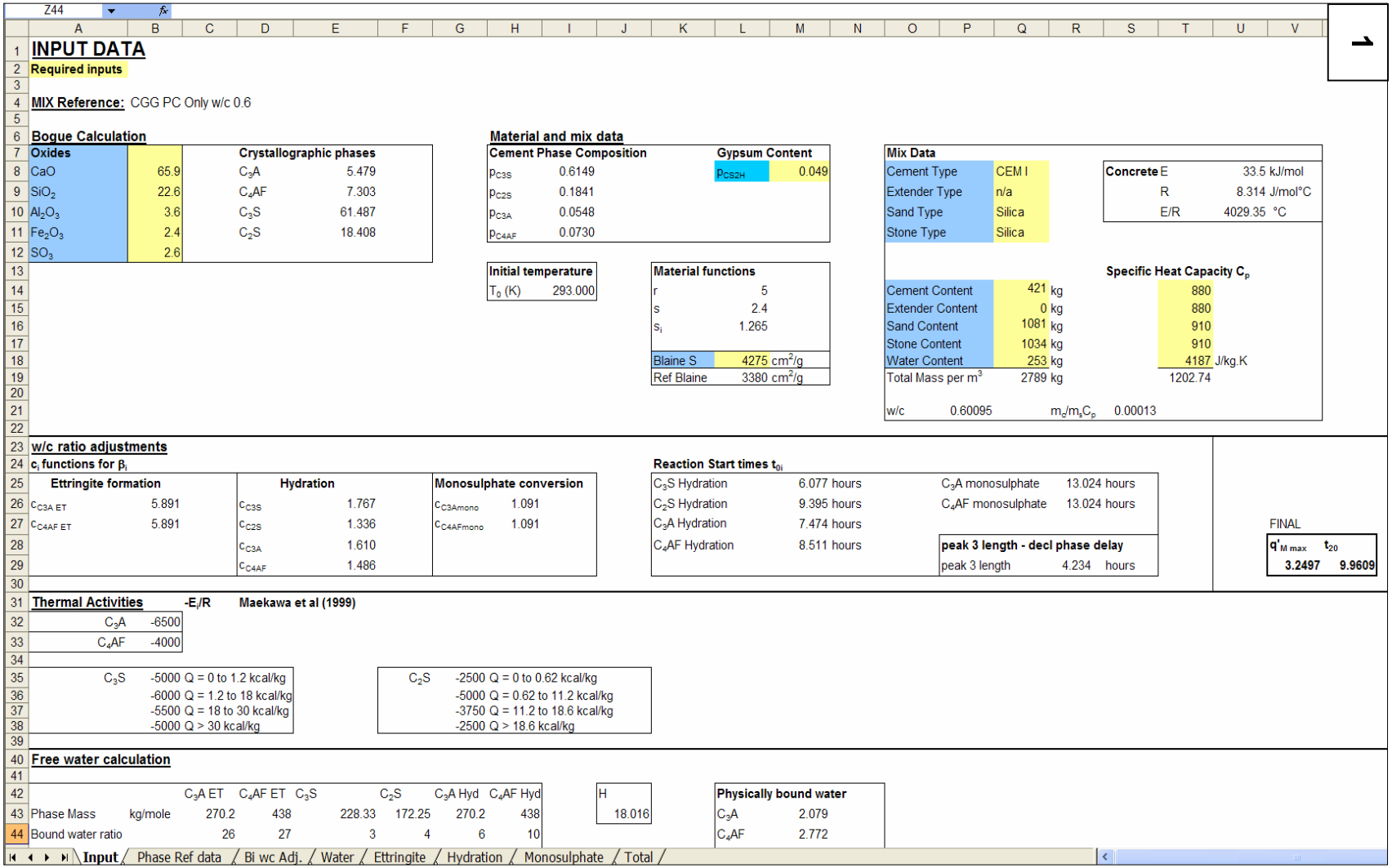

INPUT DATA

Required inputs

MIX Reference: CGG PC Only w/c 0.6

Bogue Calculation

Oxides		Crystallographic phases	
CaO	65.9	C_3A	5.479
SiO_2	22.6	C_4AF	7.303
Al_2O_3	3.6	C_3S	61.487
Fe_2O_3	2.4	C_2S	18.408
SO_3	2.6		

Material and mix data

Cement Phase Composition		Gypsum Content	
p_{C3S}	0.6149	p_{CS2H}	0.049
p_{C2S}	0.1841		
p_{C3A}	0.0548		
p_{C4AF}	0.0730		

Initial temperature	
T_0 (K)	293.000

Material functions	
r	5
s	2.4
s_i	1.265
Blaine S	4275 cm^2/g
Ref Blaine	3380 cm^2/g

Mix Data

Cement Type	CEM I		
Extender Type	n/a		
Sand Type	Silica		
Stone Type	Silica		
		Specific Heat Capacity C_p	
Cement Content	421 kg		880
Extender Content	0 kg		880
Sand Content	1081 kg		910
Stone Content	1034 kg		910
Water Content	253 kg		4187 J/kg.K
Total Mass per m^3	2789 kg		1202.74
w/c	0.60095	m_c/m_sC_p	0.00013

Concrete		
E	33.5	kJ/mol
R	8.314	J/mol°C
E/R	4029.35	°C

w/c ratio adjustments

c_i functions for β_i

Ettringite formation		Hydration		Monosulphate conversion	
$c_{C3A\ ET}$	5.891	c_{C3S}	1.767	$c_{C3Amono}$	1.091
$c_{C4AF\ ET}$	5.891	c_{C2S}	1.336	$c_{C4AFmono}$	1.091
		c_{C3A}	1.610		
		c_{C4AF}	1.486		

Reaction Start times t_{0i}

C_3S Hydration	6.077 hours	C_3A monosulphate	13.024 hours
C_2S Hydration	9.395 hours	C_4AF monosulphate	13.024 hours
C_3A Hydration	7.474 hours		
C_4AF Hydration	8.511 hours		

peak 3 length - decl phase delay		
peak 3 length	4.234	hours

FINAL

$q'_{M\ max}$	t_{20}
3.2497	9.9609

Thermal Activities $-E_i/R$ **Maekawa et al (1999)**

C_3A	-6500
C_4AF	-4000

C_3S	-5000 Q = 0 to 1.2 kcal/kg
	-6000 Q = 1.2 to 18 kcal/kg
	-5500 Q = 18 to 30 kcal/kg
	-5000 Q > 30 kcal/kg

C_2S	-2500 Q = 0 to 0.62 kcal/kg
	-5000 Q = 0.62 to 11.2 kcal/kg
	-3750 Q = 11.2 to 18.6 kcal/kg
	-2500 Q > 18.6 kcal/kg

Free water calculation

		C_3A ET	C_4AF ET	C_3S	C_2S	C_3A Hyd	C_4AF Hyd
Phase Mass	kg/mole	270.2	438	228.33	172.25	270.2	438
Bound water ratio		26	27	3	4	6	10

H	
	18.016

Physically bound water	
C_3A	2.079
C_4AF	2.772

Input / Phase Ref data / Bi wc Adj. / Water / Ettringite / Hydration / Monosulphate / Total

2

c_{C3A}	1.610	
c_{C4AF}	1.486	

C_4AF Hydration 8.511 hours

Thermal Activities $-E_i/R$ **Maekawa et al (1999)**

C_3A	-6500
C_4AF	-4000

C_3S	-5000	Q = 0 to 1.2 kcal/kg
	-6000	Q = 1.2 to 18 kcal/kg
	-5500	Q = 18 to 30 kcal/kg
	-5000	Q > 30 kcal/kg

C_2S	-2500	Q = 0 to 0.62 kcal/kg
	-5000	Q = 0.62 to 11.2 kcal/kg
	-3750	Q = 11.2 to 18.6 kcal/kg
	-2500	Q > 18.6 kcal/kg

Free water calculation

		C_3A ET	C_4AF ET	C_3S	C_2S	C_3A Hyd	C_4AF Hyd
Phase Mass	kg/mole	270.2	438	228.33	172.25	270.2	438
Bound water ratio		26	27	3	4	6	10
React. Water	kg/mole	468.416	486.432	54.048	72.064	108.096	180.160
Reqd Water	kg	25.665	35.525	33.232	13.266	5.923	13.157
Phys Bound water	kg	3.460	4.612	38.829	11.625	3.460	4.612
		29.126	40.137	72.061	24.891	9.383	17.769

H
18.016

Physically bound water	
C_3A	2.079
C_4AF	2.772
C_3S	23.334
C_2S	6.986

total water consumed	kg	ΣW_i =	193.367
End Water	kg		59.633

$\omega_{free\ end}$	0.142

Gypsum Consumption

		C_3A ET	C_4AF ET	
Phase Mass	kg/mole	270.2	438	
Comb. Ratio with gypsum		3	3	
React. Gypsum	kg/mole	504.606	504.606	
Reqd Gyspum	kg	24.776	24.776	
total gypsum	kg	20.671		
max degree Ettringite formation			0.417	
assume gypsum shared according to % of phase present				
C3A uses		8.861	0.429	0.358
C4AF uses		11.810	0.571	0.477
max gypsum consumption		1.000		

$C\acute{S}H_2$
168.202 kg/mole

Input | Phase Ref data | Bi wc Adj. | Water | Ettringite | Hydration | Monosulphate | Total

B.2.2 Reference Data (Maekawa et al., 1999)

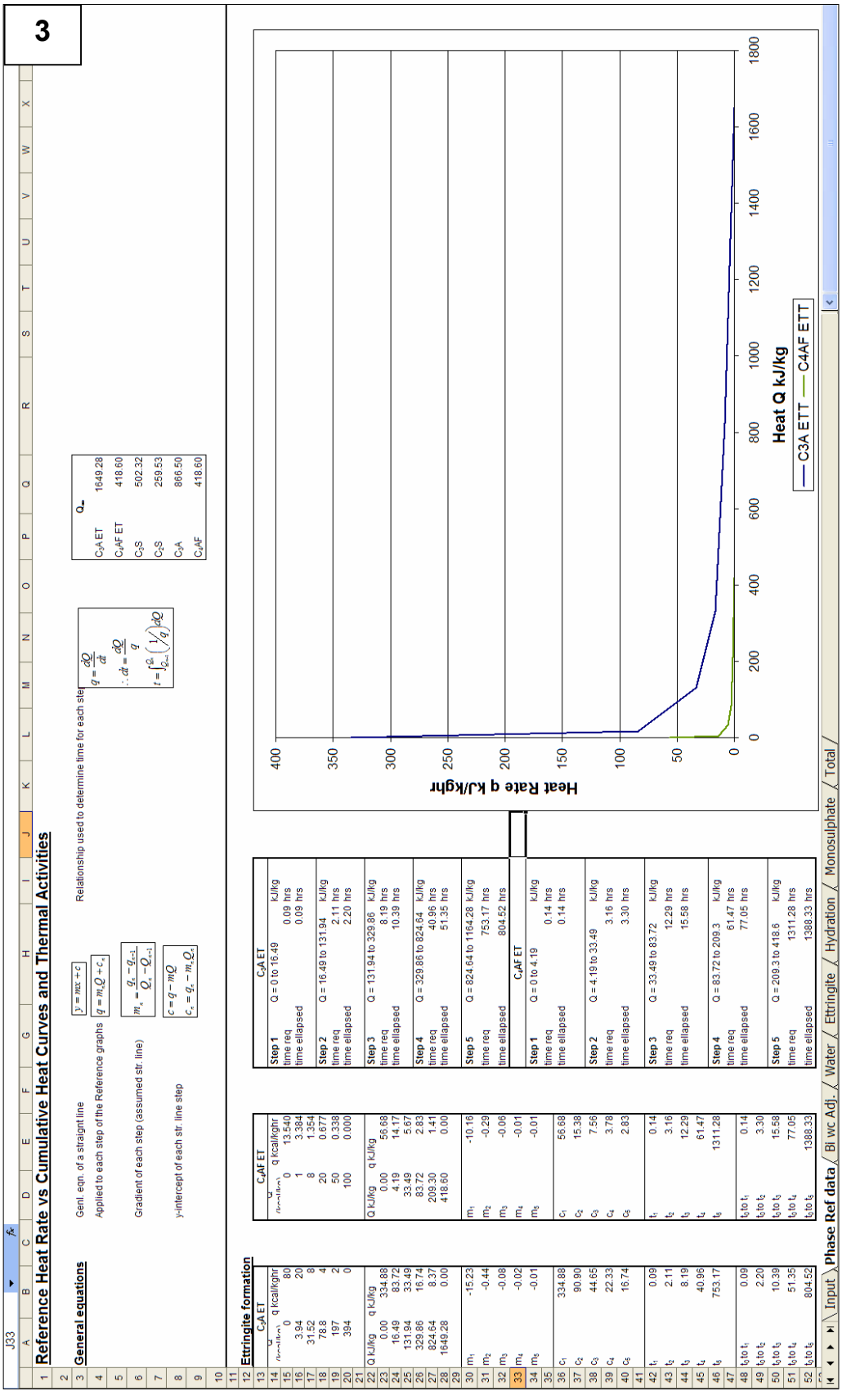

V106

Hydration

C_3A Hydration		C_4AF Hydration		C_3S hydration		C_2S hydration	
Q (kcal/kg)	q kcal/kghr	Q (kcal/kg)	q kcal/kghr	Q (kcal/kg)	q kcal/kghr	Q (kcal/kg)	q kcal/kghr
0	0	0	0	0	0	0	0
2.07	1.38	1	0.6667	1.2	0.8	0.62	0.4133
6.21	5	3	1.61	7.5	3	4.65	0.861
15.56	5	8	1.61	18	3	11.2	0.861
41.4	3.105	20	1	30	1.5	18.6	0.3513
103.5	1.656	50	0.533	60	0.8	31	0.2067
207	0	100	0	120	0	62	0
Q kJ/kg	q kJ/kg	Q kJ/kg	q kJ/kg	Q kJ/kg	q kJ/kg	Q kJ/kg	q kJ/kg
0.00	0.00	0.00	0.00	0.00	0.00	0.00	0.00
8.67	5.78	4.19	2.79	5.02	3.35	2.60	1.73
26.00	20.93	12.56	6.74	31.40	12.56	19.46	3.60
65.13	20.93	33.49	6.74	75.35	12.56	46.88	3.60
173.30	13.00	83.72	4.19	125.58	6.28	77.86	1.47
433.25	6.93	209.30	2.23	251.16	3.35	129.77	0.87
866.50	0.00	418.60	0.00	502.32	0.00	259.53	0.00
m_1	0.67	m_1	0.67	m_1	0.67	m_1	0.67
m_2	0.87	m_2	0.47	m_2	0.35	m_2	0.11
m_3	0.00	m_3	0.00	m_3	0.00	m_3	0.00
m_4	-0.07	m_4	-0.05	m_4	-0.13	m_4	-0.07
m_5	-0.02	m_5	-0.02	m_5	-0.02	m_5	-0.01
m_6	-0.02	m_6	-0.01	m_6	-0.01	m_6	-0.01
c_1	0.00	c_1	0.00	c_1	0.00	c_1	0.00
c_2	-1.80	c_2	0.82	c_2	1.59	c_2	1.44
c_3	20.93	c_3	6.74	c_3	12.56	c_3	3.60
c_4	25.71	c_4	8.44	c_4	21.98	c_4	6.83
c_5	17.04	c_5	5.49	c_5	9.21	c_5	2.38
c_6	13.86	c_6	4.46	c_6	6.70	c_6	1.73
t_1	2.63	t_1	1.54	t_1	1.81	t_1	0.82
t_2	1.47	t_2	1.87	t_2	3.79	t_2	6.61
t_3	1.87	t_3	3.11	t_3	3.50	t_3	7.61
t_4	6.50	t_4	9.37	t_4	5.55	t_4	13.02
t_5	26.94	t_5	40.42	t_5	26.94	t_5	45.48
t_6	552.74	t_6	723.29	t_6	608.73	t_6	1014.29
t_0 to t_1	2.63	t_0 to t_1	1.54	t_0 to t_1	1.81	t_0 to t_1	0.82
t_0 to t_2	4.10	t_0 to t_2	3.41	t_0 to t_2	5.60	t_0 to t_2	7.43
t_0 to t_3	5.97	t_0 to t_3	6.51	t_0 to t_3	9.10	t_0 to t_3	15.04
t_0 to t_4	12.47	t_0 to t_4	15.88	t_0 to t_4	14.64	t_0 to t_4	28.05
t_0 to t_5	39.41	t_0 to t_5	56.30	t_0 to t_5	41.58	t_0 to t_5	73.53
t_0 to t_6	592.15	t_0 to t_6	779.59	t_0 to t_6	650.31	t_0 to t_6	1087.82

C_3A Hydration		C_3S hydration	
Step 1	Q = 0 to 8 kJ/kg	**Step 1**	Q = 0 to 5 kJ/kg
time req	2.63 hrs	time req	1.81 hrs
time ellasp	2.63 hrs	time ellaspe	1.81 hrs
Step 2	Q = 8.67 t kJ/kg	**Step 2**	Q = 5.02 t kJ/kg
time req	1.47 hrs	time req	3.79 hrs
time ellasp	4.10 hrs	time ellaspe	5.60 hrs
Step 3	Q = 26 to kJ/kg	**Step 3**	Q = 31.4 t kJ/kg
time req	1.87 hrs	time req	3.50 hrs
time ellasp	5.97 hrs	time ellaspe	9.10 hrs
Step 4	Q = 65.13 kJ/kg	**Step 4**	Q = 75.35 kJ/kg
time req	6.50 hrs	time req	5.55 hrs
time ellasp	12.47 hrs	time ellaspe	14.64 hrs
Step 5	Q = 173.3 kJ/kg	**Step 5**	Q = 125.5 kJ/kg
time req	26.94 hrs	time req	26.94 hrs
time ellasp	39.41 hrs	time ellaspe	41.58 hrs
Step 6	Q = 433.2 kJ/kg	**Step 6**	Q = 251.5 kJ/kg
time req	552.74 hrs	time req	608.73 hrs
time ellasp	592.15 hrs	time ellaspe	650.31 hrs

C_4AF Hydration		C_2S hydration	
Step 1	Q = 0 to 4 kJ/kg	**Step 1**	Q = 0 to 2 kJ/kg
time req	1.54 hrs	time req	0.82 hrs
time ellasp	1.54 hrs	time ellaspe	0.82 hrs
Step 2	Q = 4.19 t kJ/kg	**Step 2**	Q = 2.6 to kJ/kg
time req	1.87 hrs	time req	6.61 hrs
time ellasp	3.41 hrs	time ellaspe	7.43 hrs
Step 3	Q = 12.56 kJ/kg	**Step 3**	Q = 19.46 kJ/kg
time req	3.11 hrs	time req	7.61 hrs
time ellasp	6.51 hrs	time ellaspe	15.04 hrs
Step 4	Q = 33.49 kJ/kg	**Step 4**	Q = 46.88 kJ/kg
time req	9.37 hrs	time req	13.02 hrs
time ellasp	15.88 hrs	time ellaspe	28.05 hrs
Step 5	Q = 83.72 kJ/kg	**Step 5**	Q = 77.86 kJ/kg
time req	40.42 hrs	time req	45.48 hrs
time ellasp	56.30 hrs	time ellaspe	73.53 hrs
Step 6	Q = 209.3 kJ/kg	**Step 6**	Q = 129.7 kJ/kg
time req	723.29 hrs	time req	1014.29 hrs
time ellasp	779.59 hrs	time ellaspe	1087.82 hrs

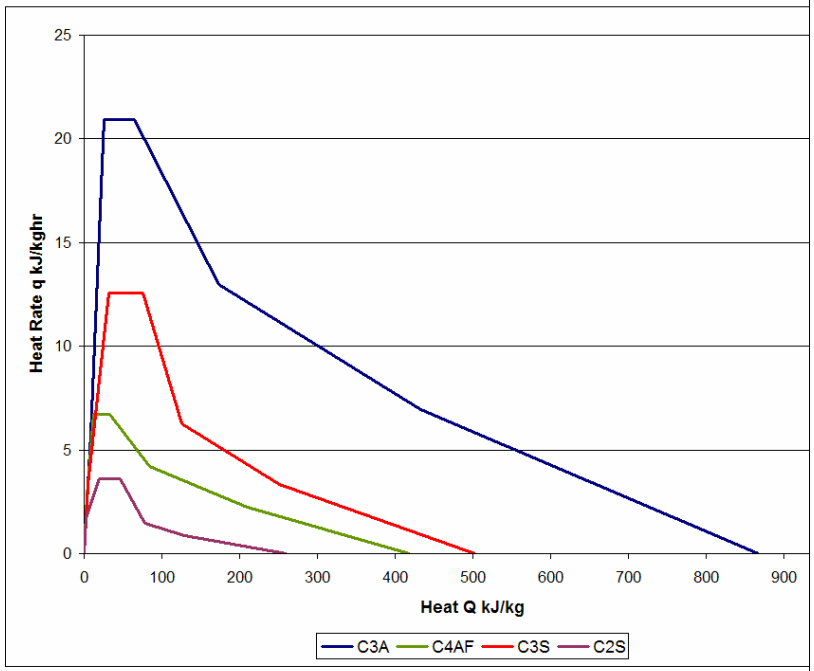

Input | **Phase Ref data** | Bi wc Adj. | Water | Ettringite | Hydration | Monosulphate | Total

V106

Monosulphate conversion

C_3A mono		
Q (kcal/kg)	q kcal/kghr	
0.00	0.00	
1.38	0.92	
4.14	3.33	
10.37	3.33	
27.60	2.07	
69.00	1.10	
138.00	0.00	
Q kJ/kg	q kJ/kg	
0.00	0.00	
5.78	3.85	
17.33	13.95	
43.42	13.95	
115.53	8.67	
288.83	4.62	
577.67	0.00	
m_1	0.67	
m_2	0.87	
m_3	0.00	
m_4	-0.07	
m_5	-0.02	
m_6	-0.02	
c_1	0.00	
c_2	-1.20	
c_3	13.95	
c_4	17.14	
c_5	11.36	
c_6	9.24	
t_1	2.02	
t_2	1.47	
t_3	1.87	
t_4	6.50	
t_5	26.94	
t_6	527.40	
t_0 to t_1	2.02	
t_0 to t_2	3.49	
t_0 to t_3	5.36	
t_0 to t_4	11.86	
t_0 to t_5	38.80	
t_0 to t_6	566.20	

C_4AF mono	
Q (kcal/kg)	q kcal/kghr
0.00	0.00
0.67	0.44
2.00	1.07
5.33	1.07
13.33	0.67
33.33	0.36
66.67	0.00
Q kJ/kg	q kJ/kg
0.00	0.00
2.79	1.86
8.37	4.49
22.33	4.49
55.81	2.79
139.53	1.49
279.07	0.00
m_1	0.67
m_2	0.47
m_3	0.00
m_4	-0.05
m_5	-0.02
m_6	-0.01
c_1	0.00
c_2	0.54
c_3	4.49
c_4	5.63
c_5	3.66
c_6	2.97
t_1	0.93
t_2	1.87
t_3	3.11
t_4	9.37
t_5	40.42
t_6	685.25
t_0 to t_1	0.93
t_0 to t_2	2.80
t_0 to t_3	5.91
t_0 to t_4	15.27
t_0 to t_5	55.70
t_0 to t_6	740.95

C_3A mono	
Step 1	Q = 0 to 5.78 kJ/kg
time req	2.02 hrs
time ellasped	2.02 hrs
Step 2	Q = 5.78 to 17 kJ/kg
time req	1.47 hrs
time ellasped	3.49 hrs
Step 3	Q = 17.33 to 4 kJ/kg
time req	1.87 hrs
time ellasped	5.36 hrs
Step 4	Q = 43.42 to 1 kJ/kg
time req	6.50 hrs
time ellasped	11.86 hrs
Step 5	Q = 115.53 to kJ/kg
time req	26.94 hrs
time ellasped	38.80 hrs
Step 6	Q = 288.83 to kJ/kg
time req	527.40 hrs
time ellasped	566.20 hrs

C_4AF mono	
Step 1	Q = 0 to 2.79 kJ/kg
time req	0.93 hrs
time ellasped	0.93 hrs
Step 2	Q = 2.79 to 8. kJ/kg
time req	1.87 hrs
time ellasped	2.80 hrs
Step 3	Q = 8.37 to 22 kJ/kg
time req	3.11 hrs
time ellasped	5.91 hrs
Step 4	Q = 22.33 to 8 kJ/kg
time req	9.37 hrs
time ellasped	15.27 hrs
Step 5	Q = 55.81 to 1 kJ/kg
time req	40.42 hrs
time ellasped	55.70 hrs
Step 6	Q = 139.53 to kJ/kg
time req	685.25 hrs
time ellasped	740.95 hrs

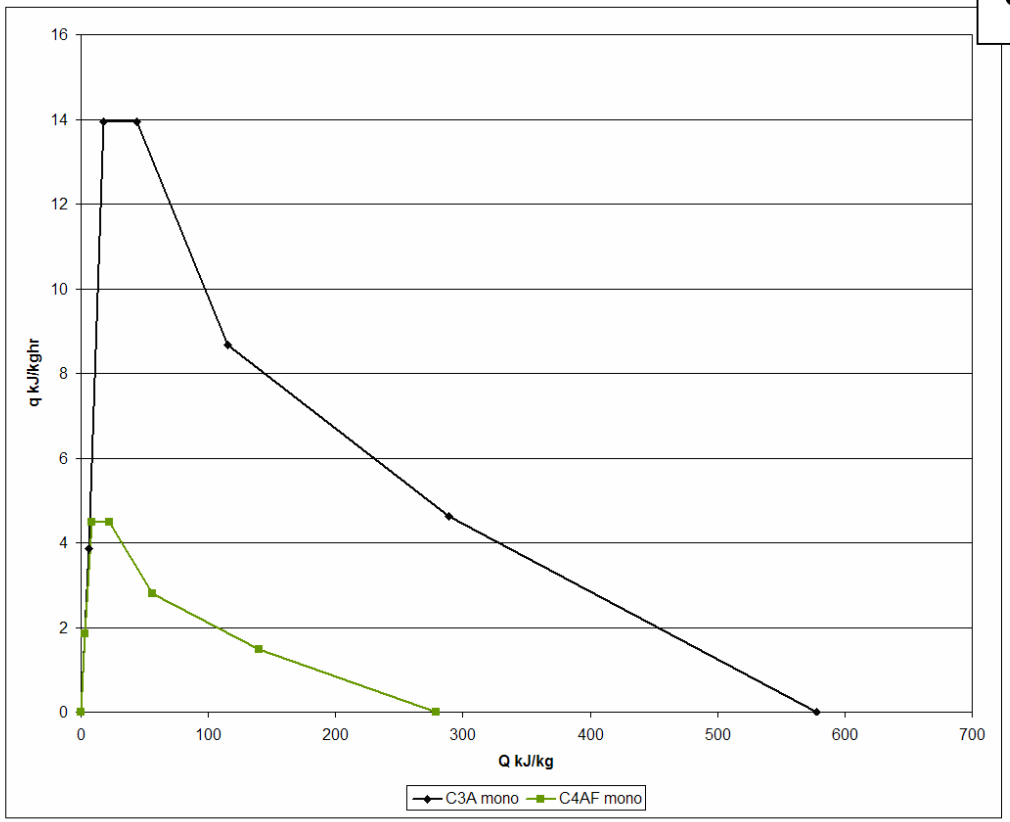

Input | **Phase Ref data** | Bi wc Adj. | Water | Ettringite | Hydration | Monosulphate | Total

Thermal Activities

-E/R — Maekawa et al (1999)

C_3A	-6500
C_4AF	-4000

C_3S	-5000	Q = 0 to 1.2 kcal/kg
	-6000	Q = 1.2 to 18 kcal/kg
	-5500	Q = 18 to 30 kcal/kg
	-5000	Q > 30 kcal/kg

C_2S	-2500	Q = 0 to 0.62 kcal/kg
	-5000	Q = 0.62 to 11.2 kcal/kg
	-3750	Q = 11.2 to 18.6 kcal/kg
	-2500	Q > 18.6 kcal/kg

C_3S		C_2S		C_3A		C_4AF	
Q kcal/kg	-E/R	Q kcal/kg	-E/R	Q kcal/kg	-E/R	Q kcal/kg	-E/R
0	-5000	0	-2500	0	-6500	0	-4000
1.2	-5000	0.62	-2500	2.07	-6500	1	-4000
7.5	-6000	4.65	-5000	6.21	-6500	3	-4000
18	-6000	11.2	-5000	15.56	-6500	8	-4000
30	-5500	18.6	-3750	41.4	-6500	20	-4000
60	-5000	31	-2500	103.5	-6500	50	-4000
200	-5000	200	-2500	200	-6500	200	-4000

C_3S		C_2S		C_3A		C_4AF	
Q kJ/kg	-E/R	Q kJ/kg	-E/R	Q kJ/kg	-E/R	Q kJ/kg	-E/R
0	-5000	0	-2500	0	-6500	0	-4000
5.0232	-5000	2.59532	-2500	8.66502	-6500	4.186	-4000
31.395	-6000	19.4649	-5000	25.99506	-6500	12.558	-4000
75.348	-6000	46.8832	-5000	65.13416	-6500	33.488	-4000
125.58	-5500	77.8596	-3750	173.3004	-6500	83.72	-4000
251.16	-5000	129.766	-2500	433.251	-6500	209.3	-4000
837.2	-5000	837.2	-2500	837.2	-6500	837.2	-4000

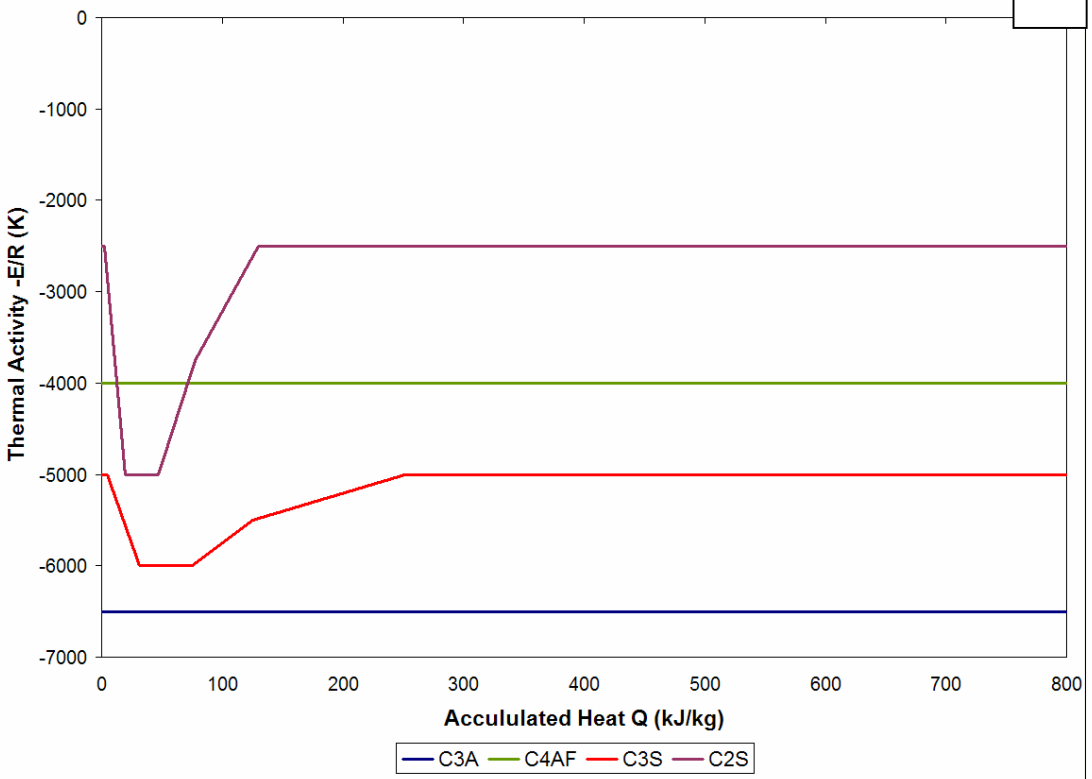

Input | Phase Ref data | Bi wc Adj. | Water | Ettringite | Hydration | Monosulphate | Total

B.2.3 w/c Adjustments

7

w/c Ratio Adjustment graphs - adjustment of β_i

Equations for Empirical Adjustment Curves

General equation applied to all curves shown in the sheet:

$$y = A \ln x + B$$

y = the adjustment function in question
x = the w/c ratio

c_i adjustment eqns

	A	B
C_3S	-2.9496	0.2654
C_2S	-2.9413	-0.1621
C_3A	-2.9529	0.1064
C_4AF	-2.9413	-0.0121
C_3A_{ETT}	1.4748	6.6423
C_4AF_{ETT}	1.4748	6.6423
Mono	1.4748	1.8423

Reaction start time eqns for t_{0i}

	A	B
C_3S	3.9328	8.0795
C_2S	3.941	11.402
C_3A	4.4244	9.727
C_4AF	4.4409	10.772
Mono	4.4244	15.277

delay of decl. phase - peak 3

	A	B
delay	4.3056	6.4264

w/c Adjustment factors

w/c: 0.601

	c_i
C_3S	1.767
C_2S	1.336
C_3A	1.610
C_4AF	1.486
C_3A_{ETT}	5.891
C_4AF_{ETT}	5.891
Mono	1.091

	t_{0i} (hours)
C_3S	6.077
C_2S	9.395
C_3A	7.474
C_4AF	8.511
Mono	13.024

length peak 3 4.234

w/c ratio	c_i adjustment eqns							Reaction start time eqns for t_{0i}						
	C_3S	C_2S	C_3A	C_4AF	C_3A ett	C_4AF ett	Mono	C_3S	C_2S	C_3A	C_4AF	Mono	delay 3
0.00001	34.224	33.701	34.103	33.851	-10.337	-10.337	-15.137	-37.199	-33.970	-41.211	-40.356	-35.661	-43.144
0.05	9.102	8.649	8.952	8.799	2.224	2.224	-2.576	-3.702	-0.404	-3.527	-2.532	2.023	-6.472
0.1	7.057	6.610	6.906	6.760	3.246	3.246	-1.554	-0.976	2.328	-0.461	0.546	5.089	-3.488
0.15	5.861	5.418	5.708	5.568	3.844	3.844	-0.956	0.619	3.925	1.333	2.347	6.883	-1.742
0.2	5.013	4.572	4.859	4.722	4.269	4.269	-0.531	1.750	5.059	2.606	3.625	8.156	-0.503
0.25	4.354	3.915	4.200	4.065	4.598	4.598	-0.202	2.627	5.939	3.593	4.616	9.143	0.458
0.3	3.817	3.379	3.662	3.529	4.867	4.867	0.067	3.345	6.657	4.400	5.425	9.950	1.243
0.35	3.362	2.926	3.206	3.076	5.094	5.094	0.294	3.951	7.265	5.082	6.110	10.632	1.906
0.4	2.968	2.533	2.812	2.683	5.291	5.291	0.491	4.476	7.791	5.673	6.703	11.223	2.481
0.45	2.621	2.187	2.464	2.337	5.465	5.465	0.665	4.939	8.255	6.194	7.226	11.744	2.988
0.5	2.310	1.877	2.153	2.027	5.620	5.620	0.820	5.353	8.670	6.660	7.694	12.210	3.442
0.55	2.029	1.596	1.872	1.746	5.761	5.761	0.961	5.728	9.046	7.082	8.117	12.632	3.852
0.6	1.772	1.340	1.615	1.490	5.889	5.889	1.089	6.071	9.389	7.467	8.503	13.017	4.227
0.65	1.536	1.105	1.378	1.255	6.007	6.007	1.207	6.385	9.704	7.821	8.859	13.371	4.572
0.7	1.317	0.887	1.160	1.037	6.116	6.116	1.316	6.677	9.996	8.149	9.188	13.699	4.891
0.75	1.114	0.684	0.956	0.834	6.218	6.218	1.418	6.948	10.268	8.454	9.494	14.004	5.188
0.8	0.924	0.494	0.765	0.644	6.313	6.313	1.513	7.202	10.523	8.740	9.781	14.290	5.466
0.85	0.745	0.316	0.586	0.466	6.403	6.403	1.603	7.440	10.762	9.008	10.050	14.558	5.727
0.9	0.576	0.148	0.418	0.298	6.487	6.487	1.687	7.665	10.987	9.261	10.304	14.811	5.973
0.95	0.417	-0.011	0.258	0.139	6.567	6.567	1.767	7.878	11.200	9.500	10.544	15.050	6.206
1	0.265	-0.162	0.106	-0.012	6.642	6.642	1.842	8.080	11.402	9.727	10.772	15.277	6.426

Input / Phase Ref data / Bi wc Adj. / Water / Ettringite / Hydration / Monosulphate / Total /

AA95

Empirical Adjustment Curves

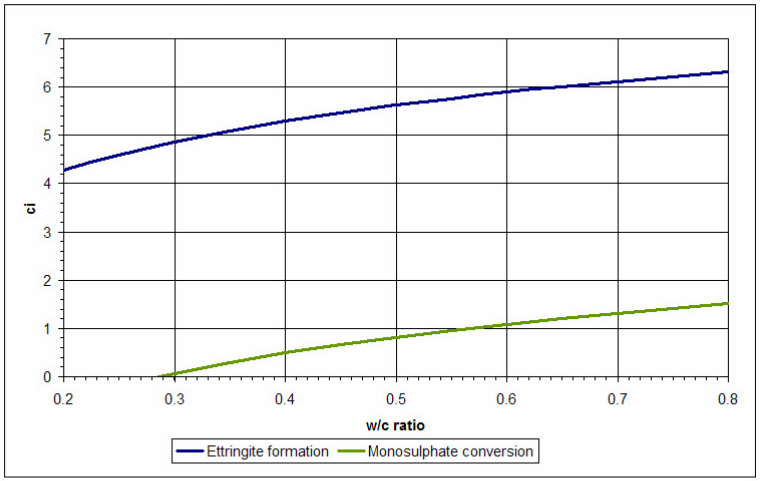

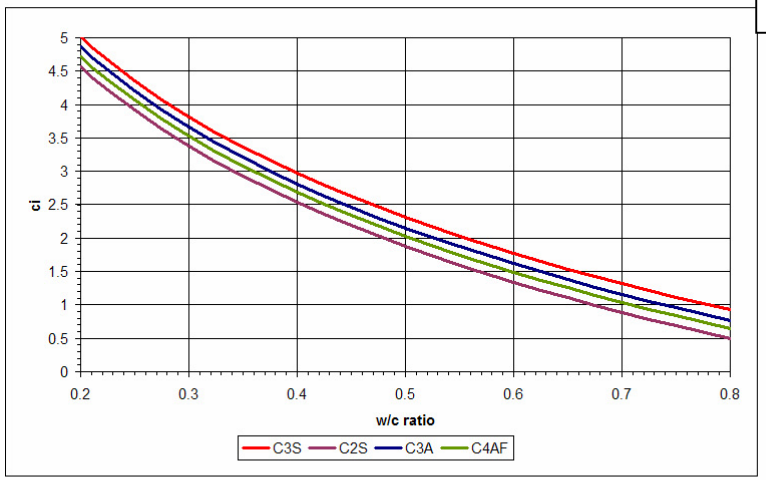

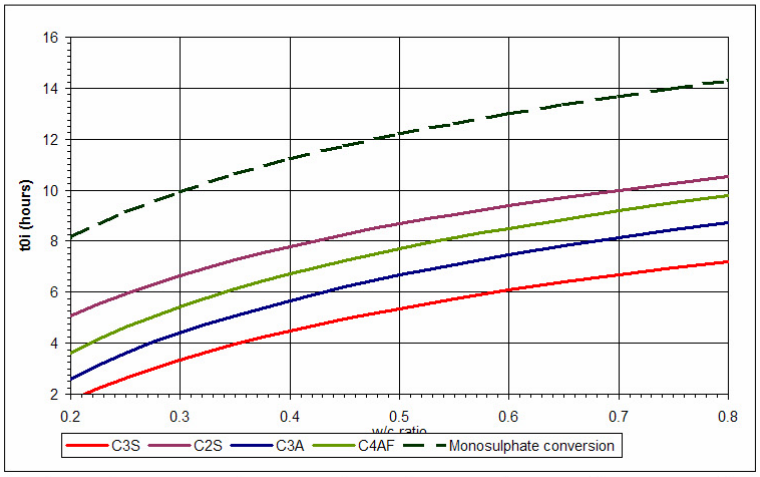

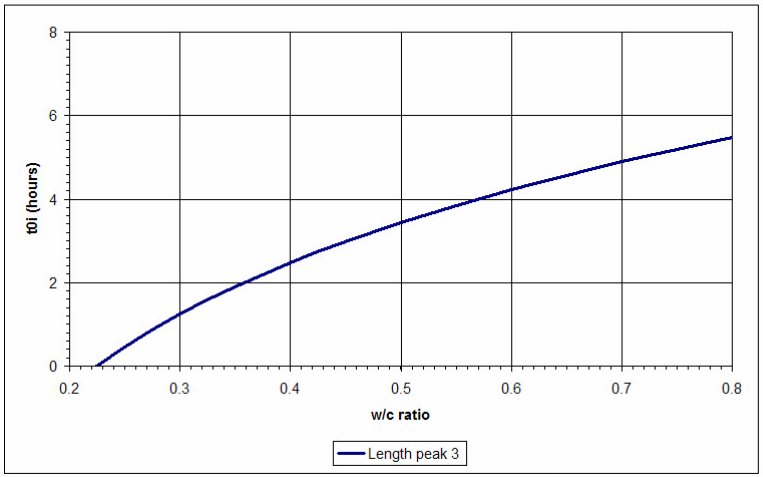

Input | Phase Ref data | **Bi wc Adj.** | Water | Ettringite | Hydration | Monosulphate | Total

B.2.4 Free Water Calculations

B.2.5 Ettringite Formation

B.2.6 Hydration of the Four Major Cement Phases

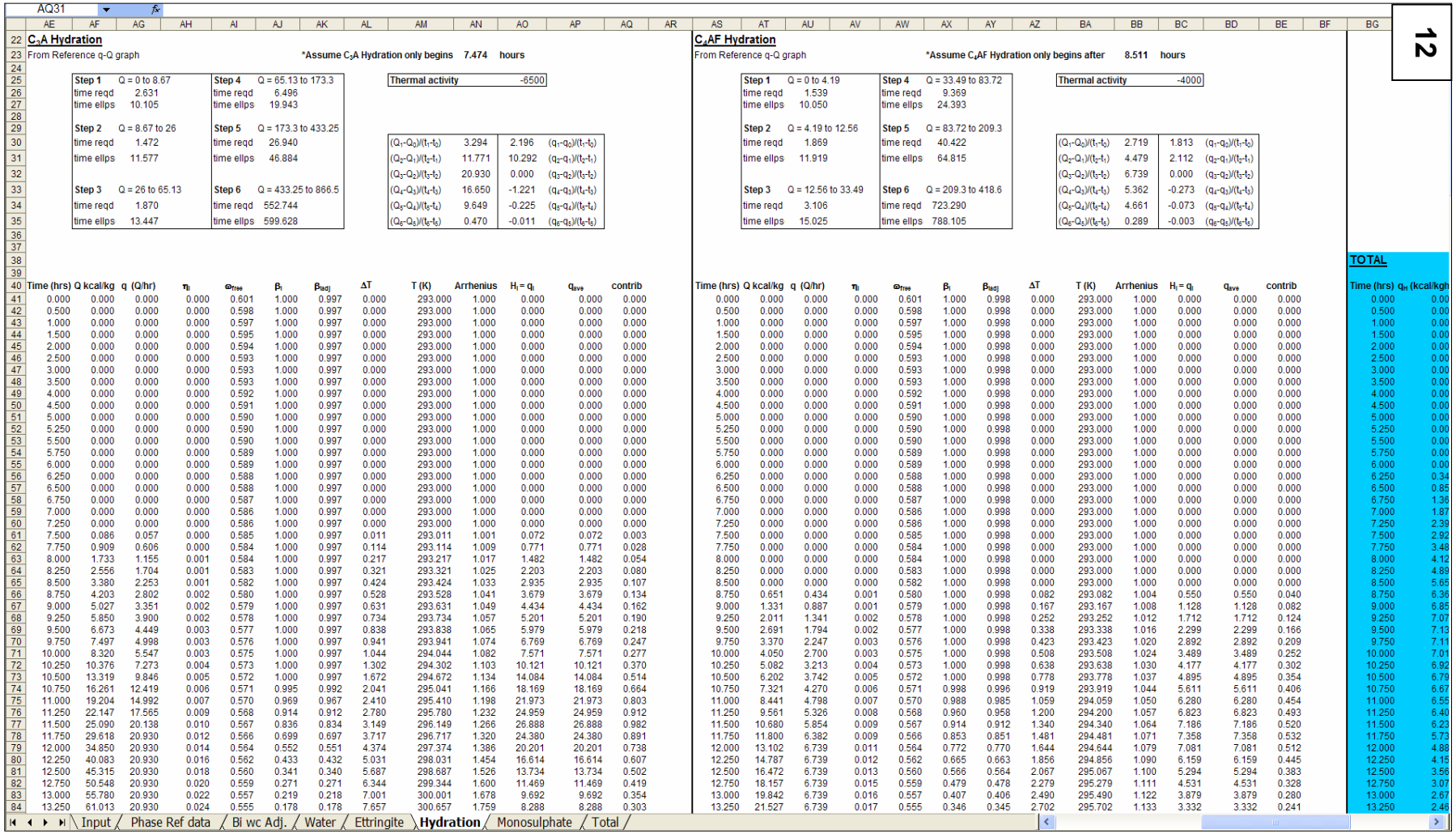

AQ31

C_3A Hydration

From Reference q-Q graph

*Assume C_3A Hydration only begins 7.474 hours

Step 1	Q = 0 to 8.67	**Step 4**	Q = 65.13 to 173.3
time reqd	2.631	time reqd	6.496
time ellps	10.105	time ellps	19.943
Step 2	Q = 8.67 to 26	**Step 5**	Q = 173.3 to 433.25
time reqd	1.472	time reqd	26.940
time ellps	11.577	time ellps	46.884
Step 3	Q = 26 to 65.13	**Step 6**	Q = 433.25 to 866.5
time reqd	1.870	time reqd	552.744
time ellps	13.447	time ellps	599.628

Thermal activity -6500

$(Q_1-Q_0)/(t_1-t_0)$	3.294	2.196	$(q_1-q_0)/(t_1-t_0)$
$(Q_2-Q_1)/(t_2-t_1)$	11.771	10.292	$(q_2-q_1)/(t_2-t_1)$
$(Q_3-Q_2)/(t_3-t_2)$	20.930	0.000	$(q_3-q_2)/(t_3-t_2)$
$(Q_4-Q_3)/(t_4-t_3)$	16.650	-1.221	$(q_4-q_3)/(t_4-t_3)$
$(Q_5-Q_4)/(t_5-t_4)$	9.649	-0.225	$(q_5-q_4)/(t_5-t_4)$
$(Q_6-Q_5)/(t_6-t_5)$	0.470	-0.011	$(q_6-q_5)/(t_6-t_5)$

Time (hrs)	Q kcal/kg	q (Q/hr)	η_{ll}	ω_{free}	β_l	β_{lacj}	ΔT	T (K)	Arrhenius	$H_l = q_l$	q_{ave}	contrib
0.000	0.000	0.000	0.000	0.601	1.000	0.997	0.000	293.000	1.000	0.000	0.000	0.000
0.500	0.000	0.000	0.000	0.598	1.000	0.997	0.000	293.000	1.000	0.000	0.000	0.000
1.000	0.000	0.000	0.000	0.597	1.000	0.997	0.000	293.000	1.000	0.000	0.000	0.000
1.500	0.000	0.000	0.000	0.595	1.000	0.997	0.000	293.000	1.000	0.000	0.000	0.000
2.000	0.000	0.000	0.000	0.594	1.000	0.997	0.000	293.000	1.000	0.000	0.000	0.000
2.500	0.000	0.000	0.000	0.593	1.000	0.997	0.000	293.000	1.000	0.000	0.000	0.000
3.000	0.000	0.000	0.000	0.593	1.000	0.997	0.000	293.000	1.000	0.000	0.000	0.000
3.500	0.000	0.000	0.000	0.593	1.000	0.997	0.000	293.000	1.000	0.000	0.000	0.000
4.000	0.000	0.000	0.000	0.592	1.000	0.997	0.000	293.000	1.000	0.000	0.000	0.000
4.500	0.000	0.000	0.000	0.591	1.000	0.997	0.000	293.000	1.000	0.000	0.000	0.000
5.000	0.000	0.000	0.000	0.590	1.000	0.997	0.000	293.000	1.000	0.000	0.000	0.000
5.250	0.000	0.000	0.000	0.590	1.000	0.997	0.000	293.000	1.000	0.000	0.000	0.000
5.500	0.000	0.000	0.000	0.590	1.000	0.997	0.000	293.000	1.000	0.000	0.000	0.000
5.750	0.000	0.000	0.000	0.589	1.000	0.997	0.000	293.000	1.000	0.000	0.000	0.000
6.000	0.000	0.000	0.000	0.589	1.000	0.997	0.000	293.000	1.000	0.000	0.000	0.000
6.250	0.000	0.000	0.000	0.588	1.000	0.997	0.000	293.000	1.000	0.000	0.000	0.000
6.500	0.000	0.000	0.000	0.588	1.000	0.997	0.000	293.000	1.000	0.000	0.000	0.000
6.750	0.000	0.000	0.000	0.587	1.000	0.997	0.000	293.000	1.000	0.000	0.000	0.000
7.000	0.000	0.000	0.000	0.586	1.000	0.997	0.000	293.000	1.000	0.000	0.000	0.000
7.250	0.000	0.000	0.000	0.586	1.000	0.997	0.000	293.000	1.000	0.000	0.000	0.000
7.500	0.086	0.057	0.000	0.585	1.000	0.997	0.011	293.011	1.001	0.072	0.072	0.003
7.750	0.909	0.606	0.000	0.584	1.000	0.997	0.114	293.114	1.009	0.771	0.771	0.028
8.000	1.733	1.155	0.001	0.584	1.000	0.997	0.217	293.217	1.017	1.482	1.482	0.054
8.250	2.556	1.704	0.001	0.583	1.000	0.997	0.321	293.321	1.025	2.203	2.203	0.080
8.500	3.380	2.253	0.001	0.582	1.000	0.997	0.424	293.424	1.033	2.935	2.935	0.107
8.750	4.203	2.802	0.002	0.580	1.000	0.997	0.528	293.528	1.041	3.679	3.679	0.134
9.000	5.027	3.351	0.002	0.579	1.000	0.997	0.631	293.631	1.049	4.434	4.434	0.162
9.250	5.850	3.900	0.002	0.578	1.000	0.997	0.734	293.734	1.057	5.201	5.201	0.190
9.500	6.673	4.449	0.003	0.577	1.000	0.997	0.838	293.838	1.065	5.979	5.979	0.218
9.750	7.497	4.998	0.003	0.576	1.000	0.997	0.941	293.941	1.074	6.769	6.769	0.247
10.000	8.320	5.547	0.003	0.575	1.000	0.997	1.044	294.044	1.082	7.571	7.571	0.277
10.250	10.376	7.273	0.004	0.573	1.000	0.997	1.302	294.302	1.103	10.121	10.121	0.370
10.500	13.319	9.846	0.005	0.572	1.000	0.997	1.672	294.672	1.134	14.084	14.084	0.514
10.750	16.261	12.419	0.006	0.571	0.995	0.992	2.041	295.041	1.166	18.169	18.169	0.664
11.000	19.204	14.992	0.007	0.570	0.969	0.967	2.410	295.410	1.198	21.973	21.973	0.803
11.250	22.147	17.565	0.009	0.568	0.914	0.912	2.780	295.780	1.232	24.959	24.959	0.912
11.500	25.090	20.138	0.010	0.567	0.836	0.834	3.149	296.149	1.266	26.888	26.888	0.982
11.750	29.618	20.930	0.012	0.566	0.699	0.697	3.717	296.717	1.320	24.380	24.380	0.891
12.000	34.850	20.930	0.014	0.564	0.552	0.551	4.374	297.374	1.386	20.201	20.201	0.738
12.250	40.083	20.930	0.016	0.562	0.433	0.432	5.031	298.031	1.454	16.614	16.614	0.607
12.500	45.315	20.930	0.018	0.560	0.341	0.340	5.687	298.687	1.526	13.734	13.734	0.502
12.750	50.548	20.930	0.020	0.559	0.271	0.271	6.344	299.344	1.600	11.469	11.469	0.419
13.000	55.780	20.930	0.022	0.557	0.219	0.218	7.001	300.001	1.678	9.692	9.692	0.354
13.250	61.013	20.930	0.024	0.555	0.178	0.178	7.657	300.657	1.759	8.288	8.288	0.303

C_4AF Hydration

From Reference q-Q graph

*Assume C_4AF Hydration only begins after 8.511 hours

Step 1	Q = 0 to 4.19	**Step 4**	Q = 33.49 to 83.72
time reqd	1.539	time reqd	9.369
time ellps	10.050	time ellps	24.393
Step 2	Q = 4.19 to 12.56	**Step 5**	Q = 83.72 to 209.3
time reqd	1.869	time reqd	40.422
time ellps	11.919	time ellps	64.815
Step 3	Q = 12.56 to 33.49	**Step 6**	Q = 209.3 to 418.6
time reqd	3.106	time reqd	723.290
time ellps	15.025	time ellps	788.105

Thermal activity -4000

$(Q_1-Q_0)/(t_1-t_0)$	2.719	1.813	$(q_1-q_0)/(t_1-t_0)$
$(Q_2-Q_1)/(t_2-t_1)$	4.479	2.112	$(q_2-q_1)/(t_2-t_1)$
$(Q_3-Q_2)/(t_3-t_2)$	6.739	0.000	$(q_3-q_2)/(t_3-t_2)$
$(Q_4-Q_3)/(t_4-t_3)$	5.362	-0.273	$(q_4-q_3)/(t_4-t_3)$
$(Q_5-Q_4)/(t_5-t_4)$	4.661	-0.073	$(q_5-q_4)/(t_5-t_4)$
$(Q_6-Q_5)/(t_6-t_5)$	0.289	-0.003	$(q_6-q_5)/(t_6-t_5)$

Time (hrs)	Q kcal/kg	q (Q/hr)	η_{ll}	ω_{free}	β_l	β_{lacj}	ΔT	T (K)	Arrhenius	$H_l = q_l$	q_{ave}	contrib
0.000	0.000	0.000	0.000	0.601	1.000	0.998	0.000	293.000	1.000	0.000	0.000	0.000
0.500	0.000	0.000	0.000	0.598	1.000	0.998	0.000	293.000	1.000	0.000	0.000	0.000
1.000	0.000	0.000	0.000	0.597	1.000	0.998	0.000	293.000	1.000	0.000	0.000	0.000
1.500	0.000	0.000	0.000	0.595	1.000	0.998	0.000	293.000	1.000	0.000	0.000	0.000
2.000	0.000	0.000	0.000	0.594	1.000	0.998	0.000	293.000	1.000	0.000	0.000	0.000
2.500	0.000	0.000	0.000	0.593	1.000	0.998	0.000	293.000	1.000	0.000	0.000	0.000
3.000	0.000	0.000	0.000	0.593	1.000	0.998	0.000	293.000	1.000	0.000	0.000	0.000
3.500	0.000	0.000	0.000	0.593	1.000	0.998	0.000	293.000	1.000	0.000	0.000	0.000
4.000	0.000	0.000	0.000	0.592	1.000	0.998	0.000	293.000	1.000	0.000	0.000	0.000
4.500	0.000	0.000	0.000	0.591	1.000	0.998	0.000	293.000	1.000	0.000	0.000	0.000
5.000	0.000	0.000	0.000	0.590	1.000	0.998	0.000	293.000	1.000	0.000	0.000	0.000
5.250	0.000	0.000	0.000	0.590	1.000	0.998	0.000	293.000	1.000	0.000	0.000	0.000
5.500	0.000	0.000	0.000	0.590	1.000	0.998	0.000	293.000	1.000	0.000	0.000	0.000
5.750	0.000	0.000	0.000	0.589	1.000	0.998	0.000	293.000	1.000	0.000	0.000	0.000
6.000	0.000	0.000	0.000	0.589	1.000	0.998	0.000	293.000	1.000	0.000	0.000	0.000
6.250	0.000	0.000	0.000	0.588	1.000	0.998	0.000	293.000	1.000	0.000	0.000	0.000
6.500	0.000	0.000	0.000	0.588	1.000	0.998	0.000	293.000	1.000	0.000	0.000	0.000
6.750	0.000	0.000	0.000	0.587	1.000	0.998	0.000	293.000	1.000	0.000	0.000	0.000
7.000	0.000	0.000	0.000	0.586	1.000	0.998	0.000	293.000	1.000	0.000	0.000	0.000
7.250	0.000	0.000	0.000	0.586	1.000	0.998	0.000	293.000	1.000	0.000	0.000	0.000
7.500	0.000	0.000	0.000	0.585	1.000	0.998	0.000	293.000	1.000	0.000	0.000	0.000
7.750	0.000	0.000	0.000	0.584	1.000	0.998	0.000	293.000	1.000	0.000	0.000	0.000
8.000	0.000	0.000	0.000	0.584	1.000	0.998	0.000	293.000	1.000	0.000	0.000	0.000
8.250	0.000	0.000	0.000	0.583	1.000	0.998	0.000	293.000	1.000	0.000	0.000	0.000
8.500	0.000	0.000	0.000	0.582	1.000	0.998	0.000	293.000	1.000	0.000	0.000	0.000
8.750	0.651	0.434	0.001	0.580	1.000	0.998	0.082	293.082	1.004	0.550	0.550	0.040
9.000	1.331	0.887	0.001	0.579	1.000	0.998	0.167	293.167	1.008	1.128	1.128	0.082
9.250	2.011	1.341	0.002	0.578	1.000	0.998	0.252	293.252	1.012	1.712	1.712	0.124
9.500	2.691	1.794	0.002	0.577	1.000	0.998	0.338	293.338	1.016	2.299	2.299	0.166
9.750	3.370	2.247	0.003	0.576	1.000	0.998	0.423	293.423	1.020	2.892	2.892	0.209
10.000	4.050	2.700	0.003	0.575	1.000	0.998	0.508	293.508	1.024	3.489	3.489	0.252
10.250	5.082	3.213	0.004	0.573	1.000	0.998	0.638	293.638	1.030	4.177	4.177	0.302
10.500	6.202	3.742	0.005	0.572	1.000	0.998	0.778	293.778	1.037	4.895	4.895	0.354
10.750	7.321	4.270	0.006	0.571	0.998	0.996	0.919	293.919	1.044	5.611	5.611	0.406
11.000	8.441	4.798	0.007	0.570	0.988	0.985	1.059	294.059	1.050	6.280	6.280	0.454
11.250	9.561	5.326	0.008	0.568	0.960	0.958	1.200	294.200	1.057	6.823	6.823	0.493
11.500	10.680	5.854	0.009	0.567	0.914	0.912	1.340	294.340	1.064	7.186	7.186	0.520
11.750	11.800	6.382	0.009	0.566	0.853	0.851	1.481	294.481	1.071	7.358	7.358	0.532
12.000	13.102	6.739	0.011	0.564	0.772	0.770	1.644	294.644	1.079	7.081	7.081	0.512
12.250	14.787	6.739	0.012	0.562	0.665	0.663	1.856	294.856	1.090	6.159	6.159	0.445
12.500	16.472	6.739	0.013	0.560	0.566	0.564	2.067	295.067	1.100	5.294	5.294	0.383
12.750	18.157	6.739	0.015	0.559	0.479	0.478	2.279	295.279	1.111	4.531	4.531	0.328
13.000	19.842	6.739	0.016	0.557	0.407	0.406	2.490	295.490	1.122	3.879	3.879	0.280
13.250	21.527	6.739	0.017	0.555	0.346	0.345	2.702	295.702	1.133	3.332	3.332	0.241

TOTAL

Time (hrs)	q_H (kcal/kgh
0.000	0.00
0.500	0.00
1.000	0.00
1.500	0.00
2.000	0.00
2.500	0.00
3.000	0.00
3.500	0.00
4.000	0.00
4.500	0.00
5.000	0.00
5.250	0.00
5.500	0.00
5.750	0.00
6.000	0.00
6.250	0.34
6.500	0.85
6.750	1.36
7.000	1.87
7.250	2.39
7.500	2.92
7.750	3.48
8.000	4.12
8.250	4.89
8.500	5.65
8.750	6.36
9.000	6.85
9.250	7.07
9.500	7.13
9.750	7.11
10.000	7.01
10.250	6.92
10.500	6.79
10.750	6.67
11.000	6.55
11.250	6.40
11.500	6.23
11.750	5.73
12.000	4.88
12.250	4.15
12.500	3.56
12.750	3.07
13.000	2.67
13.250	2.46

Input / Phase Ref data / Bi wc Adj. / Water / Ettringite / **Hydration** / Monosulphate / Total /

B.2.7 Monosulphate Conversion

B.2.8 Total Heat of Hydration of Heat Rate Determination

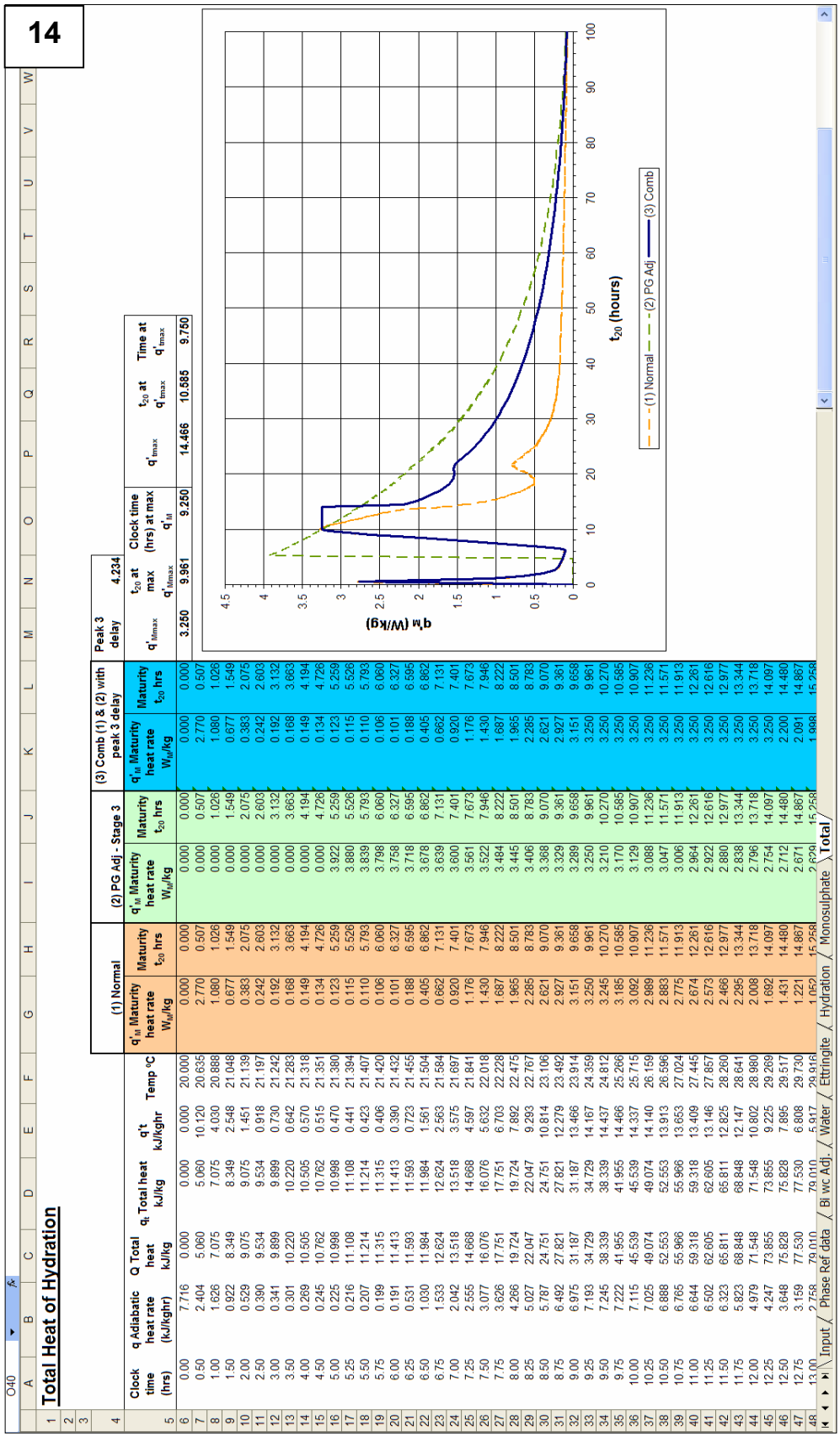

Bibliography

Addis B. (1998) *Fundamentals of Concrete*, Cement and Concrete Institute (CNCI), Midrand, South Africa.

Addis, B. and Owens, G. (ed.) (2001) *Fulton's Concrete Technology, 8th Ed.*, Cement and Concrete Institute (CNCI), Midrand, South Africa.

Addis, B.J. (ed.) (1986) *Fulton's concrete technology 6th Ed.*, Portland Cement Institute, Midrand, South Africa.

American Standard ASTM C150-04**,** *Standard Specification for Portland Cement,* ASTM International, West Conshohocken, PA, USA.

Ballim, Y. and Graham, P.C. (2003) A maturity approach to the rate of heat evolution in concrete, *Magazine of concrete research*, vol. 55 no. 3, Thomas Telford, London, UK, pp. 249-256.

Ballim, Y. and Graham, P.C. (2003) Early-age heat evolution characteristics of South African cements in relation to clinker chemistry and crystallography. In: Grieve, G. and Owens, G. (ed.) *Proceedings of the 11th International Congress on the Chemistry of Cement (ICCC)*, Durban, South Africa.

Bamford, C.H. and Tipper, C.F.N. (1969) The Practice of Kinetics. In: *Comprehensive Chemical Kinetics*, vol. 1, Elsevier Publishing, New York, USA, pp. 404.

Barret, P. and Bertrandie, D. (1986) Fundamental hydration kinetic features of major cement constituents: Tricalcium silicate (Ca_3SiO_5) and β-dicalcium silicate (β-Ca_2SiO_4), *J. Chim. Phys. Phys.-Chim.Biol*, vol. 83, no. 11-12, pp. 765-775.

Bogue, R.H. (1947) *The chemistry of Portland cement*, Reinhold Publishing, New York, USA.

Branco, F.A., Mendes, P.A. and Mirambell, E. (1992) Heat of hydration effects in concrete structures, *ACI Materials Journal*, vol. 89, no. 2, American Concrete Institute (ACI), Detroit, USA, pp. 139-145.

Bye, G.C. (1999) *Portland cement: Composition, production and properties, 2nd ed*. Thomas Telford, London, UK.

Campbell, D.H. (1999) Microscopic characteristics of clinker phases. In: *Microscopical examination and interpretation of Portland cement and clinker, 2nd Ed.*, Portland Cement Association (PCA), Skokie, USA.

Coole, M.J. (1988) Heat release characteristics of concrete containing ground granulated blast furnace slag in simulated large pours, *Magazine of Concrete Research*, vol. 40, no. 144, Thomas Telford, London, UK, pp. 152-158.

Czernin, W. (1980) *Cement chemistry for civil engineers, 2nd English Ed.*, George Godwin Ltd., London, UK.

De Schutter, G. (1998) Hydration and temperature development of concrete made with blast-furnace slag cement, *Cement and Concrete Research,* vol. 29 (1999), Pergamon Publishing, pp. 143-149.

Emborg, M. and Bernander, S. (1994) Assessment of risk of thermal cracking in hardening concrete, *Journal of Structural Engineering,* vol. 120, no. 10, American Society of Civil Engineering (ASCE), New York, USA, pp. 2893-2912.

Gibbon, G.J. (1990) *A computer controlled adiabatic calorimeter for the determination of the self-heating propensity of coal*, MSc Dissertation, University of the Witwatersrand, Johannesburg, South Africa.

Gibbon, G.J. (1995) *Laboratory test procedures to predict the thermal behaviour of concrete*, PhD Thesis, University of the Witwatersrand, Johannesburg, South Africa.

Gibbon, G.J., Ballim, Y. and Grieve, G.R.H. (1997) A low-cost computer-controlled adiabatic calorimeter for determining the heat of hydration of concrete, *Journal of Testing and Evaluation (JTEVA),* vol. 25, no. 2, American Society for Testing Materials (ASTM), West Conshohocken, USA, pp. 261-266.

Graham, P.C. (2003) *The heat evolution characteristics of South African cements and the implications for mass concrete structures*. Ph.D. Thesis, University of the Witwatersrand, Johannesburg, South Africa.

Harrison, T.A. (1981) *Early-age thermal crack control in concrete*, CIRIA Report 91, Construction Industry Research and Information Association (CIRIA), London, UK.

Hewlett, P.C. (ed.), (1998) *Lea's chemistry of cement and concrete*, Arnold, London, UK.

Holman, J.P. (1997) *Heat Transfer 8th Edition*, McGraw-Hill, New York, USA.

Kishi, T., Shimomura, T. and Maekawa, K. (1993) Thermal crack control design of high performance concrete, in the *Proceedings of Concrete 2000*, Dundee, Scotland, E&FN Spon, London, UK, pp. 447-456.

Langan, B.W., Weng, K. and Ward, M.A. (2002) Effect of silica fume and fly ash on heat of hydration of Portland cement, *Cement and Concrete Research*, vol. 32, Elsevier Science Ltd., pp. 1045-1051.

Lilkov, V., Dimitrova, E. and Petrovo, E. (1997) Hydration process of cement containing fly ash and silica fume: the first 24 hours, *Cement and Concrete Research*, vol. 27, no. 4, Elsevier Science Ltd., pp. 577-588.

Maekawa, K., Chaube, R. and Kishi, T. (1999) *Modelling of Concrete Preformance: Hydration, microstructure formation and mass transport*, Routledge, New York, USA.

Massazza, F. and Daimon, M. (1992) Chemistry of hydration of cements and cementitious materials. In: *Proceedings of the 9th International Congress on the Chemistry of Cement (ICCC)*, New Delhi, India, pp. 383-429.

Montgomery, D.C., Runger, G.C. and Hubele, N.F. (2004) *Engineering Statistics 3rd Edition*, John Wiley & Sons, Inc., New York, USA.

Neville, A.M. (1981) *Properties of Concrete, 3rd ed.*, Pitman Publishing, London, UK.

Portland Cement Association (PCA). (1994) *Research and development information: Cement*, PCA, Skokie, USA.

Ramachandran, V.S., Paroli, R.M., Beaudoin, J.J. and Delgado, A.H. (2003) *Handbook of thermal analysis of construction materials*, Noyes Publications/William Andrew Publishing, Norwich, USA.

South African Bureau of Standards (SABS). (1971) *SABS Method 747: Density of cement*, SABS, South Africa.

South African Bureau of Standards (SABS). (1971) *SABS Method 748: Specific surface of cement*, SABS, South Africa.

Springedschmid, R. (ed.) (1998) *Prevention of thermal cracking in concrete at early ages*, RILEM Report 15, E&FN Spon, London, UK.

Springenschmid, R. (ed.), (1995) *Thermal Cracking in Concrete at Early Ages: Proceedings from RILEM Symposium 25, Munich 1994*, E & FN Spon, London, UK.

Suzuki, Y., Tsuji, Y., Maekawa, K. and Okamura, H. (1990) Quantification of hydration-heat generation process of cement in concrete, *Concrete Library of JSCE*, no.19, pp 111-124.

Taylor, H.F.W (1997) *Cement chemistry, 2nd Ed.*, Telford, London, UK.

Taylor, H.F.W. (ed.), (1972) *The chemistry of cements volume 1*, Academic Press, New York, USA.

van Breugel, K. (1992) Numerical simulation of hydration and microstructural development in hardening cement-based materials, *Heron*, vol. 37, no. 2, Delft University of Technology, Delft, Netherlands.

Waller, V., d'Aloïa, L. Cussigh, F. and Lecrux, S. (2004) Using the maturity method in concrete crack control at early ages, *Cement and Concrete Composites*, vol. 26, issue 5, Elsevier Science Ltd., 9pp. 589-599.